UNIVERSITY OF CALIFORNIA,
IRVINE

Molecular and Whole Circuit Dynamics of *Drosophila* Clockwork and Light Integration

DISSERTATION

submitted in partial satisfaction of the requirements
for the degree of

DOCTOR OF PHILOSOPHY

in Biomedical Sciences

by

Logan Roberts

Dissertation Committee:
Professor Todd Holmes, Chair
Professor David Welsh
Professor Francesco Tombola
Professor Xiangmin Xu
Professor Ian Parker

2016

DEDICATION

To my family – Daniel and Trevor Roberts, Wei Fang Wu, and Sarah Huynh

To my advisor – Todd C. Holmes

And God said, “Let there be light,” and there was light. And God saw that the light was good. And God separated the light from the darkness. God called the light Day, and the darkness he called Night. (Genesis 1:3-5)

TABLE OF CONTENTS

LIST OF FIGURES

LIST OF TABLES

ACKNOWLEDGMENTS

I would like to express the deepest appreciation to my mentor and committee chair, Professor Todd C. Holmes. His scientific insights and profound guidance have been an integral part of my development as a scientist. Without his guidance and persistent help this dissertation would not have been possible.

I would also like to thank my advancement and dissertation committee members, Professor David K. Welsh, Professor Francesco Tombola, Professor Ian Parker, and Professor Xiangmin Xu for their valuable guidance and direction.

I am very thankful to current and past members of the Holmes lab for their time, input and support throughout my time in the lab. I thank Dr. Keri J. Fogle and Lisa S. Baik who have been great colleagues and supportive friends. I thank Alexis M. Galschiodt and Vinh Nguy for their assistance in my work in the lab. I am especially grateful to Dr. Tanya Leise, Dr. Takako Noguchi, and Dr. Alec Davidson for their patient guidance, generous support and incredible mentorship. They forever changed my view of science with their infectious enthusiasm and introduced me to the world of bioinformatics and bioluminescence imaging systems.

I thank my family, to whom this thesis is dedicated. I am so thankful to Trevor and Daniel Roberts, Wei Fang Wu and Sarah Huynh for their endless support, encouragement and love that made all of this possible. You guys made me who I am today (yes; it's your fault) and constantly remind me of how I am blessed. I also thank my friends who helped push me through long nights of research when needed and pull me away for fun to save my sanity when needed. I also thank God for His grace, power, sense of humor and love for allowing me to be who I am and where I am today.

I thank Cell Press for permission for the reprinting of Chapter 2, and the authors who contributed to the work: Dr. Tanya L. Leise, Dr. Takako Noguchi, Alexis Galschiodt, Dr. Jerry H. Houl and Dr. Todd C. Holmes. I also thank SAGE Publications for permission for the reprinting of Chapter 3, and the authors who contributed to the work: Dr. Tanya L. Leise, Dr. David K. Welsh, and Dr. Todd C. Holmes. I also thank the Proceedings of the National Academy of Sciences (PNAS) for permission for reprinting Chapter 4, and the authors who contributed to the work: Dr. Keri J. Fogle, Dr. Jerry H. Houl, Tri T. Tran, Nicole A. Dahm, Dr. Yu Cao, Dr. Ming Zhou, and Dr. Todd C. Holmes. I thank the authors who contributed to the work in Chapter 5, which is currently under review by PNAS, including: Lisa S. Baik, Dr. Keri J. Fogle, Alexis Galschiodt, Vinh Nguy and Dr. Todd C. Holmes. Finally, I would like to thank Dr. Alec J. Davidson, Jeff Stepkowski, David Callard, Dr. Tanya Leise, Alexis Galschiodt, Ceazar Nave, Steven DeGroot and Dr. Todd C. Holmes for their contributions to the unpublished work presented in Chapter 6. Financial support was provided by the National Science Foundation, grant number DGE-1321846, and the National Institutes of Health, grant numbers NS046750, NS078434, GM102965, and GM107405. Financial support was also provided by the National Science Foundation Graduate Research Fellowship, grant number IBN-0323466, and the Ayala/ School of Medicine Dean's Fellowship.

CURRICULUM VITAE

Logan Roberts

920 Riverview Circle
Corona, CA 92881

Cell: (949) 293-8236
loganx889@gmail.com

EDUCATION

Doctor of Philosophy in Biomedical Science **2016**
University of California, Irvine *Irvine, California*

Bachelor of Science in Neuroscience; Minor in Biomedical Research **2011**
University of California, Los Angeles *Los Angeles, CA*

LAB EXPERIENCE

Graduate Student Researcher **Sept 2012 - June 2016**
Todd Holmes Lab, University of California, Irvine

- Discovered and characterized spatiotemporal dynamics by which *Drosophila* whole circadian neural circuits reflect jet lag and are reset by light cues through process termed phase retuning.
- Assisted in the design, build, and optimization of a cutting edge bioluminescence imaging setup.
- Studied circadian, behavioral and sensory responses to light, gene mutations and social jet lag.

Graduate Laboratory Rotations **Sept 2011 – June 2012**
11 week rotations in 3 labs, University of California, Irvine

- Charlie Glabe Lab: Re-evaluated the micropathology of Parkinson's disease and multiple system atrophy using amyloid conformation-dependent monoclonal antibodies in human brain tissue.
- Kim Green Lab: Studied the role of two-pore channels in endolysosomal processing and Alzheimer's disease using mouse models and human HEK 293 cell cultures.
- Todd Holmes Lab: Optimized a protocol for stable culturing of adult *Drosophila* whole brain explants to enable longitudinal measurements of whole circuit circadian light response *ex vivo*

Undergraduate Research Assistant **Jan 2008 – June 2011**
David Krantz Lab, University of California, Los Angeles

- Performed multi-stage drug screen for potential treatments of Parkinson's disease and depression
- Developed a robust system for assaying neuroprotection and dopaminergic neuron loss due to pesticide exposure using immunohistochemistry and confocal microscopy in *Drosophila*

AWARDS

2011-2016	National Science Foundation - Graduate Research Fellowship Program (NSF-GRFP)
2016	Best Poster Award; 7th Annual Center for Circadian Biology Symposium
2011-2012	Ayala/School of Medicine Dean's Fellowship
2011	Dean's Prize Award; UCLA Science Poster Day
2011	Outstanding Presenter Award; UCLA Neuroscience Poster Day
2010	Maximizing Student Diversity Scholars Research Scholarship
2010	Center for Academic and Research Excellence (CARE) Fellow
2007-2008	UCLA Academic Competitive Grant
2007-2008	UCLA Scholarship Recognition Award

PUBLICATIONS

L. Roberts, T. Leise, D.K. Welsh, T.C. Holmes. Functional Contributions of Strong and Weak Cellular Oscillators to Synchrony and Light-Shifted Phase Dynamics. *Journal of Biological Rhythms* (2016).

L. Roberts, T. Leise, T. Noguchi, A. Galschiodt, J.H. Houl, D.K. Welsh, T.C. Holmes. Light evokes rapid circadian network oscillator desynchrony followed by gradual phase retuning of synchrony. *Current Biology* (2015).

K.J. Fogle, L.S Baik, J.H Houl, T.T Tran, **L. Roberts**, N.A. Dahm, Y. Cao, M. Zhou, T.C. Holmes. CRYPTOCHROME mediated phototransduction by modulation of the potassium ion channel beta subunit redox sensor. *PNAS* (2015).

H.O. Lawal, A. Terrell, H.A. Lam, C. Djapri, J. Jang, R. Hadi, **L. Roberts**, V. Shahi, M.T. Chou, T. Biedermann, B. Huang, G.M. Lawless, N.T. Maidment, D.E. Krantz. *Drosophila* modifier screens to identify novel neuropsychiatric drugs including aminergic agents for the possible treatment of Parkinson's disease and depression. *Molecular psychiatry* (2012).

TEACHING AND LEADERSHIP

Teaching Assistant, Physiology of Ion Channels Graduate Course **March 2015 - June 2015**
University of California, Irvine

- Provided literature reviews, discussions, grading and regular feedback for 9 students
- Held office hours and review sessions outside of class

Assistant Lab Manager and Project Leader **September 2012 - June 2016**
University of California, Irvine

- Organized lab purchasing, equipment setup, work-study training, daily tasks and safety adherence
- Mentored and trained 3 undergraduate researchers and 2 graduate students
- Led collaborations with researchers and technical professionals from various backgrounds

President of the Biomedical Research Undergraduate Society **March 2010 - June 2011**
University of California, Los Angeles

- Designed the goals, constitution, officer structure, meeting topics and workshops as co-founder
- Led workshops, meetings, lab tours and talks on biomedical topics, techniques and collaborations

LAB SKILLS

Bioluminescence imaging	Confocal microscopy	Molecular subcloning
Immunohistochemistry	*Drosophila* behavioral assays	DNA transfection
Drosophila microsurgeries	Spectrophotometry	Western blots
Whole brain and cell culture	Vibratome section preparation	Pharmacological assays
Brightfield microscopy	MATLAB	ELISA
Pharmacological drug screening	Optimizing imaging systems	Assay design
Antibody screening	Gel electrophoresis	Biostatistics

ABSTRACT OF THE DISSERTATION

Molecular and Whole Circuit Dynamics of *Drosophila* Clockwork and Light Integration

By

Logan Roberts

Doctor of Philosophy in Biomedical Sciences

University of California, Irvine, 2016

Professor Todd C. Holmes, Chair

Virtually all forms of life ranging from single-celled prokaryotes to humans have molecular and cellular clocks that calibrate essential physiological and behavioral patterns of activities. These clocks are fine-tuned by various environmental cues with light being the most powerful. Misalignment of circadian rhythms due to altered photic input by conditions such as jet lag and shift work has been linked to numerous negative health effects including diabetes, depression, Alzheimer's disease and cancer. However, the fundamental question of how circadian neural networks dynamically integrate photic input in real-time has long remained enigmatic. We address this issue by using a combination of transgenic fruit flies, immunocytochemistry, mathematical modeling and 6-day real-time bioluminescence imaging of cultured *Drosophila* whole brain explants at single cell resolution. Although desynchrony has long been perceived as a negative feature of circadian disruption, our primary findings suggest that transient circuit-wide desynchrony by light may be a key feature of photoentrainment. We also identify the functional contributions of strong and weak neuronal oscillators that permit *Drosophila* circadian neural networks to drive robust yet adaptable rhythms. Using

patch-clamp recordings, pharmacology, genetic recombination and behavioral assays, we show that light activation of the flavoprotein cryptochrome (CRY) is coupled to rapid membrane depolarization and acute behavioral arousal responses in *Drosophila* via a redox sensor called Hyperkinetic. In addition to CRY's recognized role in resetting molecular clocks in response to blue light, we show that CRY may also mediate behaviors such as phototaxis in response to ultraviolet light. We are also investigating the growing problem of social jet lag using a novel photoentrainment protocol called LD strobe in combination with a custom bioluminescence imaging system. Overall, our findings indicate that there are distinct dynamic patterns of activity at the molecular, cell-autonomous and circuit-wide levels involved in circadian photoreception which could be harnessed and amplified to treat conditions such as jet lag, shift work and seasonal affective disorder.

Supplemental Movie 1: Raw time-lapse bioluminescence recordings of adult XLG-Per-Luc *Drosophila* whole-brain explants cultured for 6 days in darkness (Roberts et al., 2015). A: Whole brain culture maintained in constant darkness throughout recording. B: Whole brain culture exposed to a 15 minute 12.57 W/m2 light pulse at CT 22 of the second day in constant darkness (DD). This movie is further discussed in Chapter 2.

Supplemental Movie 2: The animations show changes in the phase and amplitude of XLG-Per-Luc bioluminescence activity for individual oscillators from all neuronal subgroups in either DD (Left) or in response to a phase advancing light pulse (LP, Right). The angle of the disks represents phase and drift of the disks towards the center of the circle and the size of the disks indicates reduction in amplitude. The disks

are colored according to neuronal subgroup for the s-LNvs (red), l-LNvs (yellow), LNds (orange), DN1s (blue) and DN3s (green). This movie is further discussed in Chapter 3.

Supplemental Movie 3: Raw time-lapse bioluminescence recordings of cultured adult XLG-Per-Luc *Drosophila* whole-brain explants in darkness. A: Whole brain culture maintained in constant darkness throughout 7.5 days of recording. B: An 11-day recording of whole brain cultures exposed to a 15 minute 12.57 W/m2 light pulse at CT 22 of the second day in DD. This movie is further discussed in Chapter 6.

Supplemental Movie 4: The animations show changes in the phase and amplitude of XLG-Per-Luc bioluminescence activity for individual oscillators from all neuronal subgroups in either control conditions (Left, LD strobe with no phase shift) or in response to social jet lag (Right). The angle of the disks represents phase and drift of the disks towards the center of the circle and the size of the disks indicates reduction in amplitude. The disks are colored according to neuronal subgroup for the s-LNvs (red), l-LNvs (yellow), LNds (orange), DN1s (blue) and DN3s (green). This movie is further discussed in Chapter 6.

CHAPTER 1

Introduction

1.1 Biological Rhythms

Biological rhythms are endogenously generated, cyclic events ubiquitously observed in virtually all forms of life ranging from single-celled prokaryotes to complex eukaryotes (Aschoff, 1981). Biological clocks regulating these rhythms exhibit a diverse range of complexity within individual cells, tissues, organs and whole organisms. These time-dependent biological events can endogenously persist in the absence of external cues and confer essential regulation of periodic cycles in behavior and physiological functions such as endocrine rhythms (De Mairan, 1729; Hastings, 1991). Temporal oscillations are also often exogenous and are critical for coordinating internal cycles and behavior with external stimuli such as daily solar cycles. Ordinarily, we do not notice our internal biological rhythms until they are disrupted by events such as travel across different time zones – thus giving the sensation of jetlag.

Circadian rhythms

Circadian rhythms are remarkably robust yet adaptable biological time-keeping mechanisms (Aschoff, 1981). The term “circadian” is derived from *circa diem*, a Latin phrase meaning “about a day.” Circadian clocks are capable of maintaining synchronized endogenous oscillations with a periodicity of ~24 hours even in the absence of environmental cues (De Mairan, 1729). However, circadian clocks can also be fine-tuned and entrained by external environmental cues called zeitgebers (German for “time giver”) to allow organisms to coordinate optimal timing of physiological and

behavioral activities (Aschoff et al., 1971). In mammals, such as humans, the master clock is found in the suprachiasmatic nucleus (SCN) of the anterior hypothalamus. The SCN is a pair of structures that together contain ~20,000 neurons which dominantly synchronize “slave oscillators” distributed throughout peripheral tissues. Circadian time-keeping mechanisms have been implicated in a wide array of biological events including sleep/wake cycles, hormone secretion, body temperature, arousal, immune response, metabolism, cell proliferation, stem cell differentiation and drug response (Hastings et al., 2003; Schibler et al., 2003).

General approaches for studying circadian rhythms

Traditionally, studies of circadian clocks involved sampling synchronous populations of tissues at specific time points to construct phase and dose response curves. This chapter will discuss how relatively static methods of measurements such as immunocytochemistry and electrophysiology have revealed many aspects of circadian systems such as clock gene expression, circuit connections and circadian regulation of clock cell membrane excitability (Fogle et al., 2011; Helfrich-Förster, 2003; Yu and Hardin, 2006). However, these methods have poor temporal resolution due to the labor intensive nature of collecting data for large numbers of time points as well as inter-sample variability. Since circadian rhythms are dynamic processes, longitudinal methods of analysis are needed to clearly elucidate dynamic oscillations at the molecular, cell-autonomous, whole circuit and behavioral level.

Bioluminescence imaging is a powerful alternative to fluorescence imaging for longitudinal studies due to its extremely low background, low toxicity, and lack of exogenous perturbation of light-sensitive cells. Bioluminescence studies of the

mammalian SCN have revealed many aspects of cell oscillator and peptide transmitter dynamics (Ono et al., 2015; Welsh et al., 2010). However, it is not yet technically practical to test real-time light entrainment in the mammalian brain due to the difficulty of maintaining physiological photic input from the retina. Conversely, measuring real-time circadian photoreception in *Drosophila* circadian networks is feasible because the fly brain can be cultured and is directly light-sensitive due to expression of the blue light photoreceptor Cryptochrome (CRY) in approximately half of the clock neurons (Ayaz et al., 2008; Benito et al., 2008; Yoshii et al., 2008) Further, the fly circadian circuit is arrayed in a relatively flat distributed fashion. However, prior to our studies, bioluminescence studies with adult *Drosophila* only investigated cell autonomous molecular mechanisms for short recording lengths of 3-5 days (Brandes et al., 1996; Emery et al., 1997; Sellix et al., 2010). Later chapters of this thesis will discuss how we expanded bioluminescence applications by designing and/or optimizing long-term whole *Drosophila* brain culturing, bioluminescence imaging systems and sophisticated methods of single oscillator analysis. These improvements enable extended bioluminescence imaging of *Drosophila* whole circuit circadian dynamics with single neuron resolution in constant darkness (DD) and in response to light cues. These later chapters will also discuss how understanding longitudinal circadian dynamics will be useful for understanding why circadian arrhythmicity occurs and, hence how circadian rhythmicity may be restored.

Oscillation frequency: ultradian and infradian rhythms

In addition to circadian rhythms, various other biological oscillations have been reported with critical roles in physiology and behavior. Based on the cyclic frequency of

oscillations, biological rhythms can be broadly characterized as ultradian, infradian or circadian (Aschoff, 1981). Ultradian rhythms have a cyclic period of less than ~24 hours. Ultradian oscillators have been reported for their roles in regulating important physiological functions such as body temperature, hormone secretion, sleep, locomotion and feeding (Bergendahl et al., 1996; Blum et al., 2015; Daan and Slopsema, 1978; Dowse and Ringo, 1987; Ibuka et al., 1977; Kleitman, 1982). Yet despite their prevalence and purported biological importance, ultradian rhythms are still poorly understood due to their often erratic periodicity and masked expression by most robust circadian rhythms. Conversely, infradian rhythms have an oscillatory cycle period of greater than ~24 hours (Richter, 1965). Biological clocks with infradian frequency are critical for regulating biological events such as menstrual cycles, photoperiodic breeding, hibernation and seasonal rhythms (Whitton, 1978). It should be noted that heterogeneous populations of circadian, ultradian and infradian biological clocks are often observed within the same organism (Aschoff, 1981). However, the current thesis will primarily focus on various aspects of circadian systems.

The primary goal of this chapter is to give an overview of cell-autonomous circadian properties and emergent rhythms from heterogeneous neural networks in the context of the highly studied model organism *Drosophila melanogaster*. This chapter will also outline properties and functions of key players in *Drosophila* circadian photoreception. Finally, this chapter will discuss circadian disruptions and current strategies for treating circadian disorders due to events such as jet lag, shift work and seasonal affective disorder (SAD).

1.2 The Circadian System of *Drosophila Melanogaster*

Drosophila melanogaster as a model organism for circadian research

The fruit fly, *Drosophila melanogaster*, has demonstrated numerous reasons why it is an excellent model organism for studying circadian biology (Allada et al., 2001). Since their early use in 1910 by the geneticist Thomas Hunt Morgan, fruit flies have been recognized as a classic model organism for numerous biological fields as they are relatively inexpensive, prolific, and are highly amenable to a wide array of molecular tools (Morgan, 1916; Reeve, 2014). Further, *D. melanogaster* have highly characterized circadian behaviors, genetics and neural networks making them especially useful as model organisms for chronobiology studies. One of the key advantages of the *Drosophila* circadian system that is critical for the work presented in this thesis is that the master clock is directly photosensitive due to expression of the light-sensing flavoprotein cryptochrome (CRY) (Stanewsky et al., 1998). Conversely, the mammalian master clock found in the suprachiasmatic nucleus (SCN) is not directly photosensitive and requires light input from the retina. Since the SCN is not directly photosensitive, studies of mammalian circadian photoreception *in vitro* are highly impractical due to the technical difficulty of maintaining photic input from the complex and delicate retinohypothalamic tract (RHT). Nevertheless, the high conservation of circadian genes and similar principles of circadian organization between fruit flies and mammals make *Drosophila melanogaster* an outstanding model system for studying circadian rhythms and photoreception.

By the late 1960s, circadian rhythms and internal pacemakers had already been reported in numerous organisms ranging from cyanobacteria to humans. Early

research discovered that *Drosophila* eclose, or emerge from the pupal case, at dawn (Pittendrigh, 1954). Furthermore, wild-type fruit fly populations were shown to have "crepuscular" behavioral activity patterns in which they have a morning peak near subjective dawn and a larger evening peak near subjective dusk. Yet despite various behavioral and anatomical studies in a wide array of organisms, little was known about the molecular components that comprised the circadian clockwork underlying these rhythms. It was not until the 1970s that Seymour Benzer and his graduate student Ron Konopka used the mutagen ethyl methanesulfonate (EMS) to induce point mutations in *D. melanogaster* and screened the progeny for genotypes with altered eclosion rhythmicity (Konopka and Benzer, 1971). This work identified the first circadian gene called *period*. These mutants also exhibit changes in locomotor rhythmicity and indicate that a central molecular clock mechanism may underlie various outputs of circadian behavior. This work served as a catalyst to drive forward the field of circadian molecular biology. Further research has since identified numerous genetic players linked to circadian molecular clocks.

Drosophila molecular clocks are comprised of feedback loops

Molecular clocks are a fundamental mechanism central to all circadian systems. All cellular oscillators have core molecular components, although there are subtle but key differences that differentiate clock oscillators' functions. A highly conserved feature of molecular clocks is that they are comprised of interlocking, cell-autonomous transcription-translation feedback loops of cycling transcriptional repressors that regulate rhythmic gene expression (Bell-Pedersen et al., 2005). Since the identification of the first circadian mutant (*period*^{01}) in *D. melanogaster* inspired research into the molecular clock,

researchers have identified numerous clock-regulated genes. Core clock genes that comprise the core inner-workings of the *Drosophila* molecular clockwork include: *Clock* (*Clk*), *cycle* (*cyc*), *timeless* (*tim*), *doubletime* (*dbt*), *shaggy* (*sgg*), *Par domain protein 1* (*Pdp 1*), and *vrille* (*vri*) (Allada et al., 1998; Blau and Young, 1999; Cyran et al., 2003; Martinek et al., 2001; Price et al., 1998; Rutila et al., 1998; Sehgal et al., 1994). Comparative analysis has shown that these genes are highly conserved or have functional homologues in mammalian molecular clocks (Koh et al., 2006; Panda et al., 2002).

In *Drosophila*, the molecular clock is comprised of two feedback loops with positive and negative transcription factors which regulate transcription of their own genes (Figure 1.1). At the core intersection of the two loops are the two positively acting basic-helix-loop-helix (BHLH) PER-ARNT-SIM (PAS) transcription factors CLOCK (CLK) and CYCLE (CYC) (Allada et al., 1998; Hao et al., 1997; Rutila et al., 1998). During the day, CLK-CYC heterodimers bind to E-box enhancer elements to stimulate transcription of circadian genes including *per* and *tim* in the first loop and *Pdp1* and *vri* in the second loop (Blau and Young, 1999; Cyran et al., 2003; Darlington et al., 1998). PERIOD (PER) is phosphorylated during the late evening/early morning by DOUBLETIME (DBT), a homolog of mammalian casein kinase 1ε, and CK2 (casein kinase 2) leading to its degradation until it dimerizes with TIMELESS (TIM). Activation of the short wavelength photoreceptor CRYPTOCHROME (CRY) by light results in the targeting of TIM for degradation through a ubiquitin-proteasome pathway (Emery et al., 1998; Stanewsky et al., 1998). The activities and properties of CRY will be discussed in greater detail later in this chapter. In the late afternoon/early evening, PER and TIM accumulate in the

cytoplasm until TIM binds to, and stabilizes, the PER-DBT complex (Gekakis et al., 1995; Marrus et al., 1996). PP2a (protein phosphatase 2a) serves to further stabilize PER by removing phosphates that were added to PER. The TIM-PER-DBT complexes are then phosphorylated by the two kinases SHAGGY (SGG), a homolog of mammalian glycogen synthase kinase 3, and CK2 to promote translocation of the complexes into the nucleus (Lin et al., 2002; Martinek et al., 2001). However, it should be noted that immunocytochemical staining *in vivo* and *in vitro* has paradoxically provided evidence that PER and TIM can translocate into the nucleus independently (Meyer et al., 2006; Shafer et al., 2002). Once in the nucleus, PER and TIM bind to and inhibit CLK/CYC-mediated transcription and thus suppress their own transcription (Darlington et al., 1998; Nawathean and Rosbash, 2004). The second interlocked loop further ensures robust and precise timing by regulation of Clk mRNA levels (Cyran et al., 2003). The basic leucine zipper (bZip) transcription factor VRILLE (VRI) binds to Clk promoter to inhibit Clk transcription. The cycling protein PAR DOMAIN 1ε (PDP1) competes with VRI for the same binding site. In the late evening, higher PDP1 levels can outcompete VRI to allow for Clk transcription. In the morning, DBT phosphorylation of PER and CRY-mediated TIM-degradation frees CLK/CYC to stimulate transcription and repeat the cycle (Blau and Young, 1999; Cyran et al., 2003). The current thesis will focus on photic modulation of circadian gene activity as it is understood to be a highly conserved and critical mechanism of circadian systems in most organisms including *Drosophila* and humans.

Central pacemakers and peripheral cellular clocks

Cells expressing clock genes are known as clock cells. Almost all of the trillions of humans cells such as cardiomyocytes, neurons, pancreatic β cells, and immune cells contain an intracellular circadian clock that provides precise temporal control of physiological and cellular functions throughout a day (Yamazaki et al., 2000; Zylka et al., 1998). Notable exceptions include the male testis and certain cancer cells in which molecular clocks are absent (Morse et al., 2003; Winter et al., 2007). Circadian cellular oscillators can be broadly categorized as central pacemakers or peripheral clocks based on functionality and cell type. Central pacemakers found in neurons maintain robust free-running oscillations even in the absence of exogenous cues and synchronize the activities of peripheral clocks. Peripheral clocks distributed throughout various tissues exhibit their own distinct, endogenous rhythms and largely consist of oscillators that desynchronize over time in the absence of exogenous cues. In mammals, the central pacemaker is located within the suprachiasmatic nucleus (SCN) which serves to maintain synchrony between peripheral clocks to generate robust circadian output.

Molecular-genetic studies in *Drosophila melanogaster* have reported molecular clocks in neurons, glia, photoreceptors, fat bodies, rectum, the reproductive system, Malpighian (renal) tubules and the antennal lobe (Giebultowicz, 2001; Giebultowicz and Hege, 1997; Hunter-Ensor et al., 1996; Kaneko and Hall, 2000; Siwicki et al., 1988; Tanoue et al., 2004). In the absence of environmental cues, molecular oscillations in peripheral tissues dampen over time. Conversely, a small group of ~150 neurons in the brain sustain cyclic gene expression for many days even in the absence of exogenous cues. However, it is unclear whether the sustained oscillations are an intrinsic property

of the central pacemaker neurons or an emergent property of the coupled circuit. These neurons are considered the central pacemaker cells as they appear to have a key role in regulating circadian rhythms and output (Chang, 2006).

The *Drosophila* central clockwork consists of ~150 heterogeneous neurons

Each hemisphere of the *Drosophila* central circadian network is classically comprised of six neuron subgroups, along with hundreds of glial cells. These cellular oscillators were originally identified via immunohistochemical screening for *per* expression and were classified according to their anatomic locations and sizes (Figure 1.2) (Ewer et al., 1992; Kaneko and Hall, 2000). The central clock neurons are broadly classified as lateral neurons (LNs) or dorsal neurons (DNs) based on their relative positions. Both the LNs and DNs can each be further subdivided into three canonical groups that are symmetrically located in both hemispheres. The LNs consist of 5-6 dorsal lateral neurons (LNds), 5 small lateral ventral neurons (s-LNvs) and 4-6 large lateral ventral neurons (l-LNvs). The DNs consist of ~15 DN1s, 2 DN2s and ~40 DN3s. Recent studies have further subdivided these subgroups and identified new classes of circadian pacemakers based on chemical or genetic markers (Collins et al., 2012; Hamasaka et al., 2007; Johard et al., 2009; Shafer et al., 2006; Zhang et al., 2010a). Examples of these newer oscillator classes include a group of 3-4 cells called the lateral posterior neurons (LPNs) in the posterior lateral central brain as well as a single large cell in the medial central brain named the large medial cell (l-MC). Additionally, numerous glial cells have been reported to rhythmically express PER/TIM and may have a role in circadian rhythms (Ewer et al., 1992; Kaneko and Hall, 2000; Zerr et al., 1990). The DN1s have also been subdivided into highly reproducible anterior ($DN1_aS$) and posterior ($DN1_pS$) based on

expression of the neuropeptide IPNamide (IPNa), discrete anatomical locations, and axonal projections (Shafer et al., 2006). However, the current thesis will focus on further evaluation of the six classical circadian subgroups based on function in the context of free-running rhythms and circadian photoreception.

Although central clock cells were originally named for their anatomical position and size, recent studies have since subdivided the circadian circuit based on functionality. The s-LNvs are classically recognized as core pacemaker neurons as they exhibit robust oscillations in constant darkness (DD) and have been shown to be sufficient for driving rhythmic locomotor activity in DD (Grima et al., 2004; Helfrich-Forster, 1998). The circadian role of the l-LNvs in DD is still unclear. However, studies incorporating genetic and electrophysiological techniques have indicated that the l-LNvs are critical for light-mediated arousal and are necessary for light-induced phase resetting at dawn (Shang et al., 2008; Sheeba et al., 2008a). L-LNvs are ideally positioned to be coincidence detectors as they are the only clock neurons that receive extensive rhodopsin-mediated light input from the optic lobes and H-B eyelets that can be integrated with their own CRY-mediated photoreception. This light integration is discussed in further detail later in this chapter. Functional knock-out studies have implicated the LNds in rhythmic locomotor activity (Blanchardon et al., 2001). Compared to the extensive functional analysis of the more popularly studied LNs, relative little is known about the functional roles of the DNs. However, the DN1s have been suggested to have a role in light-mediated circadian behavior with subsets of the DN1s specifically exhibiting a role in driving rhythmic behavior in constant light (LL) conditions and acute response to the onset of light (Murad et al., 2007; Zhang et al., 2010a). Interestingly, the DN2s exhibit molecular oscillations

that are opposite (anti-phase) to the rhythms of the majority of the circadian neural network (Plautz et al., 1997). However, the role of the DN2s is still poorly understood. The small ~40 DN3s have been suggested to mediate synchronized locomotor activity under 12:12 hour light-dark (LD) conditions independently of the LNvs (Veleri et al., 2003). The functional roles and molecular dynamics of the heterogeneous clock neurons in the context of circadian photoentrainment will be further expanded in Chapters 2 and 3.

The *Drosophila* circadian neural network can also be parsed by neuropeptide transmitters. The roles of numerous candidate signaling molecules have been reported in distinct circadian neuron subgroups including glutamate, neuropeptide F (NPF), neuropeptide precursor-like protein 1 (NPLP1), γ-amino-butyric acid (GABA), serotonin and pigment dispersing factor (PDF) (Chang, 2006; Wang et al., 2008). PDF, a homologue to mammalian vasoactive intestinal peptide (VIP), is a highly studied neuropeptide that has been shown to be critical for circadian behavior (Helfrich-Förster, 1995; Renn et al., 1999). Four of the s-LNvs and all of the l-LNvs are unique in expressing PDF whereas the 5th s-LNv, LNd, and DNs do not express PDF (Helfrich-Förster, 1995; Kaneko and Hall, 2000; Renn et al., 1999). Genetic ablation of PDF-expressing neurons and a *pdf* null allele have shown that PDF is required for rhythmic behavior in 12:12 hour LD entrainment and DD conditions (Renn et al., 1999). The PDF G protein-coupled receptor (PdfR) was recently identified, although there is still not a consensus on its expression patterns (Hyun et al., 2005; Lear et al., 2005; Mertens et al., 2005). PdfR is most similar to Class II (family B) receptors, such as those for secretin and VIP, and increases cAMP levels upon activation. PDF is particularly important for circadian research as much of our current understanding regarding inter-neuronal connections of

the circadian neural circuit is derived from anti-PDF immunostaining of the *Drosophila* brain (Helfrich-Förster, 1995; Helfrich-Förster, 2003).

Network connections of clock neurons

Studies utilizing anti-PDF immunostaining and transgenic-driven neurite markers have revealed many of the complex inter-neuronal connections in the *Drosophila* circadian circuit (Helfrich-Förster, 1995; Kaneko and Hall, 2000; Renn et al., 1999). PDF-positive (PDF+) neurite connections are essential for synchronizing cell-autonomous oscillators, which have their own endogenous phases and activities, and driving emergent rhythmic behavioral output from the circuit (Lin et al., 2004; Renn et al., 1999). The s-LNvs send ipsilateral PDF+ projections to the accessory medulla (aMe), near the base of the optic lobe, and toward the dorsal central brain (Figure 1.2) (Helfrich-Förster, 2003). These arborizations terminate near the mushroom-body calyces, DN1s and DN2s. The l-LNvs also send PDF+ projections toward the aMe as well as contralateral neurites across the brain midline via the posterior optic tract to connect the LNvs and medulla of both hemispheres. The LNds, along with all three subsets of the DNs, primarily send arborizations to the dorsal brain (Kaneko and Hall, 2000). The LNd neurites project dorsally before splitting into a dorsal and ventral branch. The dorsal branch links with DN3 neurites whereas the ventral branch crosses the brain midline to the contralateral dorsal protocerebrum. Neurites from the DN1s and DN2s have also been shown to cross the midline in the dorso-anterior commissure. The majority of the DNs' neurite projections terminate near the axon terminals of the LNds and s-LNvs. The DN1s also send projections to the dorsal brain and ventrally to the esophagus (Mertens et al., 2005). After crossing the midline, projections from the

DN2s terminate near the inferior protocerebrum (IP) of the contralateral dorsal brain (Helfrich-Förster, 2003). The DN3s send neurite projections into the mid-dorsal brain and toward the LNvs where they terminate ventral to the IP. In summary, the *Drosophila* circadian circuit is comprised of intricate network connections between clock neurons and neurosecretory centers (Cavanaugh et al., 2014; Cavey et al., 2016). Furthermore, circadian-regulated restructuring of the complexity of PDF axon terminals has been reported in both LD and DD conditions (Fernández et al., 2008). For instance, the PDF circuit exhibits significantly greater complexity during the daytime and lower complexity during the nighttime hours. We postulate that circuit-wide plasticity is a critical mechanism for further consolidating the emergent functional output of clock cells.

An increasing level of evidence has shown that robust yet flexible intercellular communication is a critical feature of circadian neural circuits. Although clock neurons can express self-sustaining molecular rhythms, the longstanding model of cell-autonomous oscillators driving rhythmic behavioral outputs is now shown to be incomplete. Studies in both *Drosophila* and mammalian circadian neural circuits have indicated that the molecular, electrical and neurochemical activities of clock neurons are integrated in a multi-cellular network that drives self-sustaining rhythms that are also adaptable to environmental stimuli (Lin et al., 2004; Nitabach et al., 2002; Reddy et al., 2006; Welsh et al., 1995; Zhao et al., 2003). However, as discussed above, not all clock cells are created equal. Further research is needed to understand the distinct cellular physiology of the various clock cells as well as how they coordinate intercellular communication to drive behavioral rhythms. Our recent findings on cell-autonomous

and whole circuit dynamics driving robust free-running rhythms in DD and in response to light cues are discussed in Chapters 2 and 3 of this thesis.

1.3 Photoreception in *Drosophila melanogaster*

Environmental inputs into circadian systems

Circadian networks are designed to be capable of robust oscillations yet are extraordinarily adaptable to changes in the environment. These environmental temporal cues, called zeitgebers (German for "time giver"), serve to fine-tune and entrain the oscillatory gears of both *Drosophila* and mammalian clocks. This ensures that physiological events and behavior are optimally coordinated with daily environmental changes. Circadian systems are sensitive to a wide variety of zeitgebers including light, temperature, feeding, and social behavior (Levine et al., 2002; Wheeler et al., 1993). Light is considered the most powerful zeitgeber and synchronizes circadian systems with daily solar cycles (Oishi et al., 2004; Pittendrigh, 1960). This thesis will focus on light integration in the context of circadian photoreception, phototransduction pathways, and light-mediated executive behavior.

Light input pathways into the *Drosophila* circadian clock

Light is the most dominant and well-studied environmental circadian cue in *Drosophila*. Photic input can influence the circadian system in numerous ways depending on factors such as phase, duration, periodicity, intensity and wavelength of the light information. The most obvious example is day-night changes in light intensity and spectral range which can synchronize central and peripheral clocks (Myers et al., 1996; Plautz et al., 1997; Yang et al., 1998). Coordination of molecular clocks by daily solar cycles drives entrainment of *Drosophila* behavior and eclosion rhythmicity (Pittendrigh,

1954; Wheeler et al., 1993). Conversely, subjecting fruit flies to constant light (LL) conditions results in arrhythmicity and altered period lengths (Konopka et al., 1989). Acute brief pulses of light can phase-advance or phase-delay molecular and behavioral rhythms of *D. melanogaster* depending on the time of day when the pulses are applied (Cymborowski et al., 1994; Vinayak et al., 2013). In fact, application of two short pulses at times corresponding to the entrained onset and offset of daytime light exposure (e.g. 15-minute light pulses at dawn and dusk for *Drosophila*) is reported to be sufficient to simulate day-night entrainment (Kawato and Suzuki, 1981; Pittendrigh and Minis, 1964). Due to the powerful influence of light on circadian systems, it is important to understand the pathways and mechanisms of photic integration.

Studies have shown that the fruit fly, *D. melanogaster*, has five photoreceptors and/or photopigments involved in circadian photoreception (Rieger et al., 2003). Two of these are the externally visible light-sensing organs, the ocelli and the pair of compound eyes (Figure 1.2). Photic information is also received through the extraretinal photoreceptor structure called the Hofbauer-Buchner (H-B) eyelets (Hofbauer and Buchner, 1989). The compound eyes, ocelli, and H-B eyelets all express the classical retinal-based photopigment rhodopsin (Rh). Six different Rh molecules have been reported in *Drosophila* with varying peaks of spectral sensitivities (Montell, 1999). Molecular analysis and phototaxis studies have indicated that the max peaks of absorption (listed in parentheses) are Rh 1 (blue-green, λ_{max} = 480 nm), Rh 2 (violet, λ_{max} = 480 nm), Rh 3 (UV, λ_{max} = 347 nm), Rh 4 (UV, λ_{max} = 375 nm), Rh 5 (blue, λ_{max} = 436 nm) and Rh 6 (green, λ_{max} = 508 nm) (Salcedo et al., 1999; Salcedo et al., 2003). These Rh molecules are primarily expressed in the photoreceptor cells (R1 – R8) of the

compound eyes. Rh 6 is also expressed in the H-B eyelets whereas Rh 2 is expressed in the ocelli (Montell, 1999; Salcedo et al., 1999; Yasuyama and Meinertzhagen, 1999). An additional unknown photopigment is putatively expressed in the DNs as well (Rieger et al., 2006; Veleri et al., 2003). However, this thesis will primarily focus on the short-wavelength photoreceptor CRYPTOCHROME (CRY) that is expressed in ~50% of brain clock neurons. Specifically, we will focus on the molecular mechanisms of CRY phototransduction and its roles in circadian photoreception and light-driven behaviors.

Cryptochromes

Cryptochromes (CRY) are short-wavelength sensitive flavoproteins with critical roles in numerous light-driven mechanisms including circadian photoreception. This photopigment is related to bacterial photolyases which repair UV-induced DNA damage (Ahmad and Cashmore, 1993). Although CRYs were originally discovered in the flowering plant *Arabidopsis*, they have since been reported in a wide array of organisms including bacteria, plants, insects and mammals (Green, 2004; Shalitin et al., 2002). All CRYs share a highly conserved core domain called the photolyase homology region (PHR) at the N-terminus (Lin and Todo, 2005). The PHR domain is the chromophore-binding domain of CRY and has two conserved binding sites for a pterin cofactor (5,10-methenyl tetrahydrofolate, MTHF) and a flavin cofactor (FADH). The flavin adenine dinucleotide (FAD)-binding site of CRY is the most conserved region of the PHR domain. Yet despite the similarity in domain structures and amino acid sequence, cryptochromes can have a diverse range of biological roles within and between organisms. CRY functions include circadian rhythms, phototropism, cell cycles, apoptosis, immune responses and magnetoreception (Lin and Todo, 2005). Interestingly, the two mammalian isoforms

called CRY1 and CRY2 are not directly light-sensitive and are instead functionally similar to *Drosophila* TIM in acting as a circadian repressor (Griffin et al., 1999). Many invertebrates also express light-insensitive CRY isoforms which appear to be transcriptional repressors. Instead, the directly photo-activated *Drosophila* CRY is functionally similar to the mammalian blue-light sensitive photopigment called melanopsin. Melanopsin is expressed in intrinsically photosensitive retinal ganglion cells (ipRGCs) which directly communicate with the SCN to modulate light-driven circadian rhythms (Hattar et al., 2003). However, the current thesis will focus on the directly light-sensitive CRY found in *Drosophila* in the context of circadian rhythms and behavioral light response.

In 1988, a chemical mutagenesis screen identified CRY as the primary circadian photoreceptor for the *Drosophila* clock (Stanewsky et al., 1998). A severely hypomorphic CRY mutant, cry^{baby} (cry^{b}), was found to exhibit disrupted *per* expression in 12:12 hour LD conditions. CRY mutants also retain behavioral rhythmicity in constant light (LL) conditions which induce arrhythmicity in wild-type *Drosophila* (Emery et al., 2000; Stanewsky et al., 1998). Peripheral tissues that express CRY, such as the Malpighian tubules, also require CRY for rhythmic expression of PER and TIM as well as synchronization with the master clock (Ivanchenko et al., 2001). In *Drosophila,* CRY modulates circadian oscillations via degradation of the critical circadian protein TIM (Ceriani et al., 1999; Klarsfeld et al., 2004). Activation by light induces a conformational change in CRY at the C-terminus resulting in CRY binding to TIM (Busza et al., 2004; Dissel et al., 2004). The F box protein JETLAG (JET) is then recruited for ubiquitination of the TIM/CRY complex which undergoes degradation through the ubiquitin-proteasome

pathway (Koh et al., 2006). Without the stabilization provided by binding with TIM, PER is also targeted for degradation, thereby resetting the clock.

Cryptochrome is expressed in ~50% of the 150 clock neurons that comprise the *Drosophila* central clock (Benito et al., 2008; Yoshii et al., 2008). CRY is detected in all of the small and large LNvs and approximately half of the LNds and DN1s. Conversely, CRY is absent in all of the DN2s, DN3s and LPNs. In addition to its role in the circadian molecular clock, CRY has been implicated in circadian regulation of neuronal firing rate and membrane excitability (Fogle et al., 2011). Specifically, s-LNvs and l-LNvs exhibit greater spontaneous firing frequencies during the early day which gradually decrease until dusk before increasing again during the nighttime hours (Cao and Nitabach, 2008; Sheeba et al., 2008a). Electrophysiological studies in the l-LNvs have also shown that these neurons display a 20-200% increase in firing rate in response to an acute light pulse of moderate intensity (Sheeba et al., 2007). CRY-mediated phototransduction occurs via redox-based mechanisms which require membrane potassium channel conductance (Fogle et al., 2015; Fogle et al., 2011). Molecular mechanisms by which CRY is coupled to membrane depolarization are further expanded in Chapter 4 of this thesis. Chapter 5 of the current thesis will also discuss how CRY, long recognized as a blue-light photoreceptor, and certain CRY-mediated complex behaviors are particularly sensitive to ultraviolet (UV) light.

1.4 Circadian Disorders

Overview of circadian disorders: sources and consequences

Circadian disorders can result from disruptions in the internal clockwork and/or misalignment between biological clocks and the external environment. Due to the vast

influence of circadian systems on biological and physiological processes, altered circadian rhythms can have a wide array of severely detrimental effects. Acute disruptions in circadian rhythms can result from events such as jet lag, all-nighters and exposure to electronic screens at late night hours. Although these are very frequent events in modern society, these circadian disruptions have been shown to impair memory, alertness, sleep quality, metabolism and mental health (Mohawk et al., 2012). Furthermore, chronic circadian disruptions have been linked to the propensity and severity of numerous conditions such as obesity, diabetes, bipolar disorder, depression, seasonal affective disorder (SAD), sleep disorders, obesity, Alzheimer's disease, Parkinson's disease, Huntington's disease and cancer (A Quera Salva et al., 2011; Czeisler et al., 1999; Harvey, 2008; Johansson et al., 2003; Kalra et al., 2003; Videnovic et al., 2014). These circadian disorders and affiliated detrimental health effects often become more pronounced over time as circadian clocks naturally begin to break down with aging (Czeisler et al., 1992; Monk, 2005). These circadian disorders can significantly impair the quality of life for both patients and caretakers due to the disrupted and irregular sleep/activity schedules. Although circadian rhythms and sleep homeostasis are driven by different circuits, sleep is regulated by the biological clock and is often the first noticeable output of circadian disruptions.

Circadian phase disorders

Individuals with circadian phase disorders generally maintain relatively stable periods and phases, but have phase angles that are misaligned with the societal norm. Since the sleep hierarchy appears conserved, these disorders are generally not associated with sleep homeostasis but rather issues in circadian systems. Individuals

with circadian sleep phase disorders often do not notice their conditions until social schedules force them to live against their phase-shifted biological clocks. Individuals with Advanced Sleep Phase Disorder (ASPD) are considered “morning larks” as their entire sleep/wake cycle is shifted up to several hours earlier relative to the majority of the population’s rhythms which are entrained by daily solar cycles (Jones et al., 2013). This condition is reported to be more common in the elderly (Jones et al., 2013). Familial ASPD was the first circadian rhythm sleep disorder (CRSD) with an identified clock gene mutation; specifically, a mutation in the human *Period 2* gene that substitutes a serine with a glycine residue (Jones et al., 1999). Although the classic idiom of “the early bird gets the worm” makes phase-advanced sleep-wake cycles appear advantageous, this condition can result in significant sleep deprivation when social obligations force individuals to stay up later in the evening and wake earlier the next day.

Conversely, Delayed Sleep Phase Disorder (DSPD) is more common in adolescents and young adults. These individuals are considered “night owls” as they have a later onset of sleep/wake cycles (late chronotype). Clock gene polymorphisms in *Period 3* and *CLOCK* genes have been reported to putatively increase susceptibility to DSPD (Dijk and Archer, 2010; Sei et al., 2001). Similar to individuals suffering from ASPD, patients with DSPD can experience circadian disruption when artificial alarm clocks and social cues force them to awake and become active in the morning before their delayed clock-determined wake-up time. This misalignment of disrupted internal clocks and external cues underscores the importance of studying circadian gene-environment interactions.

Circadian disorders of non-entrained clocks

In addition to maintaining robust endogenous oscillations, circadian systems are critical for coordinating internal physiological events with exogenous environmental cues. Accordingly, individuals with certain circadian disorders can experience severely detrimental health effects when endogenous rhythms appear de-sensitized to, and thus disconnected from, environmental stimuli such as light. Two examples of these types of disorders are non-24-hour sleep wake syndrome (non-24) and irregular sleep wake disorder (ISWD). Non-24 is characterized by free-running rhythms that fail to entrain to environmental cues such as daily solar cycles (Bjorvatn and Pallesen, 2009; Okawa and Uchiyama, 2007). This condition is more common in patients who are blind and lack proper circadian photic input. Since the endogenous human circadian period is slightly longer than 24 hours, an inability to re-entrain with day-night cycles results in patients with non-24 exhibiting daily delays in sleep-wake onset times. Patients with Irregular Sleep Wake Disorder (ISWD) exhibit another variant of altered endogenous circadian rhythms as these individuals experience non-entrained, fragmented sleep-wake cycles (Sack et al., 2007). Individuals with this disorder often suffer from constantly-shifting sleep-wake cycles, excessive sleepiness and/or chronic insomnia. Circadian arrhythmicity has been reported in a wide array of conditions including mood disorders, Parkinson's disease, Alzheimer's disease, Huntington's disease, autism and prion diseases (Barnard and Nolan, 2008). However, it is still unclear whether these circadian disruptions are linked to the cause or effects of these conditions.

Circadian disruptions by external cues

In addition to a breakdown in the endogenous circadian clockwork, circadian rhythms can be disrupted by abnormal alterations in environmental cues. A classic example of transient disruption is observed in individuals who have recently experienced high speed travel across different time zones resulting in jet lag (Waterhouse, 1999; Wegmann and Klein, 1985). Jet lag can result in impaired cognitive performance, fatigue, gastrointestinal dysfunction, and desynchronization of circadian clock oscillators (Arendt and Marks, 1982; Winget et al., 1984). Generally, the severity of symptoms increases with the number of time zones crossed and also depends on directionality. Phase advance from traveling eastward usually results in a greater circadian disruption than phase delay from traveling westward. However, symptoms and severity can greatly vary between individuals though the mechanisms underlying this variability are still poorly understood. Due to an increasing awareness of the detrimental effects of constant disruption by events such as shift work, social responsibilities, and late night exposure to electronic screens, many researchers and clinicians are looking into the growing issue of chronic circadian disruption.

Chronic circadian disruptions can result in serious negative health effects including diabetes, heart disease and metabolic dysfunction (Fido and Ghali, 2008; Parsons et al., 2015; Scheer et al., 2009). A growing proportion of the population is experiencing chronic circadian disruption due to social obligations. Shift work disorder affects individuals who work at night or frequently change work schedules. These work schedules result in a constant state of misalignment between their body's clocks, shift schedules, and zeitgebers such as daily solar cycles. Approximately 15% of Americans

are employed as shift workers who often experience severely negative effects of health, performance and safety (Karlsson et al., 2001). Another example of chronic circadian disruption is the disorder called social jet lag, coined by Dr. Till Roenneberg in 2006.

Social jet lag is a form of habitual circadian misalignment between social cues and biological clocks (Wittmann et al., 2006). Specifically, this phenomenon refers to the time discrepancy for many individuals between work days (i.e. weekdays) and free days (i.e. weekends). Social jet lag resembles classical jet lag from high-speed travel across time zones because many individuals tend to stay up later on Friday nights (a phase delay analogous to flying West) and are forced to wake up earlier on Monday mornings for work (a phase advance analogous to a return flight East) (Wittmann et al., 2006). However, unlike classical jet lag, social jet lag occurs chronically for many people on a weekly basis and has been linked to serious health issues such as obesity, diabetes, heart disease and metabolic syndrome (Lau et al., 2013; Roenneberg et al., 2012). In Chapter 6 of the current thesis, we discuss preliminary findings and tools that we have generated for future studies of how social jet lag is reflected in circadian neural circuits *ex vivo* and circadian behavior *in vivo*.

Strategies for treating circadian disorders

Treating circadian disorders is very difficult due to the complexity of input and output signals to and from circadian clocks (Redfern, 1989; Redfern et al., 1994). However, various therapeutic options do exist for ameliorating circadian disorders. Behavioral therapy is a non-pharmacological approach with recommendations including regular sleep-wake times, avoiding caffeine and alcohol, standard work hours, regular meal times and engaging in regular exercise (Dodson and Zee, 2010; Morgenthaler et

al., 2007). Another non-pharmacological intervention is chronotherapy. Chronotherapy requires patients to progressively advance or delay their sleep-wake times 1-2 hour per day until the correct schedule is established and stable (Foldvary-Schaefer, 2009). These non-pharmacological interventions are often prescribed with pharmacological treatments.

Pharmacological interventions with the capacity to modulate circadian systems are referred to as “chronobiotics” and include classes of drugs such as indoleamines, cholinergics, peptides, antidepressants, antimanics, corticosteroids and benzodiazepines (Dawson and Armstrong, 1996). Of all the pharmacological interventions, exogenous melatonin has been the most studied (Dagan et al., 1998; Dahlitz et al., 1991; Nagtegaal et al., 1998). Melatonin is a hormone that is endogenously produced by the pineal gland in the brain with physiological roles that include regulation of circadian rhythms, blood pressure and sleep-wake cycles (Altun and Ugur-Altun, 2007). Based on the timing of ingestion, oral melatonin can advance or delay circadian systems and is currently believed to be the best pharmacological treatment for jet lag (Lewy et al., 1992). However, melatonin’s mechanism of action is poorly understood and includes side effects such as lowered body temperature (Cagnacci et al., 1992). Endogenous melatonin production is highly sensitive to light with levels of melatonin dropping during daytime hours (Brainard et al., 2001). Short-wavelength blue light is particularly effective at suppressing melatonin levels. Thus, late-night exposure to electronic displays such as laptops and tablets, which emit blue-shifted light, can lead to circadian disruption. Conversely, numerous studies have shown that the exposure of individuals to appropriately timed light can function as an effective therapy for circadian disorders (Dodson and Zee, 2010).

Since circadian systems are exquisitely sensitive to photic information, light therapy can be a very effective, non-invasive treatment for circadian disorders. Light therapies can be generally classified as dark therapy or bright light therapy. Dark therapy involves the removal of short-wavelength light at specific times of the day to prevent circadian disruption by activation of the blue-light sensitive photoreceptor melanopsin. In addition to lifestyle recommendations of deliberately avoiding evening light exposure, patients have also been prescribed amber-tinted lenses to selectively block blue-shifted light such as that emitted by electronic displays (Kayumov et al., 2005; Sasseville et al., 2006). On the other end of the spectrum, numerous studies have shown that bright light therapy (~2,500-10,000 lux) can also be used to treat circadian disorders (Boivin et al., 1996; Fetveit et al., 2003; Rosenthal et al., 1990).

Timed exposure to bright light can be used to advance, delay or reset circadian rhythms (Czeisler et al., 1981; Dodson and Zee, 2010; Morgenthaler et al., 2007). Light sources used for bright light therapy include programmable light boxes, natural sunlight and wearable therapy devices. Exposure to bright light has also been shown to improve acute alertness and to enable more rapid adaptation to shift work schedules (Boulos et al., 1995; Desan et al., 2007). Bright light therapies have shown great promise in treating circadian disruptions in conditions such as Huntington's disease and cancer (Cuesta et al., 2014; Neikrug et al., 2012). However, current treatments for circadian disorders are usually most effective when using a multimodal approach of timed light exposure, pharmacological agents and behavioral therapy (Morgenthaler et al., 2007; Okawa et al., 1998; Zhu and Zee, 2012).

1.5 Conclusions

In summary, circadian systems consist of complex input and output pathways that greatly impact numerous physiological events and behaviors. As such, disruption of circadian systems by altered internal clockwork or exogenous cues can lead to severe pathological consequences. Circadian disruptions have been linked to numerous conditions including diabetes, obesity, heart disease, metabolic syndrome, neurodegenerative conditions and cancer. However, is still unclear whether circadian disruptions are a source and/or consequence of these affiliated disorders. Further research is needed to understand the role circadian disruptions play in exacerbating these disorders.

Light appears to be the most powerful environmental cue and can influence many aspects of circadian systems. Appropriately-timed photic input is critical for natural entrainment and also holds great promise for light therapy treatments of circadian disorders. Accordingly, a better understanding of how photic information is integrated could allow us to deliberately induce, harness, and amplify light-driven circadian responses to ameliorate circadian disorders. In the following chapters, this thesis will discuss our work on novel aspects of photic integration at the molecular, cell-autonomous, whole circuit and whole organismal level in the *Drosophila* circadian system. The current thesis will also discuss the functions and dynamics of cell-oscillators comprising heterogeneous circadian circuits in the context of free-running rhythms, classical jet lag and social jet lag. Due to the many organizational similarities of *Drosophila* and mammalian circadian molecular and neural circuits, these patterns of circadian responses may be broadly observed and applicable to humans.

1.6 Figures

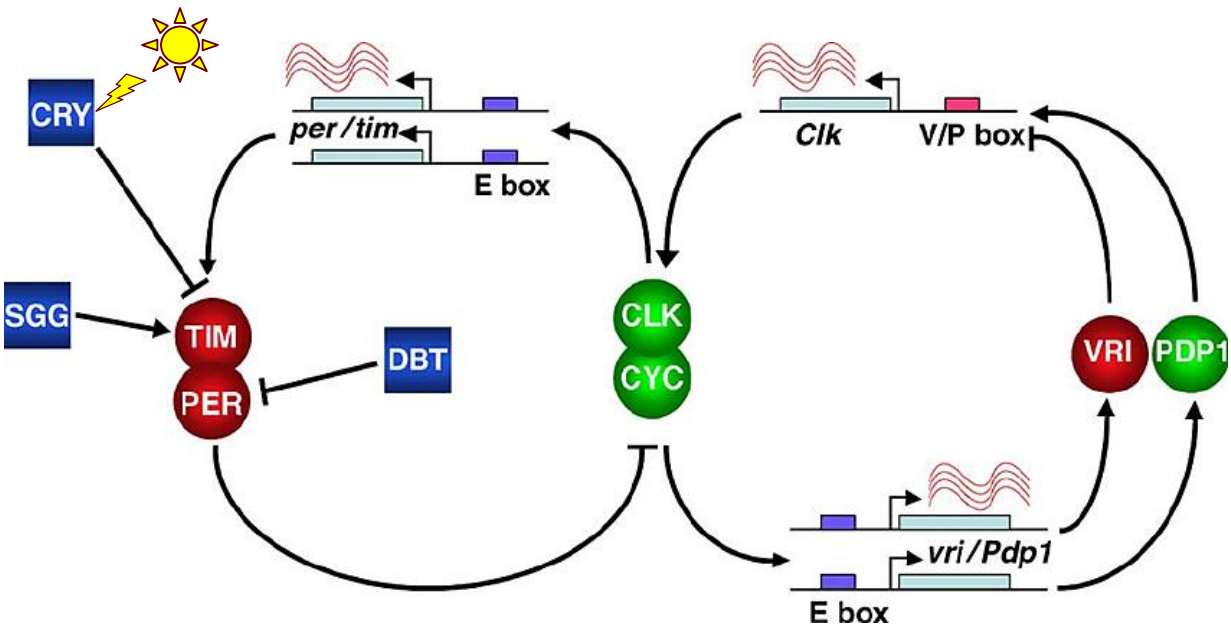

Figure 1.1 Simplified model of feedback loops found in molecular clocks. Molecular clocks in *Drosophila melanogaster* are composed of two transcriptional-translational feedback loops with positive and negative cycling transcription factors. Molecular clocks endogenously oscillate with a ~24 period but can be entrained by environmental cues, light being the most powerful (adapted from Collins & Blau. 2007).

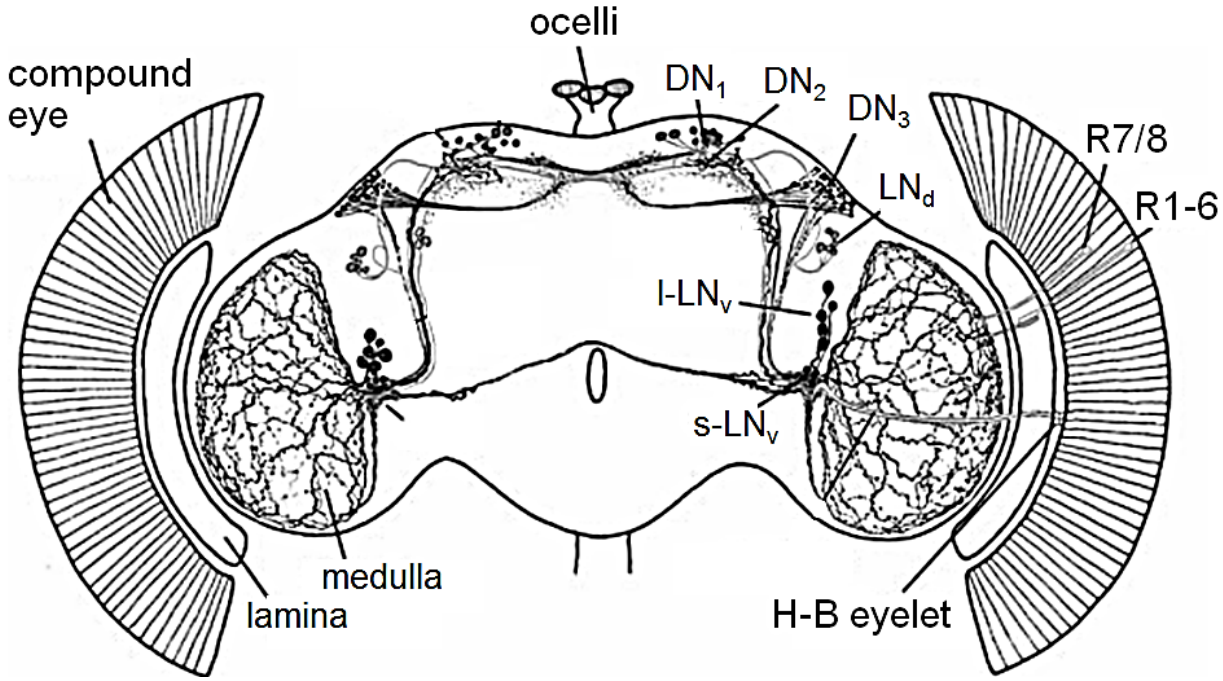

Figure 1.2 Schematic of circadian neural circuit in the adult *Drosophila* brain. Putative arborization patterns and cell locations are shown in a frontal view of the brain for the classical circadian neuron subgroups: s-LNv, small lateral ventral neuron; l-LNv, large LNv; LNd, dorsolateral neuron; DN_{1-3}, dorsal neuron subset 1-3; R1–8, photoreceptor cells of the compound eye (adapted from Helfrich-Forster et al. 2007).

CHAPTER 2

Light Evokes Rapid Circadian Network Oscillator Desynchrony Followed by Gradual Phase Retuning of Synchrony

(Roberts, Leise, Noguchi, Galschiodt, Houl, Welsh, Holmes)

Abstract

Circadian neural circuits generate near 24 hr physiological rhythms that can be entrained by light to coordinate animal physiology with daily solar cycles. To examine how a circadian circuit reorganizes its activity in response to light, we imaged period (per) clock gene cycling for up to 6 days at single neuron resolution in whole brain explant cultures prepared from per-luciferase transgenic flies. We compared cultures subjected to a phase-advancing light pulse (LP) to cultures maintained in constant darkness (DD). In DD, individual neuronal oscillators in all circadian subgroups are initially well synchronized, then show monotonic decrease in oscillator rhythm amplitude and synchrony with time. The s-LNvs and LNds exhibit this decrease at a slower relative rate. In contrast, the LP evokes a rapid loss of oscillator synchrony between and within most circadian neuronal subgroups followed by gradual phase retuning of whole circuit oscillator synchrony. The LNds maintain high rhythmic amplitude and synchrony following the LP along with the most rapid coherent phase advance. Immunocytochemical analysis of PER show these dynamics in DD and LP are recapitulated in vivo. Anatomically distinct circadian neuronal subgroups vary in their response to the LP, showing differences in the degree and kinetics of their loss, recovery and/or strengthening of synchrony and rhythmicity. Transient desynchrony

appears to be an integral feature of light response of the *Drosophila* multicellular circadian clock. Individual oscillators in different neuronal subgroups of the circadian circuit show distinct kinetic signatures of light response and phase retuning.

2.1 Introduction

Most organisms schedule their daily activity and metabolism using a circadian clock mechanism. Living organisms make daily adjustments to synchronize their circadian clock to seasonal changes of the 24-hr solar cycle by entrainment to environmental cues; light being the most powerful cue for most animals (Pittendrigh and Daan, 1976; Tauber and Kyriacou, 2001). The process of entrainment is most apparent when we travel rapidly across multiple time zones, i.e. jetlag. The brain circadian neural network of mammals is located in the suprachiasmatic nucleus (SCN), whereas the fruit fly *Drosophila melanogaster* and other insects have an anatomically distributed brain circadian neural circuit (Kaneko and Hall, 2000; Kaneko et al., 1997). Studies have revealed many similarities in the circadian biology of mammalian and *Drosophila* models, from molecular to circuit levels (Welsh et al., 2010).

Longstanding efforts have been made to understand how clock cycling of individual neuronal oscillators distributed throughout circadian circuits maps to behaviors such as entrainment. Widely used immunocytochemical (ICC) analyses of rhythmic molecular clock components in circadian circuits are limited because they cannot capture individual oscillator longitudinal activity or dynamic relationships between oscillators in a single brain. The cross-sectional ICC approach takes individual “snap shots” of clock markers and requires averaging over many brains to construct an approximate time course. To circumvent these problems, longitudinal measurements of SCN oscillators have been

made by multi-electrode recordings, or imaging of bioluminescent or fluorescent reporters of clock gene expression (Quintero et al., 2003; Schaap et al., 2003; Yamaguchi et al., 2003). These studies reveal that individual SCN oscillators express a surprisingly large range of periods and phases. Further analysis of SCN oscillators has revealed how small molecule and peptide transmitters coordinate subsets of oscillators (Welsh et al., 2010).

But the fundamental question of how a circadian network alters its distributed activity in response to a light entrainment signal in real time remains enigmatic. For the SCN, this is largely due to the technical difficulty of physiologically activating the melanopsin-mediated light input pathway in SCN slice cultures. Measuring the circuit-wide response to light is feasible in *Drosophila* because the entire fly brain can be cultured (Ayaz et al., 2008) and approximately half the neurons in the fly circadian circuit autonomously express the blue light receptor Cryptochrome (CRY) (Benito et al., 2008; Yoshii et al., 2008), which provides the primary mechanism for light resetting the circadian clock and acute light evoked increases in firing rate in circadian neurons (Fogle et al., 2011; Helfrich-Förster et al., 2001). To address how light reorganizes the activity of the *Drosophila* circadian circuit mapped at single cell resolution, we developed a culture system for *Drosophila* adult whole brains (Ayaz et al., 2008), then refined and combined high resolution imaging of circuit-wide single oscillators (Sellix et al., 2010; Yoshii et al., 2009) with sophisticated mathematical analytical tools (Cohen et al., 2012; Leise et al., 2012). For *in vivo* comparison, we performed anti-PER ICC using the same light/dark protocols used for whole brain imaging. Although ICC has limited temporal resolution for single oscillator kinetics relative to bioluminescence recordings, we can test predictions of neuronal subgroup patterns of dynamic PER activity in response to light.

2.2 Materials and Methods

XLG-Per-Luc transgenic flies

Transgenic *XLG-Per-Luc* flies were generously provided by Dr. Ralf Stanewsky (University College London, UK). The *XLG-Per-Luc* flies express the XLG-*luc* construct which consists of most of the coding sequence of the *period* gene, excluding the last ten C-terminal amino acids, fused to the *luciferase* cDNA as previously described (Veleri et al., 2003). Expression of this fusion protein allows for measurement of PER activity as reported by LUC luminescence from cultured brains using a low light camera system (more below). A study using the BG-luc fusion protein, which shares the same 5'-upstream regulatory region of period as XLG-Per-Luc, showed that most of the bioluminescence signal in whole animal imaging is emitted from the abdomen and the eyes rather than the brain, and lacks single cell resolution (Stanewsky et al., 1997).

Culturing of adult *Drosophila* whole-brain explants

Fly brain explants were dissected and cultured using a modified version of a procedure previously described (Ayaz et al., 2008). Prior to dissections, flies were entrained under standard 12 hr: 12 hr LD cycles at 25^{o}C and 50% humidity for at least 3 days. Under sterile conditions, Millicell-CM 0.4 µm culture plate inserts (Fisher) were placed in 35 mm Falcon culture dishes containing sterile PBS. The surfaces of culture plate inserts were coated with laminin and poly-D-lysine hydrobromide (BD Biosciences, NJ), each at 5 µg/cm2. Coated inserts were equilibrated for 1 hour at room temperature before aspirating excess coating, and then incubated at 37^{o}C overnight followed by extensive rinsing with sterile PBS the next day. Coated inserts were then stored at 4^{o}C for up to 3 weeks. Prior to dissection, adult male flies were anesthetized by placement

on ice, and then washed in 70% ethanol for several seconds. Anesthetized flies were transferred to a sterile petri dish and dissected in ice-cold Schneider's *Drosophila* medium (Invitrogen, CA) containing 1% Antibiotic Antimycotic solution [10,000 U/ml penicillin, 10 mg/ml streptomycin, and 25 µg/ml amphotericin (Sigma, MO)]. Brains were carefully and cleanly dissected, removing cuticles and trachea but keeping optic lobes attached to the brain. The brains were then rinsed three times with a modified version of a previously described culture medium (Ayaz et al., 2008): Schneider's *Drosophila* Medium containing 1% Antibiotic Antimycotic solution (see above), 10% fetal bovine serum, and 10 µg/ml insulin. For each experiment (3 experiments each for DD and LP condition), four brains were dissected and placed on a single insert, with ventral sides up and the brains in close proximity to allow for simultaneous imaging. Under sterile conditions, 1.2 ml of culture medium was filtered using Millex 33 mm sterile filter units into a fresh, sterile 35 mm petri dish. 1 mM luciferin (BioSynth) was filtered into the culture medium within 30 minutes of the start of recordings. A culture insert with 4 brains was transferred to this dish, which was then covered with a 40 mm circular coverslip (Thermo Scientific 40CIR1, Waltham, MA) and sealed with vacuum grease to prevent evaporation and contamination. Brain explants were maintained in the same culture medium throughout the recordings, as medium changes perturb PER activity (data not shown, see also (Morioka et al., 2012).

Bioluminescence imaging

Bioluminescence imaging was performed using a modified version of a protocol previously described (Noguchi et al., 2013). The cultured brains were mounted on the stage of an inverted microscope (Olympus IX71, Tokyo, Japan) set on an anti-vibration

table (TMC, Peabody, MA) in a dark room isolated by black curtains with temperature maintained at 25^{o}C. The microscope focus was adjusted using bright-field illumination before turning off all lights and covering the brains with a small black Lucite box. Black plastic sheets (Thorlabs BK5, Newton, NJ) were then draped over the entire microscope to minimize stray light exposure. Cycling luminescence from the cultured whole brains was collected by an Olympus 4x XLFLUOR objective (NA 0.28) and transmitted directly to a cooled charge-coupled-device (CCD) camera (Series 800, Spectral Instruments) mounted on the bottom port of the microscope. Samples were obtained at 30 minute intervals with 29.5-minute exposure duration, no binning, and 50 KHz readout for ≥ 6 days of recording at single-cell resolution. Images were then transferred to a computer using SI Image SGL D software (Spectral Instruments) before using MetaMorph software (Molecular Devices, Sunnyvale, CA) and custom MATLAB scripts to measure bioluminescence with single cell resolution. In experiments analyzing light response, brains were exposed to a white light pulse at CT 22 of the second day in DD by turning on the microscope bright field light (Olympus, TH4-100) to an intensity of 12.57 W/m2 (2,000 lux) for 15 minutes. Only experiments with all four brains still healthy, intact, contamination-free, adherent to the substrate and exhibiting bioluminescence for ≥ 6 days were considered for analysis. The total number of cells analyzed in DD and LP conditions was 122 and 126 cells, respectively

Processing of bioluminescence images

Processing of bioluminescence images was performed as described previously (Noguchi et al., 2013). Briefly, cosmic ray artifacts were removed in MetaMorph by using a running minimum algorithm, i.e. a new image was constructed from each pair of

sequential images using the minimum value of each pixel from the two images. A stack of images for each experiment was then generated and analyzed by measuring average luminescence intensity over time within regions of interest (ROIs) that were manually defined. ROIs were defined as borders of single neurons which could be clearly distinguished, isolated, anatomically identified, and exhibited bioluminescence cycling throughout the recordings. The positions of ROIs were easily tracked from frame to frame as needed to accommodate cell movement due to flattening of the brains over time with ROI sizes kept the same throughout the recording. ROIs that could not be easily distinguished and tracked were excluded from analysis. ROIs were categorized into canonical cell groups (colored-coded: red = s-LNv, yellow = l-LNv, orange = LNd, blue = DN1, green = DN3) based on classically recognized anatomical positions. Single neurons of neuronal subgroups actually became easier to identify over time as they spread out due to brain explants flattening. Raw luminescence data were then transferred to Microsoft Excel for additional processing. Single-cell luminescence was adjusted for background noise and converted to photons per minute. LumiCycle software (Dr. David Ferster, Actimetrics, IL) was used to generate clearly defined circadian peaks and troughs by subtracting linear trend (polynomial order = 0) and 13-point smoothing. For quantification of circadian parameters, smoothed data were analyzed with custom MATLAB scripts, with the first 10 hours of data excluded due to high intensities and variances in initial luminescence following dissection and addition of luciferin. Real-time bioluminescence data was analyzed for 6 day recordings.

Quantification of period activity dynamics

Custom MATLAB scripts (version 8.2) incorporating the Signal Processing and Statistics Toolboxes (MathWorks, MA) were used to analyze real-time bioluminescence data for quantification of circadian parameters including: order parameter, goodness-of-fit, period, and amplitude. The scripts incorporated the WMTSA Wavelet Toolkit (C. Cornish, U. of Washington, WA) for application of a discrete wavelet transform to all time series. The wavelet transform served to remove high frequency noise and detrend the time series, providing clearer measures of circadian fluctuations and more accurate sine-fit estimates of rhythmic parameters (Leise and Harrington, 2011). The single-cell time series were also normalized with respect to variance for computation of the order parameter R, but were not altered for calculation of other circadian parameters. Boundary conditions for the wavelet filtering were carefully adjusted to minimize edge effects. Sliding 2-day windows were used to quantify properties of oscillations over time. To quantify changes in synchrony over time, custom MATLAB scripts calculated an order parameter 'R,' defined as (Harmar et al., 2002)

$$R = \frac{\langle X^2 \rangle - \langle X \rangle^2}{\frac{1}{N}\sum_{k=1}^{N}\left(\langle {X_k}^2 \rangle - \langle X_k \rangle^2\right)}$$

where angle brackets denote time average and $\frac{1}{N}\sum_{k=1}^{N} X_k$. If the phase, period and waveform of all N cells are in perfect synchrony then R=1, whereas uniform distribution would give R=0. Custom MATLAB scripts incorporating bootstrapping was used to compute significance in R estimates. In the bootstrapping procedure, we resampled with replacement from each data set, with the size of each bootstrap sample equal to the number of cells being sampled in each data set. This procedure was repeated 10,000

times to estimate 95% and 99% confidence intervals for the difference in R (RLP – RDD¬) between cells in constant darkness (DD) and cells exposed to a light pulse (LP), with the null hypothesis being no difference. For comparison of inter-subgroup kinetics after LP, changes in synchrony over time were considered significant if they were outside the bounds of the stricter 99% confidence interval. Graphs of DD and LP values of R plotted separately were also generated for qualitative comparisons.

Custom MATLAB scripts were used for discrete wavelet transform in combination with sine-fit-estimates of circadian parameters including: (1) the goodness-of-sine-fit, (2) the proportion of reliably rhythmic cells, (3) period and (4) amplitude. These parameters were measured with 2-day sliding windows to examine changes over time and in response to a light pulse. The goodness-of-fit was used as a measure of rhythmicity and was determined as the percentage of total variance accounted for by a fitted sine wave as described previously (Veleri et al., 2003). The statistical significance of goodness-of-fit was determined by one-way ANOVA and Tukey post hoc test. Cells were considered to have reliably measurable circadian rhythms if their goodness-of-sine-fit measures were greater than a threshold value of 0.82. The criterion of 0.82 was determined by graphing all the time series against the best-fit sine curves and noting that sine-fits above 0.82 produced reliable estimates of period and amplitude. The 0.82 goodness-of-sine fit threshold was incorporated in custom MATLAB scripts to calculate changes in the proportion of reliably rhythmic cells (‘P’) over time and in response to the light pulse. The same 0.82 criterion was applied across all cell types and light conditions.

Statistically significant changes in the proportion of reliably rhythmic cells over time were determined using bootstrapping (as described above). 95% and 99% confidence

intervals were estimated by generating 10,000 bootstrap samples for each time series with the size of each bootstrap sample equivalent to the number of cells in each time series. For analysis of inter-subgroup kinetics after LP, changes in number of reliably rhythmic neurons over time were considered significant if they were outside the bounds of the stricter 99% confidence interval. Custom MATLAB scripts incorporating direct sine-fitting were used to calculate periods and amplitudes for cells meeting the 0.82 criterion of reliably measurable rhythms (Cohen et al., 2012). Statistically significant changes in periods and amplitudes were determined by one-way ANOVA, Tukey post hoc test.

Animated model comparing inter-subgroup kinetics of phase retuning

A custom MATLAB script was used to generate an animation comparing inter-subgroup kinetics of changes in phase coherence after a light pulse. A color-coded heat map representing values of R for each neuronal subgroup was mapped onto a schematic model of an adult *Drosophila* brain to allow for visualization of spatiotemporal dynamics. The model was divided into two hemispheres to allow for comparisons of neuronal subgroups maintained in DD (left side) and neuronal subgroups exposed to a light pulse (right side). The background is color-coded to provide the same general frames of reference described above.

Validation of sine-fit estimates

Custom MATLAB scripts for BPENS (Bayesian parameter estimation for noise sinusoid) calculations, employing a previously described procedure (Cohen et al., 2012), were used to quantify confidence in our criterion for reliably rhythmic cells and our sine-fit estimates of periods based on measures of uncertainty in the form of 95% and 99%

credible intervals (the Bayesian equivalent of confidence intervals). The direct sine-fit measure and the Bayesian frequency estimation method generate period estimates with correlation ρ=0.98 and p<0.0001 (688 contributions from the DD cells and 654 from the LP cells, combining across cell types and windows). The Bayesian frequency estimation of the proportion of cells with reliably measurable circadian rhythms and the goodness-of-sine-fit criterion share a correlation ρ=0.58 and p<0.0001 (combined again across cell types and windows). Custom MATLAB scripts also generated Bayesian plots for proportion of reliably rhythmic neurons for 'all cells' (from all neuronal subgroups) and individual neuronal subgroups (Figure S2.11). Qualitative comparison of these plots to sine-fit estimates of proportion of reliably rhythmic neurons confirms the same general trend of transient loss then delayed increase in proportion following a light pulse. It can be seen that the distinct patterns of light response for each subgroup are also seen by both Bayesian frequency and sine-fit estimates of the proportion of reliably rhythmic cells indicating that these trends are sufficiently reliably and consistent. Furthermore, tests were run with surrogate data from (Cohen et al., 2012) using 2-day windows to check the accuracy of the wavelet-detrending + sine-fit method we are using. The resulting period estimates had mean absolute error 1.6% with a standard deviation of 1.2%. The results of this test, in combination with the correlation of sine-fit and BPENS measures, confirm that our sine-fit measures with discrete wavelet transform using 2-day sliding windows, though not as ideal as longer recordings would allow, is sufficiently reliably and consistent for our analysis.

Qualitative comparisons of inter-subgroup per kinetics and light responses

Single-cell bioluminescence time series records were plotted to convey qualitatively distinct inter-subgroup kinetics and responses to light entrainment. Detrended records are shown for visualization of amplitude changes over time and to allow smooth continuity of the traces throughout the sliding 2-day windows used for quantitative analysis. Color-coded backgrounds were provided for general comparison of inter-subgroup kinetics. The backgrounds were color-coded to indicate three general time frames of significant trends in light response as measured by phase coherence R values. The boundaries for these time frames were based on the time points at which the differences in R between corresponding DD and LP cells (RLP – RDD) crossed the 99% confidence interval. A blue-gray background denotes the time frame in which neurons have not been exposed to a light pulse, yellow denotes the time of significant desynchrony following light entrainment, and green denotes the time of significant phase retuning of cell synchrony. These general frames of reference were used to compare inter-subgroup kinetics for all circadian measures across all cell types. Plots of values of R for oscillators in DD versus LP were also plotted separated for qualitative comparison of trends in light response.

Immunocytochemistry

Immunostaining of whole brains from adult male flies was performed using a modified version of a previously described protocol (Ayaz et al., 2008). Brains used in Figure 2.1 for spatial mapping of PER staining were fixed in 4% PFA at ZT 23 and 11. See description below for fixation times used for ‘immunocytochemical analysis of *in vivo* light response by intact flies. Primary antibodies applied and incubated for ~48 hours at

4ºC included: anti-Per (rabbit, 1:10,000) and anti-Pdf (mouse, 1:10,000). Fluorescent secondary antibodies incubated with the brain explants overnight at 4ºC were: Alexa 488 (anti-rabbit, 1:3,000) and Alexa 594 (anti-mouse, 1:500). Brains were stored at 4ºC before obtaining images with a Zeiss LSM700 confocal microscope.

Immunocytochemical analysis of *in vivo* light response by intact flies

Adult male flies are entrained for ≥3 days under standard 12 hr/12 hr LD schedule before being placed in darkness for the rest of the experiment. Control flies (hereafter referred to as 'DD flies') were maintained in constant darkness (DD) for up to 4 days. PER staining for certain neuronal subgroups after four days became too dim to reliably measure. Adult *Drosophila* denoted as 'LP flies' were exposed to a 15 min 12.57 W/m2 (2,000 lux) white light pulse from a Nikon halogen lamp (Fostec 150W fiber optic light power supply) at CT 22 of the second day in DD. Whole brains were dissected in ≤5 minutes in chilled PBS under dim orange light in an otherwise completely dark room to prevent light-triggered degradation of the Period (PER) protein. Flies maintained in DD were fixed at CT 22 on DD day 2 and CT 0 on DD days 3 and 4. Flies exposed to the phase advance white light pulse were fixed 2, 24, and 48 hours after exposure to the light pulse at CT 2 for the first time point and CT 0 for the last two time points. Note that the CT was adjusted for LP flies such that CT 0 corresponds with the time at which the light pulse was administered. 3-4 fly whole brains were dissected, fixed and stained for PER and PDF for each group and time point using the protocol described above. Images of single neurons were obtained using a Zeiss LSM 700 confocal microscope with a 63x oil immersion objective (Plan-Apochromat 63x/1.4 NA). For quantitative comparison of PER staining fluorescence intensity, regions of interest (ROIs) for all DD

and LP neuronal subgroups at every time point were imaged with the same standardized laser intensities and microscope settings ('std gain'; 488 nm laser intensity: 1.0%; gain: 740). For qualitative visualization of dimmer neuronal subgroups at later time points in DD, the same ROIs were subsequently imaged with higher gain settings ('high gain') optimized to allow the brightest and clearest visualization of individual neurons. Quantitative analysis of PER staining average fluorescence intensity was performed using the using the software Volocity (PerkinElmer). For dim images, ROIs were manually drawn using 'high gain' images with average fluorescence intensities obtained from corresponding 'standard gain' images. Statistical comparison of the average PER staining intensity of neuronal subgroups in DD and LP conditions at each time point was performed using the Student's t-test (Sigmaplot version 11) with the null hypothesis that there is no significant difference in fluorescence intensity. The experiments were performed for both w1118 and XLG-Per-Luc flies using the same protocols and standardized intensity settings.

2.3 Results

2.3.1 Imaging the *Drosophila* circadian neural circuit in organotypically cultured whole adult brains prepared from XLG-Per-Luc flies.

The *Drosophila* circadian circuit consists of at least six neuronal subgroups (Ayaz et al., 2008) which can be further subdivided by neurochemical or promoter fragment expression markers (Collins et al., 2012; Hamasaka et al., 2007; Johard et al., 2009; Zhang and Kay, 2010; Zhang et al., 2010b). These include the large and small ventral lateral neurons (l-LNv and s-LNv), the dorsal lateral neurons (LNd), and three subgroups of dorsal neurons (DN 1, 2 and 3) (Figure S2.1A, DN2s not shown). The *Drosophila*

circadian pacemaker neurons are functionally defined as cells that rhythmically express the clock proteins Period (PER) and Timeless (TIM).

Transgenic *XLG-luc (XLG-Per-Luc)* flies were used in this study because the 13.2 kb *per* gene promoter fragment drives expression of a PER-luciferase fusion protein in nearly all neurons of the circadian circuit. Normal behavioral rhythmicity is nearly restored when *XLG-Per-Luc* flies are crossed with the non-rhythmic *per* null mutant line per^{01} (Veleri et al., 2003). The spatiotemporal pattern of expression and degradation of the XLG-PER-LUC fusion protein resemble the native PER protein (Movie 2.1, Figure 2.1-6) (Veleri et al., 2003). Using a high quantum efficiency CCD camera, the anatomically defined major circadian neuron subgroups can be visualized by bioluminescence imaging of whole adult brains of *XLG-Per-Luc* flies (Figure S2.1C). Brains were maintained using a long-term organotypic culture protocol we developed in collaboration with the Hassan lab (Ayaz et al., 2008).

2.3.2 A phase-advancing light pulse induces acute desynchrony of most oscillators throughout the *Drosophila* circadian circuit followed by gradual phase retuning of synchrony.

To determine the baseline circuit-wide dynamic relationship between individual oscillators, we imaged whole adult brains of *XLG-Per-Luc* flies (previously entrained under 12:12h LD, (Veleri et al., 2003)) to measure single neuron oscillations in constant darkness (DD) for six days in organotypic culture (Ayaz et al., 2008). Time series analyses of single neuron bioluminescence oscillations for ‘all DD cells’ (from all circadian neuronal subgroups, n = 122) in continuous 6 day DD recordings show initially synchronized oscillators throughout the circadian circuit that gradually decrease their oscillator

amplitude and desynchronize with time, as shown by superimposed single-cell oscillator traces (Figure 2.1A, upper panel), averaged record (Figure 2.1B, black trace), and goodness-of-sine-fit as a measure of rhythmicity (Figure 2.1D, black trace). Average oscillator period is initially close to 24h for the first several days in DD, then decreases (Figure 2.1F, black trace). Oscillator amplitude decreases for all cells in DD, the s-LNvs dampen at a slower rate (Figure 2.1G (black trace), in agreement with whole animal and whole brain bioluminescence measurements of *XLG-Per-Luc* flies (Veleri et al., 2003).

Next, we imaged the circadian network response in adult cultured whole brains prepared from *XLG-Per-Luc* flies exposed *ex vivo* to a phase-advancing white light pulse (LP) at CT 22 of the second day of DD (6 days total recording). We compared the circadian circuit dynamics for the LP response of individual oscillators relative to control baseline measurements for corresponding oscillators in DD at matched time points. In contrast to DD conditions, the LP evokes rapid desynchrony of oscillator cycling followed by gradual recovery then strengthening of synchrony 1-2 days after the LP that can be seen qualitatively in superimposed individual oscillator traces (Figure 2.1A, lower panel) and in the averaged record (Figure 2.1B, red trace). We call the entire dynamic process of gradual emergence of phase-shifted, high amplitude, and tighter synchrony oscillations following transient phase desynchrony after exposure to the phase advancing LP “phase retuning”. The qualitatively similar phenomenon of transient phase desynchrony in SCN slices in response to bath applied vasoactive intestinal peptide (VIP) has been referred to as “phase tumbling” (An et al., 2013). Examination of the detrended traces and the averaged traces for LP cells in Figure S2.2 (bottom) clearly demonstrates that cells exposed to the LP exhibit greater synchrony and phase-shifted rhythmicity at the end of

the recording relative to cells in DD. To quantify order parameter R as a measure of the dynamic response of oscillator synchrony, we calculated values of R for a sequence of 2-day sliding windows using the definition of order parameter in (Gonze et al., 2005). R can range from 0 to 1 with higher values indicating similarity in phase, period and waveform. $R_{LP} – R_{DD}$ was then calculated for all matched time points in the LP and DD datasets. Following the light pulse, we measure significantly negative values ($R_{LP} – R_{DD} < 0$) as 'desynchrony', subsequent values with no significant difference between the conditions ($R_{LP} – R_{DD} \approx 0$) as 'recovery,' and significantly positive values ($R_{LP} – R_{DD} > 0$) at the end of the recordings as 'strengthened.' Overall analysis of 'all LP cells' (i.e. from all neuronal subgroups, n = 126) shows rapid and significant oscillator desynchrony relative to DD immediately following the LP (Figure 2.1C, yellow shaded area) which slowly phase retunes, with significantly strengthened oscillator synchrony by 2-3 days following the LP (Figure 2.1C, green shaded area). Analysis of goodness-of-sine-fit (g.o.f.) as a measure of rhythmicity over 2-day sliding windows yields a similar pattern of results: acute LP-reduced g.o.f. (Figure 2.1D, yellow shaded area) followed by gradual strengthening of oscillator g.o.f. several days later (Figure 2.1D, green shaded area). To confirm these patterns, we measured dynamic changes in the proportion of reliably rhythmic cells ($P_{LP} – P_{DD}$). The same trends of significant decreases in response to the LP relative to DD followed by recovery over several days are shown (Fig 2.1E). The periods of DD and LP cells are comparable and relatively stable with the exception of two later time points (Figure 2.1F). The overall amplitude of single-cell oscillators declines monotonically and does not differ significantly between LP and DD oscillators at time points following the

light pulse (Figure 2.1G). Thus, changes in oscillator synchrony and phase form the major qualitative and quantitative response to light.

2.3.3 Neuronal subgroups exhibit qualitatively apparent differences in dynamics of PER activity both in DD and in response to a phase-advancing light pulse.

We then longitudinally measured PER expression rhythms in single neurons from defined circadian neuronal subgroups in bioluminescence images collected at 30 min intervals for six days in DD from cultured whole adult brains of *XLG-Per-Luc* flies. The s-LNvs show the most robust rhythms and greatest inter-neuronal synchrony in DD compared with other subgroups (Figure 2.2A, top). The l-LNv also exhibit relatively large amplitude and coherent rhythms in DD, though to a lesser extent than the s-LNvs (Figure 2.2A, top). Previous reports on l-LNv oscillations dampening in DD yielded different conclusions. Some report l-LNv oscillations dampening within the first two days in DD (Shafer et al., 2002; Yang and Sehgal, 2001), while other studies report measurable l-LNv cycling of *per* mRNA after 9 days in DD (Peng et al., 2003) and protein levels (Klarsfeld et al., 2004) for at least 2.5 days in DD. We have reported considerably longer PER cycling (albeit out of phase) and phasic electrical circadian rhythmicity in the l-LNv after 15 days of DD by calibrating data collection time points to behavioral landmarks for each fly tested (Sheeba et al., 2008a; Sheeba et al., 2007). Thus our present bioluminescence results support the findings in (Klarsfeld et al., 2004; Peng et al., 2003; Sheeba et al., 2008a). The LNds, DN1s and DN3s show somewhat less robust rhythms with patterns of dampening amplitude and gradual loss of coherent rhythms over the six days of DD (Figure 2.2A, top).

Single neuron oscillators from the defined circadian neuronal subgroups exposed to a LP show strikingly different dynamics compared to DD (Figure 2.2A, bottom). The s-LNv oscillations initially show coherent, high rhythm amplitudes similar to the DD condition, then exhibit marked desynchrony immediately after the LP, followed by a gradual recovery that phase retunes to shifted synchrony after several days (Fig 2A, bottom). In contrast, the l-LNvs exhibit immediate dampening of amplitude and weak rhythmicity following the LP that does not recover (Figure 2.2A, bottom). Of all the circadian neuronal subgroups measured, the l-LNvs appear to have the most labile and immediate response to the LP, consistent with previous findings as being light sensitive (Shang et al., 2008; Sheeba et al., 2008a; Sheeba et al., 2007). In contrast, the LNds appear to maintain surprisingly high amplitude rhythms and coherence even after the LP. The DN1 and DN3 oscillators both show desynchronization, followed by recovery of synchrony several days after the LP (Figure 2.2A). The averaged traces for each circadian neuronal subgroup (Figure 2.2B) sharpen the qualitative assessments of single-cell traces for each condition. Averaged LNd oscillations show a remarkable immediate shift to an earlier phase in response to the phase-advancing LP without loss of amplitude relative to the DD condition.

2.3.4 Different circadian neuronal subgroups exhibit quantitatively distinct kinetic signatures for both DD And LP oscillator patterns.

We analyzed each of the subgroups for their single-cell order parameters, g.o.f., and proportion of reliably rhythmic cells; comparing LP relative to DD. As a measure of synchrony over time among cells within a subgroup, the order parameter R was calculated for a sequence of 2-day sliding windows (Figure 2.3A). The s-LNvs show a

significant loss of oscillator synchrony in response to the LP followed by gradual recovery ($R_{LP} - R_{DD} \approx 0$) several days after the LP. The DN3 also show a significant loss of synchrony in response to the LP, but with a slower onset and more rapid recovery relative to the s-LNvs. In contrast to the s-LNv, no significant differences in R are seen for light-evoked l-LNvs relative to the DD baseline. The LNds and DN1s show significant increases in R coinciding with s-LNv recovery several days after the LP with the LNds exhibiting the earliest and greatest strengthening of synchrony relative to DD baseline values.

Analysis of g.o.f. as an independent measure of rhythmicity for each neuronal subgroup supports the conclusions as determined by changes in the order parameter R in response to the LP (Figure 2.3B). The s-LNvs, LNds, and l-LNvs show significant decreases in g.o.f in response to the LP ranked as listed. The LNds and DN1s exhibit a significant but delayed increase in g.o.f several days after the LP. The DN3 exhibit a general trend of transient reduction followed by an increase in g.o.f though without reaching a significant difference between LP and DD. For proportion of reliably rhythmic cells (Figure 2.3C), the s-LNvs show significant decreases initially following the LP, as do the l-LNvs to a lesser extent, while the LNd, DN1 and DN3 subgroups show delayed significant increases that correspond to their phase retuning of synchrony. Thus, loss and subsequent recovery and/or strengthening of synchrony are quantifiable features of the circadian network's response to phase advancing light that vary in a stereotypic manner between circadian neuron subgroups.

We also employed BPENS (Bayesian parameter estimation for noisy sinusoids) calculations over 2-day sliding windows as previously described (Cohen et al., 2012) to quantify confidence in our criterion for reliably rhythmic cells and sine-fit estimates of

periods (Figure S2.3). BPENS calculations confirmed the same distinct trends of light response for 'all cells' and for each neuronal subgroup (see Supplemental Information for details). Additionally, we ran a test using surrogate data from (Cohen et al., 2012) using 2-day windows to further validate the accuracy of the sine-fit measures with wavelet-detrending method that we employed. The resulting period estimates had a mean absolute error of 1.6% with a standard deviation of 1.2%. This test, along with the BPENS correlation measures, confirms that the quantified trends in light response are consistent and reliable.

2.3.5 Circadian neuronal subgroups respond to the LP with temporally distinct kinetic signatures of transient desynchrony followed by phase retuned synchrony.

Under DD conditions, the different circadian neuronal subgroups are initially synchronous, but gradually decrease their inter-group synchrony over six days as seen in the aligned averaged *per* gene driven bioluminescence signals (Figure 2.4A, top panel). Surprisingly, given the proposed role of the s-LNv as 'master oscillators', the averaged peaks of the DN1s, DN3s and LNds temporally lead the lateral s-LNv and l-LNv in DD (Figure 2.4A, top panel). This may be due to shorter free-running periods in these neurons as proposed in (Dissel et al., 2014) that circadian periods may be established by synergistic interactions between multiple neuronal subgroups rather than encoded by a single neuronal subgroup like the s-LNvs. The LP induces acute desynchrony between the circadian subgroups, shown by the aligned averaged *per* driven bioluminescence signal peaks, followed by phase retuning of synchrony that varies between circadian subgroups after the LP (Figure 2.4A, lower panel). Comparison of the order parameter R within each cell subgroup shows the same temporal sequence described above of

significant light-induced acute desynchrony followed several days later by significant strengthening of oscillator synchrony (Figure 2.4B). This distributed dynamic pattern of light response is similar for the proportion of reliably rhythmic cells (Figure 2.4C). Comparative dynamic spatiotemporal patterns are depicted in Movie 2.1 with individual frames in Figure 2.4D, in which the values of R for each neuronal subgroup are converted to a color heat map (DD on the left and LP on the right).

2.3.6 Adult *XLG-Per-Luc* flies exposed to a light pulse *in vivo* exhibit transient reduction followed by delayed increase in PER staining intensity relative to DD.

After observing dynamic changes in PER activity in whole brain explants exposed to a light pulse (LP), we predicted that the same trends of light-induced network desynchrony and resynchrony would be observed for neuronal subgroups in the brains of adult, male *XLG-Per-Luc* flies exposed to a light pulse *in vivo*. Accordingly, we adapted the DD and LP protocols *in vivo* followed by brain collection for anti-PER ICC analysis of individual neuronal oscillator PER activity. Whole brains in DD were fixed near expected daily peaks of PER based on previous entrainment history. Whole brains of flies exposed to the LP were fixed at projected daily peaks of PER based on the expected phase advance by the LP (see experimental procedures for details).

In Figure 2.5, neuronal subgroups are stained for PER (green) and PDF (red) from standardized laser and imaging settings (‘std gain’) for relative comparison of staining intensity along with higher gain (‘high gain’) settings optimized to compensate for later time points and dimmer neuronal subgroups (e.g. the DN3s). In line with their proposed role as key regulators of behavior in DD (Helfrich-Förster, 2003; Shafer et al., 2002; Yang and Sehgal, 2001), the s-LNvs exhibit the greatest and most sustained PER staining

intensities over time in DD. Uniformly contrasting DD baseline measures, oscillators exposed to a LP (labeled LP + number of hours since exposure, yellow background) show a decrease in PER staining intensity immediately after the light pulse (LP + 2 hours) with the most qualitatively apparent decrease 24 hours after the light pulse (Figure 2.5). 48 hours after application of the LP, most neuronal subgroups exhibit recovery of staining intensity – recovery for dimmer subgroups such as the DN1, DN3 and l-LNv is more distinct by quantitative measurements (see below). Remarkably, phase retuning is measurable by anti-PER ICC as the LNd exhibit a qualitatively distinct and statistically significant increase in PER staining 48 hours after LP exposure relative to LNds maintained in DD. Anti-PER ICC also show significantly higher levels of PER in the DN3 for LP day 4 at 48 hr post LP relative to day 3 at 24 hr post LP (Figures 2.5 and 2.6). The 4 day range of the *in vivo* ICC staining protocol shows that all of the major features of network transient desynchrony and synchrony phase retuning following a phase advance light pulse are shared between whole brain longitudinal per-luc imaging and *in vivo*.

2.3.7 Neuronal subgroups exposed to a light pulse *in vivo* exhibit quantitatively distinct and significant changes in per staining relative to corresponding oscillators in DD.

In Figure 2.6, quantification of average PER fluorescence intensity for oscillators exposed to a phase advancing white light pulse *in vivo* reveals similar trends in phase retuning observed in our bioluminescence recordings with brain explants exposed to a light pulse *ex vivo*. Relative to baseline measurements of PER staining intensity for ‘all neurons’ in DD (averaged from all neuronal subgroups, blue), ‘all neurons’ exposed to the LP (yellow) exhibited a global significant reduction in staining intensity within 2 hours of

light exposure with the decrease in intensity continuing even up to 24 hours after the LP. 48 hours after the light pulse, the PER staining intensity has generally recovered (i.e. no significant difference in intensity between LP and DD oscillators). This general recovery of staining intensity 2 hours in advance of the original peak indicates a network phase shift induced by the phase advancing light pulse. The s-LNvs, l-LNvs and DN1s exhibit this trend to varying degrees. Furthermore, the LNds and DN3s exhibit a significant increase in PER staining intensity 48 hours after exposure to the LP relative to corresponding oscillators in DD.

In vivo ICC experiments repeated for adult *w1118* flies show the same trends of PER activity in DD and in response to phase advancing LP as *XLG-Per-Luc* ICC (Figure S2.4-S2.6). Quantitative comparison of PER levels between *w1118* (red) and *XLG-Per-Luc* (violet) flies show no significant difference in staining intensity between corresponding neurons between matched conditions and time points (Figure S2.4). The similarity of PER staining intensities between *w1118* and *XLG-Per-Luc* flies supports previous studies (Sehadova et al., 2009; Veleri et al., 2003) indicating that *XLG-Per-Luc* flies are a reliable model to study dynamics of PER activity. The common trend of transient loss then recovery and/or strengthening of PER staining intensities at expected phase-shifted peak times relative to expected peak intensities in DD provides further evidence that LP-induced transient desynchrony and delayed synchrony phase retuning observed in cultured brain explants is recapitulated *in vivo* (Figure 2.5-6).

2.4 Discussion

Multi-day functional imaging of organotypic cultures of *Drosophila* whole adult brains requires long term health of the cultures. Our previous work shows that cultures

maintain identifiable morphological characteristics of the LNvs for up to 20 days and TIM clock protein cycling identified by ICC in single LNv up to 3 days (Ayaz et al., 2008). We now reliably measure longitudinal circuit-wide function of single neuron oscillators by *XLG-Per-Luc* bioluminescence up to six days. The minimal *Drosophila* circadian network of six neuronal subgroups can be further subdivided based on neurochemical or genetic markers (An et al., 2013; Collins et al., 2012; Gonze et al., 2005; Veleri et al., 2003; Zhang and Kay, 2010; Zhang et al., 2010b). The current study is restricted to characterizing the general dynamic activity of the classical anatomically recognized s-LNv, l-LNv, LNd, DN1 and DN3 subgroups, which show distinct kinetic signatures in DD and in response to a phase advancing LP. Future studies will parse other divisions of the circuit.

The whole brain cultures tend to flatten with time, causing slight gradual positional distortion of the circadian neurons which actually makes for easier identification and isolation of single neuronal oscillators – particularly for dense subgroups such as the DN3s. We employed rigorous criteria. Oscillators that could not be clearly anatomically identified, isolated from nearby cells, distinguished from frame to frame, and did not exhibit cycling throughout the recordings were excluded from analysis. DN3 neurons do not express the CRY photoreceptor, require signaling from CRY-positive neurons to respond to light. Thus their LP response shows the circadian neural circuit remains intact in cultures (Benito et al., 2008; Yoshii et al., 2008). Intact flies can also light entrain via rhodopsin-based photic input from the eyes and other external photoreceptors (Helfrich-Förster et al., 2001). We exclude photoreceptors from cultures as they increase the risk of microbiological contamination. *Glass*^{60j} mutant flies that lack all external photoreceptors retain light responsiveness, normal behavioral entrainment and PER cycling (ICC) in a

CRY-dependent manner (Helfrich-Förster et al., 2001). We show a clear similarity of trends in light response between our bioluminescence recordings of cultured whole brains exposed to the LP and anti-PER ICC analysis of whole brains of flies exposed to the LP *in vivo*, supporting previous conclusions that cultured whole brains of *XLG-Per-Luc* flies are excellent models for studying dynamic changes in the synchrony of PER activity induced by environmental cues such as light and temperature (Sehadova et al., 2009; Veleri et al., 2003).

Our bioluminescence measurements of synchrony in DD agree with our ICC measures of PER levels and previous studies which show an apparent progressive loss of synchrony and amplitude throughout most of the circuit over time (Lin et al., 2004; Renn et al., 1999). From their previously described role as core oscillators (Helfrich-Förster, 2003; Shafer et al., 2002; Yang and Sehgal, 2001), the s-LNvs exhibit relatively robust rhythmic amplitude and synchrony in DD. The strong l-LNv amplitude and measurable phase coherence we observed even 2 days and beyond in DD is somewhat surprising based on expectations from earlier ICC studies (Klarsfeld et al., 2004; Peng et al., 2003; Shafer et al., 2002; Yang and Sehgal, 2001) and our own ICC findings of l-LNv dampening of PER levels after 2 days (Figures 2.4-5). This is possibly due to (1) the improved temporal resolution of our longitudinal *XLG-Per-Luc* imaging approach, (2) the l-LNv loss of connection with the removed optic lobes or (3) lack of modulation from peripheral tissues. However, we find the same trends in light response for l-LNvs in brain cultures exposed to a LP *ex vivo* and l-LNv in the intact brains of adult flies exposed to a LP *in vivo*. This suggests that the l-LNv oscillators' PER activity and their circuit connections

are sufficiently intact in brain culture explants, though some light input and peripheral feedback information is obviously lost for cultured brains.

One of our most notable findings is that a phase advancing light pulse induces transient damping of the synchrony and rhythmicity of single neuron oscillators followed by the gradual emergence of a new state of strengthened synchrony that reproducibly varies across the circuit network. We call this dynamic process phase retuning. The new state of circuit synchrony is characterized by a light-induced phase shift that coincides with neurons exhibiting stronger rhythms that are better synchronized both within and across neuronal subgroups relative to DD. While we have not yet measured a comprehensive phase response curve, we expect that they will vary in a systematic fashion similar to behavioral phase response curves. Desynchrony may appear to be a negative consequence of the light pulse. However, recent work suggests that transient 'phase tumbling' (An et al., 2013) of the light entrainment process may be exploited for more rapid recovery from jetlag (An et al., 2013). While much work has shown the importance of VIP peptidergic signaling in the SCN for maintaining robust rhythms (Brown et al., 2007; Colwell et al., 2003; Harmar et al., 2002), pharmacological treatment with VIP, GABAergic and vasopressin agents can transiently weaken oscillator function followed by more rapid entrainment (An et al., 2013; Evans et al., 2013; Freeman et al., 2013; Yamaguchi et al., 2013). Temporarily weakening oscillator coupling and dephasing of rhythms appears to permit circuits to more easily reset to phase shifts and overly robust oscillator networks block entrainment (An et al., 2013; Buhr and Van Gelder, 2014; Freeman et al., 2013; Hatori et al., 2014; Lamba et al., 2014; Webb et al., 2012; Yamaguchi et al., 2013).

Previous work shows that circuit connectivity (Peng et al., 2003) organizes circadian behavior and electrical outputs of cell autonomous oscillators (Nitabach et al., 2002). The *Drosophila* circadian circuit light initial response of desynchrony followed by phase retuning to a new circuit-wide synchrony pattern remarkably recapitulates many of the features we observe when LNvs are electrically hyperexcited (Ayaz et al., 2008; Nitabach et al., 2006), suggesting that such responses are dictated by circuit properties. The relatively tight homogeneous light response that we measure in longitudinally imaged *XLG-Per-Luc* fly brains in the LNds is interesting as only half of the LNds express CRY (Yoshii et al., 2008). This suggests a non-cell autonomous functional role for the LNds in light-induced circuit phase shift and maintaining behavior rhythmicity following exposure to a short light pulse. The LNds are the first neuronal subgroup to exhibit a rapid and coherent phase advance immediately following the light pulse. As suggested in (Lamba et al., 2014), the LNds may first reset their own circadian oscillations before influencing other neuronal subgroups to reset and resynchronize their own molecular pacemakers. We propose that the LNds are the actual mediators of the whole circuit phase advance and that transient phase desynchrony in other neuronal subgroups enables them to be phase retuned which ultimately drives a light induced shift in the phase of behavioral rhythms. Sub-regions of the SCN also vary in oscillator response to light input and show a wave-like spatiotemporal pattern (Evans et al., 2011; Foley et al., 2011; Nakamura et al., 2005). Comparisons of dissociated SCN cellular oscillators versus intact SCN slices suggest that many of the features of oscillator coordination are determined by anatomical connectivity (Evans et al., 2011; Evans et al., 2012; Liu et al., 2007; Welsh et al., 1995; Welsh et al., 2004).

In summary, we show by whole circuit bioluminescence imaging of single circadian neurons and immunocytochemical analysis of PER activity in response to *in vivo* light exposure that a phase-advancing light pulse induces a circuit-wide spatiotemporal pattern of acute oscillator desynchrony followed by phase retuning to synchrony that varies across circadian neuronal subgroups. The general time course of this complex circuit-wide response imaged in whole brain explants closely matches that for behavioral entrainment in intact animals (Helfrich-Förster et al., 2001). Based on the many organizational similarities of circadian circuits across the animal kingdom, entrainment appears to be constrained by connectivity of the circadian network. Our results support the hypothesis that temporarily weakened subsets of oscillators and their acute desynchrony are key initial features of entrainment. Broad features of this pattern of circadian circuit response to light may be generalized to humans and other mammals.

2.5 Figures

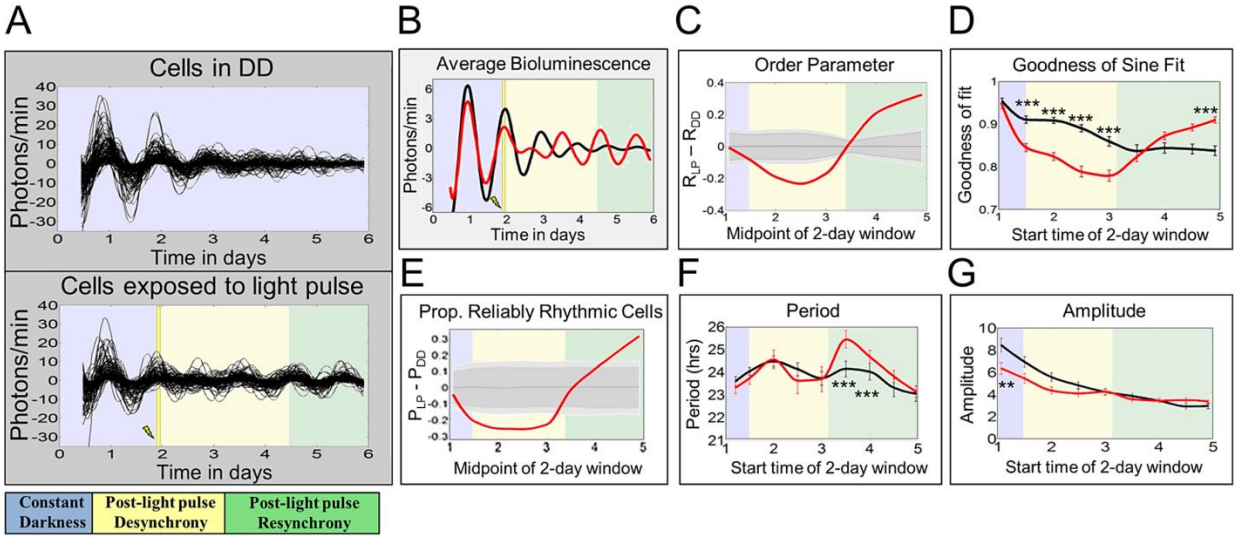

Figure 2.1. Oscillators in constant darkness exhibit gradual desynchrony over time, whereas oscillators exposed to a light pulse at CT 22 show phase retuning. Neuronal oscillators were either maintained in constant darkness ('DD cells') or exposed to a 15 min 12.57 W/m2 (2,000 lux) light pulse (LP) at CT 22 on the second day in DD ('LP cells'). The time at which the LP is applied is indicated by a yellow bar. The colored-backgrounds provide general time frames of significant changes in order parameter. Bluish-gray indicates pre-LP application, yellow indicates post-LP desynchrony, and green indicates resynchrony. **A:** *XLG-Per-Luc* bioluminescence time-series measurements show that LP cells (lower panel; n=126) exhibit transient loss then recovery and even strengthening of cell synchrony over time compared to DD cells (upper panel; n=122), which exhibit a gradual, monotonic loss of cell synchrony. **B:** Comparing averaged bioluminescence traces confirms that LP cells (red line) exhibit an acute decrease in synchronized rhythmicity after the light pulse followed by recovery and eventual strengthening of synchronized rhythmicity relative to DD cells (black line). **C:** After a LP, oscillators display significant reduction in the order parameter R followed by a delayed significant increase in R. The order parameter R varies between 0 and 1, with higher values indicating similarity in phase, period, and waveform. The solid red curve represents the difference in R between LP and DD cells ($R_{LP} - R_{DD}$). The dark and light gray zones indicate the 95% and 99% confidence zones, respectively. The null hypothesis is that there is no difference between LP and DD values of R, as determined using 10,000 bootstrap samples. **D:** Using oscillator goodness-of-sine-fit (g.o.f.) as a measure of rhythmicity, it was found that after a LP, cells (red line) demonstrate an acute reduction in g.o.f. followed by significantly greater g.o.f. over time as compared to DD oscillators at corresponding time points (black line). **E**: After a LP, relative to DD, there is a significant transient decrease in the proportion of reliably rhythmic cells ('P'), followed by a significant increase in 'P' over time. The solid red line indicates the difference between LP and DD conditions ($P_{LP} - P_{DD}$). Cells with g.o.f. ≥ 0.82 are considered to be

“reliably rhythmic.”. **F:** Sine-fit estimates of period indicate that LP cells (red line) exhibit a transient increase in period length several days after a light pulse. **G:** Sine-fit estimates of amplitude indicate that that LP cells (red lines) exhibit no significant differences in amplitude following exposure to the LP when compared to DD cells at corresponding time points. The difference in amplitude for the first 2-day window time point is likely due to slight overlap with changes in amplitude induced by the light pulse at 1.92 days. The error bars for g.o.f., period and amplitude represent ± SEM with significance analyzed using one-way ANOVA, Tukey post hoc test. *** indicates $P<0.001$ and ** indicates $P<0.005$.

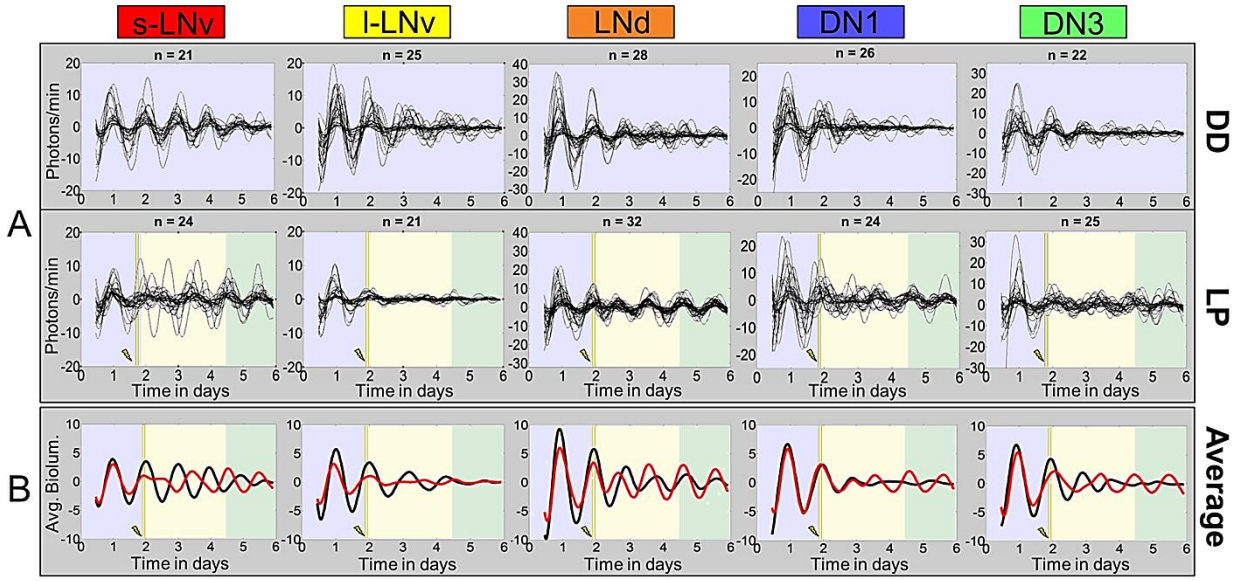

Figure 2.2. Exposure of cultured brain explants to a light pulse reveals qualitatively distinct dynamic signatures of neuronal subgroups. A: Single neuron oscillations are shown separately for each neuronal subgroup. **Top:** Neuron subgroups maintained in DD showing a general loss of intra-subgroup synchrony and amplitude over time. S-LNvs exhibit the most robust rhythms over time. **Bottom**: Neuron subgroups exposed to a 15 minute 12.57 W/m2 light pulse at CT 22 of the second day in DD *ex vivo*. LP induced transient phase tumbling followed by synchrony phase retuning is seen qualitatively at varying degrees for all groups except the l-LNv which rapidly lose oscillator synchrony and amplitude and do not phase retune following the LP by the end of the recording. Conversely, LNds do not appear to exhibit any significant loss of synchrony following the LP. The number of cells analyzed for each group is indicated by "n." The background color coding is the same as in **Fig. 2.2. B:** Averaged bioluminescence traces for LP (red line) vs. DD (black line) oscillators sharpen the qualitative patterns seen in the individual oscillator records.

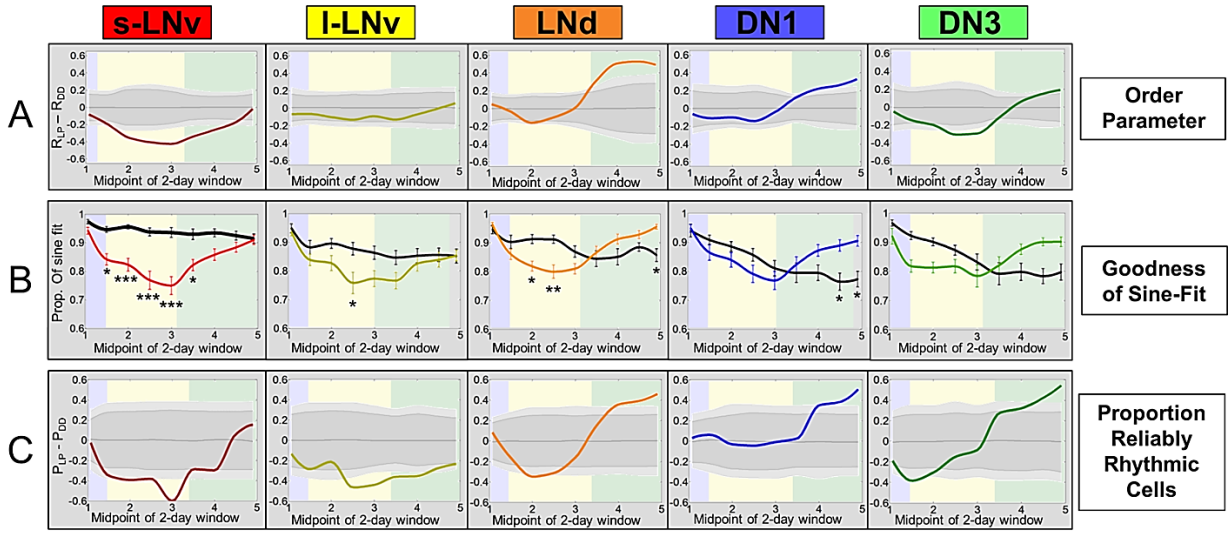

Figure 2.3. Neuronal subgroups respond to a phase-advancing light pulse with quantitatively distinct dynamics of transient desynchrony followed by recovery and strengthening of synchrony and rhythmicity. Colored-background frames of reference are the same as seen in **Fig. 2.1**. Circadian parameters are measured over 2-day sliding windows. **A:** After a light pulse (LP), neuronal subgroups exhibit transient loss and/or subsequent gain of synchrony with varying degrees and kinetics of response (s-LNv, LNd, DN1, DN3) or no significant response (l-LNv). Solid lines represent the difference in R between LP and DD conditions ($R_{LP} – R_{DD}$). Dark and light gray zones indicate 95% and 99% confidence intervals, assuming the null hypothesis of no difference between LP and DD. **B:** Exposure to LP results in a significant rapid reduction in the goodness-of-sine-fit (g.o.f.) for the s-LNvs, LNds and l-LNvs (listed by order of response). The DN1s and LNds demonstrate strengthened g.o.f. delayed by several days after the light pulse. Colored lines indicate average values for g.o.f. for LP cells, whereas solid black lines indicate values for DD cells. Error bars represent ± SEM. Significant differences between LP and DD conditions at each time point are indicated by *** for P<0.001, ** for P<0.005, and * for P<0.05 (one-way ANOVA, Tukey post hoc test). **C:** Analysis of the proportion of reliably rhythmic cells after a LP relative to the DD condition ($P_{LP} - P_{DD}$) reveals a significant initial decrease for the s-LNvs and l-LNvs and, to a lesser extent, the LNds and DN3s. The LNds, DN1s and DN3s demonstrate a later increase in proportion of reliably rhythmic cells compared to corresponding neurons in DD. Confidence intervals are plotted as described above.

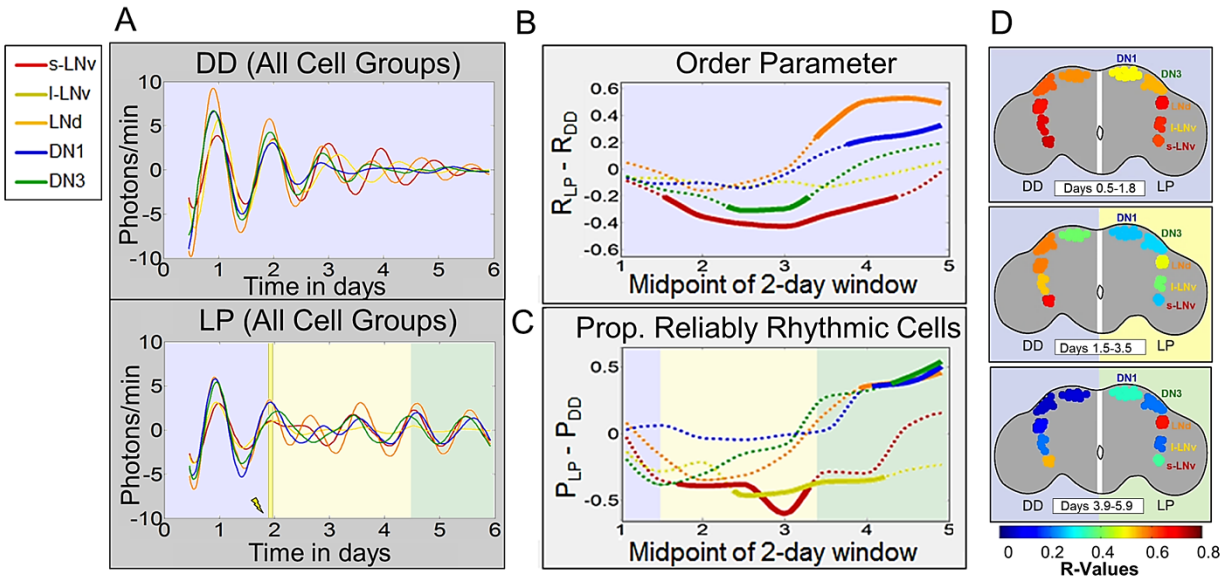

Figure 2.4. Alignment of neuronal subgroup responses to a LP reveals temporally distinct kinetic signatures of phase retuning. In **A-C**, plots of neuronal subgroup data are coded by color: s-LNv (red), l-LNv (yellow), LNd (orange), DN1 (blue) and DN3 (green). **A** (**Top)**: Average bioluminescence traces for subgroups maintained in DD exhibit a progressive and monotonic loss of rhythmicity and inter-subgroup synchrony over time. **A (Bottom):** After a light pulse (LP), average bioluminescence traces for subgroups exhibit a transient reduction in rhythmic amplitude and inter-subgroup synchrony, followed by a general strengthening of rhythmic amplitude and inter-subgroup synchrony over time relative to corresponding neurons in DD. **B, C:** Inter-subgroup comparisons of averaged single neuron circadian parameters measured using 2-day sliding windows. **B:** After a LP, s-LNvs exhibit the first and longest lasting significant reduction in R, with DN3s exhibiting similar but less extreme changes. LNds and DN1s subsequently show significant strengthening of synchrony, coinciding with recovery of s-LNv synchrony. Dotted lines indicate no significant changes in synchrony after a light pulse relative to DD ($R_{LP} – R_{DD}$) while solid lines indicate significance outside the 99% confidence interval determined by bootstrapping. **C:** Inter-subgroup comparisons of the relative proportion of reliably rhythmic cells ($P_{LP} – P_{DD}$) show that the s-LNvs and l-LNvs exhibit significant initial decreases in proportion of rhythmic cells after exposure to a light pulse, whereas the DN1, DN3 and LNd exhibit a significant delayed increase. Dotted and solid lines indicate lack or presence of statistically significant differences between LP and DD conditions as shown above for R. **D:** Images of selected time points from **Movie 2.2** comparing inter-subgroup differences in kinetics of changes in synchrony in DD or with the light pulse. The pseudo-color heat map codes values of R, with warm colors indicating high synchrony among cells within a subgroup. Left sides of brains show DD, right sides show response to LP. The colored backgrounds designating general time frames of significant changes in R are the same as previous figures.

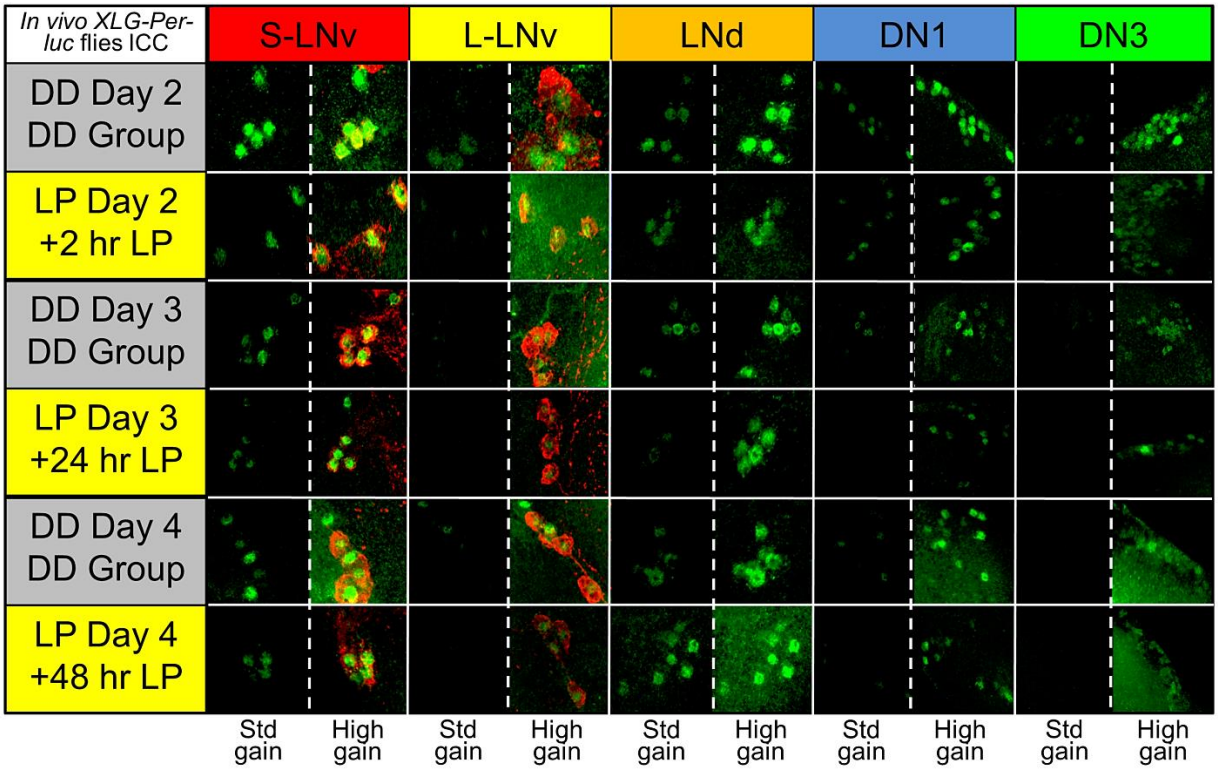

Figure 2.5. Exposure of intact *XLG-Per-Luc* adult flies to a light pulse *in vivo* reveals qualitatively apparent transient loss and subsequent increase in PER staining intensity over time. After entrainment to a standard 12h/12h LD schedule for ≥3 days, adult *XLG-Per-Luc* flies were either maintained in DD ('DD group'; gray background) or exposed to 15 min 12.57 W/m2 (2,000 lux) light pulse at CT 22 on the second day in DD *in vivo* (labeled 'LP + number of hours since exposure'; yellow background). Adult whole brains were stained for PER (green) and PDF (red). Flies in the DD group were fixed at CT 22 for DD day 2 and CT 0 for DD days 3 and 4. Flies exposed to the LP were fixed 2 hours (CT 2), 24 hours (CT 0), and 48 hours (CT 0) after the light pulse. Note that fixation times for LP flies are recalibrated such that the new CT 0 corresponds to the time when the LP is administered. In comparison to corresponding DD cells, it can be seen from representative ICC images that all neuronal subgroups demonstrate substantial dampening of PER staining intensity 24 hours after light pulse exposure with general recovery of amplitude 48 hours after the LP. The staining for each neuronal subgroup is presented at the same standardized ('std gain') laser and microscope settings to compare between time points and conditions along with staining obtained with higher intensity settings ('high gain') for visualization of dim fluorescence – particularly for later time points and the DN3s. See "Experimental Procedures" for details regarding ICC protocol and fixation times.

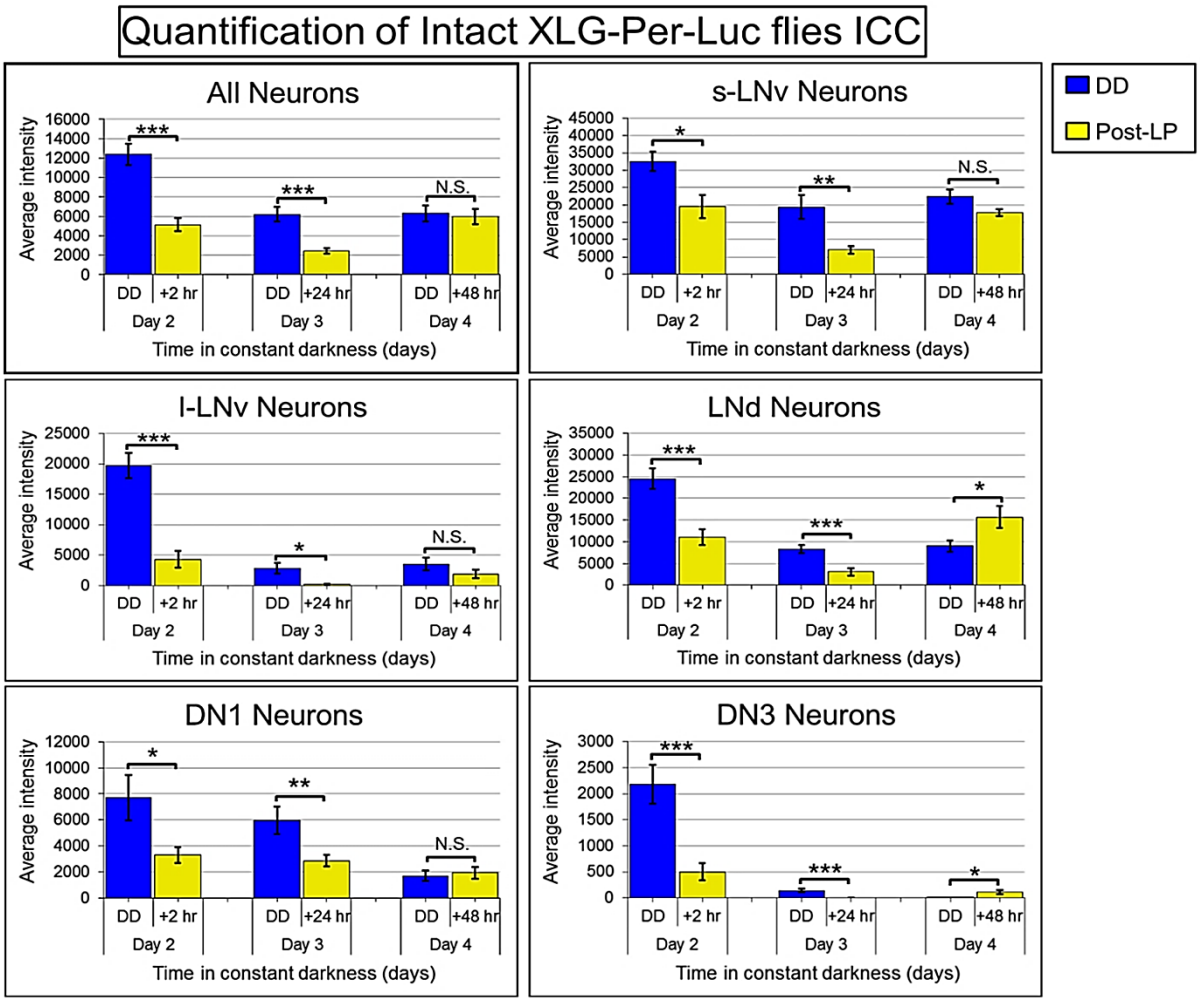

Figure 2.6. Quantification of significant changes in PER staining intensity from whole brains of *XLG-Per-Luc* flies either maintained in DD or exposed to a light pulse *in vivo*. The software Volocity (PerkinElmer) was used to measure the average fluorescence intensity of PER staining in individual neurons visualized qualitatively in **Figure 2.5.** Neuronal oscillators in DD (blue) generally exhibit a gradual reduction in the average intensity of PER staining over time with the s-LNv showing the most stable amplitude. Conversely, neuronal oscillators exposed to a light pulse (LP, yellow) exhibit a significant reduction in PER staining intensity 24 hours after the LP and a significant recovery of staining intensity 48 hours after the LP. The LNds and DN3s even appear to exhibit a significant increase in PER staining intensity 48 hours after the LP in comparison to corresponding neurons maintained in DD. However, it should be noted that very dim fluorescence at later time points and tight clustering makes analysis of DN3s difficult. The error bars represent ± SEM. N.S. indicates no significant difference, * indicates $P<0.05$, ** indicates $P<0.005$ and *** indicates $P<0.001$ determined using Student's t-test. The Student's t-test was used to compare corresponding DD and LP neuronal oscillators with the null hypothesis that there is no difference in average PER staining fluorescence intensity. The laser intensity and other settings were kept the same for all groups for comparison of fluorescence intensities.

2.6 Supplementary Information

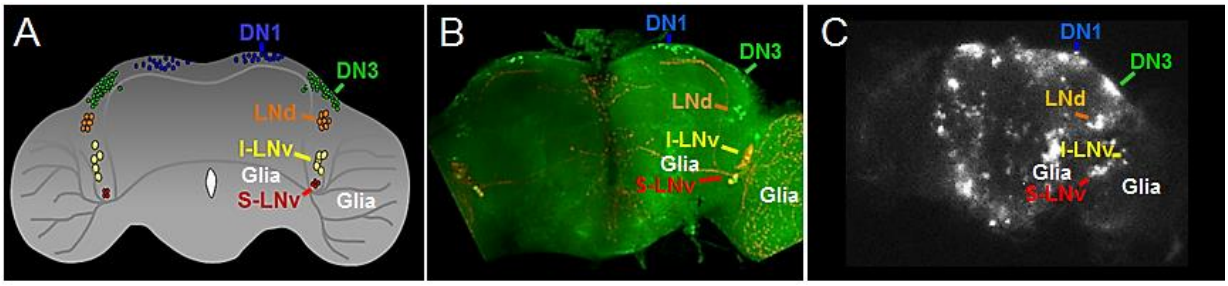

Figure S2.1. Spatial mapping of cells expressing the *period* gene in the adult *Drosophila* brain. S-LNv (red) and l-LNv (yellow) are the small and large ventral lateral neurons, respectively. LNd (orange) are the dorsal lateral neurons. DN1 (blue) and DN3 (green) are dorsal neurons subgroups 1 and 3, respectively. Clock glia cells (white text) are found throughout the brain circadian circuit. **A:** Schematic map depicting s-LNv, l-LNv, LNd, DN1, and DN3 subgroups. Neurites from the period-expressing cells are shown in gray. **B:** Confocal image of adult brain whole mount from male *XLG-Per-Luc* fly acutely fixed at ZT 23 and stained with anti-PER (green) and anti-PDF (red). Glia (white) are found throughout the brain but cannot be visualized in this image as they are dimmer and lie in different z-planes than the canonical neuronal subgroups. **C:** Bioluminescence image of single-cell *period* expression pattern in cultured adult whole-brain from male *XLG-Per-Luc* fly. The s-LNv, l-LNv, LNd, DN1, and DN3 neurons analyzed in further experiments for circadian time-course of PER expression are labeled with the same color scheme as above. DN2 neurons are not reliably detected in bioluminescence images of adult brains from *XLG-Per-Luc* flies, in agreement with (Sehadova et al., 2009; Veleri et al., 2003). Glia (white) are found throughout the brain but cannot be seen in this image for the same reasons listed above.

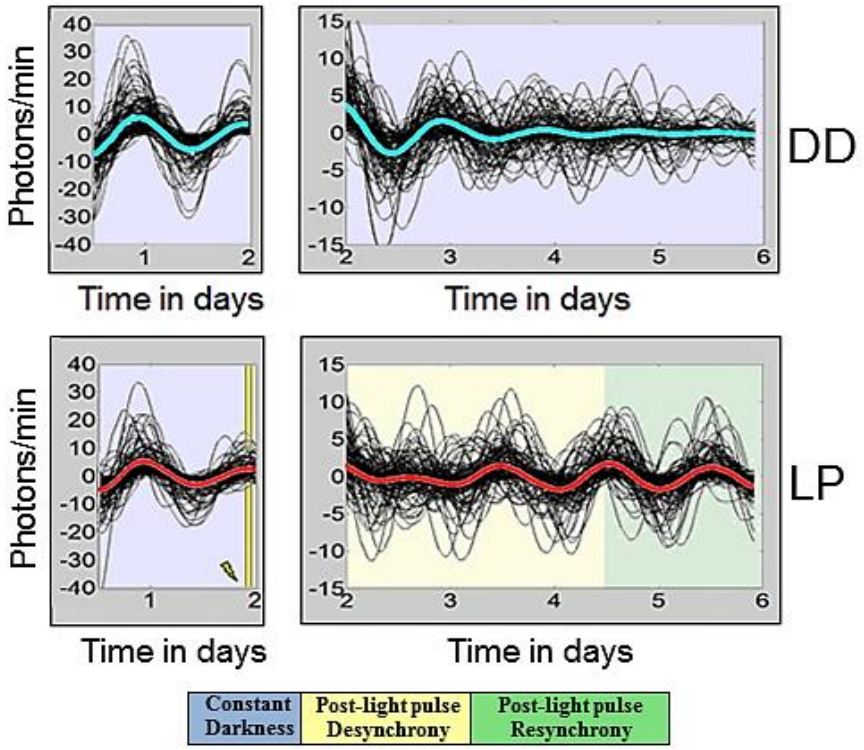

Figure S2.2. Oscillators exposed to a light pulse exhibit distinct patterns of loss, recovery then strengthening of synchrony over time relative to oscillators in DD. Averaged bioluminescence traces for DD cells (cyan; n = 122) and LP cells (red; n = 126) are superimposed on plots of detrended individual traces (black) of clock neurons seen in **Figure 2.1A**. Due to the transiently high amplitude bioluminescence at the start of recordings, the traces have been divided into two time frames (0.5-2 days and 2-6 days) with the vertical axis scaled separately for each time frame to allow for clearer visualization. **Left**: It is qualitatively apparent that oscillators in the DD and LP groups show comparable synchrony and amplitude between 0.5-1.92 days (pre-LP). **Right**: Relative to the overall monotonic, gradual dampening observed by oscillators in DD **(top)** between 2-6 days, neurons exposed to a LP **(bottom)** generally exhibit qualitatively distinct patterns of synchrony tumbling followed by phase retuning (recovery/strengthening of synchrony along with phase shift).

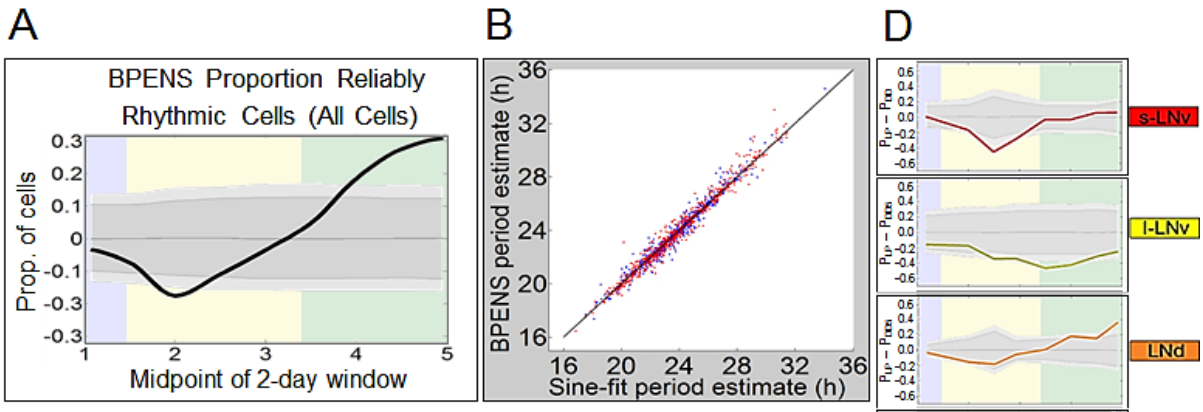

C

Correlation between Bayesian frequency estimation and sine-fit estimation		
Circadian Parameter	Correlation Coefficient (Rho)	P-Value
Period Estimate	0.98	<0.001
Reliably Rhythmic Cells	0.58	<0.001

Figure S2.3. BPENS (Bayesian parameter estimation for noisy sinusoids) calculations confirm general trends in neuronal light response seen using sine-fit criterion. A: Bayesian frequency estimates of the proportion of reliably rhythmic cells for 'all neurons' (averaged from all neuronal subgroups) validates the general trend of transient reduction and delayed recovery in proportion of neurons following a light pulse observed by sine-fit estimates. Dark and light gray zones represent measures of uncertainty in the forms of 95% and 99% credible intervals, respectively. **B**: Scatter plot of sine-fit and Bayesian frequency estimates of period show strong positive linear correlation with particularly high clustering within the circadian range. Blue spots represent DD cells (688 contributions) while red spots represent LP cells (654 contributions) from all neuronal subgroups and 2-day windows of analyses. **C**: High correlation values between BPENS and sine-fit analyses of period and proportion of reliably rhythmic cells confirm that sine-fit analysis over 2-day windows, in combination with a discrete wavelet transform, is sufficiently consistent and reliable for our measures. **D:** Colored lines for each neuronal subgroup (using the same color scheme described in **Figure S2.1**) represent the difference in proportion of reliably rhythmic cells between corresponding neurons in LP and DD conditions (PLP – PDD) over time. As observed by sine-fit estimates in Figure 2.3B, the ventral subgroups s-LNv and l-LNv exhibit significant reduction in this difference following a light pulse whereas the dorsal groups LNd, DN1 and DN3 exhibit a delayed increase following the LP. As DN3s lack CRY and share neurite connections with the s-LNvs, this provides evidence in support of previous studies that also support the idea that intercellular communication contributes to light-induced phase shifts (Tang et al., 2010). Dark and light gray zones indicate 95% and 99% confidence intervals.

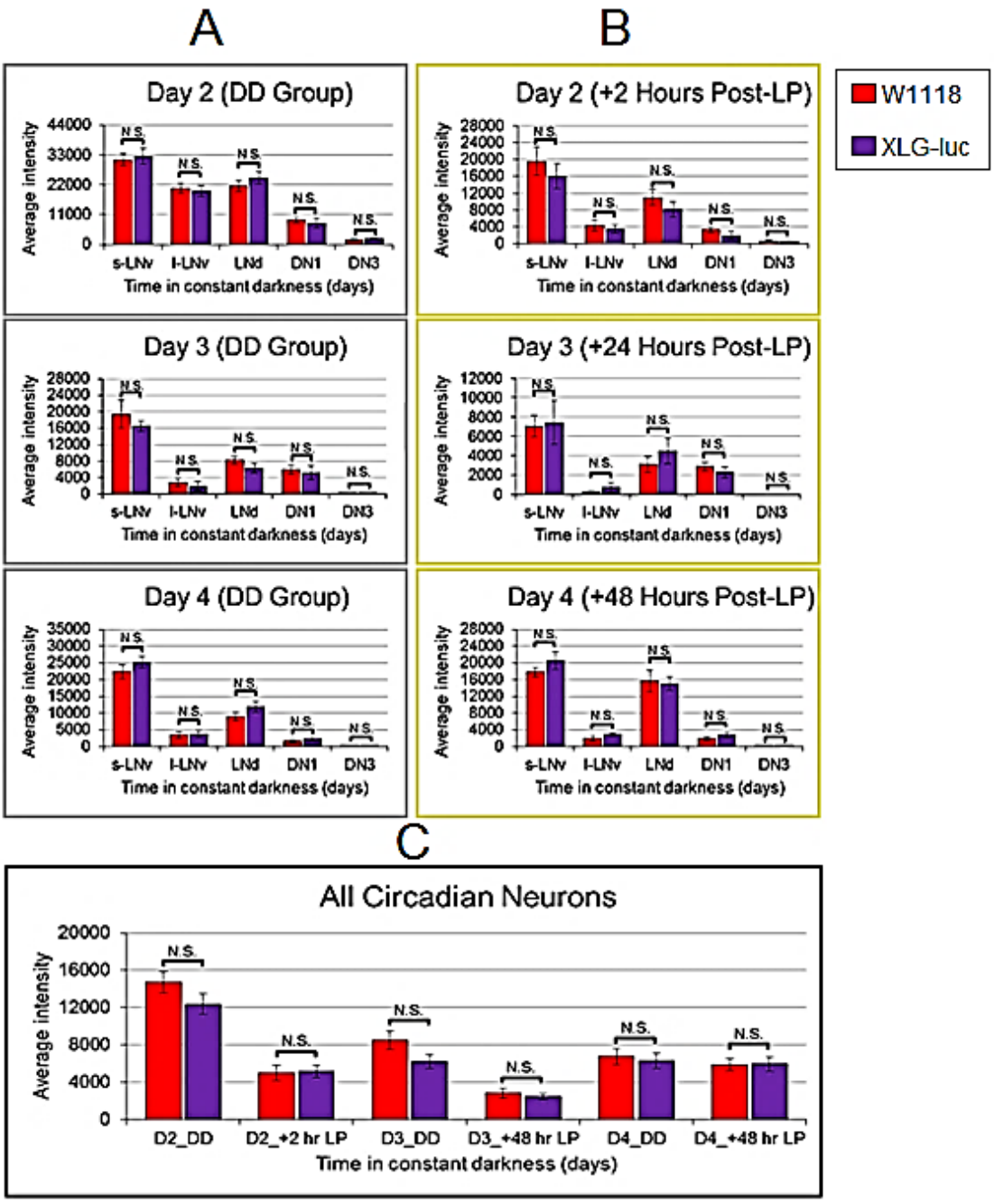

Figure S2.4. Adult *w1118* and *XLG-Per-Luc* flies show no significant difference in PER staining intensities. Quantitative comparisons of PER staining average fluorescence using the software Volocity performed for **A:** neuronal subgroups maintained in DD (gray frames) and **B:** neuronal subgroups exposed to a 15 min 12.57 W/m2 light pulse at CT 22 of the second day in DD *in vivo* (yellow frames) indicated that there is no significant difference in intensities between corresponding neurons of *w1118* flies (violet) and *XLG-Per-Luc* flies (red) at matched time points and light regimes. **C:** Comparison of 'all circadian neurons' analyzed (i.e. cells from all neuronal subgroups averaged together) revealed no significant difference in overall staining intensity between *w1118* and *XLG-Per-Luc* flies at corresponding time points and conditions. Student's t-

test was used to compare differences in average PER staining intensities between *w1118* and *XLG-Per-Luc* flies with P>0.05 considered not significant (N.S.). Laser intensity and other settings were always kept the same for comparison of PER staining intensities.

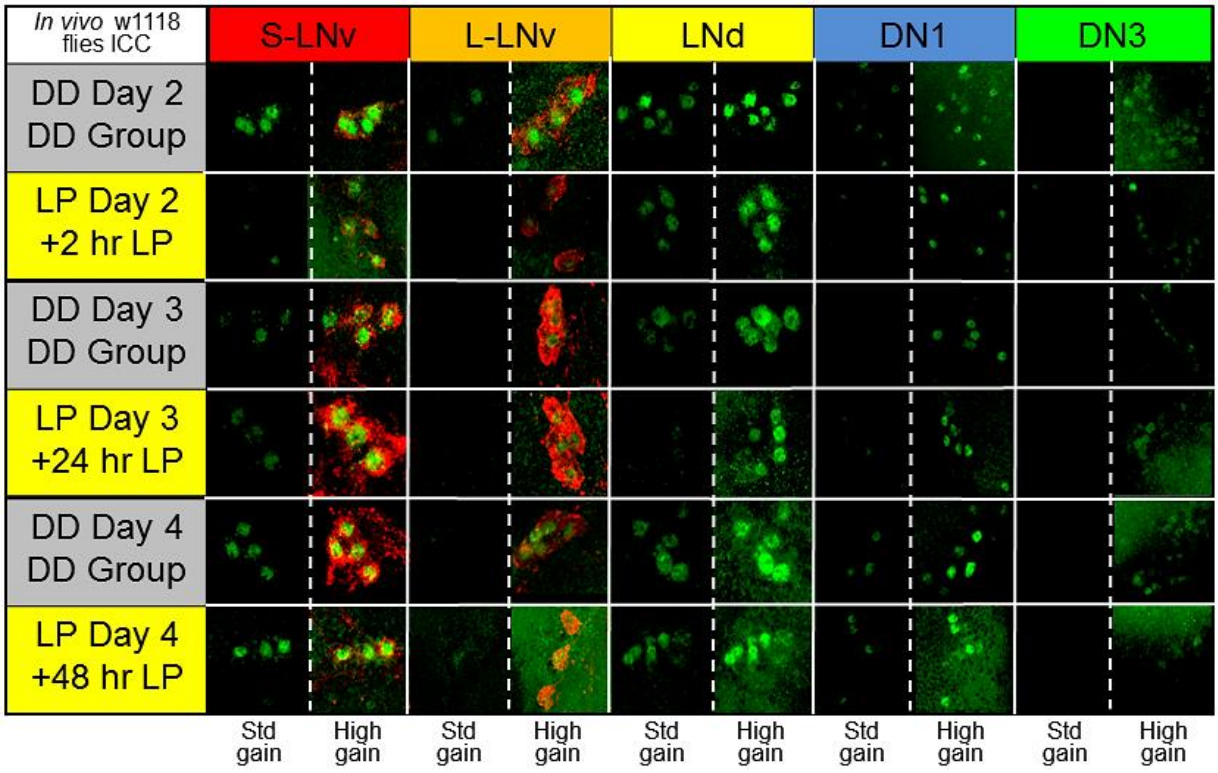

Figure S2.5. *W1118* adult flies exposed to a light pulse exhibit the same trend as *XLG-Per-Luc flies* of transient loss and subsequent recovery/increase of PER staining intensity. Representative ICC images of neuronal subgroups in *W1118* flies show the same patterns of PER staining as *XLG-luc* ICC images shown in **Figure 2.5** for adult flies either maintained in DD or exposed to a 15 min 12.57 W/m2 (2,000 lux) light pulse at CT 22 of the second day in DD in vivo. See **Figure 2.5** for description and protocol.

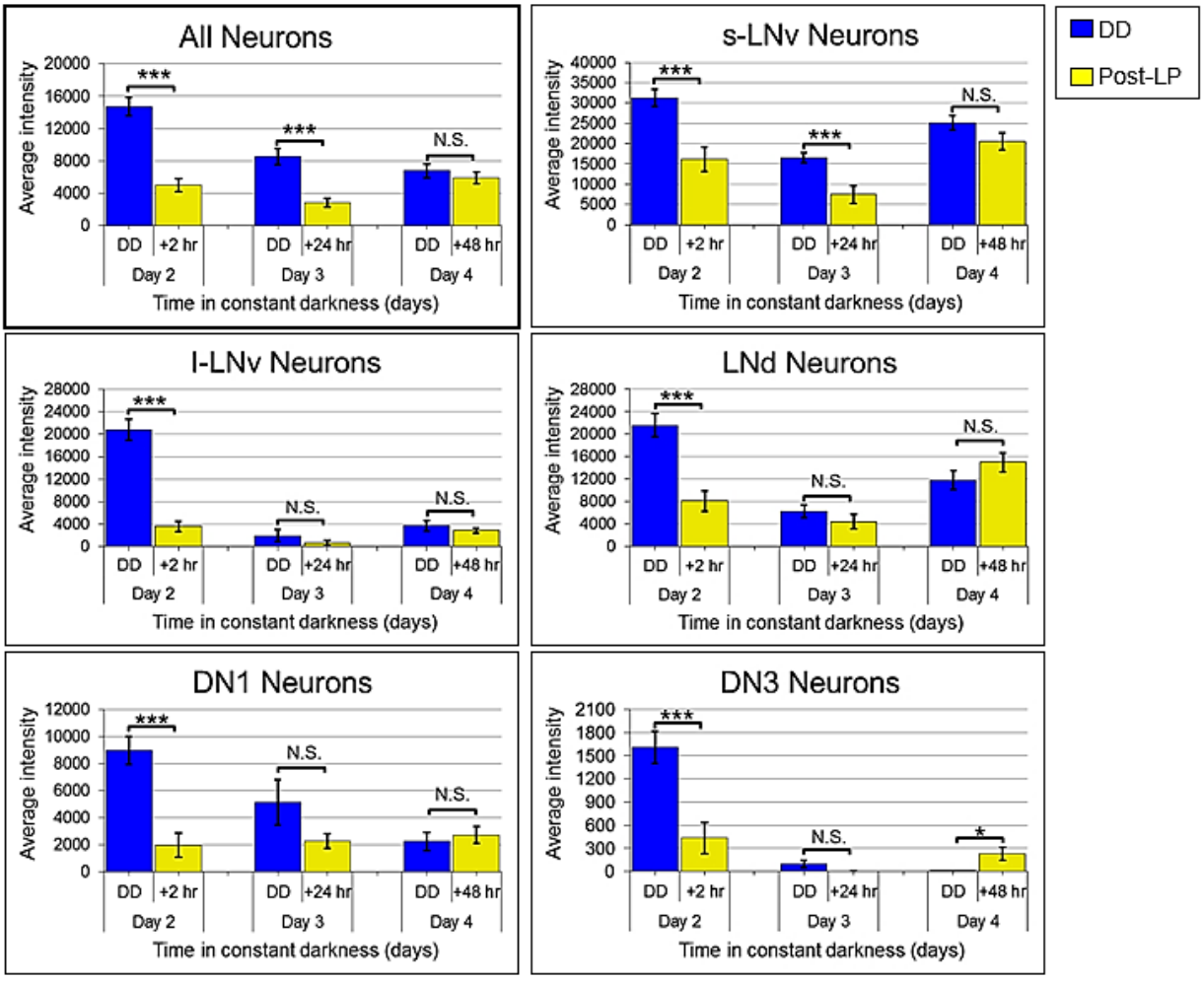

Figure S2.6. Quantification of changes in PER staining intensity for DD and LP cells qualitatively shown in Figure S2.5. Neuronal subgroups in adult *w1118* flies exhibit the same patterns of quantified changes in PER staining intensity as seen for *XLG-luc* flies in **Figure 2.6.** See **Figure 2.6** for description (same protocol and general results for both *w1118* and *XLG-luc* flies).

Movie 2.1, Related to Experimental Procedures. Raw time-lapse bioluminescence recordings of adult *XLG-Per-Luc Drosophila* whole-brain explants cultured for 6 days in darkness. A: Whole brain culture maintained in constant darkness throughout recording. **B:** Whole brain culture exposed to a 15 minute 12.57 W/m2 light pulse at CT 22 of the second day in DD. A white flash at 1.92 days indicates the time at which the light pulse was administered *ex vivo*. The time stamp at the top indicates the number of days in DD that have elapsed (movies in **A** and **B** are time matched). The first 0.42 days are excluded due to saturating and highly variable bioluminescence when the explants are first cultured. This movie can be viewed as a supplemental attachment to this thesis.

Movie 2.2, Related to Figure 2.4. Animated model comparing changes in order parameter over time for neuronal subgroups in DD versus subgroups exposed to a light pulse *ex vivo*. The animated heat map codes values of R (ranging from 0.0 to 0.8) for neuronal subgroups, with warmer colors indicating greater synchrony of phase, period and waveform among cells within a subgroup. As in **Fig. 2.4D**, the left hemisphere of the brain schematic shows DD cells and the right hemisphere shows LP cells. The background colors provide the same time frames of significant changes in R as seen in Figure 2.1. This movie can be viewed online in *Current Biology*.

CHAPTER 3

Functional Contributions of Strong and Weak Cellular Oscillators to Synchrony and Light-Shifted Phase Dynamics

(Roberts, Leise, Welsh, Holmes)

Abstract

Light is the primary signal that calibrates circadian neural circuits and thus coordinates daily physiological and behavioral rhythms with solar entrainment cues. *Drosophila* and mammalian circadian circuits consist of diverse populations of cellular oscillators that exhibit a wide range of dynamic light responses, periods, phases, and degrees of synchrony. How heterogeneous circadian circuits can generate robust physiological rhythms while remaining flexible enough to respond to synchronizing stimuli has long remained enigmatic. Cryptochrome is a short wavelength photoreceptor that is endogenously expressed in approximately half of *Drosophila* circadian neurons. In a previous study, physiological light response was measured using real-time bioluminescence recordings in *Drosophila* whole brain explants which remain intrinsically light-sensitive. Here we apply analysis of real-time bioluminescence experimental data to show detailed dynamic ensemble representations of whole circadian circuit light entrainment at single neuron resolution. Organotypic whole brain explants were either maintained in constant darkness (DD) for 6 days or exposed to a phase advancing light pulse on the second day. We find that stronger circadian oscillators support robust overall circuit rhythmicity in DD, whereas weaker oscillators can be pushed toward transient desynchrony and damped amplitude to facilitate a new

state of phase-shifted network synchrony. Additionally, we employ mathematical modeling to examine how networks composed of distinct oscillator types can give rise to complex dynamic signatures in DD conditions and in response to simulated light pulses. Simulations suggest that complementary coupling mechanisms and a combination of strong and weak oscillators may enable a robust yet flexible circadian network that promotes both synchrony and entrainment. A more complete understanding of how the properties of oscillators and their signaling mechanisms facilitate their distinct roles in light entrainment may allow us to direct and augment the circadian system to speed recovery from jet lag, shift work, and seasonal affective disorder.

3.1 Introduction

Since the relatively recent advent of high speed flight and artificial lighting, a growing proportion of the human population suffers chrono-disruption due to mismatch between biological and environmental timing. Circadian disruption by events such as jet lag and shift work are implicated in physiological disorders ranging from decreased cognitive performance and weight gain to diabetes and cancer (Knutson et al., 2007; Kreier et al., 2007; Lemmer, 2006; Maemura et al., 2007; Mazuski and Herzog, 2015; Stevens and Rea, 2001). Circadian neural circuits coordinate and synchronize physiological and behavioral activities by integrating environmental cues. Light is the most powerful cue for most organisms (Pittendrigh and Daan, 1976; Tauber and Kyriacou, 2001). Light evoked changes in mammalian cellular oscillator dynamics is still largely unexplored due to the technical difficulty of introducing a physiological light signal *in vitro* (Evans et al., 2011; Foley et al., 2011; Webb et al., 2012). For the mammalian circadian pacemaker, the suprachiasmatic nucleus (SCN), physiologically activating retina-

mediated photic responses while monitoring large numbers of deep brain individual cellular oscillators by imaging or electrophysiology remains a formidable challenge, both *ex vivo* and *in vivo*. However, in the *Drosophila* circadian system, circuit-wide responses to light can be monitored longitudinally in cultured whole brain explants (Ayaz et al., 2008; Roberts et al., 2015) due to expression of the blue light receptor Cryptochrome (CRY) in circadian neurons (Emery et al., 1998; Stanewsky et al., 1998).

To examine dynamic signatures of single-neuron oscillators and their potential roles in entrainment, we analyzed and compared *ex vivo* and *in silico* single oscillator longitudinal light responses. *Ex vivo* analysis was based on real-time bioluminescence imaging of the conserved and critical circadian gene *period* in cultured *Drosophila* whole brain explants, as previously described (Roberts et al., 2015). Explants were either maintained in constant darkness for 6 days or exposed to a circadian-time 22 h (CT22) phase advancing white light pulse after nearly 2 days in culture. The *Drosophila* circadian network minimally consists of six neuronal subgroups that include large and small ventrolateral neurons (l-LNvs and s-LNvs), dorsolateral neurons (LNds), and three subsets of dorsal neurons (DNs 1, 2 and 3) (Sheeba, 2008). Recent studies have further subdivided these subgroups by chemical or genetic markers (Collins et al., 2012; Hamasaka et al., 2007; Johard et al., 2009; Shafer et al., 2006; Zhang and Kay, 2010; Zhang et al., 2010a). Visualization and quantification of longitudinal changes in circadian network phase, amplitude, and synchrony with single oscillator resolution allows us to compare the contributions of different types of circadian oscillators to free-running behavior and light-induced phase shifts.

Motivated by the striking qualitative trends observed in the whole brain imaging data, we also developed a mathematical model of a relatively simple network consisting of three categories of oscillators with differing light responses, signaling mechanisms, and damping rates. The primary purpose of our model is to explore how and why complex dynamic signatures might emerge, with distinct patterns appearing under constant conditions and in response to a strong phase advancing stimulus. It has long been recognized that robust and synchronous circadian networks are critical for strong and healthy behavioral outputs. However, our *ex vivo* findings and computational modeling suggest that transiently desynchronizing and damping certain components of the circadian neural network may be a key adaptive feature of circadian systems that facilitates large shifts in phase while restoring synchronous rhythmicity after the adjustment is complete. The combination of single-cell resolution imaging with mathematical modeling may allow us to predict how the dynamic interplay of complementary oscillatory types and transient desynchrony could be harnessed to generate potential treatments for jet lag, shift work, and seasonal affective disorder.

3.2 Materials and Methods

Experimental bioluminescence data

Adult, male *XLG-Per-Luc* flies were entrained to a standard 12 hr:12 hr LD schedule for ≥3 days. *Drosophila* whole brains were dissected, cultured, and mounted on the stage of an inverted microscope (Olympus IX71, Tokyo, Japan) as described (Roberts et al., 2015), with cycling bioluminescence at single cell resolution measured at 30 minute intervals by the software MetaMorph (Molecular Devices, Sunnyvale, CA). Whole brain explants were either maintained in constant darkness (DD) for 6 days (n=12)

or exposed to a phase advancing 12.57 W/m^2 (2,000 lux), 15 minute white light pulse at CT 22 on the second day of DD (n=12).

Raster plots (pseudo-heat maps)

Pseudo-heat maps of individual oscillator PER-luc expression over time in cultured *Drosophila* whole brain explants were generated using MATLAB scripts (version 8.2). Analysis of experimental data used throughout this study was based on bioluminescence imaging experiments reported previously (Roberts et al., 2015). Pseudo-heat maps were generated for each neuronal subgroup and also stacked for plots of "all cells." Warmer colors indicate higher amplitude whereas cooler colors indicate lower amplitude.

Circular phase plots (sine fit)

Circular phase plots were generated based on sine-fit estimates of wavelet detrended time series using the midpoint of 2-day sliding windows. Custom MATLAB scripts integrated the WMTSA wavelet Toolkit (C. Cornish, U. of Washington, WA) for application of a discrete wavelet transform to all data sets. These plots show the phases of individual oscillators categorized by neuronal subgroup as well as for "all cells" (combined across all subgroups from 12 brains). The circular plots display phases in terms of CT, with CT 0 set equal to the overall mean phase of "all cells" for Day 1. The inner circle shows the alpha = 0.05 threshold for the resultant vector for the Rayleigh test. The null hypothesis is that phases are uniformly distributed. If the resultant vector ends outside the inner circle then the phase distribution is significantly different from the uniform distribution. The absence of plots for certain time points indicates that the rhythmicity of neurons in that subgroup at that time point was too dampened for reliable

sine-fit measures (i.e. did not meet the criteria for “reliably rhythmic cells”). Oscillators were deemed reliably rhythmic if their good-of-sine-fit was greater than a threshold value of 0.82, their period was between 18h and 30h, and their amplitude was at least 1.5, as described in (Roberts et al., 2015).

Validation of sine-fit estimates

To verify that single oscillator phases were reliably extracted through sine-fits of the wavelet detrended time series, circular phase plots were also generated using a time delay embedding method. Briefly, the time series were embedded in a higher dimension via lagging by 6 hours so that oscillations circle the origin; see *Nonlinear Time Series Analysis 2nd Edition* by H. Kantz and T. Schreiber (Cambridge University Press, 2003) for details on time delay embedding. The polar angle was then used as a phase estimate. As with the sine-fit estimates, phases are displayed in terms of CT, with CT 0 set equal to the overall mean phase of “all cells” for Day 1. Phase plots generated using 2-dimensional embedded phase analysis showed the same patterns of oscillator activity as plots generated using sine-fit estimates. MATLAB scripts were used to calculate the correlation coefficients (rho) and p-values between the time delay embedding estimates and the sine-fit phase estimates across all neuronal subgroups for all time points and conditions. The p-value is based on the null hypothesis that there is no correlation in phase estimates between these two methods. The strong positive, linear correlation (indicated by high rho values) and low p-values in Table S3.1 confirm that sine-fit estimates of phase using two-day sliding windows are sufficiently reliable and consistent. The same neurons were analyzed for both methods for corresponding time points, subgroups, and conditions.

Calculation of order parameter

To quantify changes in synchrony over time, we use the order parameter *R*, defined as in (Gonze et al., 2005) for a system of *N* oscillators with state variable *X*:

$$R = \frac{\langle X^2 \rangle - \langle X \rangle^2}{\frac{1}{N}\sum_{k=1}^{N}\left(\langle {X_k}^2 \rangle - \langle X_k \rangle^2\right)},$$

where angle brackets denote time average and $X = \frac{1}{N}\sum_{k=1}^{N} X_k$. If the phase, period and waveform of all *N* cells are in perfect synchrony then *R*=1, while a uniform distribution of phases would lead to *R*=0.

Phase ensemble animations

Custom MATLAB scripts were used to generate phase ensemble animations based on bioluminescence experimental data comparing changes in phase and amplitude over time among oscillators of brain explants either maintained in constant darkness or exposed to a phase advancing white light pulse as described (Roberts et al., 2015). The phase of each oscillator is represented by the polar angle of the disks, whereas amplitude is indicated by the radial distance of the disks from the center of the circle (drift towards the center indicates damping amplitude). The animations were generated using custom MATLAB scripts with estimates of phase and amplitude calculated using 2-dimensional embedding applied to wavelet-detrended traces. Phase and amplitude dynamics are shown at three levels of resolution: single neuron oscillators (Movie 3.1), individual neuronal subgroups (Movie 3.2), and whole network (Movie 3.3).

Model simulations

Mathematical modeling was performed using custom MATLAB scripts to explore the qualitative emergent dynamic behaviors of a network composed of different oscillator types, based on current knowledge of what we expect to be present in the *Drosophila* circadian network. This model provides a simplified negative feedback loop, roughly mimicking that of the circadian transcriptional-translational feedback loop, while remaining simple enough for an exact stability analysis (Tyson 2002). The model is built on three types of oscillators with distinct types of signaling, light responses, and degrees of dampening. However, they are not meant to specifically represent particular neuronal subgroups or neurotransmitters. The main premise is to demonstrate through a relatively simple model how different dynamic signatures could be generated and how these could be advantageous to the circadian system.

Each oscillator is simulated using a modified version of the Goodwin model (Bliss et al., 1982; Tyson, 2002) which consists of three differential equations forming a negative feedback loop:

$$\frac{dX}{dt} = \frac{a(1 + k_{act} - k_{rep})}{Z + 1} - bX \quad (1)$$

$$\frac{dY}{dt} = bX - bY \quad (2)$$

$$\frac{dZ}{dt} = bY - \frac{cZ}{Z + 1} \quad (3)$$

The parameters are set so that oscillations dampen toward steady state values over time (see Table 3.1):

$$X_{ss} = Y_{ss} = \frac{a}{b(1+a/c)} \text{ and } Z_{ss} = \frac{a}{c}.$$

Although the individual oscillators are damped, the coupled system described below generates sustained oscillations for β>0.03 under constant conditions, and also entrains to light-dark cycles. See Fig. M3.1-4 in the Mathematical Modeling Supplement.

	s	*a*	*b*	*c*	β
Group 1	0.98±0.005	(9*s*-1)*c*	0.149-0.1535	81*bs*^{2}	0.035±0.007
Group 2	0.98±0.005	(9*s*-1)*c*	0.1525-0.157	81*bs*^{2}	0.035±0.007
Group 3	0.88±0.005	(9*s*-1)*c*	0.149-0.157	81*bs*^{2}	0.175±0.035

Table 3.1. Parameter values for Goodwin model. The model generates self-sustained oscillations in individual oscillators if *s*>1 and damped oscillations if *s*<1 (with smaller *s* leading to faster damping). To create heterogeneity in the oscillator groups, values of *s* and β are normally distributed random numbers with the indicated mean and standard deviation, while values for *b* are evenly distributed in the indicated range for each group (not random). Parameters *a* and *c* are fixed functions of *s* and *b*; see (Tyson, 2002) for the derivation of these relations via a linear stability analysis. Group 3 needs a stronger coupling signal to maintain rhythmicity, due to its low value of *s* (strongly damped).

To explore the dynamic interactions of damped oscillators with different properties, we created a network of 60 Goodwin oscillators organized into 3 groups. “Group 1” oscillators (10 total, #1-10) are directly light responsive, weakly damped, and send an activating coupling signal that effectively increases the transcription rate *a* of all oscillators when the Group 1 oscillators have *X* levels above the theoretical steady state value X_{ss}. “Group 2” oscillators (10 total, #11-20) are more strongly light responsive, weakly damped, and transmit a repressing coupling signal that effectively decreases the transcription rate *a* of all oscillators when the Group 2 oscillators have *Z* levels above the steady state value Z_{ss}. These coupling functions were chosen to appropriately time the signals to promote synchronization. In both cases, higher amplitude oscillations lead to

stronger coupling. “Group 3” oscillators (40 total, #21-60) are not directly light responsive, strongly damped, and send a repressing coupling signal similar to that of Group 2.

Light response is achieved through increasing the degradation rate parameter *c* in equation (3). Both LD entrainment and response to light pulses can be effectively modeled through this mechanism. For example, a light pulse simulated by increasing *c* by 8% for Group 1 oscillators and by 16% for Group 2 oscillators for 4 hours starting 3 hours before the peak in mean *X* results in a large phase advance of nearly 9h for the coupled system. LD entrainment can be simulated by increasing *c* by 0.4% for Group 1 oscillators and by 0.8% for Group 2 oscillators for the first 10h of each 24h day.

Coupling is achieved through modifying the transcription rate parameter *a* as indicated in equation (1). Two complementary types are used for the modeling: k_{act} increases transcriptional activation while k_{rep} represses transcription in equation (1):

$$k_{act} = \frac{\beta}{10}\sum_{n=1}^{10}\frac{\max(X_n - X_{ss}, 0)}{X_{ss} + \max(X_n - X_{ss}, 0)},$$

$$k_{rep} = \frac{\beta}{50}\sum_{n=11}^{60}\frac{\max(Z_n - Z_{ss}, 0)}{Z_{ss} + \max(Z_n - Z_{ss}, 0)}.$$

All oscillators receive both types of coupling signals, but each group sends a single type of coupling signal. Note that in the alternate simulations where only one type of coupling is used, then all 3 groups send the indicated type of signal (activating or repressing). See the Mathematical Modeling Supplement for further details.

3.3 Results

3.3.1 *Drosophila* circadian neuronal subgroups exhibit distinct dynamic signatures in constant darkness and in response to a phase advancing light pulse

A longstanding question in circadian biology has been to discern which aspects of circadian rhythm dynamics and light entrainment are due to the relative contributions of cell autonomous and network properties (Liu et al., 2007; Sheeba, 2008; Wang et al., 2008; Yan et al., 2007). Real-time bioluminescence recordings have previously shown that oscillators in cultured *XLG-Per-Luc* whole brain explants maintained in constant darkness exhibit a monotonic decrease in amplitude and synchrony (Fig. 3.1A, Supp. Fig. 3.1) (Roberts et al., 2015). In contrast, perturbation of neuronal subgroups with a 12.57 W/m^2 (2,000 lux) 15 minute phase advancing white light pulse evokes transient loss of synchrony and amplitude with subsequent recovery of phase-shifted synchrony over time through the process of "phase retuning" (Fig. 3.1A). The heterogeneity of phase, period, amplitude, synchrony and light response for each of the neuronal subgroups is qualitatively apparent in raster heat map plots based on bioluminescence reporting of *period* activity (Fig. 3.1B). However, questions remain concerning how such a heterogeneous system may arise and how it may be advantageous for circadian behavior and entrainment.

3.3.2 *Drosophila* heterogeneous circadian neural networks are robust but flexible

Cellular circadian oscillators found in the *Drosophila* circadian network and the mammalian suprachiasmatic nucleus (SCN) are known to exhibit a wide range of periods, phases, amplitudes and signaling properties (Peng et al., 2003; Quintero et al., 2003; Schaap et al., 2003; Yamaguchi et al., 2003). To increase our understanding of the roles

played by different components of the circadian network, we examined how phase relationships are transiently altered during environmental adaptation. As a basis for comparison, we first observed phase relationships under constant conditions by performing quantified spatiotemporal mapping of single oscillator phase dynamics using sine-fit phase estimates for cultured adult *Drosophila* whole brain explants maintained in constant darkness (DD) for 6 days (Roberts et al., 2015). The results indicate that circadian networks consisting of oscillators with a wide range of intrinsic phases and periods are still capable of maintaining consistent mean network phase and robust phase synchrony as shown by the phase angle at or very close to CT0 over time in the absence of perturbation by environmental cues (Fig. 3.2A, Top Row). This remarkably consistent network phase relationship is highly robust in the whole brain preparation as show by little deviation of the phase vector angle for all oscillators from CT 0 over multiple days. However, the circadian neural network is also capable of a strong response when stimulated with a 15 minute phase advancing light pulse (LP) at CT 22 of the second day in DD, which evokes transient phase dispersion followed by resynchronization of phase-shifted oscillators (Fig. 3.2A, Bottom Row).

To examine the emergent roles of individual neuronal subgroups, we compared subgroups' mean phases and amplitudes in Figure 3.2B. Neuronal subgroups as a whole are considered to have significant desynchrony or damped amplitude at any time point if the mean output phase cannot be measured. This is qualitatively apparent by the absence of a color-coded disc representing a subgroup's mean phase because no phase estimates can be reliably calculated as the phase coherence and/or amplitude is too low (Fig. 3.2B). In this study, we describe oscillators as "weak" or "strong" based on the

robustness of their free-running activity in DD. As the s-LNvs and LNds are the only neuronal subgroups to exhibit robust phase coherence throughout recordings, they are considered stronger neuronal subgroups (Fig. 3.2B). Conversely, the DN3s, DN1s and l-LNvs are considered weaker oscillators as they exhibit significant desynchrony and/or damped amplitude by the end of the recordings in DD. By comparing inter-neuronal subgroup dynamics, we observe that the s-LNvs are the only subgroup to maintain a robust and consistent mean phase near CT 0 throughout the recordings. Interestingly, the s-LNvs exhibit the most rapid phase dispersion and damped amplitude in response to the phase advancing light pulse. Another pivotal subgroup is the LNds, the only subgroup to maintain phase coherence and exhibit a high fidelity rapid phase shift of 2 hours (Supp. Fig. 3.2) by Day 3 after the LP. This quantified analysis shows that the LNds did not just begin to shift on Day 3, which is observed to a lesser extent in the DN3s and s-LNvs, but immediately achieved the large final phase shift. This provides evidence that the LNds are not just first responders, but likely have a more important role in pulling the network to the new phase state. Conversely, the amplitude and phase coherence of all other subgroups are transiently suppressed following the light pulse. Snapshots of animations of bioluminescence experimental data from Movie 3.1 of single oscillator phase ensembles over time are shown to demonstrate the complexity and diverse range of oscillator activities in DD and in response to the LP (Fig. 3.2C). In order to more clearly compare complex cell autonomous and whole network dynamics in DD and in response to a phase advancing light pulse, we generated dynamic movie animations of oscillator phase ensembles based on quantified bioluminescence data at three degrees of resolution: single neuron (Movie 3.1, discs color coded by neuronal subgroup), individual

neuronal subgroup (Movie 3.2, discs color coded by neuronal subgroup), and whole network average (Movie 3.3). These movies convey the complexity of quantified circadian oscillators' dynamics and allow for clearer simultaneous, longitudinal comparisons of circadian network activity. Movie 3.1, showing single oscillator resolution, demonstrates how oscillator dynamics within and between subgroups would be practically impossible to discern using the standard static measures such as immunocytochemistry. These results motivated us to map the complex phase dynamics and explore their potential impacts on endogenous rhythms and response to light cues.

3.3.3 Quantification of neuron subgroups' phases in constant darkness reveals complementary inter-subgroup free-running phase dynamics

Studies suggest that dynamic changes in phase relationships and synchrony among autonomous oscillators distributed throughout a circadian circuit can generate distinct physiological outputs such as seasonal adaption (Coomans et al., 2015; Inagaki et al., 2007; Stoleru et al., 2007). By quantifying individual oscillator phase and overall subgroup phase coherence, we mapped the distinct dynamic signatures of neuron subgroups in whole brain explants maintained in constant darkness (Fig. 3.3). As previously described, most subgroups exhibit a monotonic decrease in rhythmic strength and phase coherence over time in DD (Roberts et al., 2015). We observe that the s-LNvs, which are considered the core pacemaker neurons (Helfrich-Förster, 2003; Shafer et al., 2002; Yang and Sehgal, 2001), appear to have the most strongly coherent and consistent phases in DD relative to other subgroups (Fig. 3.3). More importantly, the s-LNvs are the only subgroup that exhibits a robust and consistent mean phase with a phase angle very close to CT 0 that approximates the overall network's mean phase over time (compare

Movies 3.2 and 3.3). This indicates that the s-LNvs may have a predominant role in maintaining free-running rhythms over time in DD. Similarly, weaker oscillators such as the DN1s and DN3s exhibit relatively consistent mean phases with phase angles very close to CT 0 but relatively greater phase dispersion than the s-LNv after 3-4 days in DD. Intriguingly, the l-LNvs and LNds exhibit coherent but nearly opposite phase relationships over time so that the mean network phase is still consistently maintained near CT 0. The consistency of the overall mean network phase remains robust in spite of the increased spread of single oscillators' phases over time, suggesting that even free-running activity is not merely stochastic but remains measurably coordinated at the network level. The next step was to observe how these relationships might change following the application of a phase advancing light pulse to *Drosophila* whole brain explants.

3.3.4 A light-evoked phase shift pushes most oscillators towards quantitative transient desynchrony and damped amplitude before the network adopts a new state of phase-shifted synchrony

The physiological importance of robust, coordinated and consistent circadian oscillations has long been recognized. However, recent studies and models have revealed that more complex dynamics of synchrony and single oscillator activities may underlie circadian adaptations to events such as seasons, travel across time zones, and shift work (An et al., 2013; Coomans et al., 2015; Leise and Siegelmann, 2006; Muraro et al., 2013; Roberts et al., 2015; Schaap et al., 2003; Stoleru et al., 2007). To examine the response of the circadian network to light more closely, we measured the intricate spatiotemporal phase dynamics of individual oscillator responses to a phase advancing light pulse (Fig. 3.4). Intriguingly, the strong s-LNvs, which exhibit the most robust

rhythms over time in DD, conversely exhibit the most rapid phase dispersion following the LP on day 2 and do not recover significant phase coherence until day 4. However, it should be noted the mean phase shift achieved by the s-LNvs on day 5 most closely approximates the final mean phase shift achieved by the overall network (compare Fig. 3.2A to Fig. 3.4). In contrast, oscillators which exhibit generally weaker free-running oscillations, such as the DN3s and DN1s, maintain relatively greater intra-subgroup phase coherence immediately following the light pulse on Day 2 but exhibit significant loss of phase coherence by day 3. The DN3s do not express Cry and are thus not directly photosensitive. However, the DN3s exhibit a more immediate mean phase advance compared to the stronger s-LNvs. The small but immediate light-evoked phase shift observed in the "light blind" DN3s indicates that the neural connections in the organotypic whole brain explants are still sufficiently intact for communication from the Cry-expressing circadian neurons. However, it should be noted that the DN3s also exhibit the smallest mean phase shift by the end of the recordings. As observed in DD, the l-LNvs and LNds exhibit a seemingly complementary relationship in which the l-LNvs show significant dampening of rhythmicity by Day 3 following the light pulse, whereas the LNds show an increase in phase coherence by Day 3 following the light pulse (Supp. Figs. 3.2 and 3.3). The LNds are the first subgroup to complete the phase shift, achieving a large phase advance by Day 3 (Fig. 3.4, Supp. Fig. 3.3).

To verify that single oscillator phases were reliably extracted though sine-fit estimates of wavelet detrended time series, we also calculated oscillator phases in DD (Supp. Figs. 3.4 and 3.5) and in response to the LP (Supp. Fig. 3.6) using a 2-dimensional time delay embedding method (see Supplemental Information for details). The strong,

positive correlation in phase estimates between the sine-fit and time delay embedding phase methods confirms that quantified trends of dynamic oscillator activity in both light conditions and across all subgroups are reliable and consistent (Supp. Table 3.1). The complex and distinct dynamics exhibited by these neuronal subgroups motivated us to use mathematical modeling to explore what network and oscillator properties may generate these dynamics and the potential benefits.

3.3.5 Mathematical modeling of circadian network dynamics demonstrates potential benefits of complementary coupling and a mix of strong and weak oscillators

To study the key features leading to the complex emergent dynamics observed in the experimental oscillator relationships, we developed a relatively simple mathematical model of a coupled network of 60 oscillators based on a modified Goodwin model (Tyson, 2002). The oscillators are divided into three groups with differing light responses, inhibitory versus excitatory coupling signal, and oscillator damping rate. These features are based on our current ideas about qualitative features of the *Drosophila* circadian circuit guided by the literature (Collins et al., 2014; Dissel et al., 2014; Yao and Shafer, 2014) and our own experimental data. “Group 1” oscillators (10 total) are moderately light responsive, weakly damped, and send a phased coupling signal that effectively increases the transcription rate of all oscillators. “Group 2” oscillators (10 total) are strongly light responsive, weakly damped, and transmit a coupling signal that effectively decreases the transcription rate of all oscillators. The timing of the activating and repressing coupling signals were chosen to be nearly antiphase to each other in order to promote synchronization. “Group 3” oscillators (40 total) are not light responsive, are strongly

damped, and send a repressing coupling signal similar to that of Group 2. See the Methods and the Mathematical Modeling Supplement for a complete description of the model. Note that the model is not meant to directly represent particular neuronal subgroups or neurotransmitters, as we lack sufficient knowledge to create a detailed model at this time. The model simulations reproduce many of the general emergent patterns of free-running behavior and light response observed in our empirical data (Fig. 3.5A-C). In DD simulations, we observe a monotonic decrease in amplitude and synchrony for all groups, with the Group 1 oscillators maintaining relatively high amplitude, synchronous oscillations in the absence of perturbations. In contrast, a simulated phase advancing light pulse transiently suppresses the amplitudes and scrambles the phases of oscillators in Groups 1 and 3, followed by a delayed recovery and strengthening of both amplitude and phase coherence relative to corresponding oscillators in the DD condition. Note that Group 2 oscillators display an immediate increase in amplitude and phase synchrony in response to the light pulse and push the network towards a new state of phase-shifted synchrony.

To explore the potential benefits of complementary coupling, we also performed simulations with “activating only” coupling, in which all oscillators send coupling signals that increase transcription, and “repressing only” coupling, in which all oscillators send coupling signals that decrease transcription (Fig. 3.5D-E). The equations and parameters for these contrasting models are identical apart from the differences in coupling. “Activating only” coupling results in a lower order parameter *R* and reduced magnitude of phase shifts as shown on the simulated phase response curve (Fig. 3.5D) and also a reduced phase advance in response to the 4h light pulse (Fig. M3.5-6 in the Mathematical

Modeling Supplement). Furthermore, these oscillators have a longer overall period of 24.3 hours in DD compared to a period of 23.9 hours in DD for the mixed coupling model (Fig. 3.5E). On the other hand, “repressing only” coupling results in a slightly shorter overall period of 23.7 hours in DD and somewhat larger phase shifts (Fig. 3.5DE; see also Fig. M3.3 in the Mathematical Modeling Supplement). Furthermore, the “repressing only” coupling can be less stable in terms of greatly increased responses to light pulses if the coupling strength is decreased, compared to the cases of “activating only” and mixed coupling (Fig. M3.9-11 in the Mathematical Modeling Supplement). One benefit of the complementary coupling mechanisms is that increasing the coupling strength minimally effects the system’s period while greatly increasing the overall synchronization and amplitude, as shown in Figs. M3.3-4. This allows for adaptive changes in phase coherence and amplitude with only slight changes to the period. The period itself may be adjusted by altering the balance between activating and repressing coupling, which tend to respectively lengthen and shorten the period.

As shown in Figs. M3.12-15 in the Mathematical Modeling Supplement, the system exhibits a higher order parameter *R* when the system contains both weaker and stronger oscillators (indicating that the system is more easily synchronized), and the weaker oscillators are also necessary for the advancing light pulse to cause a transient dip in *R* followed by an overshoot. However, too great of a damping rate in the weaker oscillators will reduce the overall coherence of the system, as shown in Fig. M3.16. Thus, the presence of both stronger and weaker oscillators appears to play a key role in the dynamics of the system.

3.4 Discussion

The present study combines *ex vivo* experimental bioluminescence data with *in silico* model simulations to provide evidence for how circadian networks with a mix of strong and weak oscillators and complementary coupling mechanisms may contribute to robust yet responsive oscillations. Due to an increasing awareness of the detrimental effects of chronodisruption by common environmental events and features such as jet lag, shift work, and late night screen viewing time, numerous investigators have examined the importance of consistent and synchronized rhythms (Colwell et al., 2003; Yamaguchi et al., 2003). However, recent studies have shown that desynchrony is not always pathological and even varies between seasons (An et al., 2013; Coomans et al., 2015; Hastings et al., 2014; Herzog et al., 2004; Roberts et al., 2015; Schaap et al., 2003; Stoleru et al., 2007). Using custom analysis of real-time bioluminescence datasets, we show the first detailed spatiotemporal mapping of dynamic phase relationships within an entire circadian neural circuit, at single neuron resolution, both in DD and in response to a light pulse. The complexity of multiday single oscillator phase dynamics revealed here underlines the difficulty in understanding biological clocks by cross-sectional methods such as immunocytochemistry or acute electrophysiology, and the importance of longitudinal analysis of single-cell circadian rhythms by methods such as whole brain bioluminescence imaging.

Accordingly, we endeavored to quantify and map the spatiotemporal dynamics of oscillators in whole *Drosophila* brain explants either maintained in constant darkness (DD) or exposed to a phase advancing light pulse (LP). Although recent studies have further subdivided the *Drosophila* circadian circuit based on neuropeptide or genetic markers (An

et al., 2013; Collins et al., 2012; Gonze et al., 2005; Nitabach and Taghert, 2008; Veleri et al., 2003; Zhang and Kay, 2010; Zhang et al., 2010a), analysis in this study was limited to the classical anatomically recognized s-LNv, l-LNv, LNd, DN1 and DN3 subgroups. Future studies will functionally dissect further subdivisions of the circuit. Numerous studies have investigated how the intrinsic and heterogeneous activities of autonomous single-cell oscillators distributed throughout circadian circuits map to daily behavioral rhythms and entrainment. Sub-regions of the SCN have been shown to have a diverse range of periods, phases, and dynamics of light response (Evans et al., 2011; Foley et al., 2011). In this study, we confirm that, even in the absence of perturbation by external cues, different components of the *Drosophila* circadian circuit display a wide range of intrinsic oscillator phases, periods, and phase coherence. Interestingly, the heterogeneous circadian oscillators have complementary activities in whole brain explants maintained in DD so that the network has a whole still exhibits a remarkably robust and consistent overall mean phase over time in spite of the increase spread in oscillators' periods and phases over time. This indicates that the activity of these heterogeneous groups does not merely become stochastic in DD, but that their phases remain coordinated to some extent. The stability and coherence of oscillator phases over time in DD also further supports the robustness and utility of cultured *XLG-Per-Luc* whole brain explants. We observe that the s-LNvs, which exhibit strongly consistent and coherent free-running rhythms, have a mean phase that most closely matches the overall network mean phase for all 6 days of recording. Though the weaker DN1s and DN3s also show a relatively consistent mean phase over time, they exhibit more rapid damping of amplitude and phase dispersion over time. The LNds and l-LNvs also exhibit coherent

phases over time in DD but do not maintain a consistent mean phase near CT 0. This supports previous studies indicating that the s-LNvs have key roles as pacemaker neurons (Helfrich-Förster, 2003; Shafer et al., 2002; Yang and Sehgal, 2001). However, the mean phase of the circuit as a whole also appears to be generated by the complementary dynamics of the fast-paced (<24 hour period) l-LNvs and slow-paced (>24 hour period) LNds. Although these subgroups both exhibit significant and coherent phase drift in DD, the network mean phase is maintained due to the nearly exact mirroring of their opposite phase drifts over time. The complementary activities of the l-LNvs and LNds agree with previous findings of slow-paced and fast-paced oscillators (Dissel et al., 2014). This is intriguing, as these two subgroups also appear to have complementary responses to a phase-advancing light pulse, in which the LNds exhibit an immediate increase in amplitude and phase coherence whereas the l-LNvs show an immediate decrease in amplitude and phase coherence. The complementary activities of the LNds and l-LNvs in DD and in response to a phase advancing light pulse suggest that the l-LNvs and LNds may play unique roles in circadian network responses to cues of different phases. We also emphasize the potential roles of the weaker DN1s and DN3s which recover synchrony much more quickly than the stronger s-LNvs following exposure to the light pulse. This agrees with previous work indicating that weaker oscillators can adjust their phase more readily and enhance resynchrony (Webb et al., 2012). These findings suggest that certain cells may intrinsically maintain more stable phases for supporting robust free-running circadian rhythms, whereas more weakly circadian cells may have faster or slower intrinsic rhythms to enable more flexible adaptation to environmental changes.

The dual importance of the strength of circadian rhythms along with plasticity of circadian networks to enable adaptation to various environmental cues is a critical feature. By combining single-cell phase dynamic analysis of *ex vivo* whole circuit bioluminescence experimental data with computational modeling of emergent network dynamics, we provide evidence that transiently desynchronizing and damping most oscillators in a neural network may actually be a key feature for facilitating entrainment by light for the whole circuit. We postulate that a phase advancing light pulse at CT 22 scrambles most oscillators' phases and suppresses amplitudes so that stronger oscillators such as the LNds, which exhibit an increase in phase coherence and amplitude, can lead the rest of the transiently weakened network towards a new state of phase-shifted synchrony. Although altering oscillators' phase coherence or amplitudes may have different downstream consequences, we observe that dynamic changes in coherence and amplitude appear to coincide in response to the phase advancing light pulse. This is also important for the mammalian SCN for which the phase and amplitude of coupling for both damped and sustained oscillators have been shown to be critical for synchrony and entrainment (Ananthasubramaniam et al., 2014). Thus, there is considerable experimental precedent for this coupling paradigm in circadian models.

In both the DD and LP conditions, we observe that there is always at least one group of strong oscillators, such as the s-LNvs and LNds, which appear to contribute to maintaining robust network mean phase over time. We previously showed that the LNds have an unexplained increase in phase coherence by the end of the recording following a phase advancing light pulse (Roberts et al., 2016). However, our new analysis here shows that the LNds exhibit an immediate increase in phase coherence and amplitude

following the LP that coincides with their phase advance. Our mathematical modeling suggests that this increase in amplitude may be critical for shifting the rest of the network into a new advanced phase. Although the LNds exhibit the most immediate phase shift and increase in amplitude followed the LP, we note that the phase shift achieved by the s-LNvs on Day 5 most closely approximates the mean network phase shift on Day 5. This suggests that although the LNds appear to lead the phase shift, the new state of phase-shifted network synchrony is not achieved for behavioral output until the s-LNvs have achieved their final coherent phase shift. This indicates that both these strong oscillator groups may have distinct contributions for the emergent behavioral output in response to the phase advancing light pulse. Though the weaker DN1s and DN3s maintained relatively consistent, but less coherent mean phase in DD, a phase advancing light pulse appears to transiently desynchronize and dampen their rhythms so that strong oscillators can drive the network toward the new state of phase shifted synchrony. We observe that the DN3s, which are not directly light-sensitive, show a more immediate coherent phase shift than any other subgroup except the LNds. However, the DN3s subsequently exhibit the most gradual phase shift that does not reach the mean network phase shift by the end of the recordings. These findings support previous studies indicating that transiently weakening oscillator coupling and rhythmicity may enable circuits to more easily adapt to phase shifts, whereas networks that are too rigid and fixed may have reduced entrainment capacities (An et al., 2013; Freeman et al., 2013; Hatori et al., 2014; Lamba et al., 2014; Roberts et al., 2015; Tsumoto et al., 2011; Webb et al., 2012; Yamaguchi et al., 2013).

Our computational modeling allowed us to explore the potential roles of complementary coupling mechanisms in producing the key features of the distinct

dynamic signatures observed in our experimental imaging. Although this is a relatively simple model derived from general circadian trends observed in previous literature and our own experimental data, previous studies have shown that varying just a few key parameters can reproduce experimentally observed circadian features (Tokuda et al., 2005). Our model simulations demonstrate how a complementary system of mixed signaling may enable robust but flexible period length, amplitude, synchrony and capacity for large phase shifts. These simulations agree with previous experimental and modeling studies which showed that complementary excitatory and inhibitory interactions between faster-paced and slower-paced neuronal oscillators allow for fine-tuning of emergent period and phase (DeWoskin et al., 2015; Dissel et al., 2014; Stoleru et al., 2007; Yao and Shafer, 2014). Our modeling also suggests that adjusting the balance between coupling types may enable either more robust rhythms or greater network adaptability to environmental cues.

By combining quantitative single oscillator phase dynamics analysis of *ex vivo* whole circuit bioluminescence experimental data with mathematical modeling of complementary oscillator types, we provide evidence that stronger circadian neurons contribute to maintaining robust rhythms whereas weaker oscillators confer the flexibility to respond to environmental cues by large phase advances. However, it is still unclear how the complex phase relationships found among oscillators across and even within neuronal subgroups precisely map to circadian behavior and entrainment. Further research is also necessary to assess the precise interplay of neurochemical and/or gene signaling during a light-evoked phase shift that increases the amplitude of certain oscillators such as the LNds but may push other oscillators toward a transient state of

desynchrony and damped amplitude. Future studies may incorporate pharmacological and genetic targeting of network coupling between stronger and weaker oscillators to explore how this dynamic process may be induced, amplified, and harnessed to treat conditions such as jet lag, shift work and seasonal affective disorder.

3.5 Figures

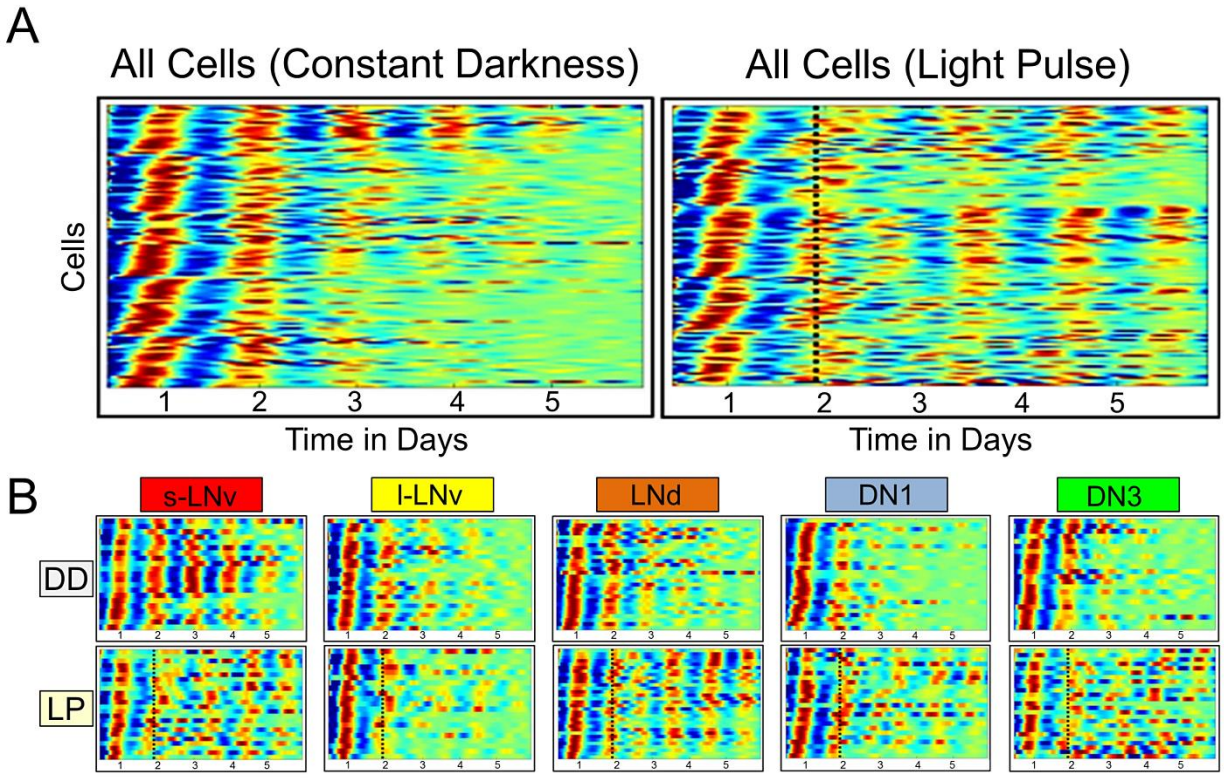

Figure 3.1. Circadian neurons of cultured whole brain explants exhibit distinct dynamic signatures in constant darkness and when exposed to a phase advancing light pulse. Pseudo-heat maps of individual oscillator *XLG-Per-Luc* expression over time are provided for **A:** 'all cells' (combined across 12 brains per condition) and **B:** each neuronal subgroup. Warmer colors indicate higher amplitude whereas cooler colors indicate lower amplitude of rhythmic *Per* expression. **A (Left):** Cells in DD (n=122) exhibit a wide range of free-running phases with decreasing phase coherence over time. **A (Right):** Cells (n=126) exposed to a 15 min 12.57 W/m^2 white light pulse (LP) at CT 22 on the second day in DD (indicated by dotted black line) generally exhibit a transient reduction in phase coherence and amplitude followed by a phase shift and gradual recovery of phase coherence and amplitude over time. **B (Top**): L-LNvs (n=25), LNds (n=28), DN1s (n=26), and DN3s (n=22) in DD generally exhibit a loss of phase coherence and amplitude over time to varying degrees with the s-LNvs (n=21) exhibiting the most consistent and robust phase coherence. **B (Bottom**): S-LNvs (n=24), l-LNvs (n=25), DN1s (n=26), and DN3s (n=22) exposed to the LP exhibit distinct dynamic signatures of transient loss followed by delayed recovery of phase-shifted oscillator synchrony (phase retuning) and amplitude following the LP. Note that the LNds (n=28) appear to exhibit relatively consistent phase coherence and amplitude following the LP, as well as the most rapid phase shift. Raster plots were generated using MATLAB scripts analyzing bioluminescence data reported previously (Roberts et al., 2015).

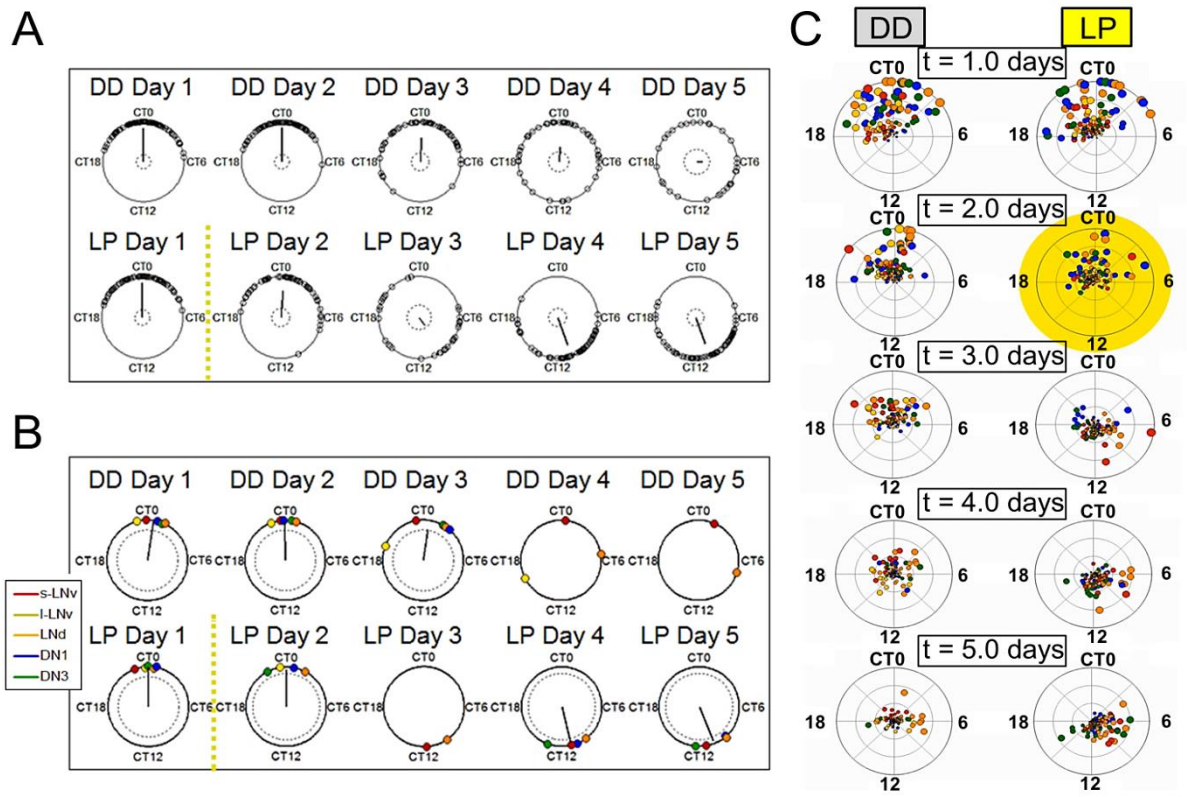

Figure 3.2. *Drosophila* circadian neural networks show significant differences in inter- and intra-subgroup dynamics in constant darkness and in response to a phase-advancing light pulse. Circular plots of sine-fit phase estimates using the midpoint of 2-day sliding windows are shown for **A:** individual phases of 'all cells' (combined across all neuronal subgroups from 12 brains) and **B:** phases taken from the mean trace of each neuronal subgroup in **(A, B Top)** constant darkness (DD) and **(A, B Bottom)** following the phase advancing light pulse (LP). The phase angles are shown for s-LNvs (red), l-LNvs (yellow), LNds (orange), DN1s (blue), and DN3s (green). A yellow dotted line divides the general time frames of pre-LP and post-LP exposure. If the resultant vectors end outside of the inner circles (representing the **α** =0.05 threshold for each Rayleigh test; test is not run if there are fewer than 4 rhythmic subgroups), then the phases are significantly concentrated around the mean phase. The null hypothesis is that the phases are uniformly distributed. In **2B**, the mean phases for neuronal subgroups were excluded at certain time points if the subgroup: (1) did not have any reliably rhythmic cells at that time point or (2) did not have sufficient phase coherence to provide a reliable mean phase estimate. **C:** Snapshots of selected time points from **Movie 3.1** showing changes in single oscillator phase and amplitude over time in DD (left) and in response to the LP (right). The LP is represented by a yellow highlight on day two. The disks representing each of the subgroups are colored the same as previous figures. The angle of the disks around the circle represents phase and the distance of the disks from the center represents amplitude. Phase and amplitude were estimated using 2-dimensional embedding applied to wavelet detrended traces for each individual oscillator. Circular phase plots were generated using MATLAB scripts. See 'Experimental Procedures' for details.

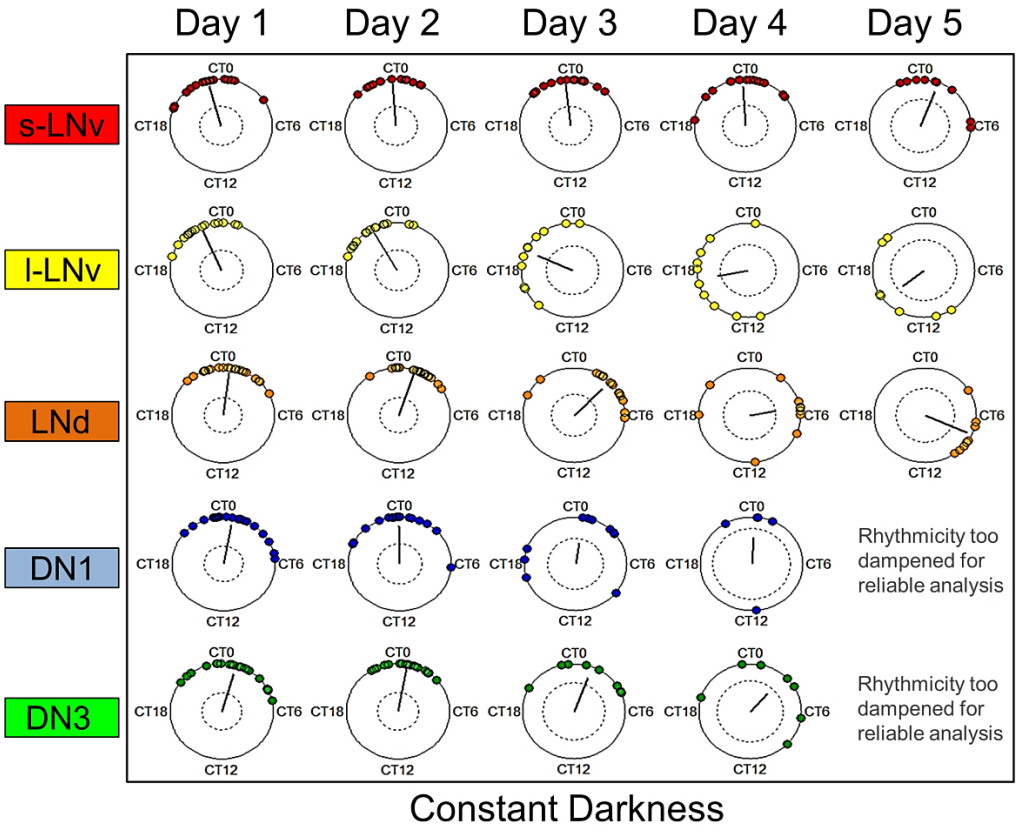

Figure 3.3. Quantification of neuron subgroups' dynamics in constant darkness reveals distinct differences in phases, periods, and degrees of phase dispersion over time. Phases of individual oscillators categorized by neuronal subgroup are shown in circular plots based on sine-fit phase estimates using the midpoint of 2-day sliding windows. To compare relative phase shifts over time, phases were normalized such that overall mean phase for Day 1 for 'all cells' is circadian time 0 (CT 0). Neuronal subgroups in DD reveal a wide range of phases and periods and generally exhibit gradual phase dispersion over time; with the notable exception of the s-LNvs. If the resultant vectors end outside the inner circles, then the phase distribution significantly differs from the uniform distribution. The absence of plots for certain time points indicates that rhythmicity for all oscillators was too damped for reliable sine-fit measures.

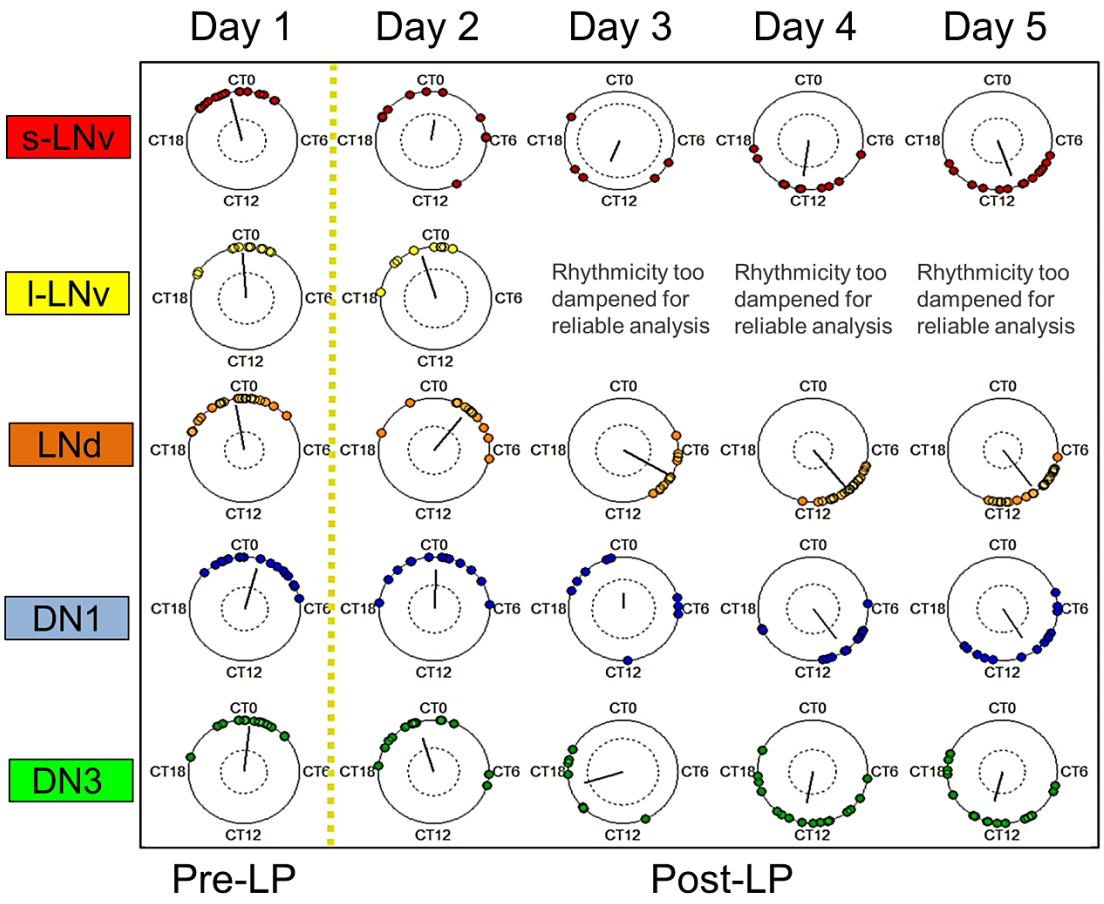

Figure 3.4. Neuronal subgroups exposed to a phase-advancing light pulse exhibit distinct dynamics of loss and recovery of phase-shifted synchronous oscillations. Circular phase plots reveal distinct neuronal subgroups' dynamics of phase response to a light pulse (the yellow dotted line divides the general time frames of pre-LP and post-LP exposure). Neuronal subgroups generally exhibit significant phase dispersion following exposure to the LP, with the exception of the LNds and DN3s. Relative to corresponding subgroups in DD, neuronal subgroups also generally exhibit significantly greater phase coherence and a shift in mean phase 3-4 days after the light pulse. The inner circles represent the **α** =0.05 threshold for each Rayleigh test, with the null hypothesis that phases are uniformly distributed.

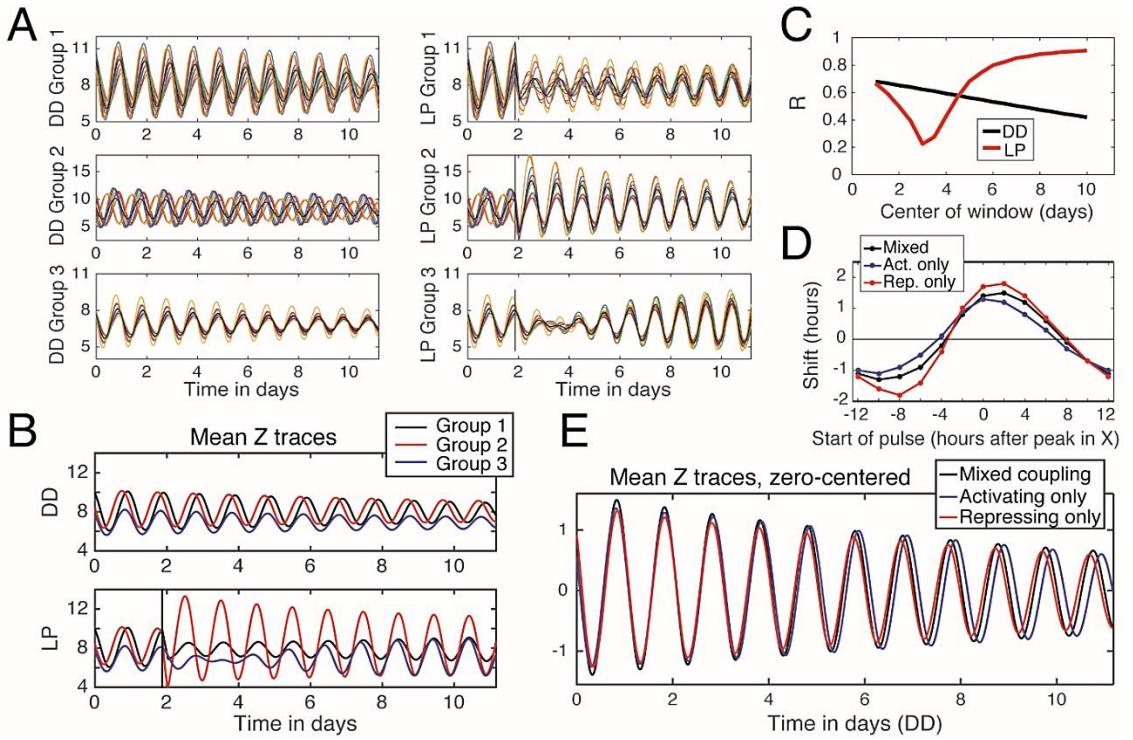

Figure 3.5. Mathematical modeling of circadian network dynamics indicates importance of complementary coupling of strong and weak oscillators in synchronization and adaptation. The general dynamic signatures of oscillator synchrony and phase retuning by light are modeled using three oscillator groups coupled by complementary activating and repressing signals. **A:** Three oscillator groups (60 oscillators total) are simulated in either constant darkness (**A, Left**) or in response to a phase advancing light pulse (**A, right**), using a modified version of the Goodwin model (Tyson, 2002). Traces of the *Z* variable are shown here. Rate parameters are set to generate damped circadian oscillations. Group 1 (10 oscillators) is light responsive and sends a signal that increases transcription rate. Group 2 (10 oscillators) is light responsive, has a shorter period, and sends a signal that decreases transcription rate. Group 3 (40 oscillators, but only 10 representative oscillators shown in figures for clarity) is not directly light responsive, more strongly damped, and send a signal that decreases transcription rate. **B:** Mean traces of the Z variable from each of the three groups of oscillators show that group 2 oscillators exhibit an increase in amplitude following the LP and are the first group to exhibit a phase advance. **C:** As observed with bioluminescence data, the simulated oscillators exposed to a phase advancing light pulse (red trace) exhibit a mean decrease in order parameter R, followed by a delayed increase in R relative to oscillators in DD (black trace). R varies between 0 and 1 with higher values indicating similarity in phase, period, and waveform. **D:** Phase response curves of simulated systems, with all oscillators having only excitatory signals (activating only), only inhibitor signals (repressing only), or a complementary system with a mix of both signaling types. **E:** Simulations in constant darkness show that the complementary system shows an intermediate period length relative to activating only and repressing only systems. Simulations were generated using custom MATLAB scripts. See Materials and Methods for details.

3.6 Supplementary Information

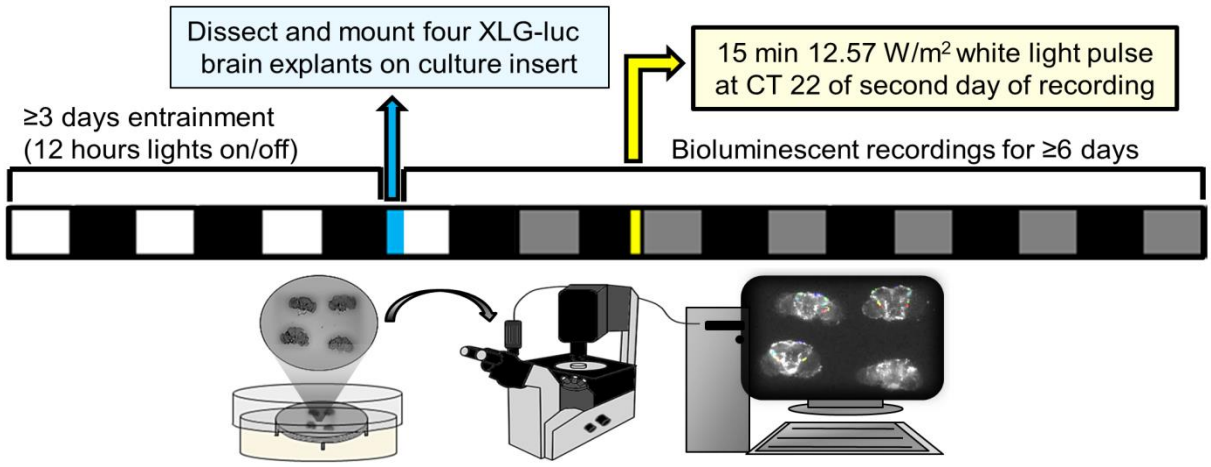

Figure S3.1. General schematic of the experimental setup for bioluminescence recordings. Adult, male *XLG-Per-Luc* flies are entrained to a standard 12 hr:12 hr LD schedule for ≥3 days (white and black squares represent 12 hour light and dark periods, respectively). Four adult male flies are then dissected and mounted on a culture membrane insert in a 35 mm dish containing 1.2 ml of culture medium. 1 mM luciferin is added to the culture medium 30 minutes prior to recording. The cultured brains are then placed on the stage of an Olympus IX71 inverted microscope set in a dark room. Light from the samples is collected by a 4x objective and transmitted directly to a cooled charge-coupled device (CCD) camera mounted on the microscope's bottom port. *XLG-Per-Luc* bioluminescence images are collected by a computer at 30 minute intervals and analyzed with the software MetaMorph and custom MATLAB scripts. For baseline measurements, bioluminescence recordings were obtained for whole brain explants maintained in constant darkness. These recordings were compared to brain explants exposed to a 12.57 W/m2 (2,000 lux), 15 minute light pulse at CT 22 on the second day of imaging. Only experiments which had all four brains still healthy, intact, free of contamination, adherent to the insert membrane, and exhibiting bioluminescence for ≥ 6 days were analyzed. See "Materials and Methods" for specific details on setup.

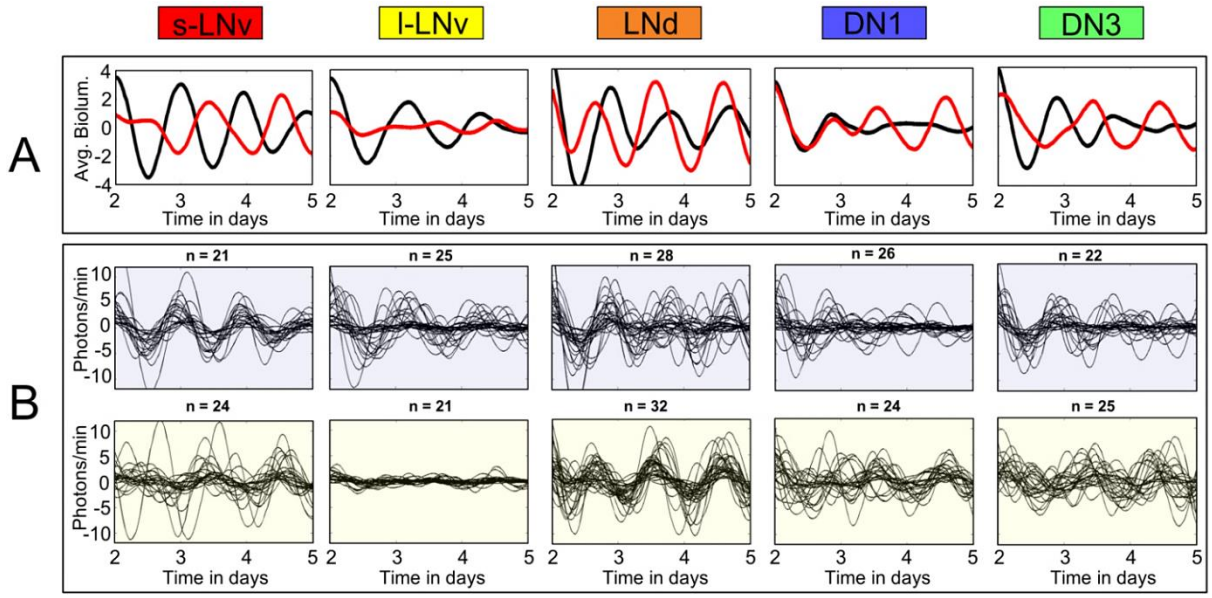

Figure S3.2. Distinct differences in phase, synchrony and amplitude observed between strong versus weak oscillators in DD and in response to a phase advancing light pulse. *XLG-Per-Luc* bioluminescence time-series measurements show the dynamics of neuronal oscillators either maintained in constant darkness ("DD cells") or after exposure to a 15 minute light pulse at CT 22 on the second day in DD ("LP cells") as previously reported (Roberts et al., 2015). The time frames were narrowed to cover day 2 to day 5 of the recording in order to more clearly highlight the dynamic changes in activity during this critical window. **A:** Comparing mean bioluminescence traces confirms that LP cells (red line) exhibit a transient loss then recovery of phase shifted synchrony in response to the light pulse relative to DD cells (black line). Note that the LNds also exhibit the most immediate, high fidelity phase shift of two hours following the LP. **B**: Wavelet-detrended time series are shown comparing neuronal subgroup dynamics in either DD (top panel) or LP (bottom panel) conditions. The number of neuronal oscillators analyzed for each condition and subgroup are shown above each panel.

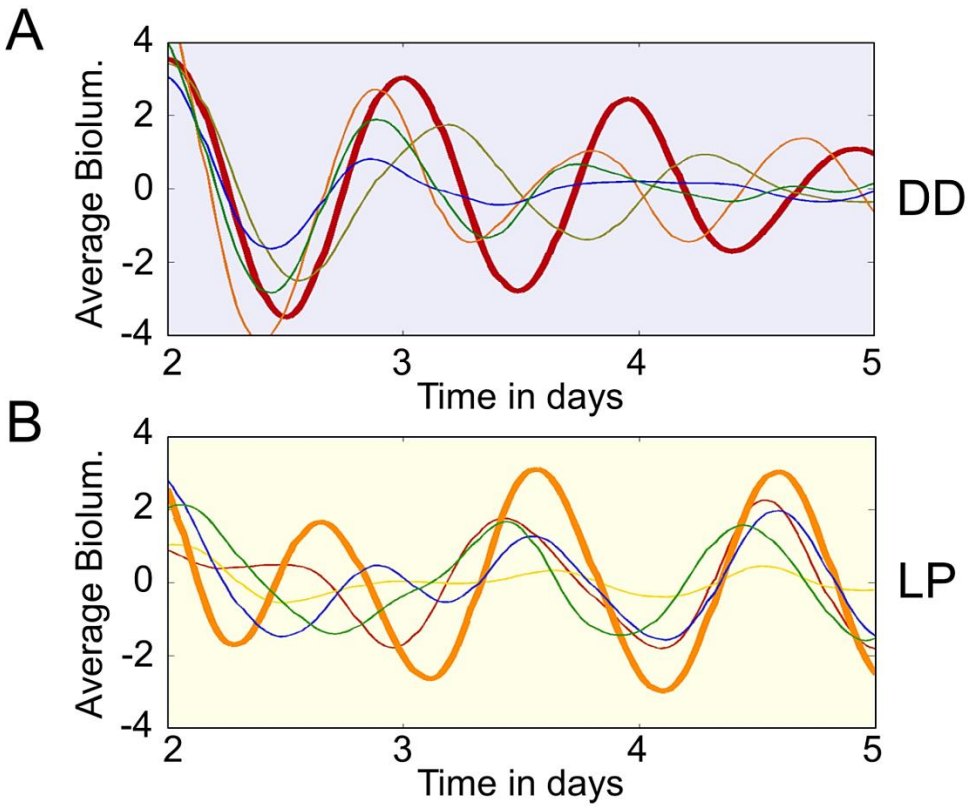

Figure S3.3. Alignment of inter-subgroup dynamics indicates role of strong oscillators in both DD and LP conditions. Mean bioluminescence traces are provided for the sLNvs (red), l-LNvs (yellow), LNds (orange), DN1s (blue) and DN3s (green). **A:** Subgroups in DD exhibit a gradual decrease in rhythmicity and inter-subgroup synchrony over time. Note that the s-LNv trace is slightly thicker to highlight this subgroup having the most consistently high amplitude oscillations in DD relative to other subgroups. **B:** After exposure to a phase-advancing light pulse, most subgroups show suppressed amplitudes and scrambled phases. The LNds are represented with a thicker trace to highlight that these oscillators exhibit an increase in amplitude and synchrony following exposure to the LP.

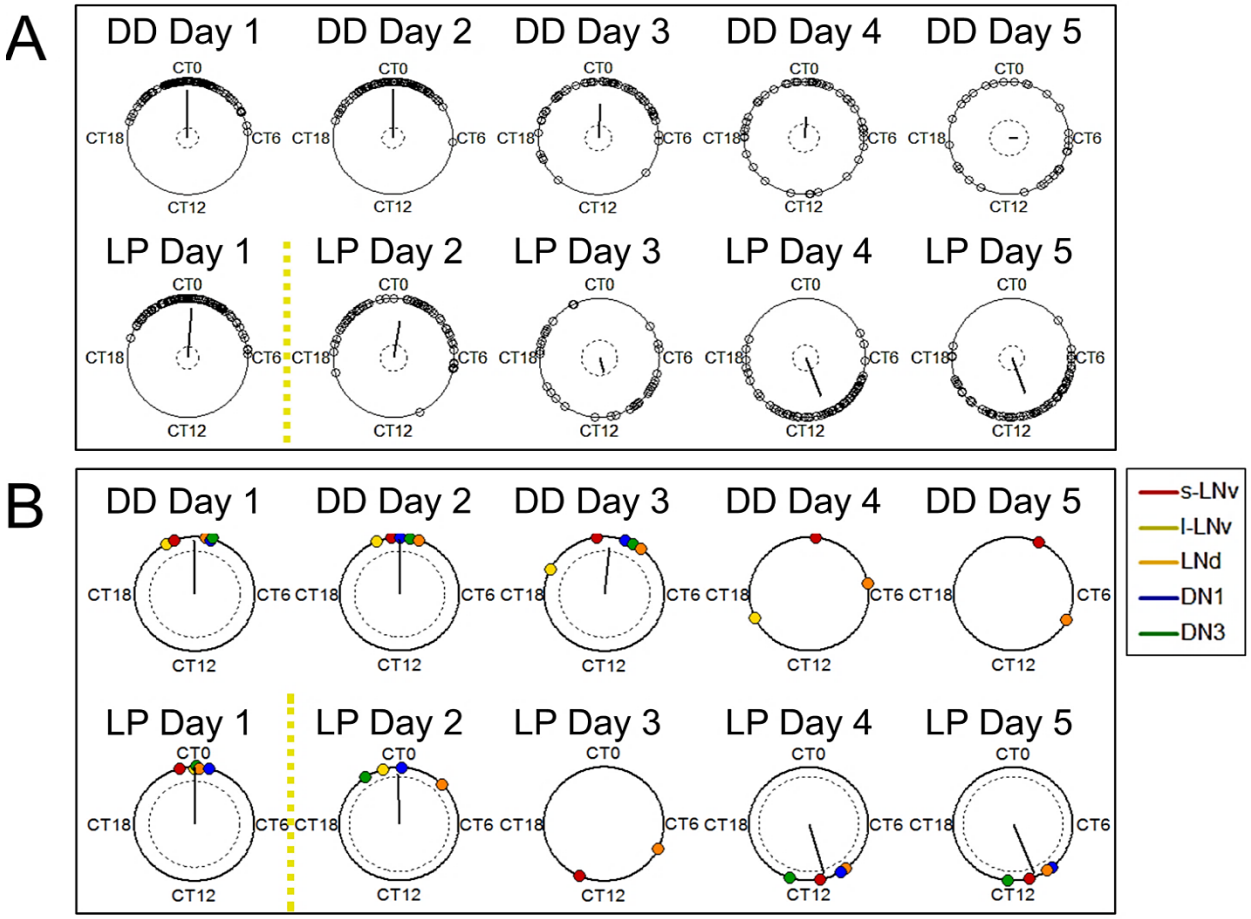

Figure S3.4. Nonlinear embedded phase estimates show the same trends in phase coherence and mean phase over time in DD and after LP as observed with sine-fit estimates. Circular phase plots for 'all cells' (combined across all neuronal subgroups) in **A:** DD and **B:** after a light pulse reveal the same patterns in phase coherence and phase shift as observed for sine-fit estimates in Fig. 3.2A. The similarity in trends using both methods confirms the reliability and consistency of observations made using the sine-fit estimates in combination with discrete wavelet transform. Custom MATLAB scripts were used to generate nonlinear embedded phase plots. See Fig. 3.2A for description of phase plots.

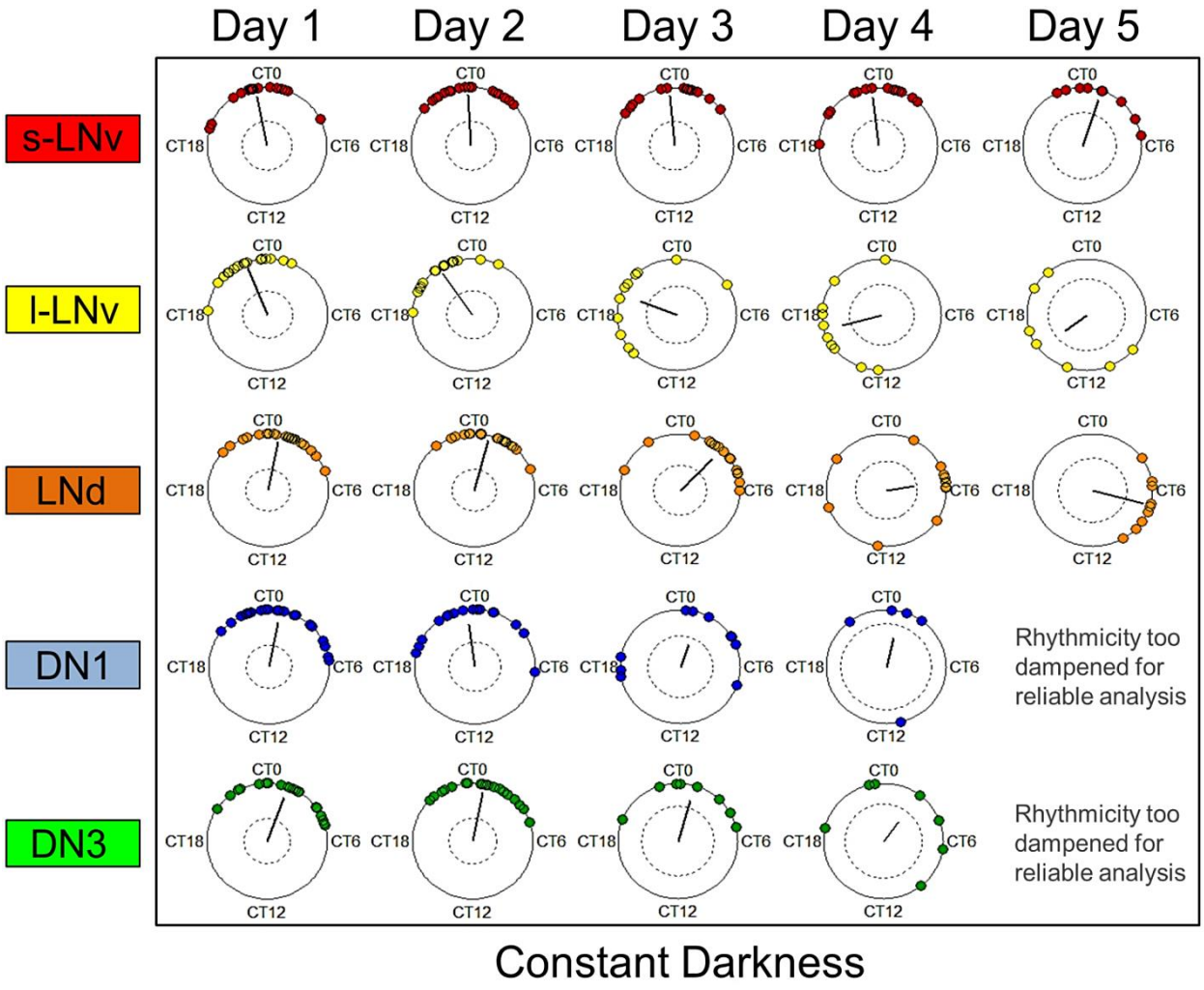

Figure S3.5. Nonlinear embedded estimates of neuronal subgroups maintained in DD show general phase dispersion and phase drift over time in DD. Embedded phase plots for neuron subgroups maintained in DD confirm the same trends of phase dispersion as observed using sine-fit estimates in Fig. 3.3. See Fig. 3.3 for description of circular phase plots for neurons in DD.

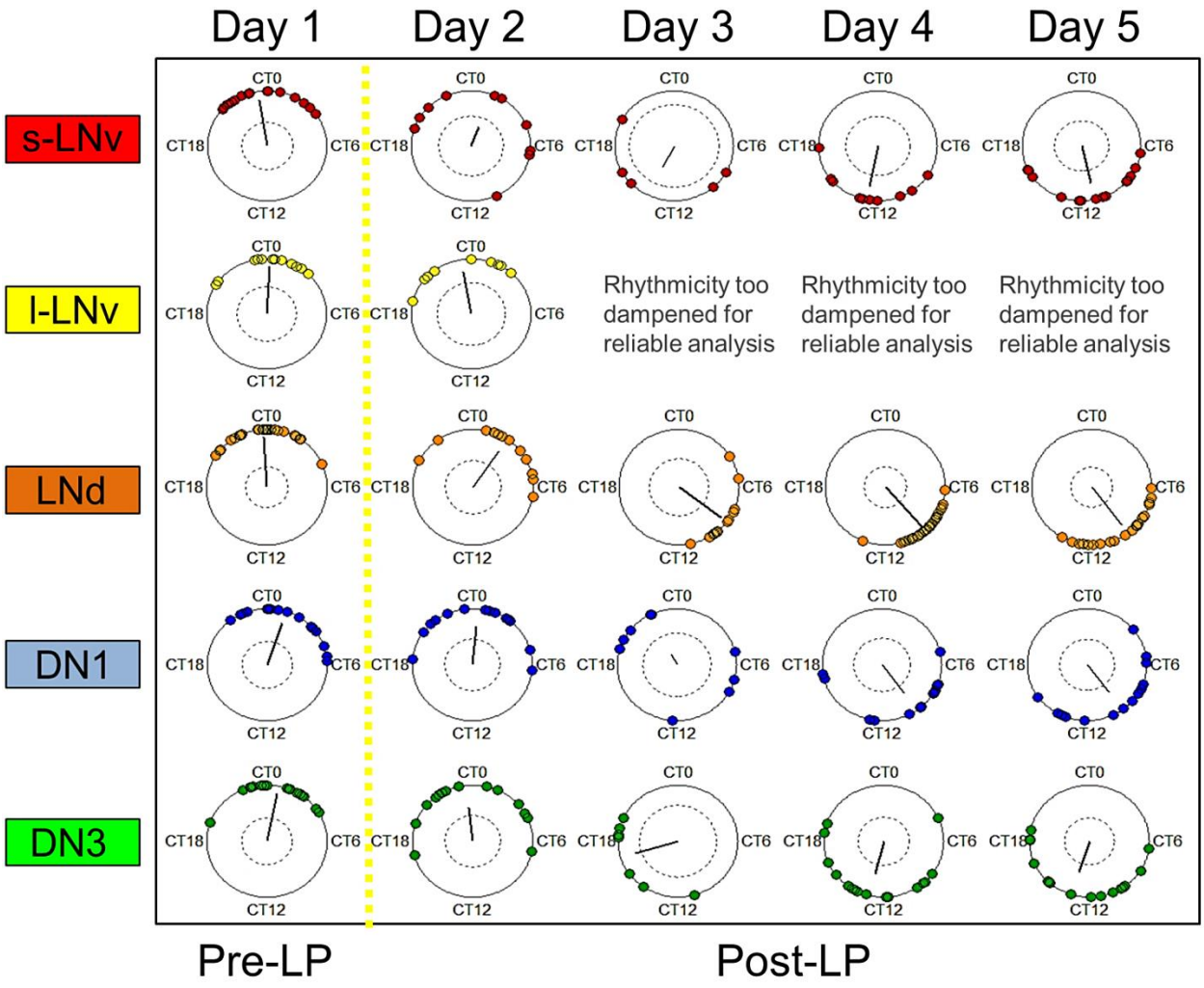

Figure S3.6. Nonlinear embedded phase estimates of neuronal subgroups exposed to a light pulse generally show transient phase dispersion followed by delayed increase in phase coherence. Circular phase plots for neurons exposed to a light pulse show the same general patterns of transient phase dispersion followed by delayed phase increase and phase shift, using the nonlinear embedded method (as seen here) and the sine-fit method (seen in Fig. 3.4). See Fig. 3.4 for details regarding circular phase plots for neurons exposed to a LP.

Statistics on Phase Sine vs Embed Phase Estimates (Circ. correlation for phase)		
Condition + Day	Rho	p-value
DD day 1	0.98	3.60E-12
LP day 1	0.98	3.60E-12
DD day 2	0.94	3.20E-10
LP day 2	0.93	1.80E-09
DD day 3	0.96	3.40E-10
LP day 3	0.97	3.10E-09
DD day 4	0.96	6.40E-08
LP day 4	0.96	1.90E-07
DD day 5	0.96	9.50E-06
LP day 5	0.98	7.90E-11

Table S3.1. Nonlinear embedded phase analysis validates sine-fit estimates of phase. Custom MATLAB scripts were used to calculate the correlation coefficients (rho) and p-values between nonlinear embedded and sine-fit phase estimates across all neuronal subgroups for all time points and conditions. The p-value is based on the null hypothesis that there is no correlation in phase estimates between these two methods. The strong positive, linear correlation (indicated by high rho values) and low p-values confirm that sine-fit estimates of phase using two-day sliding windows are accurate. The same neurons were analyzed using both methods for corresponding time points, subgroups, and conditions.

Movie S3.1. Please see online for animations of individual oscillator dynamics in DD and in response to a phase advancing light pulse show the complexity of the network phase ensemble. The animations show changes in the phase and amplitude of XLG-Per-Luc bioluminescence activity for individual oscillators from all neuronal subgroups in either DD (Left, n=122) or in response to a phase advancing light pulse (Right, n=126). The timing of the LP is indicated by a yellow highlight around the circle. The angle of the disks represents phase and drift of the disks towards the center of the circle and the size of the disks indicates reduction in amplitude. The disks are colored according to neuronal subgroup for the s-LNvs (red), l-LNvs (yellow), LNds (orange), DN1s (blue) and DN3s (green). Animations were generated using custom MATLAB scripts. This movie can be viewed as a supplemental attachment to this thesis.

Movie S3.2. Animations of individual subgroup dynamics show that the activities of neuronal subgroups are transiently scrambled before a phase advance by a light pulse. Changes in average phase and amplitude over time are animated for circadian neuronal subgroups. Note that the LNds appear to lead the phase advance while the phases and amplitudes of the other neuronal subgroups are transiently scrambled following the light pulse. The same color scheme, nonlinear dynamics method, and data sets were used as seen in Movie S1. This movie can be viewed online in the *Journal of Biological Rhythms*.

Movie S3.3. Animations of averaged network kinetics show a transient reduction in amplitude by the light pulse followed by delayed recovery of phase-shifted amplitude over time. The average activity of whole network (i.e. averaged from all neuronal subgroups) dynamics in either DD (Left) or in response to the phase advancing light pulse (Right) are represented by black disks. See Movie S1 for details regarding measures and representations of phase and amplitude. This movie can be viewed online in the *Journal of Biological Rhythms*.

3.7 Modeling Supplement

We developed a simple mathematical model to explore the qualitative dynamics of a network composed of different oscillator types, based on current knowledge of the *Drosophila* circadian network. The modeling aim here is to observe the key general features of the various oscillator types and demonstrate how a mix of activating and repressing coupling mechanisms in a system with different oscillator types may support circadian properties like amplitude, synchrony, period length, and entrainment. We are not trying to employ the model to provide evidence for how the circadian circuit responds to a phase shifting light pulse in such a fashion but suggest why it appears to respond in such a way (i.e. potential consequences of the heterogeneous network). Previous studies have shown that alterations in coupling between heterogeneous oscillator types can result in different emergent periods and phases (Tokuda et al., 2005).

The *Drosophila* clock consists of clusters of clock neurons with distinct circadian properties, with both excitatory and inhibitory intercellular signals playing roles in determining the system's overall properties, such as period length (Dissel et al., 2014). Rather than one cluster acting as a master pacemaker controlling the others, the different clusters each play important and functionally distinct roles (Yao and Shafer, 2014). Multiple coupling signals are released from and perceived by various *Drosophila* clock neurons, including PDF, which stimulates cAMP near dawn, and glutamate, which inhibits cAMP around dusk, thereby generating differentially timed synchronizing signals to promote robust oscillations (Collins et al., 2014). Inspired by these general principles underlying the *Drosophila* circadian clock, we built a model system involving three groups of oscillators with distinct types of signaling, light responses, and degrees of

dampening. However, the groups in this model are not intended to specifically represent particular clock neuron clusters, and the coupling mechanisms in the model are not meant to represent specific neurotransmitters. The main premise is to demonstrate through a relatively simple model how different dynamic signatures could be generated through a heterogeneous circadian system and what the advantages of such a system might be.

Each oscillator is simulated using a modified version of the Goodwin model (Bliss et al., 1982; Tyson, 2002):

$$\frac{dX}{dt} = \frac{a(1 + k_{act} - k_{rep})}{Z + 1} - bX \quad (1)$$

$$\frac{dY}{dt} = bX - bY \quad (2)$$

$$\frac{dZ}{dt} = bY - \frac{cZ}{Z + 1} \quad (3)$$

Various versions of Goodwin-type models have been employed to study the circadian system (Ruoff et al., 2001; Cheng et al., 2009; Saithong et al., 2010; Komin et al., 2011; Leise et al., 2013; Gu et al., 2014; Kidd et al., 2015; Gu et al., 2015). The parameters for our system (see Table 3.1) are set so that uncoupled oscillations dampen over time toward the steady state values,

$$X_{ss} = Y_{ss} = \frac{a}{b(1+a/c)} \text{ and } Z_{ss} = \frac{a}{c}.$$

Although the individual oscillators are damped, the coupled system described below generates sustained oscillations for β>0.03 under constant conditions, and also entrains to light-dark cycles (see Figure 3.1).

	s	*a*	*b*	*c*	β
Group 1	0.98±0.005	(9*s*-1)*c*	0.149-0.1535	81*bs*^{2}	0.035±0.007
Group 2	0.98±0.005	(9*s*-1)*c*	0.1525-0.157	81*bs*^{2}	0.035±0.007
Group 3	0.88±0.005	(9*s*-1)*c*	0.149-0.157	81*bs*^{2}	0.175±0.035

Table M3.1. Parameter values for modified Goodwin model. The model generates self-sustained oscillations in individual oscillators if *s*>1 and damped oscillations if *s*<1 (with smaller *s* leading to faster damping). To create heterogeneity in the oscillator groups, values of *s* and β are normally distributed random numbers with the indicated mean and standard deviation, while values for *b* are evenly distributed in the indicated range for each group (not random). Parameters *a* and *c* are fixed functions of *s* and *b*; see (Tyson, 2002) for the derivation of these relations via a linear stability analysis. Group 3 needs a stronger coupling signal to maintain rhythmicity, due to its low value of *s* (strongly damped).

To explore the dynamic interactions of damped oscillators with different properties, we created a network of 60 modified Goodwin oscillators organized into 3 groups. “Group 1” oscillators (10 total, #1-10) are directly light responsive, weakly damped, and send an activating coupling signal that effectively increases the transcription rate *a* of all oscillators when the Group 1 oscillators have *X* levels above the theoretical steady state value X_{ss}. “Group 2” oscillators (10 total, #11-20) are more strongly light responsive, weakly damped, and transmit a repressing coupling signal that effectively decreases the transcription rate *a* of all oscillators when the Group 2 oscillators have *Z* levels above the steady state value Z_{ss}. These coupling functions were chosen to appropriately time the signals to promote synchronization. In both cases, higher amplitude oscillations lead to stronger coupling. “Group 3” oscillators (40 total, #21-60) are not directly light responsive, strongly damped, and send a repressing coupling signal like that of Group 2.

Light response is achieved through increasing the degradation rate parameter *c* in equation (3). Both LD entrainment and response to light pulses can be effectively

modeled through this mechanism. For example, a light pulse simulated by increasing *c* by 8% for Group 1 oscillators and by 16% for Group 2 oscillators for 4 hours starting 3 hours before the peak in mean *X* results in a large phase advance for the coupled system. LD entrainment can be simulated by increasing *c* by 0.4% for Group 1 oscillators and by 0.8% for Group 2 oscillators for the first 10h of each 24h day. In all simulations, the system is entrained to LD for 500 days, released into DD for 2 weeks, then the light pulse is administered.

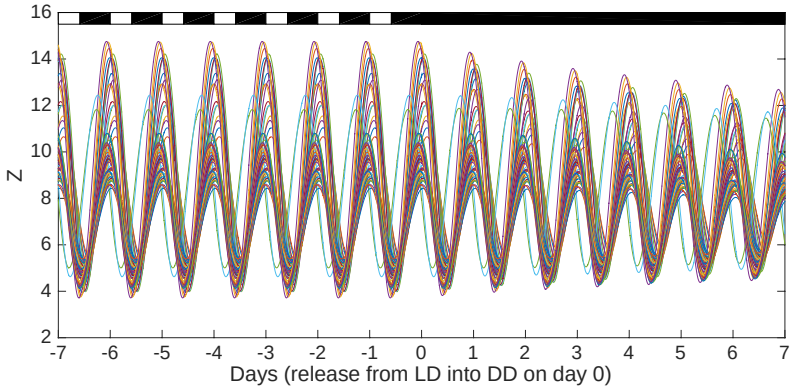

Figure M3.1. Oscillations of the 60-oscillator system under LD entrainment, showing release into DD. Mixed coupling, with parameters as shown in Table 3.1.

Coupling is achieved through modifying the transcription rate parameter *a* in equation (1). Two complementary types are used for the modeling: k_{act} increases transcriptional activation while k_{rep} represses transcription (see Figure 3.2):

$$k_{act} = \frac{\beta}{10}\sum_{n=1}^{10}\frac{\max(X_n - X_{ss}, 0)}{X_{ss} + \max(X_n - X_{ss}, 0)},$$

$$k_{rep} = \frac{\beta}{50}\sum_{n=11}^{60}\frac{\max(Z_n - Z_{ss}, 0)}{Z_{ss} + \max(Z_n - Z_{ss}, 0)}.$$

All oscillators receive both types of coupling signals, but each group sends a single type of coupling signal. Note that in the alternate simulations where only one type

of coupling is used, then all three groups send the indicated type of signal (activating or repressing). For the case of activating-only coupling signals, the coupling functions are

$$k_{act} = \frac{\beta}{10}\sum_{n=1}^{10}\frac{\max(X_n - X_{ss},0)}{X_{ss}+\max(X_n - X_{ss},0)} + \frac{\beta}{50}\sum_{n=11}^{60}\frac{\max(X_n - X_{ss},0)}{X_{ss}+\max(X_n - X_{ss},0)}, \quad k_{rep} = 0\,,$$

while for the case of repressing-only coupling signals, the coupling functions are

$$k_{act} = 0\,,\ k_{rep} = \frac{\beta}{20}\sum_{n=1}^{10}\frac{\max(Z_n - Z_{ss},0)}{Z_{ss}+\max(Z_n - Z_{ss},0)} + \frac{\beta}{50}\sum_{n=11}^{60}\frac{\max(Z_n - Z_{ss},0)}{Z_{ss}+\max(Z_n - Z_{ss},0)}\,.$$

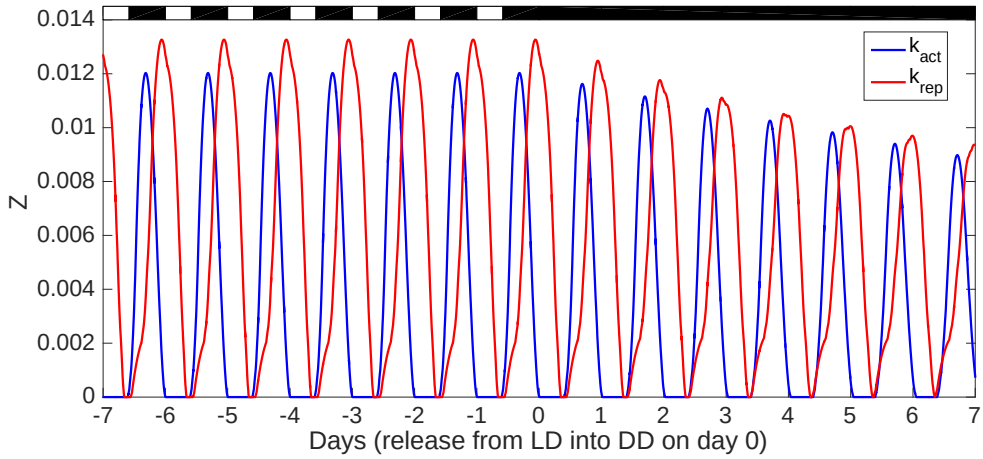

Figure M3.2. Coupling functions k_{act} and k_{rep} under LD entrainment followed by DD. Mixed coupling, with parameters as shown in Table 3.1.

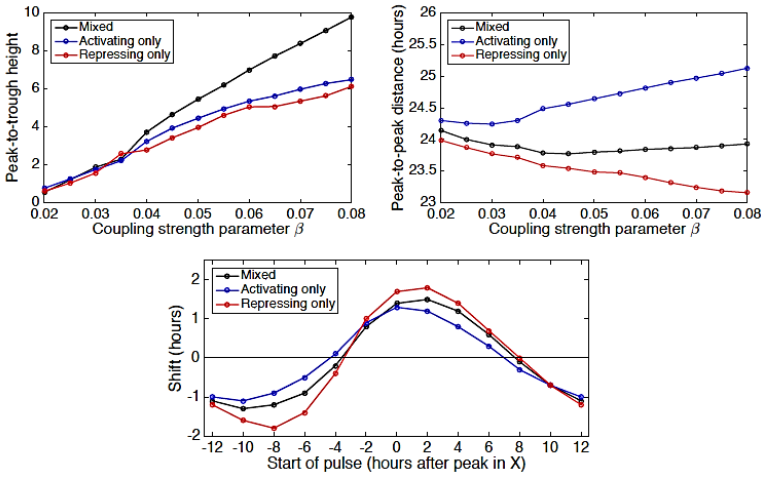

Figure M3.3. Short-term characteristics of system after release from LD into DD. *Upper left*: Peak-to-trough height of the mean *Z* waveform 2 weeks after release from LD entrainment to DD. *Upper right*: Distance between consecutive peaks of the mean *Z* waveform 2 weeks after release from LD entrainment to DD. *Lower*: Phase response curve for 30-minute light pulse for β=0.035. Simulations used the parameter values in Table 3.1 (except β as indicated in the graphs), with three different types of coupling. As β increases, the mixed coupling results in a more slowly changing cycle length and higher amplitude compared to the activating-only and repressing-only cases.

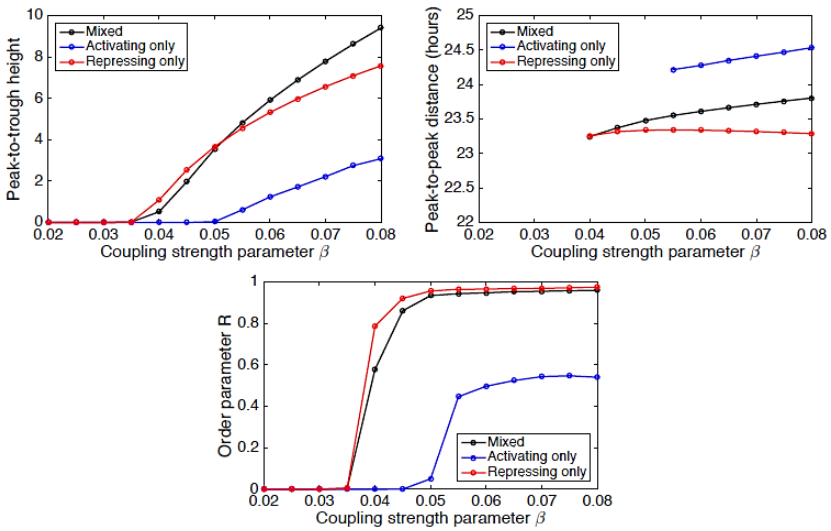

Figure M3.4. Long-term characteristics of the system under DD. *Upper left*: Amplitude of the mean *Z* waveform under long-term DD, with positive amplitude indicating self-sustained oscillations of the coupled system. *Upper right*: Period under long-term DD for cases with self-sustained oscillations. *Lower*: Order parameter *R* calculated using *Z* under long-term DD. Simulations used the parameter values in Table 3.1 (except β as indicated in the graphs) for 1000 days, with three different types of coupling. As β increases, the mixed coupling results in a more moderate cycle length and higher amplitude compared to the activating-only and repressing-only cases. β=0.035 is the threshold for the system to exhibit stable oscillations over long term for mixed and repressing-only cases. The presence of repressing coupling supports stable oscillations over the long run for the system (after transients settle out, which usually took 200-300 days).

To quantify changes in synchrony over time, we use the order parameter *R*, defined as in (Gonze et al., 2005) for a system of *N* oscillators with state variable *X*:

$$R = \frac{\langle X^2 \rangle - \langle X \rangle^2}{\frac{1}{N}\sum_{k=1}^{N}\left(\langle {X_k}^2 \rangle - \langle X_k \rangle^2\right)},$$

where angle brackets denote time average and $X = \frac{1}{N}\sum_{k=1}^{N} X_k$. If the phase, period and waveform of all *N* cells are in perfect synchrony then *R*=1, while a uniform distribution of phases would lead to *R*=0.

Figures M3.5-7 below show the results of a strong advancing light pulse for the 60-oscillator system with 10 in group 1, 10 in group 2, and 40 in group 3. In all light pulse simulations, the system is first entrained to a light-dark cycle for 500 days as described above, then released to constant conditions for two weeks before the 4-hour light pulse is administered, with the start of the light pulse 3 hours before the peak in mean *X*. For comparison, Figure M3.8 shows the results of a strong delaying light pulse for the same system, using a 4-hour light pulse starting 8 hours before the peak in mean *X*.

Shifts are determined by comparing the peak times of the mean *Z* trace for unpulsed versus light-pulsed conditions on the 6^{th} day following the light pulse, chosen because the experiments only ran that length of time.

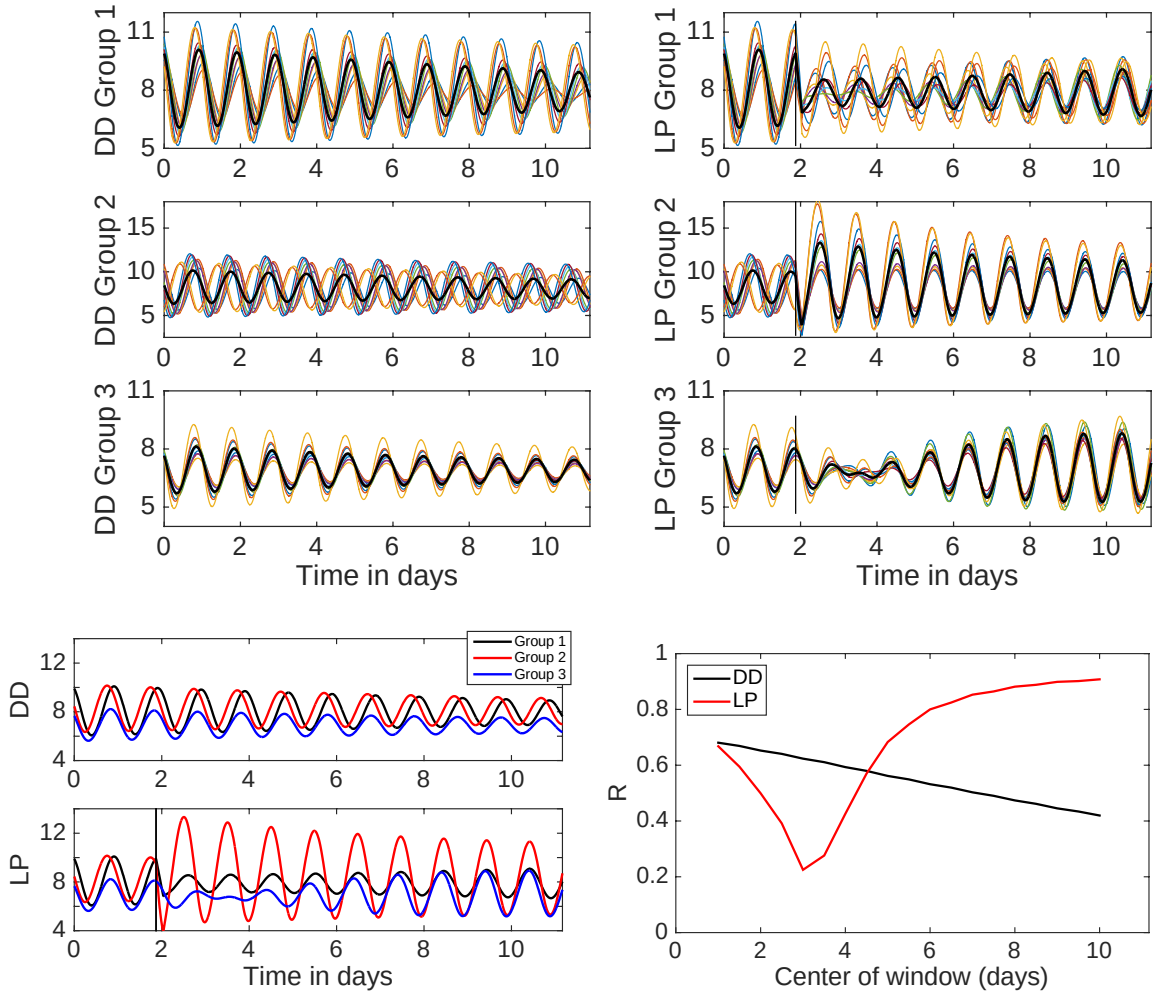

Figure M3.5. Large phase advance of 8.6h for 60-oscillator system with mixed coupling and β =0.035. *Top*: traces of the 10 group 1 oscillators, traces of the 10 group 2 oscillators, and traces of 10 representative group 3 oscillators under constant conditions (DD) or with a 4h light pulse applied 3h before the peak in mean *X* (LP). A vertical line marks the time of start of the light pulse. *Lower left*: mean traces for each group. *Lower right*: order parameter *R* for 2-day windows, calculated using *Z*.

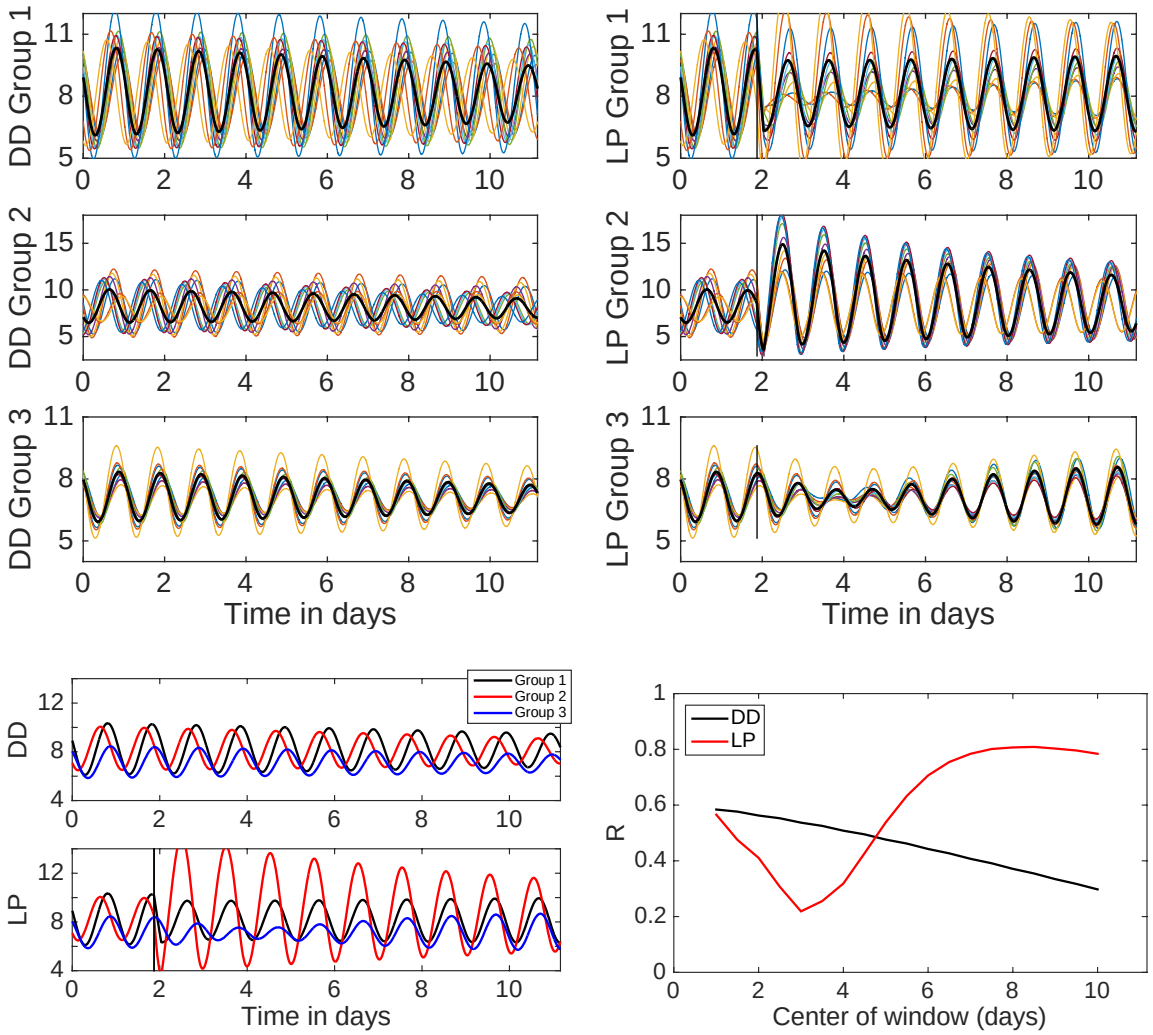

Figure M3.6. Large phase advance of 6.6h for 60-oscillator system with activating-only coupling and β =0.035. *Top*: traces of the 10 group 1 oscillators, traces of the 10 group 2 oscillators, and traces of 10 representative group 3 oscillators under constant conditions (DD) or with a 4h light pulse applied 3h before the peak in mean *X* (LP). A vertical line marks the time of start of the light pulse. *Lower left*: mean traces for each group. *Lower right*: order parameter *R* for 2-day windows, calculated using *Z*.

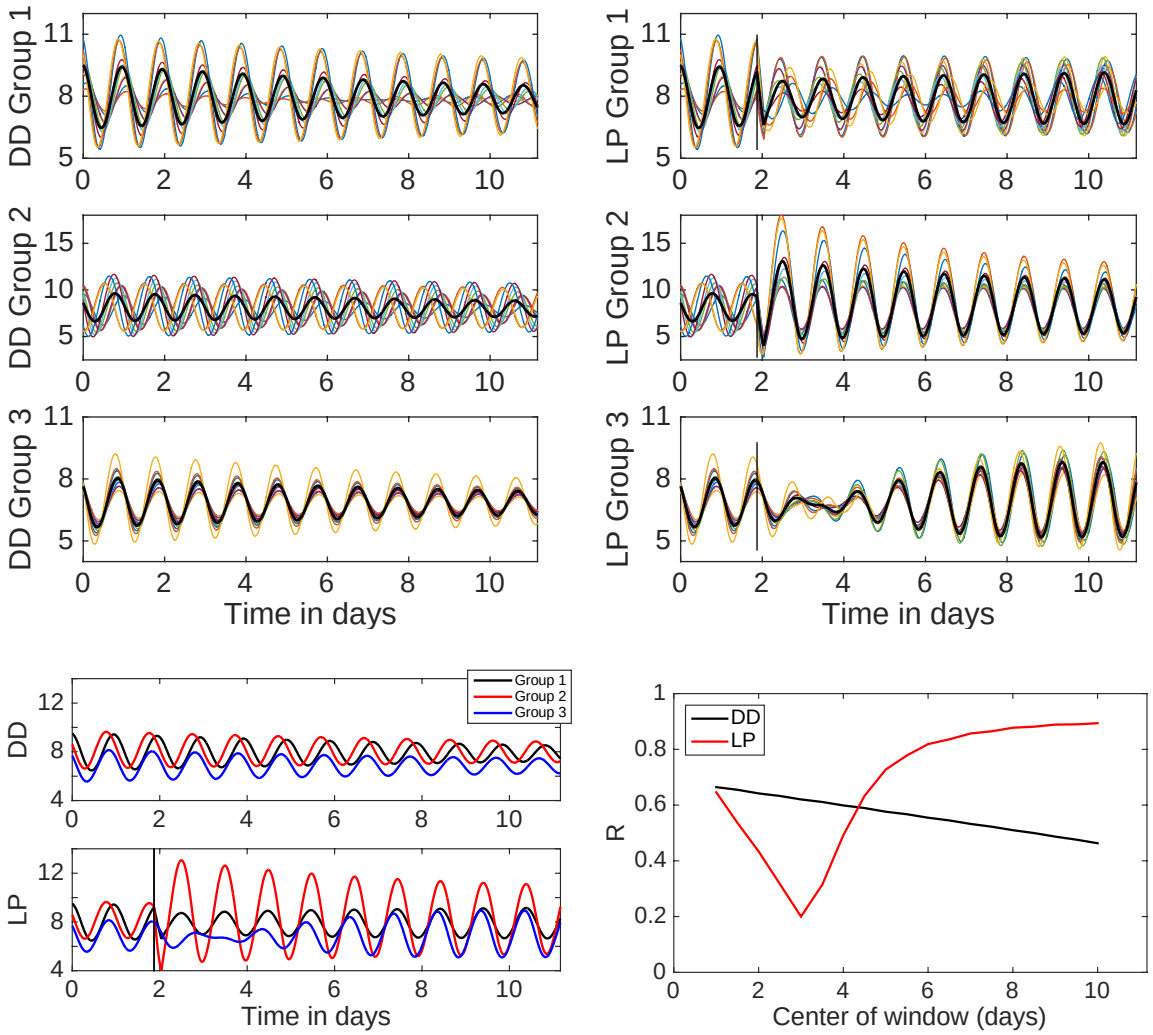

Figure M3.7. Large phase advance of 8.4h for 60-oscillator system with repressing-only coupling and β =0.035. *Top*: traces of the 10 group 1 oscillators, traces of the 10 group 2 oscillators, and traces of 10 representative group 3 oscillators under constant conditions (DD) or with a 4h light pulse applied 3h before the peak in mean *X* (LP). A vertical line marks the time of start of the light pulse. *Lower left*: mean traces for each group. *Lower right*: order parameter *R* for 2-day windows, calculated using *Z*.

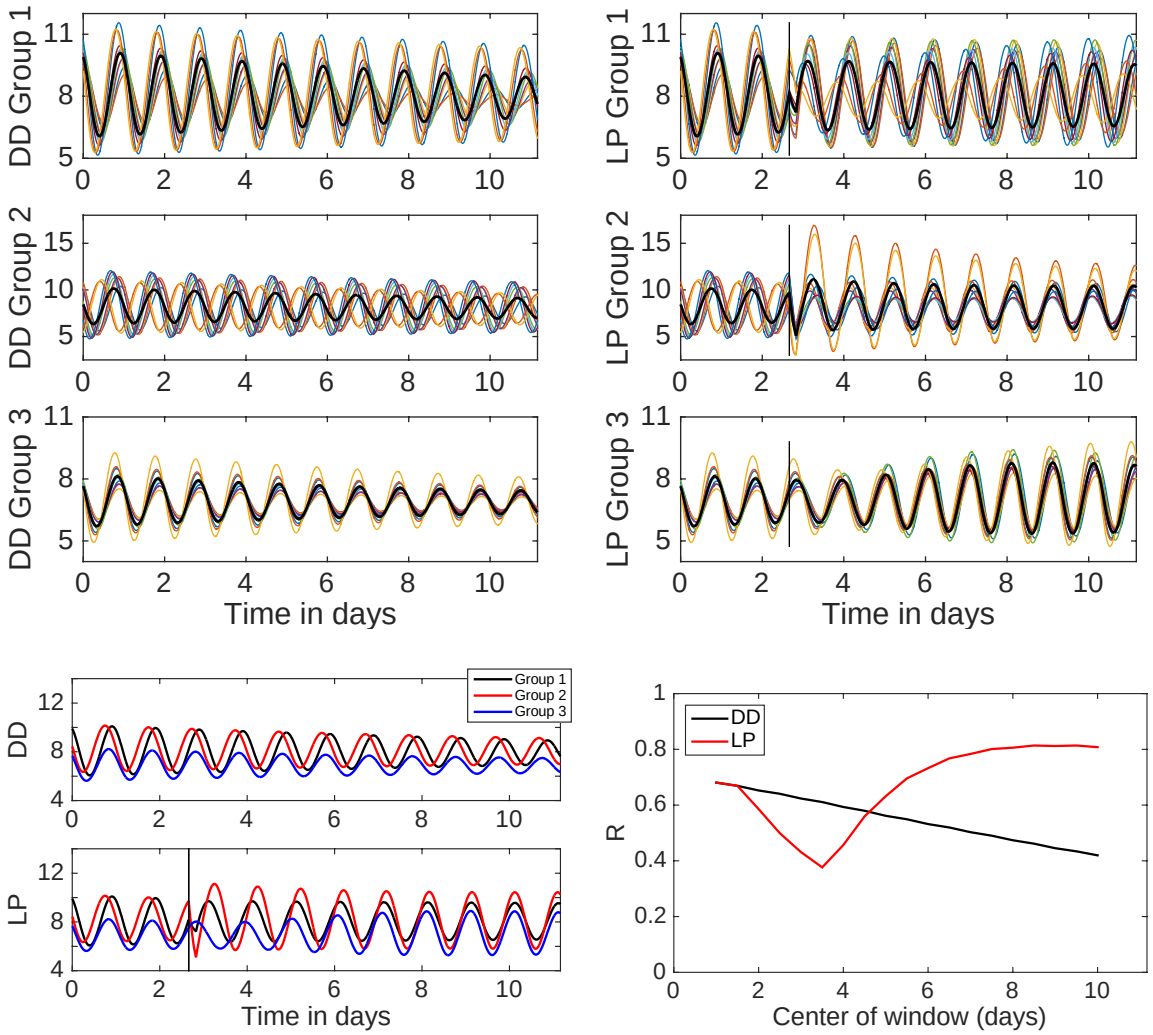

Figure M3.8. Large phase delay of 8.1h for 60-oscillator system with mixed coupling and β =0.035. *Top*: traces of the 10 group 1 oscillators, traces of the 10 group 2 oscillators, and traces of 10 representative group 3 oscillators under constant conditions (DD) or with a 4-hour light pulse applied 8 hours before the peak in mean *X* (LP). A vertical line marks the time of start of the light pulse. *Lower left*: mean traces for each group. *Lower right*: order parameter *R* for 2-day windows, calculated using *Z*.

To further assess the roles of each group and type of coupling, the figures below examine different scenarios through phase response curves to half-hour light pulses and through the order parameter *R* for the stronger 4-hour light pulse (applied 3 hours before peak in mean *X*). The cases of mixed coupling and repressing-only coupling lead to stronger synchronization in DD as the coupling strength β increases. In the case of

activating-only coupling, increasing the coupling strength has a more limited effect. For all three cases and values of β near 0.035, the advancing light pulse causes a transient dip in *R* followed by an overshoot.

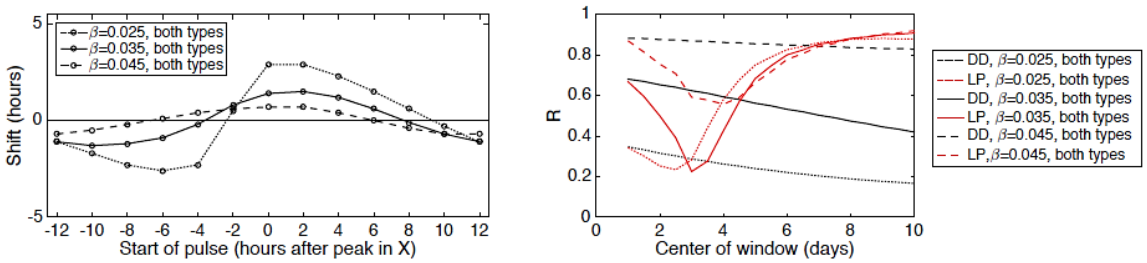

Figure M3.9. Both types of coupling signals are present (the base model)

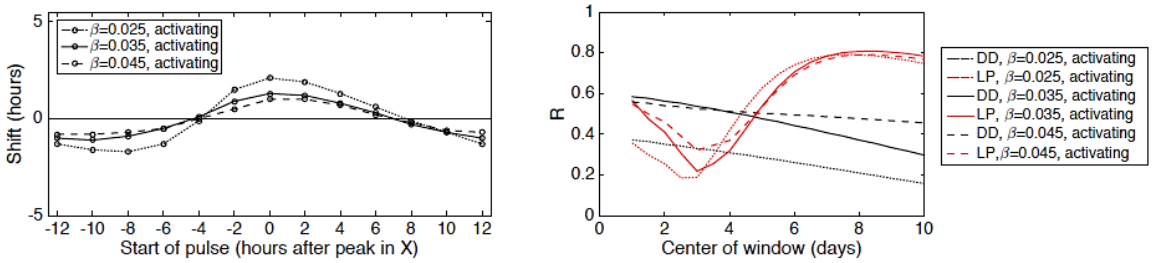

Figure M3.10. Coupling from all three groups is activating

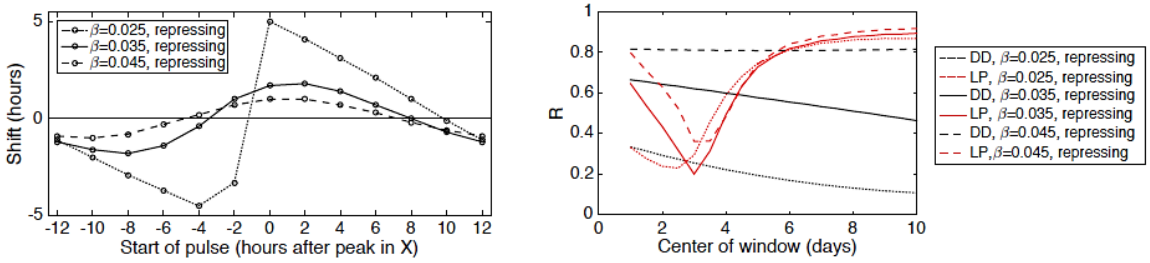

Figure M3.11. Coupling from all three groups is repressing

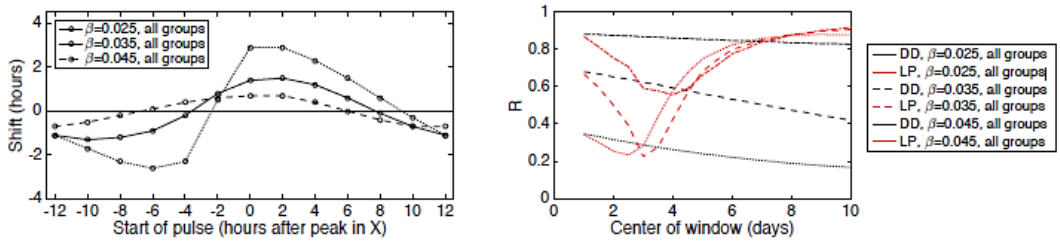

Figure M3.12. All groups (10 in group 1, 10 in group 2, 40 in group 3)

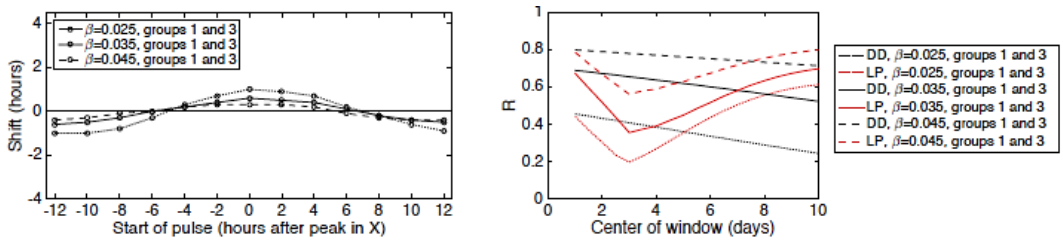

Figure M3.13. Groups 1 and 3 only (20 in group 1, 40 in group 3)

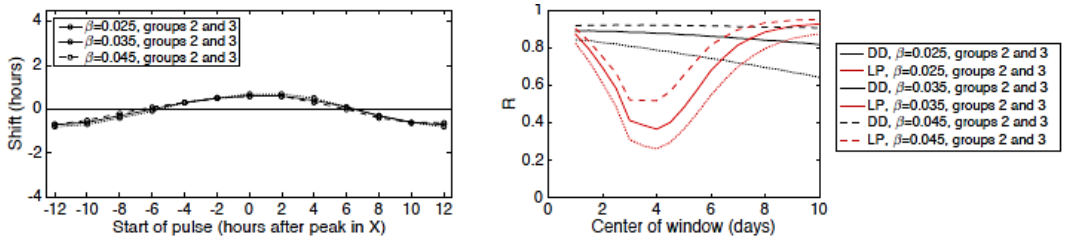

Figure M3.14. Groups 2 and 3 only (20 in group 2, 40 in group 3)

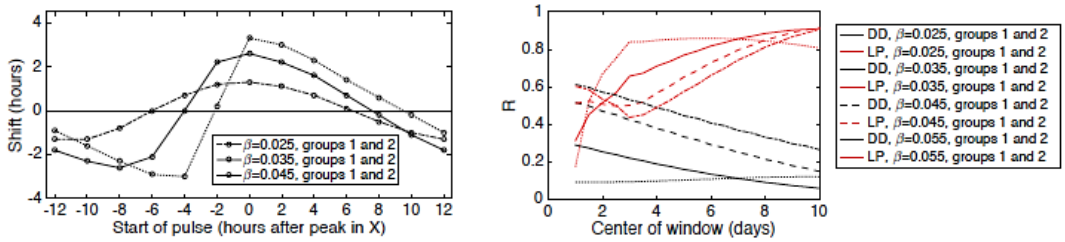

Figure M3.15. Groups 1 and 2 only (30 in group 1, 30 in group 2)

Left: Phase response curve for a 30-minute light pulse. Negative shifts indicate delays, while positive shifts correspond to advances.
Right: Order parameter *R*, calculated using *Z*, in DD versus following a 4h light pulse that begins 3 hours before peak in *X*, which results in a large phase advance.

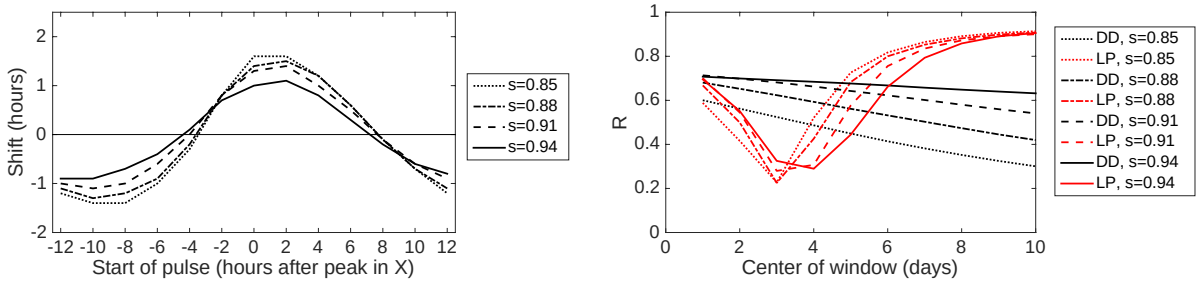

Figure M3.16. Effect of group 3's mean damping rate in mixed coupling system with all groups. Increasing the mean value of *s* in group 3 results in a system that is

more resistant to shifting and that exhibits a higher order parameter. (Lower *s* results in faster damping.)

CHAPTER 4

CRYPTOCHROME-mediated phototransduction by modulation of the potassium ion channel β-subunit redox sensor

(Fogle, Baik, Houl, Tran, Roberts, Dahm, Cao, Zhou, Holmes)

Abstract

Blue light activation of the photoreceptor CRYPTOCHROME (CRY) evokes rapid depolarization and increased action potential firing in a subset of circadian and arousal neurons in *Drosophila melanogaster*. Here we show that acute arousal behavioral responses to blue light significantly differ in mutants lacking CRY, as well as mutants with disrupted opsin-based phototransduction. Light-activated CRY couples to membrane depolarization via a well conserved redox sensor of the voltage-gated potassium (K+) channel β-subunit (Kvβ) Hyperkinetic (Hk). The neuronal light response is almost completely absent in hk−/− mutants, but is functionally rescued by genetically targeted neuronal expression of WT Hk, but not by Hk point mutations that disable Hk redox sensor function. Multiple K+ channel α-subunits that coassemble with Hk, including Shaker, Ether-a-go-go, and Ether-a-go-go–related gene, are ion conducting channels for CRY/Hk-coupled light response. Light activation of CRY is transduced to membrane depolarization, increased firing rate, and acute behavioral responses by the Kvβ subunit redox sensor.

4.1 Introduction

CRYPTOCHROME (CRY) is a photoreceptor that mediates rapid membrane depolarization and increased spontaneous action potential firing rate in response to blue

light in arousal and circadian neurons in *Drosophila melanogaster* (Fogle et al., 2011; Sheeba et al., 2007). CRY regulates circadian entrainment by targeting circadian clock proteins to proteasomal degradation in response to light (Emery et al., 1998; Helfrich-Förster et al., 2001; Koh et al., 2006; Stanewsky et al., 1998). CRY is expressed in a small subset of central brain circadian, arousal, and photoreceptor neurons in *D. melanogaster* and other insects, including the large lateral ventral neuron (LNv; l-LNv) subset (Fogle et al., 2011; Sheeba et al., 2007). The l-LNvs are light-activated arousal neurons (Fogle et al., 2011; Parisky et al., 2008; Shang et al., 2008; Sheeba et al., 2008a; Sheeba et al., 2007), whereas the small lateral ventral neurons (s-LNvs) are critical for circadian function (Helfrich-Forster, 1998; Helfrich-Förster et al., 2001). Previous results suggest that light activated arousal is likely attenuated in *cry*-null mutants. In addition to modulating light-activated firing rate, membrane excitability in the LNv neurons helps maintain circadian rhythms (Nitabach et al., 2002; Nitabach et al., 2006; Sheeba et al., 2008a), and LNv firing rate is circadian regulated (Cao and Nitabach, 2008; Sheeba et al., 2007).

Based on our previous work suggesting that l-LNv electrophysiological light response requires a flavin-specific redox reaction and modulation of membrane K^+ channels, we investigated the molecular mechanism for CRY phototransduction to determine how light-activated CRY is coupled to rapid membrane electrical changes. Sequence and structural data suggest that the cytoplasmic Kvβs are redox sensors based on a highly conserved aldo-keto-reductase domain (AKR) (Chouinard et al., 1995; Gulbis et al., 2000; Long et al., 2005; McCormack and McDonnell, 1994). Although no functional role for redox sensing by Kvβ subunits has been established yet *in vivo*, studies with

heterologously expressed WT and mutant Kvβ subunits show that they confer modulatory sensitivity to coexpressed K^+ channels in response to oxidizing and reducing chemical agents (Pan et al., 2008; Pérez-García et al., 1999; Weng et al., 2006). Mammals express six Kvβ genes, whereas *Drosophila* expresses a single Kvβ designated HYPERKINETIC (Hk) (Chouinard et al., 1995). We find that the light-activated redox reaction of the flavin adenine dinucleotide (FAD) chromophore in CRY has a distinct phototransduction mechanism that evokes membrane electrical responses via the Kvβ subunit Hk, which we show is a functional redox sensor *in vivo*.

4.2 Materials and Methods

Electrophysiology and pharmacology

Patch-clamp measurements were performed on acutely dissected adult fly brains as described previously (Fogle et al., 2015; Sheeba et al., 2007). L-LNv recordings were made in whole-cell current-clamp mode. After allowing membrane properties to stabilize after whole-cell break-in, 30–60 s of recording in current-clamp configuration (unless otherwise stated) was obtained under dark conditions (~0.05 mW/cm^2) before lights were turned on. For most experiments, unless stated otherwise, lights-on data were then collected for 30–60 s and followed by another 30–60 s of darkness. DPI and H2O2 were obtained from Sigma and stock solutions prepared in double distilled H2O or standard external recording solution and bath-perfused onto the brain preparation in standard recording solution (Sheeba et al., 2007).

Optics

Multiple light sources were used for these studies (Fogle et al., 2011; Sheeba et al., 2007). The standard halogen light source on the Olympus BX51 WI microscope

(Olympus) was used for all experiments with white light. Wavelength isolation of 375–450 nm, 550 nm for electrophysiological recordings was achieved by placing appropriate combinations of 25-mm long- and short-pass filters (Edmund Industrial Optics) over the halogen light source directly beneath the recording chamber. Filters were changed during recordings to internally match neuronal responses to varying wavelength ranges. Some recordings using intense blue light (450–490 nm, 19 mW/cm^2) were obtained by using the standard mercury light source fitted to the Olympus BX51 WI microscope with cut-on and cutoff wavelengths determined by the standard GFP filter cube. In most cases, the entire matrix of white and isolated wavelengths was obtained from each single recording, with at least two light/dark cycles per wavelength range per recording. For the behavioral experiments, we used ultra-high-power LEDs implemented by Stanford Photonics, with the UHP-Mic-LED-460, which provides >1 W collimated blue light (460 nm peak, 27 nm spectrum half width, 85% peak power at 450 nm) or the UHP-Mic-LED-595, which provides >650 mW collimated orange light (595 nm peak, 16 nm spectrum half width). The LED devices were triggered on and off manually for behavioral experiments. Light was measured for all sources by using a quantum sensor and a light meter (LI-250A; LI-COR) and expressed as mW/cm^2.

Light response behavioral testing

The automated TriKinetics *Drosophila* Activity Monitor system was used to assay the locomotor activity of individual flies (Nitabach et al., 2002; Sheeba et al., 2008b). Adult male flies (1–4 d old) were individually placed in glass tubes, and their locomotor activity was tracked by the breaking of an IR beam recorded on a data acquisition computer. Behavioral activity counts were collected throughout the experiment in 1-min bins. For all

assays flies were entrained to at least 3 d of standard 12-h:12-h light: dark cycles (light phase illumination was 50–100 mW/cm^2). LED light pulses (5-min duration, blue 460 nm or orange 595 nm) were given at three hourly intervals starting at 6 h after lights off for three nights in a row. For data analysis, the locomotor activity of individual flies are summed during the 5-min light pulses. This sum is divided by the locomotor activity of the same individual for 5 min immediately preceding the light pulse, then these values are averaged across each genotype and expressed as the mean and SEM of beam crossings per pulse. ANOVA is used to determine statistical differences between genotypes.

Genetics

The control genotype w; pdfGAL4-dORK-NC1-GFP was generated by recombination between the driver and channelGFP fusion lines. “Rescue” experiments were performed with genotypes w or hk−/− ;pdfGAL4-dORK-NC1-GFP/UAS-(dCRY, Hk-WT, Hk-D260N, Hk-K289M); cry01 (homozygous) or + as described in Dataset S1.

Cell culture and transfection

HEK 293 human embryonic kidney cells were maintained as described previously (Fadool et al., 1997; Holmes et al., 1996). Cells were cultured in MEM with L-glutamine and Earle salts supplemented with 10% FBS. Each 60-mm dish of ∼80% confluent cells was transfected as previously described (Fadool et al., 1997). All cDNA constructs for transfection of HEK 293 cells were under the control of the mammalian cytomegalovirus CMV promoter using the pCS2+ vector (Nitabach et al., 2001).

Statistics

Data are presented as mean ± SEM. Values of n refer to number of measured lights on/off cycles; in all cases, the n values were obtained from at least five separate recordings. All statistical tests of ANOVA were performed with SigmaPlot 11. Variables were first tested for normality; if found to fail normality testing, Kruskal–Wallis one-way ANOVA on ranks was performed, followed by Dunn test. ANOVA on normally distributed variables was followed by Tukey test to determine significant differences between genotypes. For before and after lights-on comparisons of two sets of normally distributed variables, paired t tests were performed with SigmaPlot; for non-parametrically distributed variables, values were compared by using a signed-rank test (SigmaPlot)

4.3 Results

4.3.1 Acute behavioral responses to blue light are altered in CRY mutants.

Mutants lacking CRY or opsin-based phototransduction exhibit defects in light entrainment (Helfrich-Förster et al., 2001). Subsequent work on the LNv indicates that these neurons also mediate light-driven arousal behavior (Parisky et al., 2008; Shang et al., 2008; Sheeba et al., 2008a). The CRY-dependent rapid electrophysiological response to blue light recorded in the LNv suggests that the loss of CRY attenuates acute behavioral arousal responses to blue light, but not to wavelengths beyond its absorbance cutoff above 530 nm (Fogle et al., 2011). The behavioral locomotor responses were compared with 460-nm blue vs. 595-nm orange 5-min LED light pulses given in the middle of the night at ZT18, ZT19, and ZT20 for three successive nights to control, $cry^{-/-}$, and *gl60j* mutant flies (which lack all opsin-based external photoreceptors). The averaged behavioral actograms of control flies to blue light for two successive nights are shown

(Fig. 4.1A). We examined flies which were asleep, defined as inactive for at least 5 min, immediately before the light pulse for the percentage that awakened during the pulse. For control flies, a 5-min pulse of blue light woke 41 ± 3.7% of the sleeping flies; the numbers of *cry*$^{-/-}$ and *gl60j* mutant flies awakened were significantly lower (Fig. 4.1B). We also scored the behavioral response of awake flies to light pulses. For awake control flies, blue and orange light pulses in the middle of the night evoked twofold and threefold increases in locomotor activity relative to baseline activity in the dark (Fig. 4.1C). In contrast, both *cry*$^{-/-}$ and *gl60j* mutant awake flies show significantly attenuated behavioral responses to nighttime blue light pulses (Fig. 4.1C). CRY- and opsin-mediated phototransduction pathways contribute to the arousal behavioral response to nighttime blue light and mediate weaker responses to nighttime blue light when either component is absent. As expected, *gl60j*mutant awake flies do not behaviorally respond to nighttime orange light pulses (Fig. 4.1C), whereas *cry*$^{-/-}$mutant awake flies show significantly greater behavioral response to nighttime orange light pulses (Fig. 4.1C).

4.3.2 The CRY-mediated electrophysiological light response is attenuated in mutants lacking the Kvβ subunit Hyperkinetic.

Acute pharmacological block of K+ channel currents eliminates the CRY-mediated l-LNv light response (Fogle et al., 2011). Acute block of the l-LNv light response by the flavin-specific redox inhibitor diphenyleneiodonium (DPI) requires light-activated reduction of CRY flavin (Fig. 4.S1). As redox signaling appears to be important for the CRY light response, we tested light responses in l-LNv recordings of flies null for hyperkinetic (hk−/−) Kvβ subunit (Chouinard et al., 1995). Kvβ proteins are highly conserved members of the NADP+-dependent AKR superfamily, but as yet are not linked

to any known in vivo physiological function (Chouinard et al., 1995; Gulbis et al., 1999; Gulbis et al., 2000; Long et al., 2005; McCormack and McDonnell, 1994; Pan et al., 2008; Weng et al., 2006). The l-LNv blue light response (firing frequency light on/light off) in hk−/− flies is significantly attenuated (Fig. 4.2B and C) relative to control (Fig. 4.2A and C). This electrophysiological property is CRY light response-specific, as the l-LNv dark spontaneous firing rate in hk−/− vs. control does not differ from control or cry−/− ($P = 0.769$, ANOVA; Fig. 2D and Dataset S1). The l-LNv light response to white and blue wavelengths is significantly decreased in hk−/− flies relative to control (ANOVA; Fig. 4.2C). Control, hk−/−, and cry−/− all show no response to orange light and do not differ.

4.3.3 LNv-directed expression of Hyperkinetic RNAi attenuates the CRY-mediated light response.

K+ channel subunits are widely expressed in the *Drosophila* nervous system and photoreceptors (Hardie, 1991). To test the contribution of Hk to the CRY-mediated light response in the 8–10 pair of LNv neurons, the electrophysiological light response was measured in neurons that express Hk RNAi and Dicer directed by the pdf-GAL4 promoter. Normal electrophysiological responses to blue, white, and orange light (firing frequency light on/light off) were measured in l-LNv whole-cell patch-clamp recordings by using the RNAi genetic background control genotype (Fig. S4.2A and C), but blue and white (but not orange) light responses are significantly reduced relative to controls in transgenic flies that express HkRNAi and DICER in the LNv (Fig. S4.2B and C). As an additional control, we tested the effects of LNv-directed ShabRNAi knockdown of the Kv2-family voltage-gated K+ channel Shab subunit and found no effect on the light response recorded in l-LNv to blue, white, or orange light, which are all indistinguishable vs. RNAi controls (Fig.

S4.2C). The baseline l-LNv action potential firing rates recorded in the dark were calculated for each genotype, and none significantly differed from control (Fig. S4.2C and Dataset S1). Thus, RNAi knockdown restricted to the LNv closely resembles the electrophysiological phenotype of loss of l-LNv response to blue and white light seen in hk−/−.

4.3.4 The l-LNv light response is occluded by genetic or acute disruption of the cellular redox environment and is dependent on the Hk redox sensor.

To test whether the l-LNv light response is modulated by the cellular redox environment, we measured the l-LNv light response under conditions that genetically or chemically disrupt the cellular redox environment. Superoxide dismutase (SOD) enzymes (SOD1, expressed in cytoplasm; and SOD2, expressed in mitochondria) regulate the redox environment by limiting cellular superoxide radicals (Godenschwege et al., 2009). Blue and white, but not orange, light responses in the l-LNv are significantly lower in sod1−/− (but not sod2−/−) relative to genetic WT control (Fig. S4.3A and B). Acute treatment with the oxidizer H2O2 abolishes response to blue light relative to vehicle control. Conditions that disrupt the cellular redox environment lead to increased spontaneous action potential firing in the absence of light thus occlude the l-LNv light response. Dark spontaneous firing frequency of l-LNv is significantly increased in sod1−/− and sod2−/− flies relative to genetic controls (Dataset S1). Dark spontaneous firing rate of l-LNv is significantly increased following acute H2O2 treatment relative to vehicle controls in genetic WT control flies (Fig. S4.3C, D, and G and Dataset S1). Acute H2O2-induced increases in dark spontaneous firing rate of l-LNv are Hk dependent, as no significant increase in dark spontaneous firing rate of l-LNv is observed following acute

H2O2 treatment in hk−/− flies (which resemble vehicle controls for the hk−/− genotype and the genetic controls), but the dark spontaneous firing rate of l-LNv is significantly increased in flies with LNv-directed WT Hk expression in the hk−/− genetic background, which in turn resemble the H2O2 response of WT controls (Fig. S4.3E–G). Thus, acute H2O2-induced increases in dark spontaneous firing rate of l-LNv are Hk dependent, demonstrating an in vivo role for Hk connecting cellular redox environment and membrane firing properties.

4.3.5 WT Hk expression functionally rescues the Cry-mediated light response in hk−/− flies, whereas mutants that disrupt the Hk redox sensor fail to rescue.

Ion channels express motifs that confer modulation to signaling pathways (Holmes et al., 1996; Nitabach et al., 2001) or metabolic cues (Noma, 1983). Structural analysis of fly and mammalian Kvβ proteins reveal that they are functional AKRs (Chouinard et al., 1995; Gulbis et al., 1999; Gulbis et al., 2000; Long et al., 2005; McCormack and McDonnell, 1994), measured by using heterologous expression systems (Pan et al., 2008; Pérez-García et al., 1999; Weng et al., 2006). To determine whether the loss of the CRY-mediated l-LNv light response in hk−/− is a result of the loss of the redox sensor in this Kvβ subunit, we tested a matrix of genetic rescue experiments in the hk−/− genetic background by LNv-targeted expression of functional WT Hk or point mutants that disable the enzymatic activity of Kvβ without affecting protein expression levels (Campomanes et al., 2002; Pan et al., 2008; Weng et al., 2006). Fig. 4.3A shows a structural model of the Kvβ subunit in blue, with the NADP cofactor depicted in yellow. Two highly conserved residues (Scott et al., 1994) near the NADP+ cofactor, D260 and K289, depicted in magenta, are critical for enzymatic activity of Kvβ (Fig. 4.3B) (Pan et al., 2008; Weng et

al., 2006). We focused on these two sites because extensive previous work shows that mutations at these residues impair redox sensing without influencing protein expression or trafficking (Campomanes et al., 2002; Pan et al., 2008; Weng et al., 2006). To confirm that the *Drosophila* Hk D260 and K289 mutations do not affect protein expression or trafficking, they were tested in a GFP-tagged K isoform of Hk, and they express at equivalent or higher levels relative to WT Hk with no discernible changes in cellular protein distribution (Fig. S4.4). The l-LNv light response to blue light is cell-autonomously restored to levels indistinguishable from controls by WT Hk expression in the hk−/− genetic background (Fig. 4.3C). In contrast, the l-LNv light response to blue light is not functionally rescued by expression of the D260N-Hk mutant (Fig. 4.3D) or the K289M-Hk mutant in the hk−/− genetic background (Fig. 4.3E). The blue and white light response recorded in l-LNv neurons with LNv-targeted expression of WT Hk in the hk−/− genetic background is indistinguishable from the control light response, whereas similar LNv targeted expression of D260N- and K289M-Hk are significantly lower than the control light response and are indistinguishable from the severely attenuated light response seen in hk−/− (Fig. 4.3F, middle bars). Control, hk−/−, and WT Hk, D260N-Hk, and K289M-Hk expressed in the LNv in the hk−/− genetic background all show no response to orange light (Fig. 4.3F). The baseline l-LNv spontaneous firing rate recorded in the absence of light for control, hk−/−, and WT Hk, D260N-Hk, and K289M-Hk expressed in the hk−/− genetic background show no significant differences, indicating that the electrophysiological effects noted previously are specific for Cry-mediated light response (Fig. 4.3G and Dataset S4.1).

4.3.6 The ether-a-go-go family K+ channels underlie CRY-mediated membrane depolarization and increased neuronal firing rate in response to light.

Hk also coassembles with *D. melanogaster* EAG-family Kvα subunits (Petersen et al., 2004; Wilson et al., 1998). To determine whether EAG-family Kvα subunits contribute to the l-LNv CRY-mediated light response, including membrane depolarization, we expressed the dominant-negative eag∆932 transgene (eag-DN) (Broughton et al., 2004) in the LNv driven by the pdf-GAL4 promoter. LNv-targeted expression of eag-DN eliminates blue and white light responses seen in controls (Fig. 4.4 A, B, and F). Similar to the LNv targeted expression of eag-DN, no blue or white light responses are seen in l-LNv recordings prepared from eag genetic null mutants (eag amorphic; Fig. 4.4F). In contrast, blue and white light responses recorded from the l-LNv of dslo-null mutant flies, a Ca-sensitive K channel that is not reported to interact with Hk but has been reported to be modulated by redox state (Santarelli et al., 2006; Tang et al., 2004), are indistinguishable from control (Fig. 4.4F). No orange light responses were observed for all genotypes tested (Fig. 4.4F).

As eag-DN expression could potentially disrupt the function of all three closely related members of the *Drosophila melanogaster* EAG family [EAG, EAG-related gene (ERG), and EAG-like K+ channel gene (ELK)], we measured the blue and white light response following LNv-targeted expression of a single RNAi line for EAG and two independent RNAi lines each for ERG and ELK. Compared with the normal blue and white light responses seen in l-LNv recordings prepared from an RNAi control line (Fig. 4.4G), significantly lower blue and white light responses are recorded following the LNv targeted expression of eag RNAi and both lines for erg RNAi (Fig. 4.4 C, D, and G). In contrast,

the blue and white light responses are indistinguishable from controls in l-LNv recordings following LNv targeted expression of both elk RNAi lines (Fig. 4.4 E and G). No orange light responses were observed for all RNAi line genotypes tested (Fig. 4.4G). Baseline l-LNv firing rate in the dark was measured for all genotypes tested and all were indistinguishable from control, except for the eag amorphic-null mutant, which exhibits a significantly higher baseline firing rate (Fig. 4.4H and Dataset 4.S1). Membrane depolarization response to blue light in the dslo-null mutant is indistinguishable from control recordings (Fig. 4.4I), but is significantly lower in neurons recorded from the eag amorphic-null mutant or following LNv-targeted expression of eag-DN (Fig. 4.4I). Similarly, blue light-evoked l-LNv depolarization is significantly lower relative to control following LNv targeted expression of eag RNAi and two independent erg RNAi lines, but not two independent elk RNAi lines (Fig. 4.4I). EAG-family channels regulate membrane resting potential and the action potential repolarization (Ganetzky et al., 1999), whereas Shaker-type K+ channels, which also coassemble with Hk, have very little effect on membrane resting potential, but regulate firing rate subject to rapid inactivation that contributes to cumulative inactivation (Hoffman et al., 1997). Taken together, the results indicate that Hk-coassembled EAG and ERG (but not ELK) K+ channels underlie CRY-mediated light-evoked increased firing rate and depolarization.

4.4 Discussion

Acute behavioral arousal to blue light is significantly attenuated in CRY mutants. We identify a redox signaling couple between blue light-activated CRY and rapid membrane depolarization via the redox sensor of Kvβ channel subunits coassembled with Kvα channel subunits. Additional unknown factors may act as intermediates between

CRY and Hk. This finding provides in vivo validation of a very longstanding hypothesis that the highly conserved redox sensor of Kvβ subunit functionally senses cellular redox events to physiological changes in membrane electrical potential. Genetic loss of any single component functionally disrupts the CRY-mediated blue light response, which is functionally rescued by LNv restricted expression of their WT genes in the null backgrounds. Although little is known about the structural contacts between Kvβ and EAG subunits, Kvβ subunits make extensive physical contacts in a fourfold symmetric fashion in 1:1 stoichiometry with the T1 assembly domain of other coassembled tetrameric Kvα subunits that form the complete functional channel (Gulbis et al., 1999; Gulbis et al., 2000; Long et al., 2005). Application of Kvβ redox chemical substrate modulates voltage-evoked channel peak current, steady-state current, and inactivation in heterologously expressed α-β channels, which are reversed by fresh NADPH (Pan et al., 2008; Weng et al., 2006). These results indicate that measurements of channel biophysical properties can reflect the redox enzymatic cycle of Kvβ as these channel modulatory effects are absent in preparations that lack the expression of WT Kvβ subunits or express redox sensor mutant Kvβ subunits (Pan et al., 2008; Weng et al., 2006). Whether direct chemical redox reactions occur between CRY and Hk is unclear. For CRY, light or chemical reduction induces one-electron reduction of the FAD cofactor of CRY (Berndt et al., 2007; Kao et al., 2008; Vaidya et al., 2013), whereas the reductive catalytic mechanism of AKRs (such as Hk) requires a hydride ion transferred from NADPH to a substrate carbonyl, then a solvent-donated proton reduces the substrate carbonyl to an alcohol (Barski et al., 2008). These differences in redox chemistry between CRY and Hk suggest that other intermediates, such as oxygen, are possibly required for redox coupling.

Spectroscopic analysis of animal and plant CRYs suggest that light activation causes reduction of the FAD oxidized base state (Berndt et al., 2007; Kao et al., 2008; Lin et al., 1995; Vaidya et al., 2013). Light activation of *Drosophila* CRY also evokes conformational changes in the C terminus of CRY that clearly promotes CRY C-terminal access to proteolytic degradation and subsequent interactions with the TIMELESS clock protein, thus signaling degradation and circadian entrainment (Dissel et al., 2004; Ozturk et al., 2011; Ozturk et al., 2014; Peschel et al., 2009). However, all existing evidence suggests that light activated CRY-mediated circadian entrainment and membrane electrical phototransduction operate under different mechanisms, including their different activation thresholds and relative dependence on the C terminus of CRY (Fogle et al., 2011). Further distinguishing the distinct mechanisms of the downstream effects of light-activated CRY, the light-induced conformational changes that couple CRY to ubiquitin ligase binding (thus causing circadian entrainment) occur in oxidized and reduced states of CRY and are unaffected in CRY tryptophan mutants that presumably are responsible for intraprotein electron transfer reactions following light-evoked reduction of the FAD cofactor (Ozturk et al., 2014). Another recent study shows that light- or chemical-evoked reduction of *Drosophila* CRY FAD is coupled to conformational changes of the CRY C terminus (Vaidya et al., 2013), along with reporting a surprising negative result that DPI has no effect on the reoxidation of the reduced anionic semiquinone of purified *Drosophila* CRY. DPI could hypothetically influence the electrophysiological light response by blocking the pentose phosphate pathway (Riganti et al., 2004) which produces the Hk redox cofactor NADPH, but this does not explain the light dependence for DPI blocking the electrophysiological light response herein. The available evidence indicates that CRY-

mediated light evoked membrane depolarization occurs independently of conformational changes in the CRY C-terminal domain but depends on redox changes in CRY, whereas CRY-mediated light evoked circadian entrainment depends on conformational changes in the CRY C-terminal domain and may or may not depend on CRY redox state.

Light-activated CRY evokes rapid membrane depolarization through the redox sensor of the Kvβ subunit Hk. A general role for circadian regulation of redox state coupled to membrane excitability has been described recently in mammalian suprachiasmatic neurons (Wang et al., 2012). Redox modulation of circadian neural excitability may be a well-conserved feature.

Author Contributions

T.C.H. designed research; K.J.F., L.S.B., J.H.H., T.T.T., and N.A.D. performed research; L.R., Y.C., and M.Z. contributed new reagents/analytic tools; K.J.F., L.S.B., J.H.H., N.A.D., and T.C.H. analyzed data; and K.J.F. and T.C.H. wrote the paper.

4.5 Figures

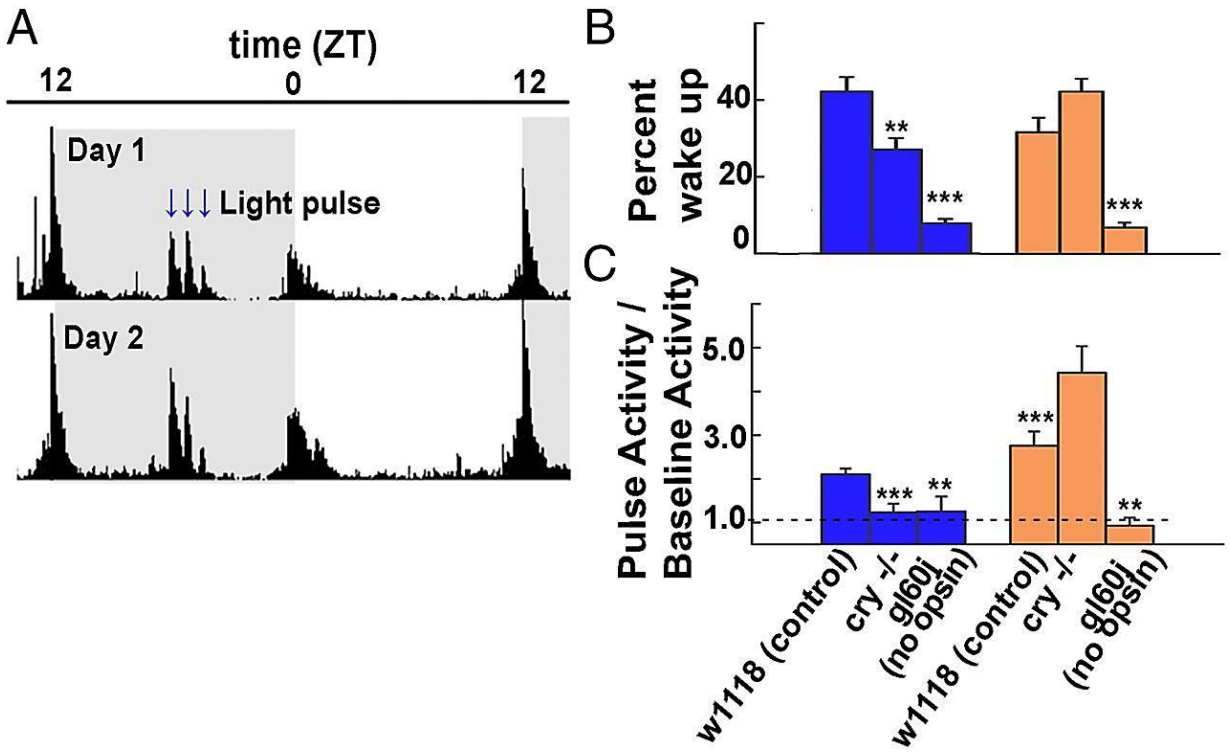

Figure 4.1. Blue light activation of CRY contributes to rapid acute behavioral arousal responses. (A) Two days of averaged locomotor activity of control flies maintained in 12-h:12-h light:dark cycles. Entrainment shifts following the blue or orange nighttime light pulse protocol do not occur for any genotypes tested. (B) The averaged values of sleeping flies that wake in arousal response to blue and orange nighttime light pulses are shown for control (41 ± 4%, n = 40 blue; 32.6 ± 4%, n = 32 orange), cry−/− (26.3 ± 3%, n = 26 blue; 43.6 ± 3%, n = 17 orange), and gl60j (7.6 ± 1%, n = 14 blue; 7.1 ± 1%, n = 18 orange) mutant flies. Significantly fewer sleeping cry−/− flies wake in response to blue light pulses (P = 0.007), whereas the percentage of sleeping cry−/− flies that wake in response to orange light pulses does not differ from control (P = 0.09). Sleeping flies lacking all external opsin-based photoreceptors (gl60j mutants) show similar severe defects in their wake arousal responses to blue (P < 0.001) and orange (P = 0.001) light pulses. (C) The averaged normalized (pulse activity/baseline activity) values of behavioral arousal locomotor responses of awake flies are shown for control (2.1 ± 0.1, n = 509 blue; 2.8 ± 0.3, n = 286 orange), cry−/− (1.2 ± 0.2, n = 173 blue; 4.4 ± 0.6, n = 79 orange), and gl60j (1.3 ± 0.3, n = 86 blue; 0.9 ± 0.2, n = 112 orange) flies. The arousal response to blue light pulses is significantly attenuated in awake cry−/− flies (P = 0.002), but these flies show a significantly higher arousal response to orange light pulses (P = 0.02). In contrast, the arousal response to blue (P = 0.034) and orange (P = 0.003) light is significantly decreased in awake gl60j mutant flies. All data values and statistics are presented in detail in Dataset S1.

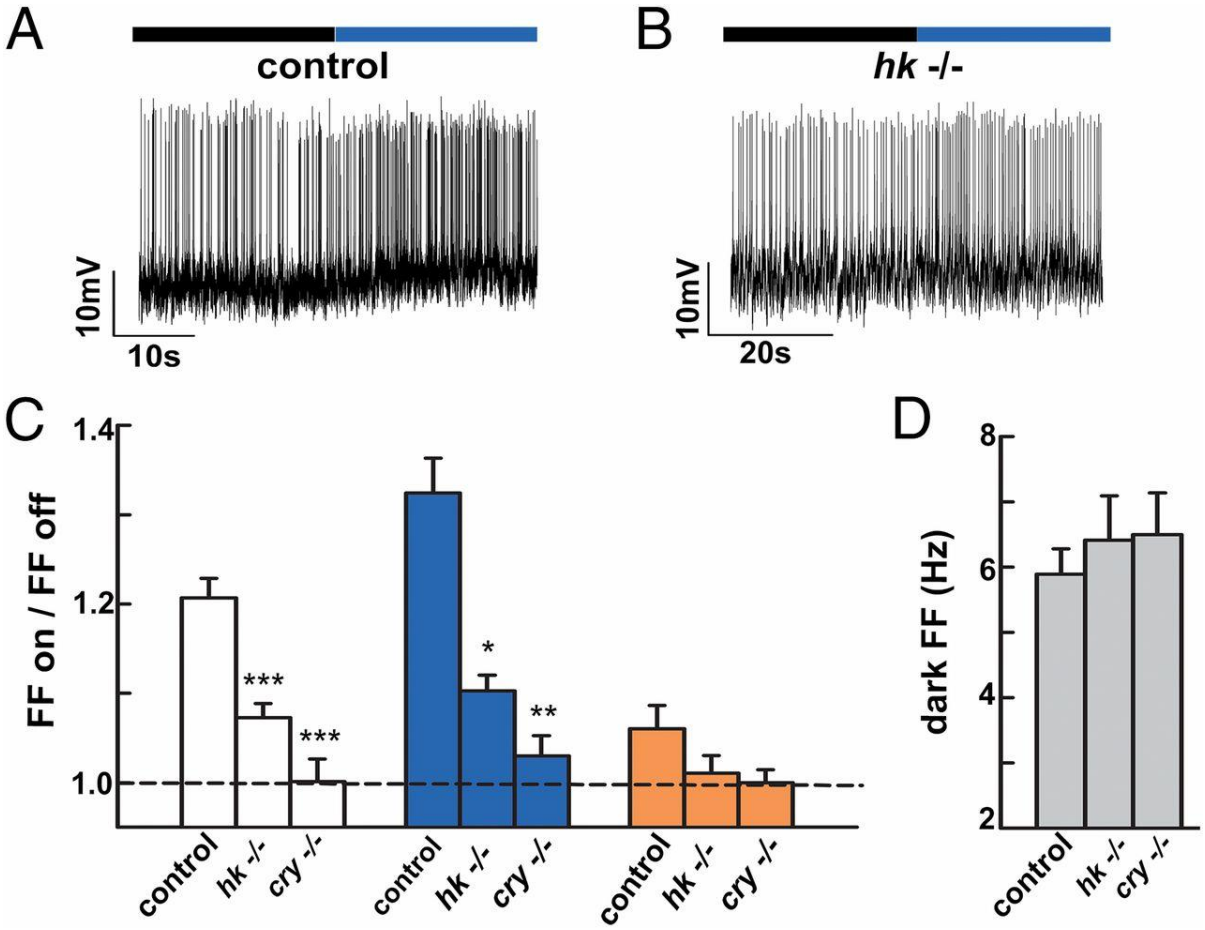

Figure 4.2. Mutant flies lacking the redox-sensor Kvβ subunit hyperkinetic have a significantly reduced l-LNv light response that is indistinguishable from cry−/−. (A) Representative traces for control blue l-LNv light response (0.6 mW/cm^2, 375–450 nm, purple bar; black bar indicates no light) vs. (B) genetic null hk−/−. (C) Bar graph quantifies the l-LNv light response for control, hk−/−, and cry−/− flies. In white light (4 mW/cm^2), control flies (1.21 ± 0.02, n = 26) are significantly different from hk−/− (1.07 ± 0.02, n = 16, P < 0.001) and cry−/− (1.00 ± 0.03, n = 14, P < 0.001 vs. control) flies. In blue light, control flies (1.32 ± 0.04, n = 30) are also significantly different from hk−/− (1.10 ± 0.02, n = 23, P = 0.001) and cry−/− flies (1.03 ± 0.02, n = 17, P = 0.0001). The severely attenuated light responses of hk−/− and cry−/− flies do not differ from each other (P = 0.14 in white; P = 0.36 in violet). In orange light (4 mW/cm^2, >550 nm), control (1.04 ± 0.11, n = 23), hk−/− (1.01 ± 0.08, n = 17), and cry−/− (1.00 ± 0.05, n = 13) flies, responses do not differ (P > 0.35 in all pairwise comparisons). (D) Basal firing frequencies under dark conditions. The values for control (5.89 Hz ± 0.39, n = 77), hk−/− (6.41 Hz ± 0.68, n = 37), and cry−/− (6.5 Hz ± 0.64, n = 38) do not differ (P = 0.77 and P = 0.69 vs. control, respectively). All data values and statistics are presented in detail in Dataset S1.

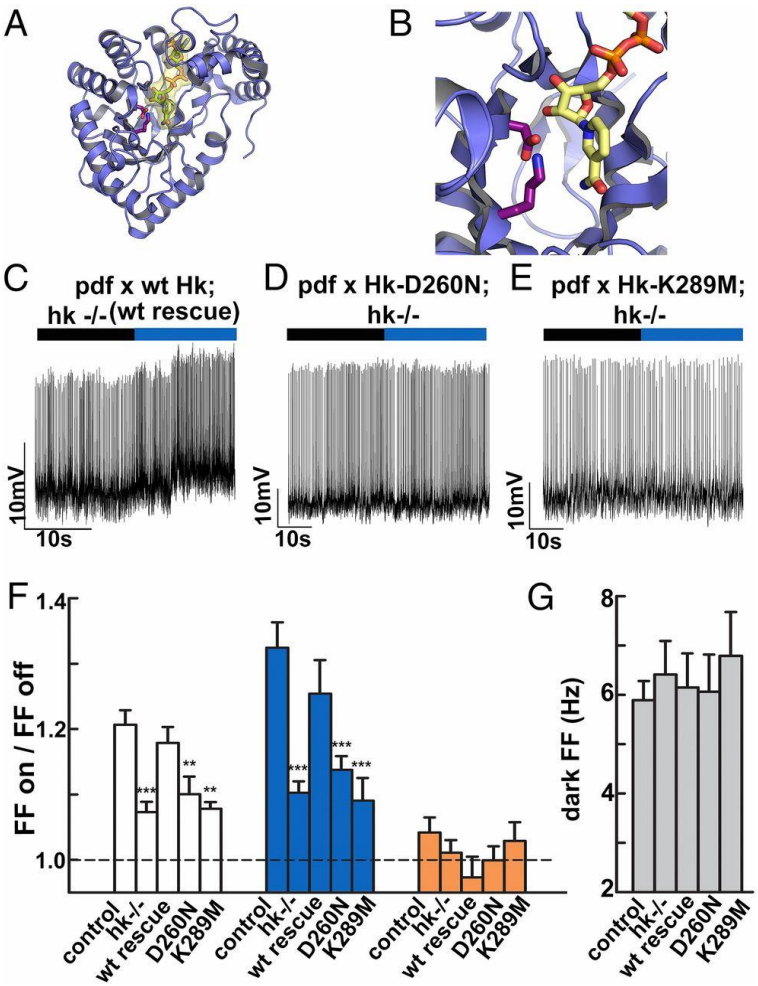

Figure 4.3. LNv-directed expression of WT Hk in hk−/− flies functionally rescues the Cry-mediated light response, whereas expression of Hk redox sensor-disabling mutants fail to rescue. (A) Structural model of the Kvβ subunit (blue) bound to the NADP+ cofactor (yellow). (B) Positional model of two key residues for Kvβ redox sensing (D260 and K289) depicted in stick form in magenta relative to the NADP+ cofactor (yellow). (C) WT Hk expressed in LNv neurons in the hk−/− genetic background rescues the l-LNv light response (black bar indicates no light; purple bar indicates 375–450 nm blue light, 0.6 mW/cm^2). In contrast, LNv-directed expression of redox-disabled point mutants D260N-Hk (D) and K289M-Hk (E) in hk−/− fail to rescue the l-LNv blue light response. (F) The white light response (firing frequency lights on/lights off, 4 mW/cm^2) recorded in l-LNv expressing WT Hk in hk−/− (WT rescue, 1.18 ± 0.02, n = 22) is indistinguishable from the control response (1.21 ± 0.02, n = 26, P = 0.79) but is significantly different from hk−/− (1.07 ± 0.02, n = 16, P = 0.004), showing functional rescue. In contrast, LNv-directed expression of the redox-disabled D260N-Hk mutant in hk−/− (1.12 ± 0.03, n = 13) is significantly different from control (P = 0.036) but not hk−/− (P = 0.58) recordings, indicating failure to rescue. Similarly, the white light response recorded in l-LNv expressing the redox disabled K289M-Hk mutant in hk−/− (1.08 ± 0.01, n = 12) is significantly different from control (P < 0.001) but not null (P = 0.99) recordings. The response to blue light in WT rescue l-LNv recordings (1.25 ± 0.05,

n = 16) is not different from control (P = 0.61), but differs from hk−/− (1.10 ± 0.02, n = 23, P = 0.038); the light response in recordings of l-LNv expressing D260N-Hk is significantly less than from control (1.15 ± 0.02, n = 15, P = 0.01) and not different from null (P = 0.88); the light response in recordings of l-LNv expressing K289M-Hk in hk−/− (1.06 ± 0.02, n = 13) is significantly less than control (P < 0.001) and not different from null (P = 0.95). In orange light (4 mW/cm^2, >550 nm), WT rescue (0.96 ± 0.1, n = 11), D260N-Hk (1.00 ± 0.06, n = 8), and K289M-Hk (1.03 ± 0.09, n = 10) are not significantly different from each other, control (1.04 ± 0.11, n = 23), or hk−/− (1.01 ± 0.08, n = 17) recordings (P > 0.1 in all comparisons). (G) The basal firing frequencies in the dark for control (5.89 Hz ± 0.39, n = 77), hk−/− (6.41 Hz ± 0.68, n = 37), Hk WT rescue (6.15 Hz ± 0.69, n = 31), Hk D260N rescue (6.06 Hz ± 0.76, n = 23), and Hk K289M rescue (6.79 Hz ± 0.89, n = 18) do not differ (P = 0.77, P = 0.941, P = 0.999, and P = 0.874 vs. control, respectively). All data values and statistics are presented in detail in Dataset S1.

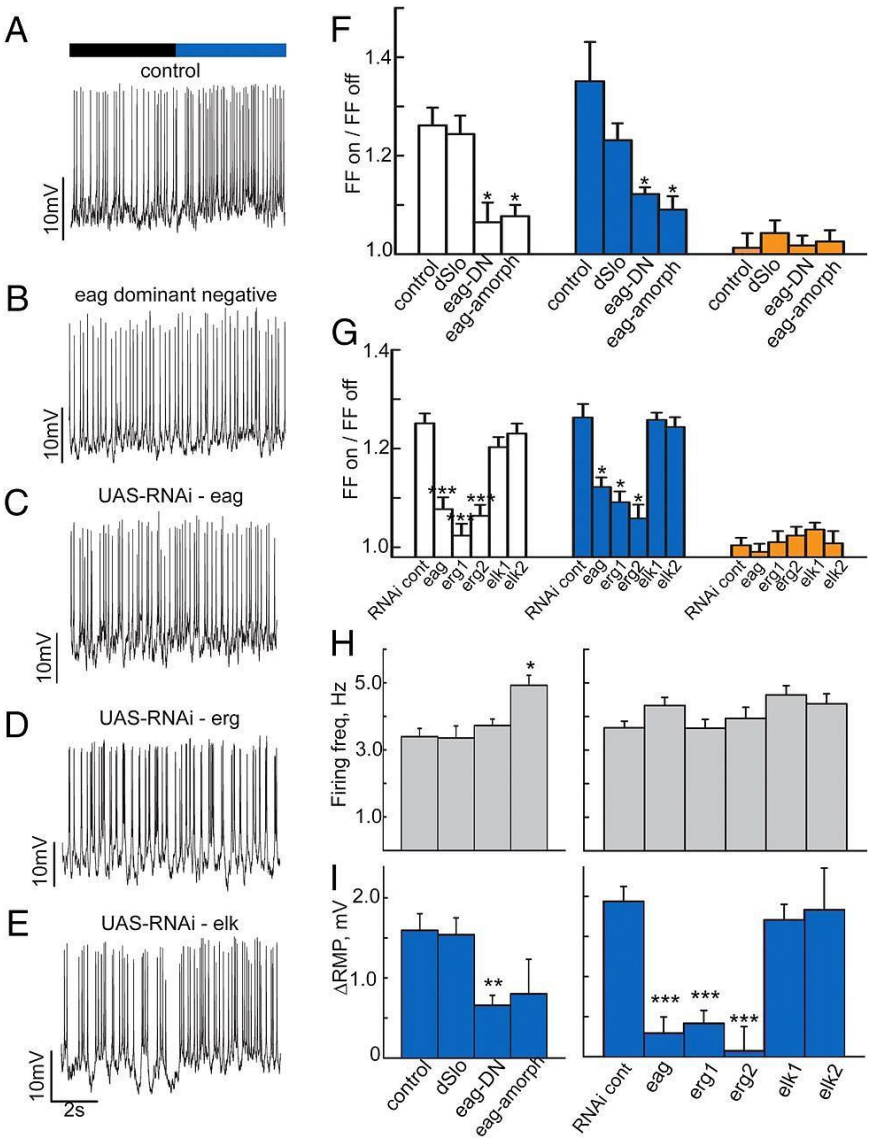

Figure 4.4. The Ether-a-go-go family K+ channels underlie light evoked membrane depolarization and increased neuronal firing rate. Representative traces for control (A), eag-dominant negative (B), pdfGAL4-driven UAS-RNAi against eag (C), pdfGAL4-driven UAS-RNAi against erg (D), and pdfGAL4-driven UAS-RNAi against elk (E). Bar graphs (F) quantify firing frequency change for control flies in white light (1.26 ± 0.04, n = 19), which is not different from the response of dSlo flies (1.23 ± 0.03, n = 24, P > 0.05). Eag-dominant negative (1.06 ± 0.04, n = 18) and eag amorphic flies (1.08 ± 0.02, n = 13) are both different from control and dSlo (P < 0.05 in each case). In blue light, control (1.35 ± 0.08, n = 19) and dSlo (1.23 ± 0.03, n = 26) do not differ (P > 0.05). However, eag-DN (1.12 ± 0.01, n = 19) and eag amorphic (1.09 ± 0.03, n = 13) both differ from control and dSlo (P > 0.05 in each case). The responses to orange light do not differ. (G) The white light response for RNAi genotype-control flies is 1.25 ± 0.02 (n = 19). This is significantly different from the response of flies with pdfGAL4-driven RNAi against eag (1.08 ± 0.02, n = 16, P < 0.001), against erg line 1 (1.02 ± 0.02, n = 16, P < 0.001), and against erg line 2 (1.06 ± 0.02, n = 17). It is not different from the responses

of the two elk RNAi lines (1.20 ± 0.02, n = 24, P = 0.50; and 1.23 ± 0.02, n = 17, P = 0.98, respectively). In blue light, the control response (1.26 ± 0.03, n = 23) is different from that of the eag RNAi line (1.12 ± 0.02, n = 19, P < 0.05) and both erg RNAi lines (1.09 ± 0.02, n = 18, P < 0.05; and 1.06 ± 0.03, n = 16, P < 0.05), but not the elk lines (1.26 ± 0.02, n = 19, P > 0.05; and 1.24 ± 0.02, n = 19, P > 0.05). The responses to orange light again do not differ. (H) The basal dark firing frequencies for control (3.39 Hz ± 0.24, n = 58), dSlo (3.35 Hz ± 0.36, n = 42), and eag-dominant negative (3.72 Hz ± 0.19, n = 47) do not differ (P > 0.05), but that of eag amorphic (eagsc29; 4.92 Hz ± 0.30, n = 25) is different from control (P < 0.05). The firing frequencies for RNAi control (3.66 Hz ± 0.20, n = 43), eag-RNAi (4.32 Hz ± 0.24, n = 39), erg RNAi-1 (3.65 Hz ± 0.26, n = 33), erg RNAi-2 (3.94 Hz ± 0.33, n = 30), elk RNAi line 1 (4.64 Hz ± 0.28, n = 41), and elk RNAi line 2 (4.37 Hz ± 0.30, n = 30) do not differ (P > 0.5 in each case.) (I) Bar graphs quantify the change in resting membrane potential during periods of blue light vs. darkness. Control (1.60 mV ± 0.21, n = 22) and dSlo (1.54 mV ± 0.21, n = 17) do not differ (P > 0.05). eag-DN, however, is different from control and dSlo (0.66 mV ± 0.12, n = 30, P < 0.05). eag amorphic (0.80 mV ± 0.43, n = 13) trended lower, but its difference does not reach significance (P > 0.05). The change in RMP for RNAi control flies is 1.94 mV ± 0.19 (n = 27). This is significantly different from eag RNAi-expressing flies (0.30 mV ± 0.20, n = 15), erg RNAi 1 flies (0.42 mV ± 0.16, n = 16), and erg RNAi 2 flies (0.07 mV ± 0.30, n = 10; P < 0.001 in each case). Elk RNAi-expressing flies lines 1 and 2 (1.71 mV ± 0.19, n = 18; and 1.83 mV ± 0.52, n = 13) do not differ from control (P = 0.978 and P = 1.00, respectively). All data values and statistics are presented in detail in Dataset S1.

4.6 Supplementary Information

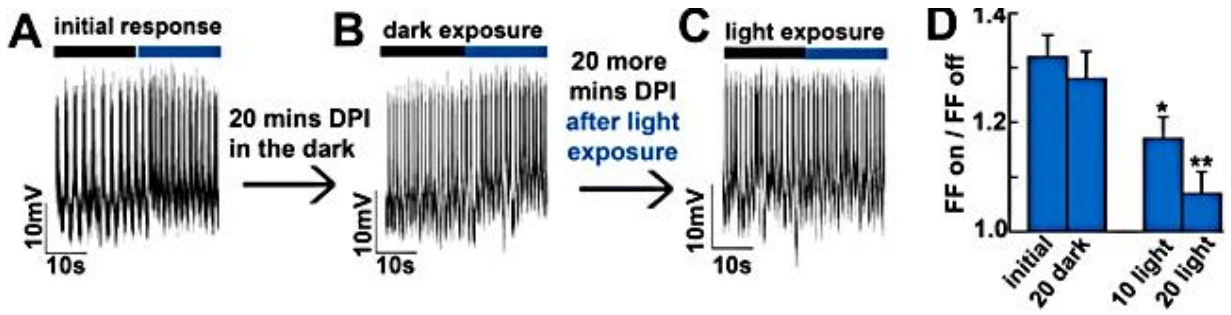

Figure S4.1. The l-LNv light response requires a CRY-specific FAD redox reaction. (A) Representative recording of control l-LNv blue light response (black bar indicates no light, purple bar indicates 375–450 nm blue light, 0.6 mW/cm^2). (B) Representative intact l-LNv light response (firing frequency lights on/lights off) following 16.8 μM DPI perfusion in the dark for 20 min. (C) At 15 min after first light exposure (35 min total DPI), the light response is reduced. (D) Bar graphs quantifying the l-LNv response to blue light. The initial blue light response following 20 min of DPI (1.28 ± 0.05, n = 10) does not differ from non-DPI controls (1.32 ± 0.04, n = 39, P = 0.93). After 10–15 min DPI following initial exposure to light (35 min DPI exposure), the blue light response is lower (1.17 ± 0.04, n = 9, P = 0.15 vs. non-DPI control recordings). By 20–25 min after light exposure (40–45 min DPI exposure), the blue light response is significantly lower (1.07 ± 0.04, n = 7, P = 0.011 vs. controls).

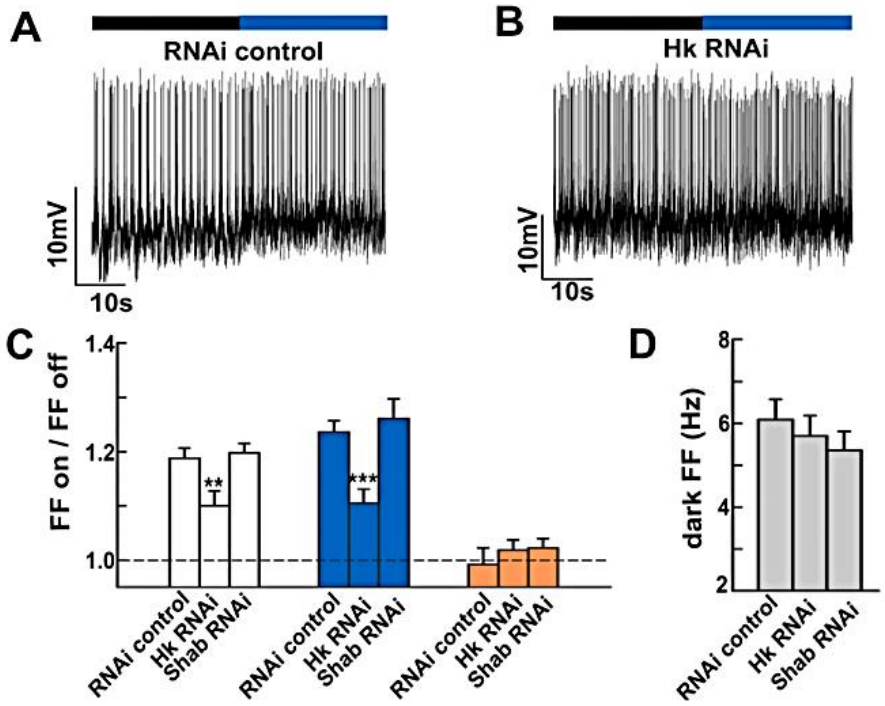

Figure S4.2. LNv-directed expression of hyperkinetic RNAi significantly knocks down the l-LNv light response. (A) Representative traces for the intact control blue l-LNv light response (0.6 mW/cm^2), 375–450 nm, blue bar; black bar indicates no light recorded from RNAi control genotype flies (w, pdfGAL4;pdfGAL4-UASDCR/p12c) vs. (B) Significant attenuation of the blue light response recorded from the l-LNv of flies that express Hk RNAi and DICER in the LNv (w, pdfGAL4; pdfGAL4-UAS-dcr/p12c;UAS-hk-RNAi). (C) Bar graph quantifies the l-LNv white (white bars, 4 mW/cm^2 unfiltered halogen), blue (blue bars, 0.6 mW/cm^2, 375–450 nm blue), and orange (orange bars, 4 mW/cm^2, >550 nm orange) light response for RNAi control, Hk RNAi, and Shab RNAi flies. The l-LNv white light response of control flies (1.19 ± 0.02, n = 16) is significantly different from Hk RNAi (1.10 ± 0.03, n = 28, P = 0.03) but not control Shab RNAi flies (1.20 ± 0.02, n = 17, P = 0.96). Similarly, the l-LNv blue light response of control flies (1.23 ± 0.02, n = 18) is significantly different from Hk RNAi (1.10 ± 0.03, n = 31, P = 0.006) but not control Shab RNAi flies (1.26 ± 0.04, n = 20, P = 0.78). The l-LNv orange light responses do not differ between the RNAi control (0.99 ± 0.03, n = 15), Hk RNAi (1.02 ± 0.02, n = 20, P = 0.79), and Shab RNAi (1.02 ± 0.02, n = 13, P = 0.84) genotypes. (D) The basal dark firing frequencies for RNAi control flies (6.09 Hz ± 0.49, n = 27), Hk RNAi flies (5.70 Hz ± 0.49, n = 37), and Shab RNAi flies (5.36 Hz ± 0.45, n = 29) do not differ (P = 0.96 and P = 0.80 vs. control, respectively). All data values and statistics are presented in detail in Dataset S1.

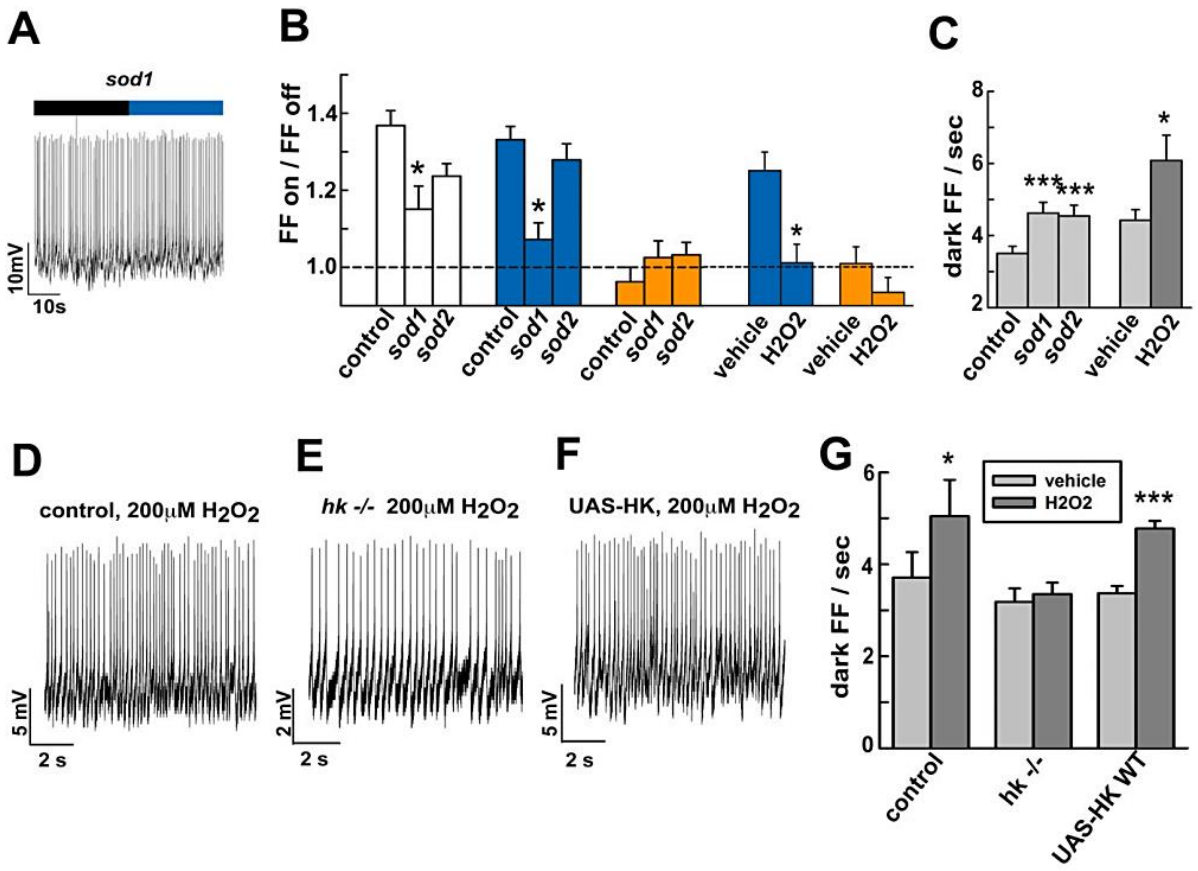

Figure S4.3. The l-LNv light response is occluded by genetic or chemical disruption of the cellular redox environment in an Hk redox sensor-dependent manner. (A) Representative recording of sod1−/− (sod1) l-LNv. (B) The l-LNv response of sod1−/− (1.15 ± 0.06, n = 11) to white light (4 mW/cm^2) is significantly lower than control (1.36 ± 0.04, P = 0.023, n = 13), whereas that of sod2−/− (sod2) (1.23 ± 0.03, n = 14) does not differ from control (P = 0.14). sod1−/− also exhibits significantly attenuated l-LNv blue light (0.6 mW/cm^2, 375–450 nm) response (1.07 ± 0.04, n = 8) relative to control (1.33 ± 0.03, n = 16, P = 0.01), whereas sod2−/− mutants do not differ from control (1.27 ± 0.04, n = 14, P = 0.53). Control (0.96 ± 0.04, n = 16), sod1−/− (1.025 ± 0.04, n = 8), and sod2−/− (1.03 ± 0.03, n = 14) all show no significant response to orange light (4 mW/cm^2, >550 nm). Acute treatment with H2O2 (200 μM) significantly abolishes the l-LNv response to blue light (1.01 ± 0.05, n = 11, P = 0.0007, 375–450 nm blue light, 0.6 mW/cm^2) relative to control (1.25 ± 0.05, n = 8), whereas there is no significant response to orange light (4 mW/cm^2, >550 nm) in vehicle control (1.01 ± 0.04, n = 7) or H2O2 conditions (0.93 ± 0.04, n = 11). (C) Dark spontaneous firing frequency is significantly greater (P < 0.01) in sod1−/− (4.62 Hz ± 0.3, n = 41, P = 0.001) and sod2−/− (4.54 Hz ± 0.3, n = 61, P < 0.001) relative to control (3.50 Hz ± 0.2, n = 49). Dark spontaneous firing frequency is significantly greater following H2O2 treatment (6.08 Hz ± 0.7, n = 21) relative to vehicle control (4.42 Hz ± 0.3, n = 23, P = 0.03). (D) Representative recording of l-LNv firing in dark in 200 μM H2O2 treatment for WT genetic control vs. (E) genetic null hk−/−, (F) and WT Hk expressed in LNv in hk−/−

genetic background (Hk WT rescue). (G) Dark spontaneous firing frequency in l-LNv is significantly higher following H_2O_2 treatment (5.04 ± 1.58, n = 5) compared with vehicle treatment (3.71 ± 1.10, n = 5, P = 0.020) in neurons from WT control flies. Dark spontaneous firing frequency in l-LNv following H_2O_2 treatment in genetic null hk−/− (3.35 ± 0.60, n = 7) does not differ from vehicle control treatment (3.18 ± 0.71, n = 7, P = 0.249). Expression of WT Hk in the LNv of genetic null hk−/− shows significant increase in l-LNv dark spontaneous firing frequency following H_2O_2 treatment (4.77 ± 0.37, n = 6) compared with vehicle treatment (3.37 ± 0.35, n = 6, P ≤ 0.001), showing functional rescue and Hk dependence for the H_2O_2 induced increase in dark spontaneous firing rate. l-LNv Firing rates for vehicle controls for genetic WT control flies, genetic null hk−/− flies, and Hk WT rescue flies do not differ. All data values and statistics are presented in detail in Dataset S1.

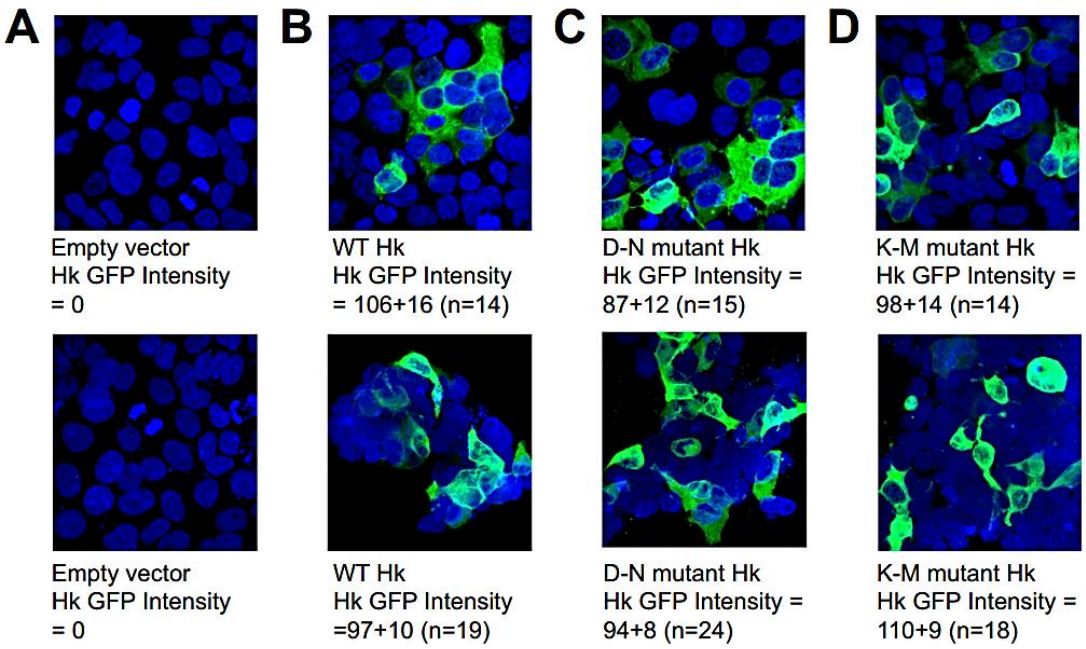

Figure S4.4. Hk mutants express at equivalent levels to WT Hk. Expression of *Drosophila* Hk WT GFP, Hk D260N GFP, and Hk K289M GFP (A–D) in HEK293a grown in DMEM media. Cells (2 × 105) were plated in each well in a 12-well plate maintained overnight at 37 °C. HEK293a cells were transfected with 1.2 µg empty pCS2+ vector (A), Hk WT GFP-pCS2+ (B), Hk D260N GFP pCS2+ (C), or Hk K289M GFP pCS2+ (D). At 48 h later, cells were fixed, immunostained with anti-EGFP (green), and counterstained with DAPI (blue). The images were scanned with a Zeiss LSM700 confocal microscope by using Zen software. (A–D) Z-stack image ranges from 16 to 26 µm in thickness. Cell images were analyzed with Volocity 6.3 software (Perkin-Elmer). Hk mutant expression normalized to DAPI express at equivalent levels compared with WT Hk. Fluorescence values are expressed as pixel intensity per cubic millimeter. There are no significant differences between WT and mutant Hk expression (one-way ANOVA). Results of two of six representative experiments are shown in the upper and lower panels.

CHAPTER 5

CRYPTOCHROME Mediates Behavioral Executive Choice in Response to Ultraviolet Light

(Baik, Fogle, Roberts, Galschiodt, Nguy, Holmes)

Abstract

Drosophila melanogaster CRYPTOCHROME (CRY) mediates behavioral and electrophysiological responses to blue light in circadian and arousal neurons. However, spectroscopic and biochemical assays of heterologously expressed CRY suggest that CRY may mediate functional responses to ultraviolet (UV) light as well. To determine the relative contributions of distinct phototransduction systems for UV light responses, we tested mutants lacking CRY and mutants with disrupted opsin-based phototransduction with a battery of behavioral and electrophysiological tests. While both CRY and opsin-based external photoreceptor systems cooperate as UV light activated sensory systems, CRY mediates behavioral responses related to executive function, consistent with its expression in central brain neurons.

5.1 Introduction

For nearly a century, it has been assumed that insect responses to ultraviolet (UV) light are mediated by UV-sensitive opsins expressed in eyes and other external photoreceptors. However, various organisms often express other non-opsin photoreceptors including the blue-light sensitive flavoprotein CRYPTOCHROME (CRY). In *Drosophila melanogaster*, CRY mediates rapid membrane depolarization and increased spontaneous action potential firing rate in the lateral ventral neurons (LNvs)

which are involved in arousal and circadian responses (Sheeba et al., 2008a). Blue light activated CRY couples to membrane depolarization in *Drosophila* LNv neurons by a redox based mechanism to potassium channel heteromultimeric complexes consisting of the redox receptor cytoplasmic potassium beta (Kvβ) HYPERKINETIC (Hk), and ion conducting voltage-gated potassium (Kvα) ether-a-go-go family subunits (Fogle et al., 2015). Electrical activity in the LNvs contributes to circadian rhythms (Nitabach et al., 2002; Nitabach et al., 2006; Sheeba et al., 2008a) and, reciprocally, circadian neuronal firing rate is circadian regulated (Flourakis et al., 2015; Sheeba et al., 2008a). Circadian regulation of firing rate is also observed in other species (Belle et al., 2009; Michel et al., 1993). CRY is best characterized as the primary photoreceptor responsible for blue light-activated circadian entrainment (Busza et al., 2004; Emery et al., 1998; Helfrich-Förster et al., 2001; Lin et al., 2001; Peschel et al., 2009; Rosato et al., 2001; Stanewsky et al., 1998). CRY expressing large lateral ventral neurons (l-LNvs) also mediate acute behavioral arousal responses to blue light (Fogle et al., 2015; Fogle et al., 2011; Kumar et al., 2012; Shang et al., 2008; Sheeba et al., 2008a; Sheeba et al., 2008b). Further work shows that arousal and circadian functions are not strictly segregated between the LNv subsets as the small LNvs (s-LNvs) contribute also to arousal (Parisky et al., 2008) and clock cycling is robustly altered in the l-LNv in response to light entrainment cues (Roberts et al., 2015).

Many insects, including *Drosophila*, display a strong spectral sensitivity for short wavelength light. The ability to sense and respond to UV light is important as it guides physiological and behavioral responses to sunlight that are crucial to an organism's survival. The absorbance spectra of purified CRY from *Drosophila* show a strong UV

peak near 365 nm in addition to the 450 nm blue light peak (Berndt et al., 2007; Bouly et al., 2007; Hoang et al., 2008). Further, UV light triggers CRY degradation in cultured cells that heterologously express CRY (VanVickle-Chavez and Van Gelder, 2007). To test the *in vivo* functional significance of these earlier findings, we measured behavioral and electrophysiological responses to UV light near the CRY UV peak.

5.2 Materials and Methods

Electrophysiology

The ultraviolet wavelength range was isolated using a filter cube designed for DAPI imaging (Olympus). Light intensities were determined by a Newport 842-PE Power/Energy meter. The UV dose response curve was performed by placing neutral density filters of varying degrees of opaqueness in the light path from the mercury bulb to the brain prep. Most recordings lasted for the duration of the full dose-response curve, and all intensities for all genotypes include at least five different brains.

Behavioral experiments

To determine the UV light induced phase response curve in control, $cry^{-/-}$ null mutant and gl^{60j} mutant flies lacking external photoreceptors, flies were entrained for a minimum of three days in standard white light 12:12 hr LD (0.46 mW/cm^2), followed by three days of uninterrupted darkness (DD). On the fourth day, a ten-minute pulse of UV light (365nm, 0.85 mW/cm^2) was given at varying CTs at 4 hr intervals (2, 6, 10, 14, 18 and 22hr) to induce a phase shift. This was followed by four more days of DD. Each time point of PRC was analyzed by at least two individual behavioral runs and represents at least 60 flies. The time of peak morning activity for each day before the UV pulse and each day after the pulse was calculated and averaged. The data points presented are

the average difference between these peaks (phase shift). Bins are 12 minutes in length and each graph is an average of four separate entrainment runs, three days pre-pulse and three days post-pulse (twelve total days of activity per condition).

Light choice

Standard Trikinetics activity monitors were modified to remove the center barrier in order to accommodate 5 mm glass tubes (Trikinetics, Waltham, MA). Two air holes were drilled into the tube equidistant from the ends, which were both plugged with fly food and sealed with paraffin wax after the fly was introduced to the tube. Flies were entrained in the tubes for 3 days in white light 12:12 hr LD (0.46 mW/cm^2) and three days in UV light (365 nm, 400 µW/cm^2). Following entrainment, one half of the monitor was covered with either neutral density filters or cardboard, providing the flies with a choice of a darkened environment during the 12 hours of light. Activity for each fly in the lighted versus darkened side of the tube was averaged over 10 days and statistical preferences were determined by t-test. Each genotype was tested over five separate behavioral runs with 80 flies total per genotype.

Light pulse arousal

Flies were entrained for a minimum of three days to a normal LD 12:12 cycle. During the dark phase, they were given three consecutive 5-minute pulses of UV (365nm, 0.85 mW/cm^2) or orange (595nm, 1.25 mW/cm^2) at ZT 18, 19, and 20, for three nights. Activity during all of these pulses and for the subsequent 40 minutes were binned in five-minute intervals and averaged. Statistical tests between genotypes at each bin of five minutes were conducted by one-way ANOVA. Sleeping flies, defined by inactivity for five minutes preceding the pulse, were assessed for the percentage that woke up during the

pulse. Active flies were assessed for the change in their activity during and after the pulse; changes were expressed as activity of bin/activity during baseline.

Behavioral phototaxis

An electrophoresis system photo-documentation hood (15 x 20 cm, Fisher Biotech) was converted into a light-tight chamber to hold populations of flies for recordings. A DAM2 *Drosophila* Activity Monitor (32 channels with dual infrared beams, Trikinetics) was mounted to the front of the chamber and sealed with a glass cover on the outer face. For each experiment, a group of 40 adult flies was directly placed into the chamber. W^{1118}, and cry^{01} flies were independently tested. The entire apparatus was then placed in a light-sealed enclosure where the flies are left to habituate for 30 minutes before recording. To capture time-of-day effects for phototactic responses, behavioral activity was recorded from CT 21 to CT 3. An LED light source was turned on for 5 cycles of 5 minute pulses followed by 55 minutes of constant darkness. The LED light source was either: (1) a Prizmatix UHP-Mic-LED-595 (595nm) or (2) a Prizmatix Mic-LED-365, High Power UV LED (365nm). The light intensity for both LED sources was set to 2.97 $\mu W/cm^2$. Due to the narrow collimated light emission of these two light sources, they were reflected off an inner surface of the enclosure so that their light emissions covered all 32 channels of the activity monitor. Data was collected by the DAM2 *Drosophila* Activity Monitor to be analyzed in 1 minute bins. Excel was used for quantitative analysis of average population activity in response to the light pulses relative to baseline measurements of activity in darkness. Statistical significance was determined using one-way ANOVA, Tukey post-hoc test.

Transparency of *Drosophila* cuticles to UV light

The proportion of UV light (365nm) that is transmitted through head and eye cuticles was measured using a modified version of a protocol previously described in (Fogle et al., 2011). Briefly, adult male flies were dissected in ice cold PBS for removal of head or compound eye cuticle tissue within 3 days of eclosion. Three blue-black light strips were mounted facing downward in a light-tight enclosure to shine UV light on a Li-Cor LI-250A light meter with the Li-Cor Quantum sensor facing upward. The quantum sensor was wrapped in aluminum foil with a small pinhole made in the foil with a diameter smaller than the cuticle samples. The transparency of the cuticles was measured as the amount of 365 nm transmitted through the cuticle tissues divided by baseline measurements of the amount of UV light that passes through a small droplet of PBS covering the pinhole. The amount of light transmitted was measured for 10 compound eye and 7 head cuticle tissue samples. A statistical comparison of the percentage of UV light that passes through eye versus head cuticles was determined using student t-test.

5.3 Results

5.3.1 CRY mediates opsin-independent electrophysiological response to UV light in large lateral ventral neurons.

The CRY-expressing small lateral ventral neurons (s-LNVs) are critical for circadian rhythmicity (Helfrich-Forster, 1998), while the large lateral ventral neurons (l-LNvs) mediate acute arousal behavioral response to blue light spectra (Fogle et al., 2015). Light-modulated behaviors, such as the circadian entrainment and acute arousal, are driven by the modulation of membrane excitability in contributing neurons, such as the l-LNvs (Fogle et al., 2015; Nitabach et al., 2002; Nitabach et al., 2006; Sheeba et al.,

2008a). The l-LNv electrophysiological light response is mediated by blue light activation of CRYPTOCHROME (CRY) coupled to membrane depolarization by the redox sensor of the voltage-gated potassium (K^+) channel β-subunit (Kvβ) HYPERKINETIC (Hk) (Fogle et al., 2015; Fogle et al., 2011; Sheeba et al., 2008a). Based on UV-visible light spectroscopy analysis of purified CRY, we tested whether similar l-LNv electrophysiological response (firing frequency light on/light off) was observed in response to UV-light. The control fly l-LNv responds to UV-light with varying degrees to different intensities (Fig. 1A and E). The l-LNv response to UV-light is significantly attenuated in *cry*$^{-/-}$ (Fig. 1B and E) and *hk*$^{-/-}$ (Fig. 1C and E) flies relative to control (Fig. 1A and E) at all intensities.

To determine whether if the CRY-mediated l-LNv UV-light response is cell-autonomous, we performed a series of genetic rescue experiments. Genetic rescue of LNv-targeted expression of CRY in *cry*$^{-/-}$ genetic background is able to cell-autonomously rescue l-LNv light response to UV light at low intensity (20μW/cm^2), but is incomplete for intermediate and high intensities (150μW/cm^2 and 640μW/cm^2, respectively) (Fig. 1D and F). Similarly, LNv-targeted expression of WT Hk in *hk*$^{-/-}$ genetic background rescues l-LNv UV-light response at low intensities, but not at high intensity (Fig. 1G). Expression of redox sensor-disabled Hk point mutant, Hk D260, does not rescue l-LNv response to UV-light (Fig. 1G). Thus, electrophysiological response to UV-light is specifically mediated by light-activated CRY coupled to the membrane via Hk redox sensor, consistent with our previous findings (Fogle et al., 2015).

To determine whether opsin-based photoreceptors contribute also to the l-LNv response to UV-light, we recorded from the l-LNv neurons of mutant *glass60j* (*gl60j*) flies

which lack eyes and other external photoreceptors. The l-LNv UV-light responses of *gl60j* flies are qualitatively lower, but do not differ significantly from that of control flies (Fig. 1H,I). We also observe that crossing *gl60j* mutants with either $cry^{-/-}$ or $hk^{-/-}$ mutants results in complete loss of light response (Fig. 1H). Thus, CRY and UV-sensitive opsins expressed in external photoreceptors both account for the full intensity-dependent light response in a subset of circadian neurons. These results suggest that CRY and UV-sensitive opsins act together for UV-light driven behaviors in fruit flies.

5.3.2 Acute arousal response to UV-light is CRY- and opsin-dependent.

CRY is expressed in a specific subset of neurons in the *Drosophila* central brain, including a subset of circadian, arousal, and photoreceptor neurons (Benito et al., 2008; Fogle et al., 2011; Sheeba et al., 2008a; Yoshii et al., 2008). The CRY-expressing large lateral ventral neurons (l-LNvs) mediate acute arousal behavioral response to blue light (Fogle et al., 2015). We measured the proportion of UV-light transmittance through eye and head cuticle tissue using a 365 nm LED light source as described in (Fogle et al., 2011). Eye cuticles are over 85% transparent and head cuticles are nearly 50% transparent to 365 nm UV light (Fig. S1). We also measured acute behavioral responses to 5 minute pulses of 365nm UV or 595nm orange LED light in the middle of the subjective night at ZT18, ZT19, and ZT20 for three consecutive nights in control, $cry^{-/-}$, $hk^{-/-}$, and *gl60j* mutant flies. The averaged behavioral actogram of control flies in response to UV light is shown (Fig 2A). We examined flies that were asleep immediately prior to the light pulse, with sleep defined as five minutes of inactivity. The percentage of flies that awakened in response to UV light was comparable between control, $cry^{-/-}$, and $hk^{-/-}$ flies but was significantly lower in *gl60j* mutant flies (Fig 2B). In response to orange light, the

percentage of flies that awakened was comparable between control and *cry*$^{-/-}$ flies. However, a significantly higher percentage of *hk*$^{-/-}$ flies awakened showing flies of this genotype are more readily aroused in response to orange light relative to controls in comparison to the significantly lower percentage of *gl60j* flies that awakened relative to controls (Fig 2B).

We also examined the behavioral response of flies that were awake immediately prior to the light pulse. During the UV light pulse (just after 0 min), awake control flies show a dramatic increase in arousal activity, while *cry*$^{-/-}$ awake flies remain relatively inactive during the UV light pulse, and show a delayed response minutes later following the UV light pulse. Like *cry*$^{-/-}$ flies, *hk*$^{-/-}$ flies have a significant defect in arousal response during the UV light pulse, and also exhibit a delayed response minutes later following the UV light pulse. *Gl60j* awake flies do not respond to UV light pulses (Fig 2C). Acute arousal behavioral responses to pulses of UV light show contributions from both CRY- and opsin-based photoreception, for which opsin-based photoreception is primary and CRY plays a modulatory role. Arousal activity in *cry*$^{-/-}$ flies does not differ from that of control flies during the orange light pulse, while *cry*$^{-/-}$ flies show significantly higher activity in the subsequent five minutes after the orange light pulse. *hk*$^{-/-}$ flies have significantly higher activity compared to control flies during and 20 minutes following the orange light pulse. *Gl60j* flies do not respond to orange light pulses, showing that opsin-based photoreception is primary for orange light arousal responses in awake flies (Fig 2D).

5.3.3 Both CRY and external photoreceptors contribute to circadian entrainment by UV light.

Both CRY and opsins mediate light-activated circadian entrainment in visible wavelengths, particularly blue light (Busza et al., 2004; Emery et al., 1998; Helfrich-Förster et al., 2001; Peschel et al., 2009; Rosato et al., 2001; Stanewsky et al., 1998). We measured the UV light induced circadian phase response curve (PRC) at 4 hr intervals from CT2-22, comparing wild-type control, mutants lacking *cry* (*cry*$^{-/-}$) and *glass60j* mutants lacking all opsin-based photoreceptors (*gl60j*). All flies were entrained for a minimum of three days in standard white light 12:12 hours LD followed by three days of constant darkness (DD) to establish the pre-pulse behavioral baseline, then were exposed to a ten-minute pulse of UV light (365nm, 0.85 mW/cm^2) at the varying CT times followed by four more days of DD. The PRC was calculated by comparing the time of peak morning activity the day before versus day after the UV light pulse. The average difference between these peaks (phase shift) are shown for the UV light PRCs for control versus *cry*$^{-/-}$ flies (Fig.3A) and for control versus *gl60j* flies (Fig.3B). Control flies robustly entrain to UV light pulses given during subjective night, with the greatest phase delay response at CT14 and the greatest phase advance response at CT22 (Fig. 3A, C, E) and show relatively little response to UV light pulses given during the subjective day ("the dead zone"), similar to visible light entrainment (Helfrich-Förster et al., 2001; Pittendrigh and Minis, 1964). Mutant *cry*$^{-/-}$ flies show clear defects in UV light entrainment with significantly lower entrainment for both phase delay (CT 14) and phase advance (CT 18 and 22) along with a significant entrainment defect at CT 2 (Fig. 3A, C, D). The entrainment defects in *cry*$^{-/-}$ mutant flies are not due to a pre-pulse phase shift of the

baseline as shown by comparing the pre-pulse waveforms for control (Fig. 3C) and *cry*$^{-/-}$ mutant flies (Fig. 3D). UV light entrainment defects are restricted to phase advancing light pulses (CT 18 and 22) in *gl60j* mutant flies (Fig. 3B), providing further evidence that CRY and UV sensitive photoreceptors opsins both contribute to *Drosophila* light entrainment (Helfrich-Förster et al., 2001).

5.3.4 CRY mediates executive choice attributes of positive phototaxis and avoidance behaviors to different intensities of UV light.

Light can serve as either a repellent or an attractive signal for an animal's behavior, depending on intensity and spectra. Many insects, including adult *Drosophila*, exhibit an innate spectral attraction to low intensity UV light as shown by phototaxis behavioral assays (Gao et al., 2008; Heisenberg and Buchner, 1977; Yamaguchi et al., 2010). In contrast, high intensity UV light induces avoidance behavior, particularly in larvae and egg-laying females (Xiang et al., 2010; Zhu et al., 2014), and reduces mating activity in adult male *Drosophila* (Sakai et al., 2002). Subsets of circadian pacemaker neurons and core clock genes modulate UV light aversive behavior in larvae, suggesting circadian modulation of behavioral UV light response (Kane et al., 2013; Keene et al., 2011).

Positive phototaxis behavior of male adult flies to low intensity UV light exposures (2.97 μW/cm^2, 5 minutes per exposure) was measured using a retrofitted Trikinetics DAM5 *Drosophila* Activity Monitor attached to light-tight chamber holding a population of 40 flies (Fig. S2). Wild-type control flies show robust attraction towards the low intensity UV light (365nm LED) exposure (Fig. S2B, D). Positive phototaxis towards UV light is significantly attenuated in cry-null mutant (*cry*$^{-/-}$) flies compared to control flies (Fig. S2B, D). Interestingly, control flies linger in the previously light-exposed region following the

light-pulse long after the light has been turned off, indicating that CRY mediates aspects of executive choice as well as simple acute sensory function (Fig. S2B, D). *Gl60j* flies show no attraction towards UV light (Fig. S2B, D). Thus, external photoreceptors have a primary acute sensory role for UV phototaxis while CRY appears to play a modulatory role for the magnitude and duration of the response. We also confirmed spectral sensitivity for strong phototaxis for UV light versus very weak phototaxis for orange light (595nm LED) for control and $cry^{-/-}$ flies (Fig. S2B-E).

The results above indicate that CRY serves as a distinct sensory input channel for UV light sensing that includes attributes of executive choice. To test this, we measured behavioral choice responses to high intensity UV light. 12:12 LD-entrained adult male flies were presented with a choice between an environment exposed to high-intensity UV light ($400uW/cm^2$) versus escape to a "dark" environment which blocked UV exposure during the subjective day time (ZT0-12). We refer to this as the "Mad Dogs and Englishmen" experiment (after Coward, 1931). A modified Trikinetics *Drosophila* Activity Monitor system fitted for long tubes allowed us to measure the choice of either locomotor activity in the high intensity UV light exposed versus the dark covered environment (Fig. 4A, B). Control flies significantly avoid UV light and strongly prefer to be in the dark environment, especially during the mid-day: ZT1-8 (Fig. 4C-E in blue, and S3A). *Gl60j* flies also avoid high-intensity UV light which is remarkable as they lack eyes and all other external photoreceptors, but their UV avoidance is not as effective as control flies during the mid-day (Fig. 4E in orange, and S3D). In contrast, $cry^{-/-}$ and $hk^{-/-}$ flies actually prefer the high intensity UV light environment over the dark environment at during the day-time, particularly during the early morning and all afternoon hours and exhibit significantly

attenuated avoidance behavior to high intensity UV light compared to control at all times of day (Fig. 4C, D and S3B, C). While *cry*$^{-/-}$ and *hk*$^{-/-}$ flies have significantly higher preference to high intensity UV light compared to control and *gl60j* flies during the UV light-exposed daytime hours (ZT0-12), environmental preference for either side of the monitor does not differ between all four genotypes during the subjective nighttime (ZT12-24) when the UV light is off (Fig. 4F). On an hour-by-hour basis, there is no systematic preference for control flies for either side during the night (Fig. S3A, when there is no UV light), however *cry*$^{-/-}$, *hk*$^{-/-}$, and *gl60j* flies show small but significant preferences for the covered “dark side” during much or all of the night (Fig. S3B, C, D). This might reflect residual olfactory cues. The results show clearly that CRY and its downstream redox sensor Hk mediate choice in avoidance behavior in response to high intensity UV light.

5.4 Discussion

The l-LNv electrophysiological response to UV light is nearly abolished in neurons from mutants lacking either CRY or its membrane redox sensor Hk (Fig. 1). CRY- and Hk-mediated electrophysiological l-LNv UV-light responses increase with UV light intensity. The remainder of the l-LNv light response is due to external photoreceptor inputs, suggesting that the l-LNv may be critical integrators for different input channels of UV light. Mutants lacking CRY show significantly altered behavior in response to UV light by four very different assays: 1) acute arousal response to light flashes during the night, 2) circadian entrainment, 3) positive phototaxis for low intensity UV light and 4) avoidance of high intensity UV light. The loss of both behavioral and l-LNv electrophysiological functional responses to UV light in *cry*$^{-/-}$ and *gl60j* mutants is consistent with our

hypothesis that LNv neurons integrate multiple UV light inputs to regulate behavioral responsiveness to UV light.

In addition to the ability to sense the presence of light, the ability to discern the changes in intensity, spectral content, timing and exposure length of light provides valuable information about the changing environment that is crucial to an organism's well-being and survival. UV light avoidance behavior has been demonstrated in foraging larva and egg-laying activity in females. We demonstrate UV light avoidance behavior in adult male *Drosophila* that is mediated by the CRY/Hk signaling pathway. During peak UV light intensity, which is mid-day in most natural environments, flies tend to take a "siesta" rest and thus avoid heat exposure and desiccation. UV light avoidance behavior peaks during the mid-day followed by a gradual decrease in UV avoidance/dark preference (Fig. 4), despite unvarying UV intensity for our experimental conditions during the daytime (ZT0-12). This suggests that CRY/Hk-mediated UV light avoidance behavior may be under circadian control. Interestingly, larval avoidance behavior has been shown to be dependent on opsin-based photoreceptors, as well as a subset of circadian pacemaker neurons and circadian genes (Kane et al., 2013; Keene et al., 2011). However, the clock controlled putative mechanism and neuronal groups underlying UV light preferential behavior in adult flies still requires further investigation.

CRY dually mediates attraction and avoidance behaviors to UV light depending on UV light intensity. The differences in CRY-mediated behavioral response to different intensities of UV light poses an interesting question of whether CRY may be important not only for the acute sensory detection of the light, but also for modulating more complex aspects of behavior such as executive choice. CRY-mediated behavioral responses likely

depend on spectral composition, intensity, and duration of light exposure, as well as integration with other sensory cues, most notably temperature (Das et al., 2015, 2016; Hamada et al., 2008; Zhong et al., 2012). CRY-mediated electrophysiological light responses vary monotonically depending on UV light intensity, thus the cell autonomous neuronal CRY light sensor codes for graded responses to UV light intensity rather than gated on/off responses. CRY-mediated graded UV light responses are translated directly as changes in neuronal membrane potential and firing rate. While both CRY- and opsin-based external photoreceptors contribute to regulate UV light responses, CRY-mediated response is independent and functionally distinct from that of opsin-based responses as shown by both electrophysiological and behavioral results. In conclusion, our results indicate that CRY is a major regulator of a wide range of fly behavioral responses to UV light.

Author Contributions

T.C.H., K.J.F., L.R. and L.S.B. designed research; K.J.F., L.R., L.S.B., A.G., and V.G. performed research; T.C.H., K.J.F., L.R. and L.S.B. contributed new analytic tools; K.J.F., L.R., L.S.B., A.G., and V.G., N.A.D., and T.C.H. analyzed data; and L.S.B. and T.C.H. wrote the paper.

5.5 Figures

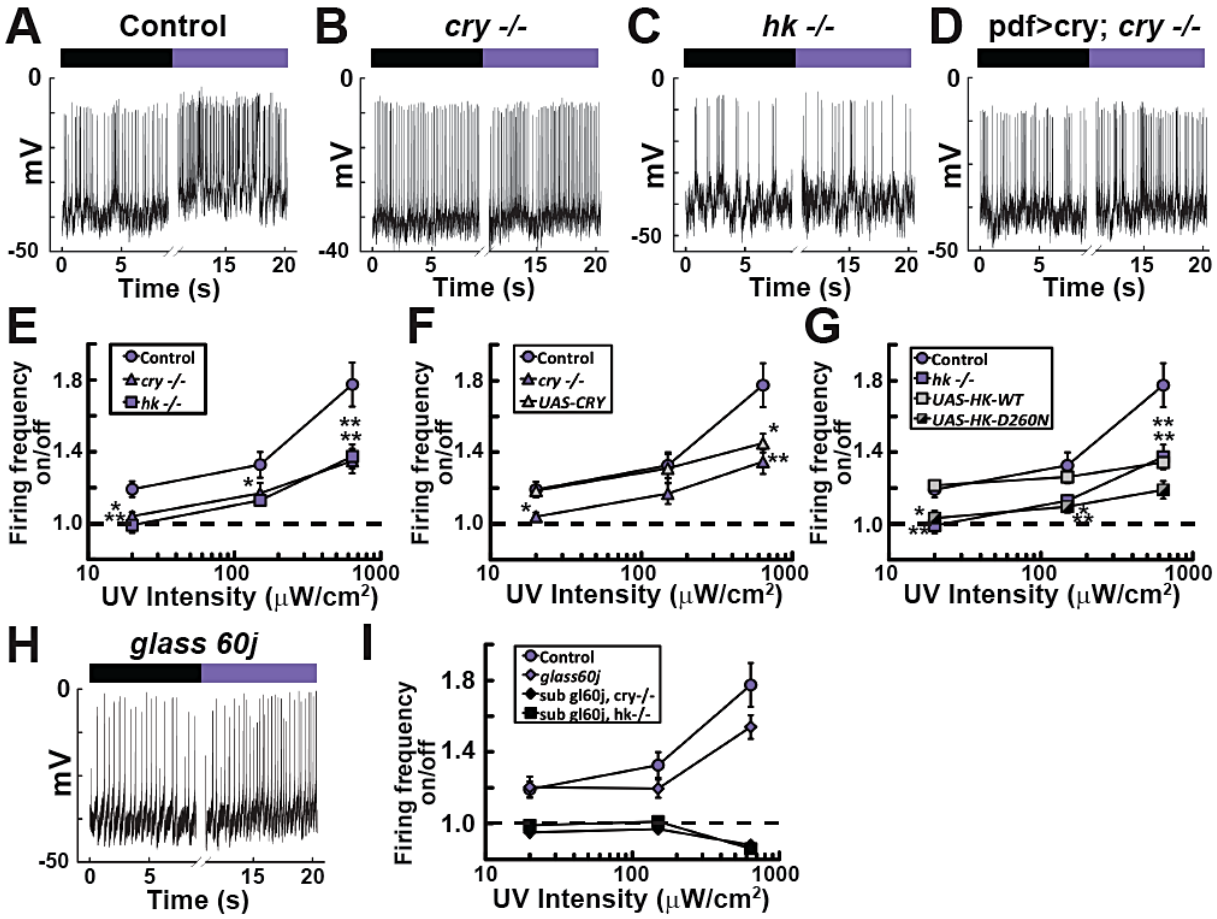

Figure 5.1. L-LNv electrophysiological response to UV-light is attenuated in flies lacking CRY-based phototransduction. (A) Representative trace for control l-LNv UV-light response. (350nm, 640μW/cm^2, violet bar; lights off, <0.01μW/cm^2, black bar) The gap in the x-axis removes <1s wherein a noise transient is caused by manual opening of the shutter to expose the prep to light vs. representative traces for **(B)** *cry*$^{-/-}$, **(C)** *hk*$^{-/-}$, and **(D)** "cry rescue" flies (pdfGAL4-driven LNv UAS-cry expression in a *cry*$^{-/-}$ background). **(E-G)** Dose response quantification of l-LNv firing frequency (FF) response (FF on/ FF off) to UV light at low (20μW/cm^2), intermediate (150μW/cm^2), and high (640μW/cm^2) intensities. **(E)** Electrophysiological response of control flies increase with increasing intensities of UV light (1.19 ± 0.04, n=17, low; 1.33 ± 0.07, n=15, intermediate; 1.77 ± 0.12, n=15, high intensity). The significantly attenuated UV-light responses of *cry*$^{-/-}$ (1.04 ± 0.02, n=17, p=0.01, low; 1.17 ± 0.06, n=15, p=0.129, intermediate; 1.35 ± 0.07, n=15, p=0.005 vs. control, high intensity) and *hk*$^{-/-}$ (0.99 ± 0.04, n=15, p=0.002, low; 1.13 ± 0.03, n=14, p=0.049, intermediate; 1.37 ± 0.07, n=26, p=0.008 vs. control, high intensity) flies do not differ from each other (p=0.622, low; p=0.879, intermediate; p=0.978, high intensity). **(F)** Dose response quantification of FF for control vs. *cry*$^{-/-}$ and "*cry* rescue" flies. Full rescue is achieved cell-autonomously at low intensity (1.18 ± 0.03, n=15, p=.99

vs. control and p=.011 vs. *cry*$^{-/-}$), but is incomplete for intermediate intensity (1.24 ± 0.03, n=15; where it differs neither from control nor cry$^{-/-}$) and high intensity UV-light (1.45 ± 0.05, n=15, p=.03 vs. control and p=.68 vs. *cry*$^{-/-}$). **(G)** Dose response quantification of FF for control vs. *hk*$^{-/-}$ and pdfGAL4-driven rescue of wild type Hk (UAS-Hk-WT) or of redox sensor-disabled point mutant Hk (UAS-Hk-D260N), both in *hk*-null background. Similar to the "*cry* rescue" flies, wild-type Hk rescue flies follow the same pattern, achieving rescue at lower intensity (1.21 ± 0.03, n=16, p=0.97 vs. control, and p<0.001 vs. *hk*$^{-/-}$), but not at intermediate (1.26 ± 0.03, n=16, p=0.732 vs. control, and p=0.18 vs. *hk*$^{-/-}$) and high intensities (1.34 ± 0.04, n=16, p=0.001 vs. control, and p=0.99 vs. *hk*$^{-/-}$). The redox sensor-disabled point mutant Hk-D260N fails to rescue the light response at all UV-light intensities (1.03 ± 0.04, n=13, p=0.033, low; 1.09 ±0.03, n=15, p= 0.004, intermediate; 1.19 ± 0.05, n=11, p<.001 vs. control, high intensity). **(H)** Representative trace for *glass60j* l-LNv UV-light response. **(I)** Dose response quantification FF for *glass60j* flies. Glass60j flies trend toward having a smaller UV response at intermediate and high intensity UV-light, but do not significantly differ from control (1.20 ± 0.06, n=18, p=0.87, low; 1.19 ± 0.05, n=14, p=0.15, intermediate; 1.54 ± 0.07, n=16, p=0.098 vs. control, high intensity). The *gl60j* plus *cry*$^{-/-}$ response (black diamonds) or plus the *hk*$^{-/-}$ response (black squares) shows CRY and opsins together account for the full light response.

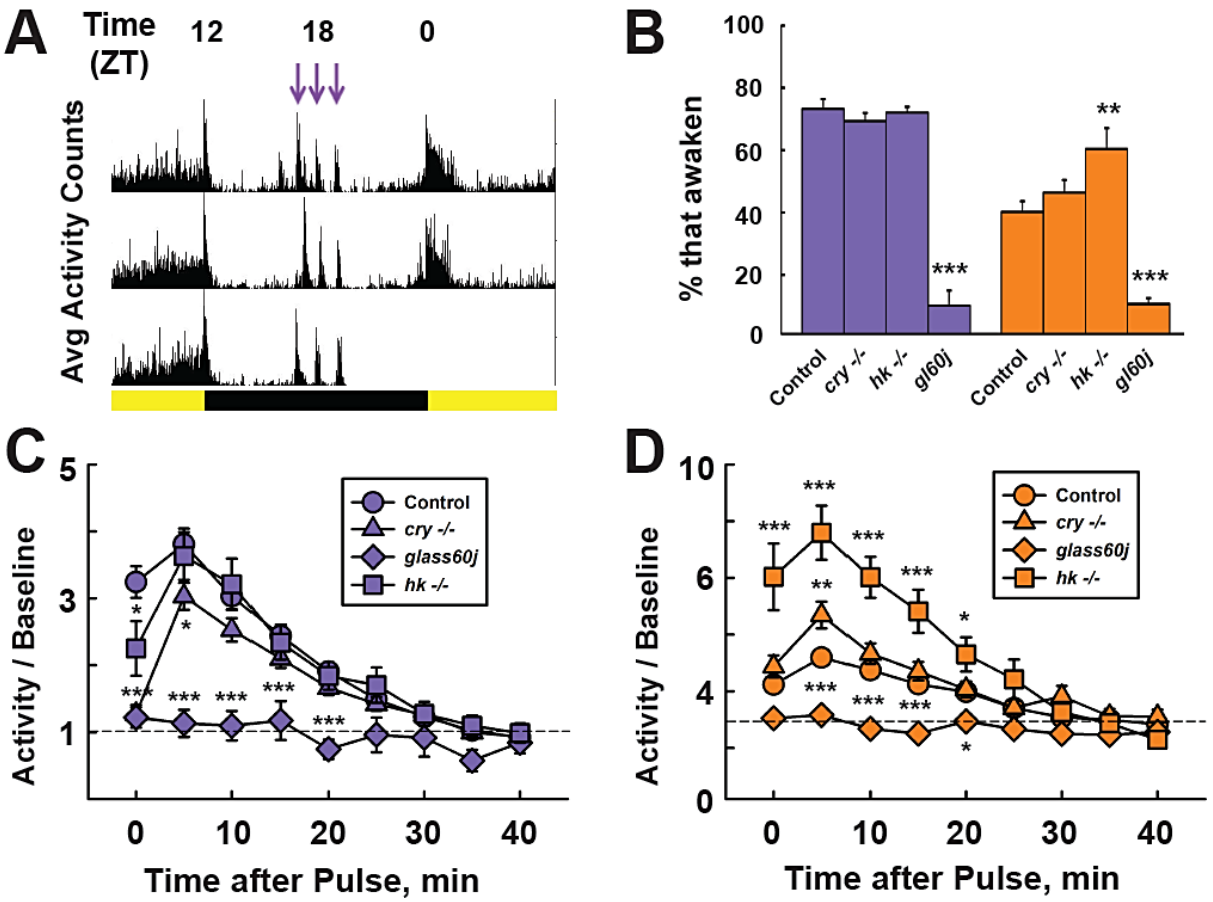

Figure 5.2. *Drosophila* acute arousal response to UV-light is CRY- and opsin-dependent. **(A)** Averaged double-plotted actogram of flies given three 5-minute light pulses (365nm, 3.4µW/m^2) during three consecutive nights. Flies respond acutely to light pulses but remain entrained to the LD 12:12 environmental cues. **(B)** Percentage of sleeping flies which awaken during the light pulse for UV (365nm, 3.4µW/m^2) and orange light (595nm, 6.5µW/m^2). Significantly lower percentage of flies which lack opsins (*glass60j)* awaken compared to the control flies (10.1% ± 2, n=17, p<.001 vs. control for UV and 10.6% ± 2, n=18 p <.001 vs. control for orange). **(C)** Time course of activity of awake flies during and after UV light pulses. Each point on the graph represents a bin of five minutes, with the first bin collected during the pulse. During the light pulse, control flies show a dramatic increase in arousal activity (activity/baseline is 3.24 ± 0.2, n=515 flies) while *cry*$^{-/-}$ flies remain relatively inactive (1.27 ± 0.1, n=432, p = <.001 vs. control), only responding after the pulse (3.0 ± 0.2, n=432, p =.046 vs. control, 3.8 ± 0.2, n=515). *Hk*$^{-/-}$ flies, like *cry*$^{-/-}$ flies, have a significantly decreased arousal activity during the light pulse (2.2 ± 0.4, n=181, p=.043 vs. control) but become active after the pulse ends (3.6 ± 0.35, n=181, p=.972 vs. control for bin 2). Flies lacking opsins (*glass60j*) do not respond to UV pulses (p <.001 vs. control for bins 1-5). **(D)** Time course of activity of awake flies during and after orange light pulses. *hk*$^{-/-}$ flies show significantly greater activity than control flies during the light pulse (6.0 ± 1.1, n=72, p <.001 vs. control 2.2 ± 0.2, n=379) and in the subsequent 20 minutes (p <.001 *hk*$^{-/-}$ vs. control for bins 2-5). *Cry*$^{-/-}$ flies and

control flies do not differ during the orange light pulse (2.9 ± 0.4, n=158, p=.551 vs. control) while *cry*$^{-/-}$ actually show higher activity in the subsequent five minutes (3.2 ± 0.2, n=379 vs. 4.7 ± 0.5, n=158, p=.005). Flies lacking opsins (*glass60j*) do not respond to orange pulses (p <.001 vs. control for bins 2-4).

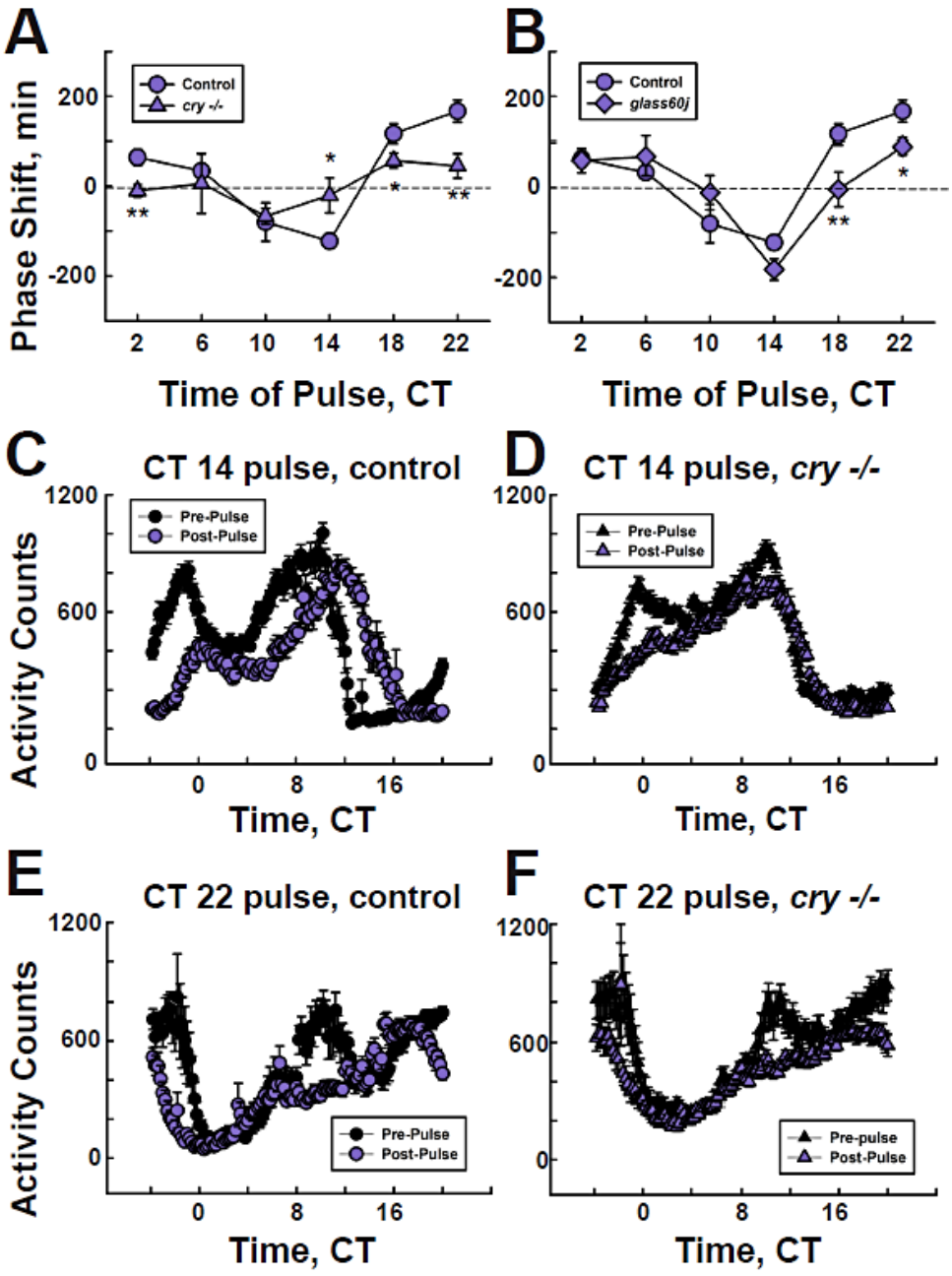

Figure 5.3. *Drosophila* circadian entrainment by ultraviolet light. **(A)** Phase response curve (PRC) for morning peak of activity for control and *cry*-null mutant (*cry*$^{-/-}$) flies. *cry*$^{-/-}$ flies do not re-entrain as well to UV light pulses (365nm, 3.4μW/cm^2, 10 minutes) at ZT2 (64 min ±18, n=4, -10 min ± 14, n=4, p=.009), ZT14 (-122 min ± 17, n=7, -20.5 min ± 40, n=4, p=.032), ZT18 (117 min ± 22, n=5, 57 min ± 17, n=5, p=.044), and ZT22 (167 min ± 24, n=5, 45 min ± 27, n=5, p=.006) compared to control flies. **(B)** PRC for control vs. *glass60j* flies, which fail to entrain at ZT18 as compared to control flies (117 min ± 22, n=5, -3.8 min ± 38, n = 5, p=.017) and not as well as the control flies at ZT22 (167 min ± 24, n=5, 91 min ± 18, n=5, p =.022). **(C)** Averaged activity profiles for control flies pre- (black symbols) and post- (violet symbols) UV pulse (365nm) at ZT14. Control

flies display a phase delay in the morning and evening peaks of activity. **(D)** Averaged activity profile for *cry*$^{-/-}$ flies before (black symbols) and after (violet symbols) a UV pulse at ZT14. *cry*$^{-/-}$ flies display a weak phase delay of the morning peak (45 min ± 27) that is significantly lower than that of control flies (167 min ± 24, n=12 days of activity per condition, p=.006). **(E)** Averaged activity profiles for control flies before (black symbols) and after (violet symbols) a UV pulse (365nm) at ZT22. Control flies display a phase advance in the morning and evening peaks of activity. **(F)** Averaged activity profile for *cry*$^{-/-}$ flies before (black symbols) and after (violet symbols) a UV pulse at ZT14. *cry*$^{-/-}$ flies display a weak phase advance (20.5min ± 38) of the morning peak that is significantly lower than of control flies (122min ± 16, n=12 days of activity per condition, p=.032).

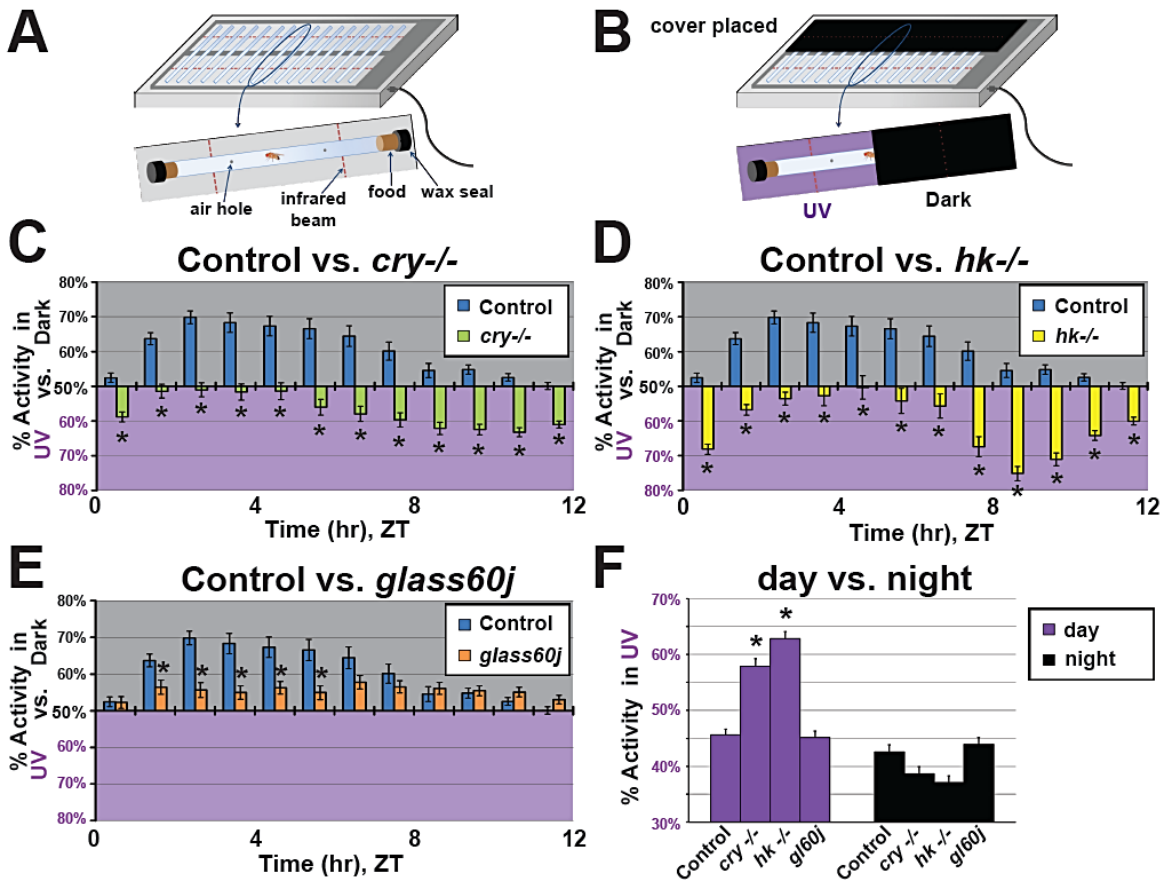

Figure 5.4. CRY-based phototransduction contributes to UV-light avoidance behavior in *Drosophila.* **(A)** Diagram of the "light choice" apparatus. Standard Trikinetics *Drosophila* activity monitors were modified to fit behavior tubes of 2x length. **(B)** Half of the monitor is covered with cardboard to provide flies a choice between UV-light exposed (400μW/cm^2) and dark environments. 80 flies were tested for each genotype over 5 individual experimental runs. **(C-E)** Preference for UV-exposed vs. dark environment is measured by percent of activity in each environment over total amount of activity for each ZT. Gray-shade indicates dark environment preference (light avoidance), and violet-shade indicates UV environment preference. **(C)** *cry*-null mutant (*cry*$^{-/-}$) flies have a significant defect UV light avoidance behavior at all times of the day compared to control flies, and prefer the UV environment over the dark (All $p<0.05$) **(D)** Similarly, *hyperkinetic*-null (*hk*$^{-/-}$) flies also have a significant defect in UV light avoidance behavior at all times of the day compared to control flies, and prefer the UV environment over the dark (All $p<0.05$). **(E)** Mutant flies lacking all opsin-based external photoreceptors (*glass60j* or *gl60j*) show significantly less UV avoidance control flies only during the midday, ZT1-6 (All $p<0.05$). **(F)** Average percent activity in UV-exposed environment during the day vs. night. *Cry*$^{-/-}$ and *hk*$^{-/-}$ flies have significantly higher activity in the UV-exposed environment during the day compared to control flies ($p<0.05$). Daytime percent activity in UV-exposed environment of *glass60j* flies does not significantly differ from control. Percent activities in UV-exposed environment for *cry*$^{-/-}$, *hk*$^{-/-}$, and *gl60j* flies during the nighttime do not differ from control.

5.6 Supplementary Information

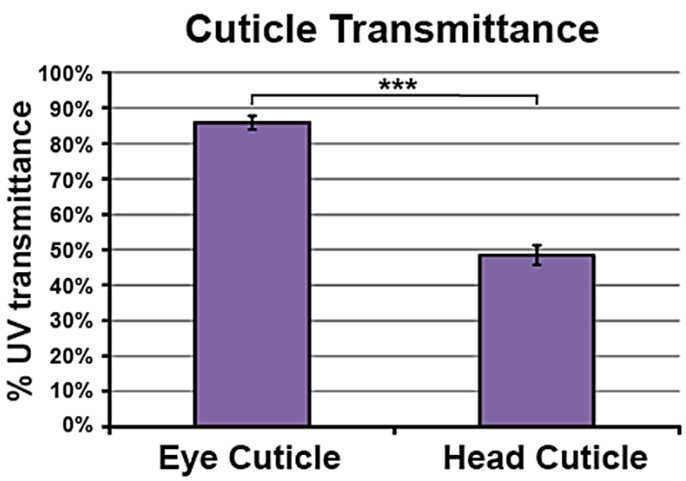

Figure S5.1. *Drosophila* head and eye cuticles transmits UV light. The proportion of 365 nm (UV) light transmitted through cuticle tissues was calculated as the amount of UV light transmitted through either eye (n=10) or head (n=7) cuticle tissues divided by baseline measurements of transmittance through a droplet of PBS.

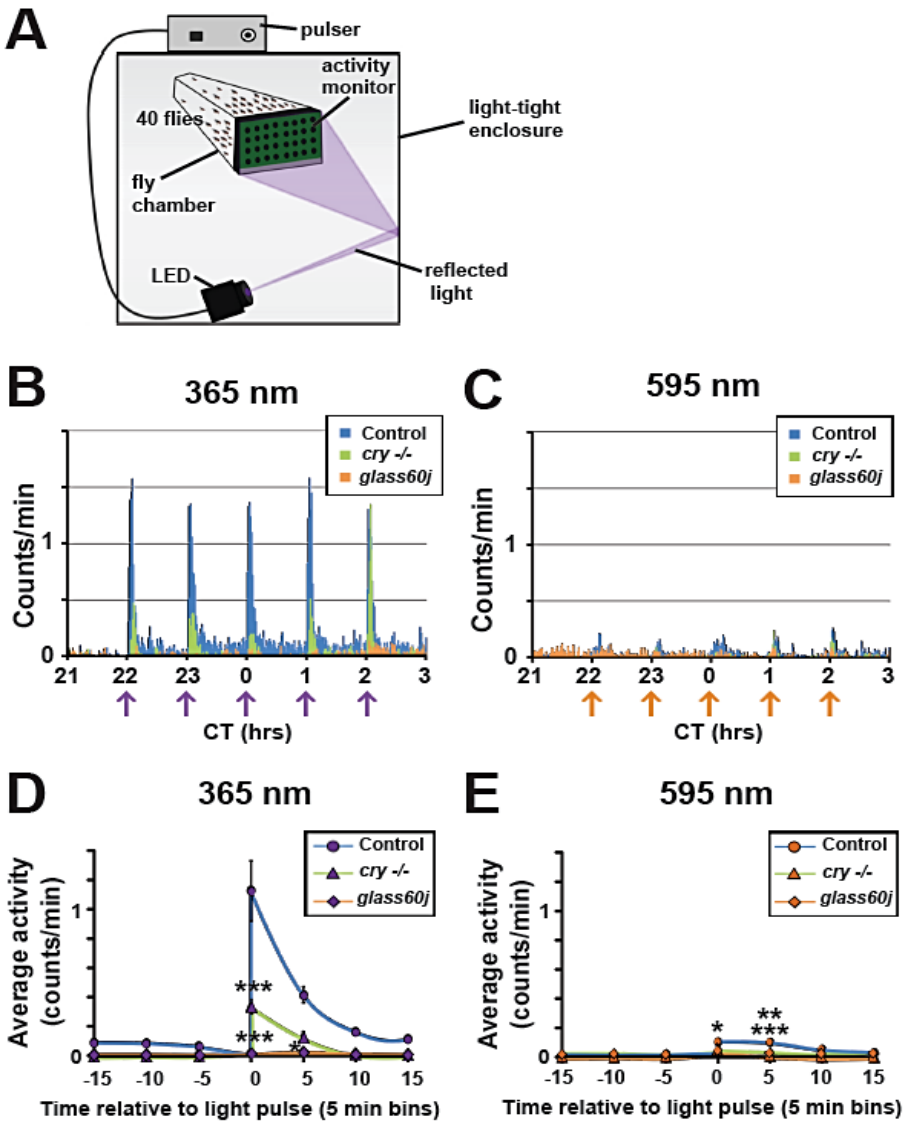

Figure S5.2. *Drosophila* positive phototaxis behavior towards UV-light is attenuated in mutants lacking CRY- and in mutants lacking external photoreceptors. **(A)** An electrophoresis system photo-documentation hood was converted into a light-tight chamber to hold populations of flies for recordings. A DAM2 *Drosophila* Activity Monitor (32 channels with dual infrared beams, Trikinetics) was mounted to the front of the chamber and sealed with a glass cover on the outer face. For each experiment, a group of 40 adult flies was directly placed into the chamber. **(B)** Average phototaxis activity counts per minute towards a dim, five 5-minute UV light pulse (365nm, indicated by violet arrows) followed by 55 minute of darkness starting at CT 21 to CT 3. Control flies (n=6) are shown in blue, *cry-/-* (n=3) flies in green, and *gl60j* (n=4) flies in orange. **(C)** Average phototaxis activity counts per minute towards five 5-minute orange light pulse (595nm, indicated by orange arrows) followed by 55 minute of darkness starting at CT 21 to CT 3. **(D-E)** Average phototaxis activity in 5-minute bins relative to the (D) UV-light or (E) orange-light pulse averaged from the same flies measured in panels (A-B).

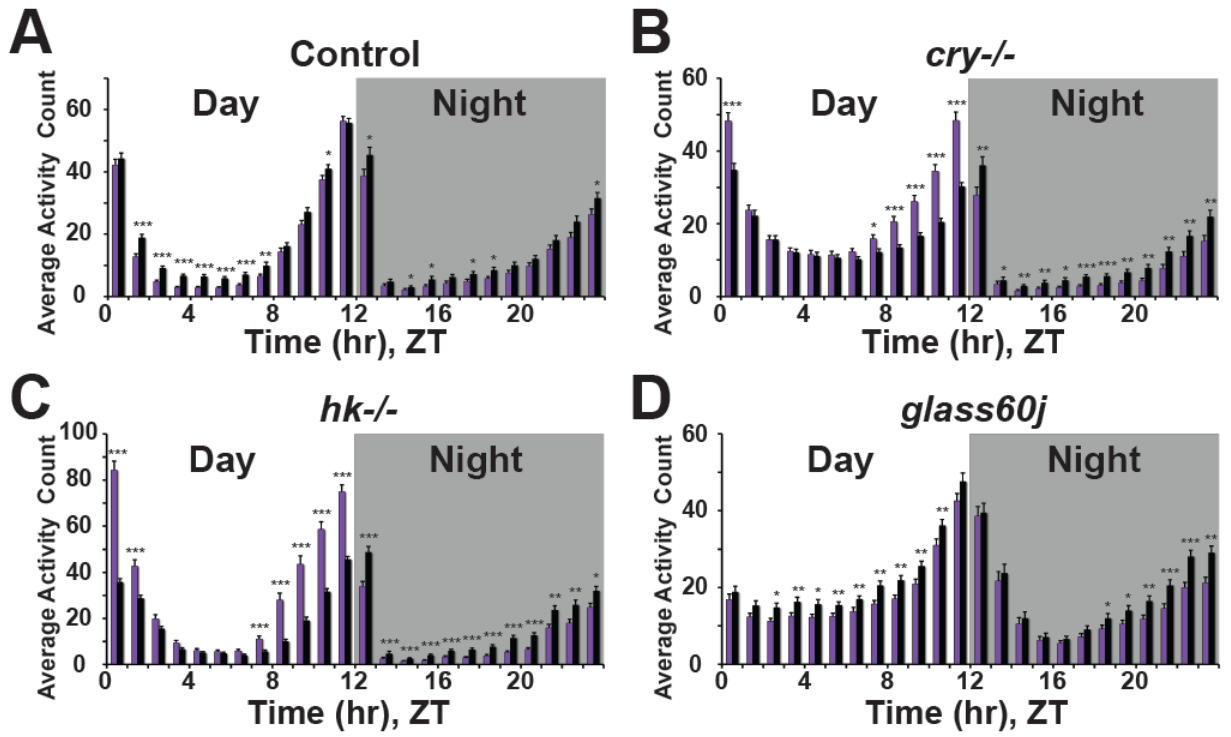

Figure S5.3. CRY-based phototransduction mediates *Drosophila* choice of light environment. Average activity count over ZT time in the UV-exposed environment (365nm, 400μW/cm^2, violet bars) versus the dark environment (black bars) are shown. The UV light was on during the daytime (ZT0-12) and off during the nighttime (ZT12-24; shaded gray on the graphs) **(A)** Control flies prefer the dark environment over the UV-exposed one during the mid-day **(B)** cry-/- flies and **(C)** *hk-/-* flies both lack the preference for dark environment in the mid-day, and prefers the UV-exposed environment at other times of the day. **(D)** *Glass60j* flies choose the dark environment over the UV-exposed one during the mid-day, similar to control flies.

CHAPTER 6

Conclusions and Future Directions

6.1 Overview of Thesis Work

Circadian systems are essential for the survival of most organisms. Our lives are largely governed by repeating patterns of purposeful behaviors (e.g. meal times) and a wide range of rhythmic physiological processes (e.g. metabolism). We and virtually every other multicellular organism (and even many single cell organisms) have molecular and cellular clocks that calibrate the dynamics of these processes. These clocks are fine-tuned by various environmental cues. Light appears to be the most powerful of these cues and drives many circadian aspects of physiology, biology and behavior. Throughout my thesis work, I have characterized novel aspects of light integration at the molecular, cell-autonomous, circuit and behavioral levels.

Chapter 2 of the current thesis discusses our discovery and characterization of the novel process of “phase retuning” by which *Drosophila* circadian neural networks adapt to a phase advancing light cue. We mapped the spatiotemporal dynamics of circuit-wide photoentrainment by performing continuous bioluminescence imaging over 6 days at single cell resolution in organotypic whole brain cultures prepared from transgenic XLG-Luc *Drosophila melanogaster.* We showed that exposure of the *Drosophila* circadian network to a phase advancing white light pulse results in transient desynchrony followed by a delayed recovery in phase-shifted synchrony through a process we called “phase retuning.” This work suggests that desynchronization may be a key feature of entrainment and that treatments which hasten oscillator desynchronization may speed recovery from jet lag.

In Chapter 3, this thesis addresses the longstanding question of how heterogeneous circadian circuits drive synchronous yet adaptable rhythms. By employing a combination of *ex vivo* analysis of real-time bioluminescence datasets with mathematical modeling of complementary oscillator types, we show that circadian networks contain a mix of strong and weak components that enable robust yet flexible responses to external perturbations. Specifically, transiently desynchronizing weaker oscillators may actually be a key adaptive feature that permits stronger oscillators to more easily pull circadian networks into a new state of phase-shifted synchrony. We also provide the first detailed spatiotemporal map of whole dynamic network phase ensembles, at single neuron resolution, in free-running and light-shifting conditions (see Movie 2). Our results suggest that dynamic coupling between weak and strong oscillators may contribute to seasonal adaptability and could be deliberately directed and amplified for treatment of conditions such as jet lag and seasonal affective disorder.

Chapters 4 and 5 discuss the molecular mechanisms and behavioral outputs of CRYPTOCHROME-mediated phototransduction. Using patch-clamp recordings from the large lateral ventral neurons of acutely dissected adult fly brains, we show that blue light-activation of CRYPTOCHROME (CRY) evokes increased firing rate, rapid membrane depolarization and acute behavioral arousal responses via the well-conserved voltage-gated potassium channel β-subunit (Kvβ) redox sensor called Hyperkinetic (HK) (Chapter 4). Although CRY has long been recognized as a blue-light sensitive photoreceptor, our findings in Chapter 5 suggest that *Drosophila* CRY may mediate executive behaviors in response to ultraviolet (UV) light such as positive versus negative phototaxis. Since CRY is a highly conserved photoreceptor, elucidation of CRY phototransduction could enable

optimization of better insect disease vector control systems (i.e. bug zappers) as well as a better understanding of circadian photoreception.

Taking everything together, I hypothesize that there is a complex interplay between cell-autonomous molecular clocks and circuit-wide integration that drives light-mediated circadian rhythms. Specifically, transient damping of weaker neuronal oscillators such as the DN3s by light appears to enable stronger neuronal oscillators such as the LNds to pull the *Drosophila* circadian neural network into a new state of phase-shifted synchrony. Although desynchrony was long perceived as a negative feature of circadian disruption, the work presented in this thesis suggests that transient desynchrony by light may be a key feature of circadian photoentrainment. Accordingly, treatments such as light therapy may be able to harness desynchrony in order to accelerate recovery from circadian disruptions due conditions such as jet lag, shift work and seasonal affective disorder.

6.2 Unresolved Issues and Future Directions

The current thesis has addressed various aspects of the *Drosophila* circadian clockwork and light integration. However, there many key questions that still need to be addressed in future studies. Here I briefly discuss some of the important unresolved issues that I believe are critical for understanding circadian photoreception and circadian disorders. I will also discuss some of our preliminary data, novel light entrainment protocols and design of a custom imaging system that have already laid the groundwork for how to approach these key issues.

Unresolved Issue 1: Elucidating how the activities of cell-oscillators are coupled to drive phase retuning by light. Although we have characterized distinct neuron oscillator dynamics involved in circadian adaptation to phase advancing light cues, it is

still unclear how the complex phase relationships between and within neuronal subgroups precisely map to circadian behavioral entrainment. Future experiments should examine how cell-autonomous and network properties drive phase retuning by light. Since the neuropeptide pigment dispersing factor (PDF) is known to be important for intercellular communication, we are currently working on generating XLG-luc flies with mutations in the PDF receptor to examine the importance of coupling between circadian oscillators in driving circadian light entrainment.

Unresolved Issue 2: Characterizing the interplay of neurochemical and/or gene signaling during a light-evoked phase shift that drives functional contributions of strong and weak circadian oscillators. Our studies suggest that phase-shifting light cues increase the amplitude and synchrony of certain oscillators such as the LNds whereas other oscillators such as the l-LNvs are pushed toward a transient state of damped amplitude and desynchrony. Future studies should incorporate genetic and pharmacological targeting of specific neuron oscillators to identify the molecular basis that distinguishes weak and strong cell oscillators. Elucidating the sources of the observed oscillator dynamics could potentially allow for treatments which shift circadian systems toward greater synchrony or plasticity as needed for therapy.

Unresolved Issue 3: Assessing how cryptochrome activity is coupled to complex light-driven behaviors. In our studies, we show that cryptochrome (CRY) can mediate light-driven circadian activity and phototactic behavior independently of the classical opsins. Furthermore, CRY appears to drive behavioral arousal by blue light via redox reactions whereas CRY resets circadian clocks by undergoing conformational changes.

Future studies should distinguish the distinct mechanisms, and likely unknown intermediates, that regulate the various downstream effects of light-activated CRY.

Unresolved Issue 4: Identifying circadian components and properties of light which distinguish positive and negative phototaxis in insects. Although we showed that CRY mediates phototaxis response to ultraviolet (UV) light, the factors which influence the attraction versus avoidance to UV light by adult *Drosophila* remains enigmatic. As *Drosophila* are known to avoid sunlight due to the risk of desiccation, I hypothesize that light intensity and time of day affect whether phototaxis is positive or negative. Future studies should examine light-driven behavior with varying light intensities in different clock mutant backgrounds. This work would be useful for optimizing light control methods such as bug zappers for insect disease vectors.

Unresolved Issue 5: Understanding how chronic circadian disruption affects circadian network properties and output. Although we have examined how *Drosophila* circadian neural networks respond to transient disruption by a phase-advancing light pulse analogous to jet lag, the real-time effects of chronic circadian disruption by events such as social jet lag on circadian neural networks is still largely unknown. We have laid the groundwork for addressing this issue by designing and optimizing novel photoentrainment protocols to enable bioluminescence imaging during intermittent light cues simulating social jet lag. Further, we have designed and optimized a custom imaging system to enable real-time recordings of social jet lag reflected in the *Drosophila* circadian neural network at single neuron resolution. I will discuss below our toolkit design and preliminary findings of how circadian neural networks respond to social jet lag.

6.3 LD Strobe: A Novel Light Protocol to Permit Bioluminescence Recordings of Real-Time Photoentrainment

6.3.1 Introduction

Although circadian clocks are capable of endogenous oscillations in free-running conditions, studies have shown that coordination of these clocks with daily solar cycles is critical for regulating physiological and behavioral activities (Hardin, 2005; Oishi et al., 2002; Pauley, 2004). Accordingly, misalignment of clocks induced by events such as shift work and jet lag has been correlated with reduced cognition and health (Davidson et al., 2009; Pauley, 2004). However, current bioluminescence imaging protocols are limited to imaging in the dark as light exposure would mask relatively low levels of luminescence and damage the highly sensitive CCD cameras needed to detect weak bioluminescence signals. Our goal is to develop a novel entrainment protocol called “LD strobe” which divides the daytime hours of standard 12:12 hour day-night entrainment into 12 cycles of short light and dark intervals to allow for semi-continuous bioluminescence imaging while simulating day-night photoentrainment.

We know by common experience that we can move between bright sunlight outdoors and darkened rooms indoors without apparent disruptions in our circadian rhythms. This indicates that the timing of photic input and not just the level of exposure may be critical for photoentrainment. Furthermore, previous studies have shown that photoentrainment is maintained under “skeleton photoperiod” (SPP) conditions where a complete 12:12 hour light-dark photophase (hereby referred to as 12:12 LD) is replaced with two brief (< 1 hour) light pulses at the beginning and end of subjective day (Oishi et al., 2002; Pittendrigh and Daan, 1976; Sharma et al., 1997). However, entrainment by

SPP is not stable when day length varies. Specifically, SPP protocols with longer day lengths can result in a “phase jump” in which behavioral activity abruptly crosses one of the light pulses so that activity is greater during the subjective day (Geetha et al., 1996; Pittendrigh and Daan, 1976; Sharma et al., 1997; Stephan, 1983). We hypothesize that more constant light input from an LD strobe protocol will more reliably simulate the parametric actions of complete 12:12 LD in providing stable entrainment. Since molecular clocks are known to drive behavioral rhythms, we are optimizing the LD strobe protocol using classical behavioral assays.

6.3.2 Materials and Methods

Behavioral analysis of day-night entrainment

The automated Trikinetics *Drosophila* Activity Monitor system was employed to record the locomotor activity of wild-type (W^{1118}[5905]) and XLG-luc adult flies (Nitabach et al., 2002; Sheeba et al., 2008b). Individual flies were placed in 5 mm pyrex glass tubes with fly food on one end and a cotton plug on the other. Every experiment was run with 64 adult male flies with the fly-containing tubes mounted in a DAM5 *Drosophila* activity monitor (Trikinetics) which records the number of infrared beam crossings over time as a measure of activity. Flies are first entrained under standard 12:12 LD conditions for ≥3 days. Following this, flies are exposed to LD strobe, SPP or standard 12:12 LD light protocols with consistent phases and a consistent white light intensity of 1.1 mW/cm^2 for 5 days. LD and SPP protocols were performed with light pulse durations of 5, 15 or 30 minutes. Finally, the free-running activity of these flies is recorded for 5 days under constant darkness (DD) conditions.

Quantification of locomotor activity

The software FaasX (M. Boudinot and F. Rouyer, Centre National de la Recherche Scientifique) was used for analysis of locomotor activity recorded by the automated Trikinetics *Drosophila* Activity Monitor system. Cycle-P was utilized to quantify period length, amplitude and rhythmicity using 15 minute bins of individual fly locomotor activity. Individual flies were defined as rhythmic based on chi-square periodogram analysis with the following criteria (high frequency filter on): power ≥ 40, width ≥ 4 hours and period length of 24 ± 8 hours. Double-plotted actogram graphs were generated by the software ClockLab (Actimetrics) showing normalized activity over 1 minute intervals.

6.3.3 Preliminary results

Behavior analysis of adult *Drosophila* locomotor activity indicates that both the LD strobe (LDS) and skeleton photoperiod (SPP) protocols appear capable of simulating day-night entrainment (Figure 6.1). Stable photoentrainment is observed for 5,15 and 30-minute light pulses under both LDS and SPP conditions for wild-type and XLG-Luc flies as indicated by period length, amplitude and rhythmicity (Table 6.1). However, based on quantitative analysis and qualitative comparisons of locomotor activity profiles, we have determined that an LD strobe protocol with alternations of 15 minutes of light followed by 45 minutes of darkness (hereby referred to as 15L45D LD strobe) simulates classical 12:12 hour LD entrainment with the greatest fidelity.

6.3.4 Conclusions

The development of a novel “LD strobe” protocol permits real-time bioluminescence imaging of circadian photoentrainment without the risk of damaging the CCD camera or masking low amplitude luminescence signals with light. It will also allow investigations of whether short periods of darkness during daytime hours (e.g. when we enter a darkened

room or take a nap) have a discernable effect on circadian clocks and behavioral rhythms. We are currently optimizing the 15L45D LD strobe protocol to study photoentrainment and social jet lag in adult *Drosophila* whole brain explants using real-time bioluminescence imaging *ex vivo*. Future studies should also look into the underlying molecular and cellular mechanisms for why LD strobe protocols appear to provide more robust photoentrainment than skeleton photoperiod protocols.

6.4 Designing, Building and Optimizing a Custom Bioluminescence Imaging System to Study Social Jet Lag and Photoentrainment Dynamics

We previously showed that physiological light response could be measured using real-time bioluminescence recordings in *Drosophila* whole brain explants which are directly light-sensitive due to expression of the photoreceptor cryptochrome (Roberts et al., 2015). These experiments were performed with an Olympus IX71 inverted microscope (Tokyo, Japan) in a dedicated dark room. However, these studies were limited to imaging in only constant darkness (DD) conditions, a temporal resolution of 30 minutes, four explants per experiment, 6 day recordings and manual activation of the microscope bright field light (Olympus, TH4-100) for photic input. In order to improve spatiotemporal resolution and functionality, we have designed, built and optimized a new bioluminescence imaging system (Figure 6.2). Here I will briefly discuss the key factors contributing to the improved imaging capabilities and the significant increase in signal-to-noise.

Signal optimization and protection of cooled intensified CCD camera: Photons are detected by a MEGA-10Z cooled intensified CCD camera (Stanford Photonics). This camera has high quantum efficiency and extremely low intrinsic dark current due to new

intensifier technology and Peltier cooling. We installed an automated mechanical shutter to act as a fail-safe to protect the camera from automated LED exposure and accidental light exposure. This shutter is closed by default and requires a 5V TTL input to open. We have also installed a 700 nm short-pass IR filter in the camera to further prevent noise from red-shifted LEDs within the connected Zeiss microscope. Since luciferase emission has a peak of ~550 nm, the signal is still strong with the filter in place. The camera is positioned in an isolated lower shelf and is connected via an adapter to a microscope above through an opening in the shelf.

Removing microscope light contamination: An Axio Observer.Z1 Microscope (Zeiss) is equipped with 5x (NA 0.25) and 10x (NA 0.50) objectives. Imaging with the 5x objective enables recordings of 6 whole brain explants simultaneously while proving sufficient depth-of-field to image all circadian neuronal subgroups in different z-planes. In order to reduce noise induced by internal light contamination, the microscope needed to have over a dozen LED sources (used for encoding moving parts or diagnostics) manually isolated, deactivated, removed and/or blanked using black silicone caulk and a custom jumper. Military-spec night-vision goggles were used to confirm that the system is light-tight with virtually no noise from internal light sources.

Automated XYZ Stage: An Applied Scientific Instrumentation (ASI) stage is connected to the microscope and is designed to hold a single 35 mm petri dish or 6-well plates. This stage has automated XYZ movement that is controlled by the software Piper to enable greater spatial control and higher imaging throughput. The movement speed of this stage is optimized to reduce unwanted vibrations that could displace samples being imaged. A fan is also positioned next to the stage to provide constant laminar air flow across the

surface of samples and prevent condensation from building up on cover glasses that can obscure imaging.

Light-tight incubator: The entire imaging system is contained within a custom incubator built by Dr. Alec Davidson (Morehouse School of Medicine, GA). The incubator is light-tight with a blackened interior and enables contained imaging without the need for a dedicated light-tight room. The temperature is set to maintain the internal temperature at ~25.5^{o}C ± 0.5^{o}C.

Temperature regulation: Temperature is an important zeitgeber for *Drosophila* and many other organisms (Barrett and Takahashi, 1995; Buhr et al., 2010; Glaser and Stanewsky, 2005). Accordingly, temperature must be maintained consistently within a tight range for our experiments to ensure that light is the only entraining environmental cue. The incubator is maintained within a cooled room (<19^{o}C) with a heating plate and two custom wooden light baffles built into the roof of the incubator to ensure that the temperature is maintained at ~25.5^{o}C ± 0.5^{o}C. These baffles are designed with an internal labyrinth (including at least five 180^{o} turns) with flat black paint to prevent reflection and to allow airflow without light passage. A fan is also installed on each baffle (one inflow, one outflow) to circulate cooler ambient room air.

Custom Automated LED Setup: We have designed an integrated multi-LED setup with automated triggering via TTL input. An FC5-LED High Multi-Wavelength LED Light Source (Prizmatix) provides four preset wavelengths of light including 365 nm, 450 nm, 550 nm and 630 nm. A fifth slot provides flexibility by being fitted with an electrical connector and SMA fiber coupler to enable any Mic-LED to be connected to the FC5-LED light source. The LED source is connected to a single large diameter SMA fiber optic

cable that bifurcates into two fiber optic light guides. These light guides terminate at two off-axis area illuminators that are positioned by wall-mounted articulated arms to provide equal field illumination over a 6-well surface area of 128 mm x 86 mm. These LEDs are set to provide a light intensity of 30 $\mu W/cm^2 \pm 0.5 \mu W/cm^2$ over the entire surface. Light intensity can be adjusted via 10-turn potentiometers or TTL input of 0-5V. The TTL input permits rapid light control with a speed of approximately 10 microseconds. The LED source, computer, PC supply, power supply and chiller are connected to two uninterruptible power supply (UPS) units providing surge protection and backup power.

Optimization of the software Piper: The software Piper provides automated control of light exposure during imaging experiments via 5V TTL input to the LEDs and a 3.3 V input to the mechanical shutter to protect the CCD camera. This enables complex iterations of light protocols (~214 players) to simulate social jet lag *ex vivo* for 11 days of imaging. We have also optimized Piper to filter out noise from cosmic rays in real-time.

Conclusions

Our new imaging system has significantly improved spatiotemporal resolution and functionality. Our current experiments demonstrate that the system has an excellent signal-to-noise ratio with virtually no dark counts (<1 photon/min). This reduction in noise is matched by enhanced single neuron resolution with over 30-fold improvement in signal relative to the imaging system used in our previous studies (Roberts et al., 2015). This imaging system has also increased our temporal resolution from 30 minute intervals to 5 minute intervals. The augmented bioluminescence imaging system will enable future studies of how photic entrainment and social jet lag are reflected in real-time in *Drosophila* whole brain explants with increased spatiotemporal resolution.

6.5 Studying how Circadian Neural Circuits Reflect Social Jet Lag

6.5.1 Introduction

The growing problem of "social jet lag" represents the chronic discrepancy between social schedules and circadian clocks (Wittmann et al., 2006). Specifically, the weekly misalignment for many individuals between work days (i.e. weekdays) and free days (i.e. weekends). Social jet lag resembles classical jet lag from high speed transmeridian flight as many individuals often stay up later on Friday nights due to social cues and sleep in on the weekends resulting in a phase delay similar to flying westward across time zones. Following this phase delayed weekend schedule, social obligations and artificial alarm clocks then often force many individuals to begin waking up earlier on the first work day back (i.e. Monday) resulting in a phase advance similar to a return flight eastward across time zones. However, unlike the transient disruptions of classical jet lag, social jet lag is a chronic misalignment that has been linked to serious physiological and psychological issues. An increasing number of researchers and medical professionals have linked social jet lag to obesity, depression, cardiovascular disease, cognitive deficits, alcohol consumption and tumor progression (Cho et al., 2000; Filipski et al., 2004; Gonnissen et al., 2012; Hasler et al., 2012; Levandovski et al., 2011; Roenneberg et al., 2012; Scheer et al., 2009; Wittmann et al., 2010). However, the manner in which social jet lag alters circadian systems and molecular clocks resulting in these negative effects is poorly understood. By using our custom bioluminescence imaging system and LD strobe protocol described above, we are able to examine how social jet lag is reflected in circadian neural networks *ex vivo* using 11-day bioluminescence recordings of cultured adult *Drosophila* whole brain explants. In order to simulate social jet lag, phase shifts of

3 hours are used in our experiments as weekly 3-hour phase shifts are commonly experienced by the general populace and have been shown to be sufficient to result in numerous negative health effects including obesity and metabolic syndrome (Parsons et al., 2015; Wittmann et al., 2006).

6.5.2 Materials and Methods

Bioluminescence imaging

Bioluminescence imaging was performed using adult, male *XLG-Per-Luc* transgenic flies provided by Dr. Ralf Stanewsky (University College London, UK). *XLG-Per-Luc* flies are first entrained to ≥3 days of 12:12 hour LD entrainment before dissection. Six whole fly brain explants were dissected and cultured on a single insert per experiment using a modified version of a previously described protocol (Roberts et al., 2015). The cultured brains were mounted on a stage (Applied Scientific Instrumentation) with automated XYZ movement that is controlled by the software Piper. The stage is connected to an upright Axio Observer.Z1 Microscope (Zeiss) set in a custom light-tight incubator (designed by Dr. Alec Davidson, Morehouse School of Medicine, GA) with temperature maintained at 25^{o}C ± 0.5^{o}C. Bioluminescence from the cultured whole brains is collected by a Zeiss 5x (NA 0.25) objective and transmitted directly to a MEGA-10Z cooled intensified CCD camera (Stanford Photonics) mounted on the bottom port of the microscope. The XY position of the samples is manually set using bright-field illumination. The optimal z-plane of focus for bioluminescence imaging is obtained by performing 10 z-steps at 40-50 µm intervals with 5-10 minute exposures. Experimental bioluminescence imaging of the samples is obtained with 15 minute exposures at 30 fps for ≥ 11 days of recording at single-cell resolution. Light exposure and entrainment were

performed using the 15L45D LD Strobe protocol described above. Images are processed by Piper and ImageJ before using MetaMorph (Molecular Devices, Sunnyvale, CA), Microsoft Excel and custom MATLAB scripts to measure circadian parameters of bioluminescence cycling with single cell resolution. Only experiments with all six brain explants still healthy, contamination-free, adhering to the insert substrate, and exhibiting bioluminescence for ≥ 11 days were considered for analysis.

Simulating day-night entrainment and social jet lag *ex vivo*

To establish baseline measurements of day-night entrainment, one group (hereby referred to as the "Control Group") consists of whole brain explants exposed to a 15L45D LD strobe schedule simulating 12:12 hour LD entrainment for 9 days with no phase shifts followed by 2 days of constant darkness (DD). White light exposure is performed using an LED set to provide a light intensity of 30 $\mu W/cm^2 \pm 0.5 \mu W/cm^2$ with automated timing set via TTL input from Piper. During intervals of light exposure, the CCD camera is protected by a mechanical shutter that is controlled via TTL input from Piper to allow for semi-continuous imaging. For samples exposed to a social jet lag protocol (hereby referred to as the "SJL Group"), the first three "weekdays" (same phase for simulated "Wednesday" – "Friday" schedules) are in-phase with the Control Group. This is followed by a 3-hour phase delay on the evening of the third day ("Friday night") followed by two "weekend" days with no phase shift ("Saturday – Sunday"). The whole brain explants are exposed to a phase advance of 3 hours on the morning of sixth day ("Monday morning") with no phase shift on the following "weekdays" ("Monday" – "Wednesday") before finally ending with 2 days of free-running conditions in DD. Three hour phase shifts are used because they correspond with social behaviors that are commonly observed in

the general populace. LED light exposure and imaging are automated via TTL input from the Piper software (208 players for the Control Group and 214 players for the SJL Group).

Processing of bioluminescence images

Cosmic rays are removed in real-time using the Piper cosmic ray filter set to discriminate the sum of all pixel values above 800 and reject frames that are >3 standard deviations over the running average (run over 30 frames). The software ImageJ is then used to generate images with bioluminescence averaged over 45 minute intervals. These images were then processed in MetaMorph as previously described (Noguchi et al., 2013; Roberts et al., 2015). Briefly, noise from dark current and cosmic rays were removed by using a running minimum algorithm to generate new images constructed from pairs of sequential images using the minimum values of each pixel from the two images. MetaMorph was used to generate a stack of images for each experiment with average luminescence intensity over time measured for regions of interest (ROIs) that were manually defined based on a previous protocol (Roberts et al., 2015). ROIs were classified into canonical circadian neuron groups (colored-coded: red = s-LNv, yellow = l-LNv, orange = LNd, blue = DN1, green = DN3) based on consistent and classically recognized anatomical locations. Raw bioluminescence data were then processed by Microsoft Excel to adjust for background noise and convert raw luminescence over time to photons-per-minute as previously described (Noguchi et al., 2013; Roberts et al., 2015). Circadian parameters were analyzed for 11 day recordings using modified versions of previously described MATLAB scripts with the first 12 hours excluded due to initially high amplitude and highly variable bioluminescence following dissection and addition of luciferin (Roberts et al., 2015).

6.5.3 Preliminary Results

LD strobe day-night entrainment results in robust synchrony and rhythmicity within and between canonical circadian neuron subgroups

Drosophila whole brain explants exposed to a 15L45D LD strobe entrainment protocol simulating 12:12 hour day-night entrainment with no phase shifts (Control Group, n = 100 cells) exhibit network-wide robust rhythmicity, high amplitude oscillations, ~24-hour period and consistent phase throughout the 9 days of LD strobe (Figure 6.3A, green trace). Order parameter R was quantified for 2-day sliding windows as a measure of dynamic synchrony as previously described (Gonze et al., 2005; Roberts et al., 2015) Robust rhythmicity and synchrony is also observed between and within the s-LNvs, l-LNvs, LNds, DN1s and DN3s (Figure 6.3 A-B). Upon transitioning to constant darkness (DD) conditions on Day 9, an immediate decrease in amplitude, rhythmicity and synchrony is observed for all circadian neurons (Table 6.2; Figure 6.3, dark blue trace). However, the canonical circadian neurons are still relatively synchronized for the initial days in DD as previously observed (Roberts et al., 2015; Sehadova et al., 2009). The robust rhythmicity and consistent phase of explants exposed to the Control LD strobe protocol provide baseline measurements of day-night entrainment (Movie 3, left side) for comparison to whole brain explants exposed to the social jet lag light protocol (Movie 3, right side).

Social jet lag disrupts circadian neurons' intrinsic rhythmicity and synchrony

In order to simulate social jet lag, *Drosophila* whole brain explants (SJL Group, n = 107 cells) were exposed to a 15L45D LD strobe protocol that simulated a 3-hour phase delay from "weekdays" (black trace) to "weekends" (red trace) followed by a 3-hour

phase-advance to return from the “weekend” schedule back to “weekdays.” Although clear phase shifts were observed at the network-wide and single-cell levels, surprisingly strong synchrony and amplitude were maintained between and within canonical circadian neuron subgroups throughout the 9 days of exposure to social jet lag conditions (Figure 6.3). Intriguingly, circadian neuron oscillators exhibit an immediate damping of amplitude, rhythmicity and synchrony upon transitioning to free-running conditions in DD that is significantly greater in reduction than corresponding neurons in the DD portion of control experiments (Figure 6.3, blue trace). Inter-subgroup desynchrony is particularly pronounced with an immediate drop in synchrony from an R value of 0.88 on the final weekdays to an R value of 0.19 in DD (Table 6.2). Motivated by the clear differences in inter-subgroup responses to social jet lag, we investigated single oscillator dynamics within each canonical circadian subgroup.

Distinct circadian neuron subgroup dynamics in response to social jet lag

We analyzed each of the canonical circadian subgroups’ responses to social jet lag (SJL) in comparison to their baseline activities in “control conditions” of day-night entrainment with no phase shifts (Figure 6.4). During control conditions, all circadian oscillators exhibit robust rhythmicity and amplitude to varying degrees (Figure 6.4A, black traces). The classical pacemaker s-LNvs have the most robust synchrony over time whereas the DN1s have the highest amplitude oscillations (Table 6.2, Figure 6.4A). Upon changing to constant darkness (DD) conditions on Day 9, each of the neuronal subgroups exhibit a clear and immediate decrease in amplitude and synchrony (Figure 6.4A, blue traces). The large and small LNvs both maintain the highest synchrony in DD whereas the LNds exhibit the lowest synchrony (Table 6.2). Conversely, exposure to social jet lag

results in the small and large LNvs both exhibiting significant damping of amplitude and synchrony relative to LNvs in control conditions (Figure 6.4B). Averaged bioluminescence traces are shown for clearer comparisons of the neuron subgroup qualitative dynamics in SJL and control conditions (Figure 6.4C). The s-LNvs show particularly pronounced damping of synchrony and amplitude during the “weekend” schedule following the 3-hour phase delay with a slight recovery of synchrony following the 3-hour phase advance returning entrainment back to the original “weekday” schedule. However, the l-LNvs show significantly reduced amplitude and synchrony following the 3-hour phase delay with synchrony and amplitude becoming even more damped following the 3-hour phase advance. Further, the small and large l-LNvs have significantly lower synchrony in DD relative to corresponding s-LNvs and l-LNvs in the Control Group. Conversely, the dorsal LNd, DN1 and DN3 subgroups maintain relatively robust synchrony and amplitude in SJL conditions. These dorsal subgroups all exhibit greater synchrony in DD than both the LNv subgroups (Table 6.2). Interestingly, the light-blind DN3s are the only subgroup to exhibit greater synchrony by Day 9 in the SJL conditions relative to DN3s in the control conditions.

6.5.4 Conclusions

By employing a combination of LD strobe entrainment with our custom bioluminescence imaging system, we are able to investigate how circadian neural systems respond to social jet lag at the circuit-wide, individual neuron subgroup and single cell oscillator levels. *Drosophila* whole brain explants are directly light-sensitive due to the expression of the blue-light sensitive photoreceptor CRYPTOCHROME (CRY) in circadian neurons and can thus be used to study physiological photic entrainment in

real-time (Benito et al., 2008; Veleri et al., 2003; Yoshii et al., 2008). To the best of our knowledge, semi-continuous imaging with the novel 15L45D LD strobe protocol provides the first longitudinal bioluminescence recordings of whole circadian neural networks responding to day-night photic entrainment in real-time with single cell resolution. The coherent and consistent mean network phase in response to the continuous light pulses of the LD strobe protocol suggest that properly timed zeitgebers at the start and end of the daytime hours with consistent nighttime darkness are critical for proper entrainment as has been described by skeleton photoperiod protocols (Oishi et al., 2002; Pittendrigh and Daan, 1976; Sharma et al., 1997). This may be why naps during midday might not disrupt circadian rhythms whereas late night exposure to electronic blue-light emitting screens can reset circadian systems. Furthermore, our observations that oscillators exhibit an immediate damping of rhythmicity and synchrony upon switching from LD strobe entrainment to constant darkness indicate that entrainment is critical for maintaining robust oscillator synchrony and rhythmicity in addition to consistent phase.

Interestingly, circadian neuron oscillators in social jet lag conditions maintain relatively high amplitude synchronous oscillations despite exposure to a 3-hour phase delay and 3-hour phase advance. However, the significant and immediate decrease in amplitude and synchrony upon transitioning to DD conditions suggests that the intrinsic rhythmicity of these oscillators has already been disrupted by exposure to social jet lag and is only being maintained by constant photic input from the LD strobe protocol. Future studies will need to investigate precisely how these circadian neurons are being disrupted and the emergent behavioral and physiological consequences. Our single-cell analysis has also revealed that the ventral s-LNvs and l-LNvs appear to be particularly disrupted

by exposure to SJL whereas the dorsal LNds, DN1s and DN3s maintain relatively robust rhythmicity and synchrony. As previously observed, the LNds and light-blind DN3s actually exhibit an increase in synchrony and amplitude in response to phase shifts suggesting that these two subgroups may have critical roles in pulling the rest of the circadian neural network into a new state of phase-shifted synchrony (Roberts et al., 2015). Sub-regions of the mammalian master clock found in the suprachiasmatic nucleus (SCN) have also been shown to have spatiotemporal variances in light response (Evans et al., 2011; Foley et al., 2011; Nakamura et al., 2005). Future studies should investigate whether certain neuron oscillators in the SCN are particularly susceptible to social jet lag.

In summary, our combination of a novel LD strobe protocol in combination with bioluminescence imaging of whole *Drosophila* brain explants has shown that exposure to social jet lag conditions results in a circuit-wide change in intrinsic oscillator rhythmicity and synchrony. These bioluminescence recordings represent the first visualization of whole circadian network response to light-induced social jet lag in real-time with single neuron resolution. Our preliminary findings suggest that certain circadian neurons may be more susceptible to disruption by social jet lag whereas other neuron oscillators may be critical for facilitating circuit adaptation to the phase shifts. As circuit connectivity appears critical for photoentrainment, we plan to examine how pharmacological or genetic alterations of inter-neuronal communication may accelerate adaptability to and recovery from social jet lag. Based on the numerous organizational similarities between *Drosophila* and mammalian circadian circuits, these patterns of circadian neural network response to social jet lag may be generally observed in humans and other mammals.

6.6 Concluding Remarks

In conclusion, light input can powerfully influence many aspects of physiological, psychological and behavioral activities. Circadian neural systems are particularly driven by photic signals with daily solar cycles providing the most dominant environmental cues for entrainment. However, abnormal changes in proper timing of light exposure due to situations such as jet lag and late night electronic display exposure can result in misalignment of internal biological clocks and the external environment. Chronic misalignment of circadian systems has been linked to a wide array of negative health effects including obesity, diabetes, depression, bipolar disorder, Parkinson's disease and cancer. Our studies suggest that circadian neural networks are composed of a complementary ensemble of strong and weak cellular oscillators that permit circadian systems to maintain robust, synchronous oscillations while also remaining adaptable to environmental cues. Our work further suggests that pharmacological agents which transiently weaken the activities of certain neuron oscillators such as the l-LNvs while enhancing the function of other key circadian oscillators such as the LNds may enable circadian systems to more rapidly adapt to conditions such as social jet lag and seasonal affective disorder. In this thesis, I have described our efforts to develop a toolkit for future studies of circadian systems by designing a new bioluminescence imaging system and developing novel light entrainment regimes for studying the longitudinal dynamics of whole circadian network photoentrainment at single neuron resolution. It is my hope that our findings and new tools will open new avenues of research into the precise consequences of circadian disruptions and, hence, how they may be treated.

6.7 Figures

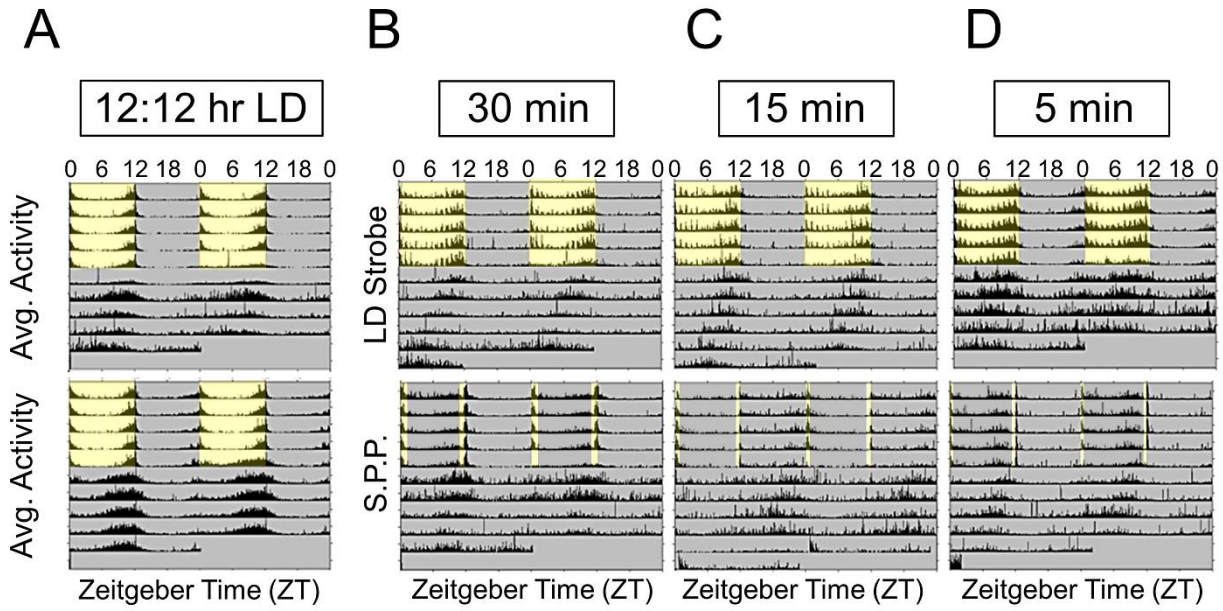

Figure 6.1. Day-night entrainment of locomotor activity by LD strobe and skeleton photoperiod light protocols. The averaged locomotor activities of adult *Drosophila* are shown for 5 days of entrainment by various light protocols followed by 5 days of constant darkness (DD). All flies were first entrained to ≥3 days of 12:12 hour LD entrainment. Yellow shading indicates intervals of light exposure whereas gray shading indicates intervals of darkness. **A**: XLG-Luc flies (**top row**) and wild-type W^{1118}[5905] (**bottom row**) flies were exposed to 5 days of 12:12 hour LD entrainment. **B-D**: XLG-Luc flies were entrained for 5 days by either LD strobe (**top row**) or skeleton photoperiod (S.P.P., **bottom row**). LD strobe and skeleton photoperiod entrainment was performed with **B**: 30 minute, **C:** 15 minute, or **D:** 5 minute light pulses. The automated Trikinetics *Drosophila* Activity Monitor system was used to record the locomotor activities of 64 male fruit flies per experiment. Double-plotted actograms were generated by ClockLab (Actimetrics) for 1 minute bins.

	W1118			XLG-Luc		
30L30D LD Strobe	**n**	**%Rhythmic**	**Period**	**n**	**%Rhythmic**	**Period**
LD	54	100	23.8	46	95.7	23.8
DD	53	100	23.5	45	64.4	23
15L45D LD Strobe	**n**	**%Rhythmic**	**Period**	**n**	**%Rhythmic**	**Period**
LD	61	100	23.7	41	97.6	23.9
DD	60	100	23.5	36	75	23.2
5L55D LD Strobe	**n**	**%Rhythmic**	**Period**	**n**	**%Rhythmic**	**Period**
LD	56	98.2	23.6	58	98.3	23.8
DD	51	94.1	23.4	54	74.1	23.3
30 min SPP	**n**	**%Rhythmic**	**Period**	**n**	**%Rhythmic**	**Period**
LD	61	98.4	23.9	56	94.6	23.9
DD	59	98.3	23.6	51	82.4	23.3
15 min SPP	**n**	**%Rhythmic**	**Period**	**n**	**%Rhythmic**	**Period**
LD	62	100	23.6	55	74.5	23.8
DD	61	98.4	23.4	50	54	23.7
5 min SPP	**n**	**%Rhythmic**	**Period**	**n**	**%Rhythmic**	**Period**
LD	63	100	23.6	62	95.2	23.7
DD	63	98.4	23.3	62	87.1	23.1

Table 6.1. **Quantification of behavioral entrainment by LD strobe and skeleton photoperiod.** FaasX was used for analysis of behavioral experiments shown in **Figure 6.1**. Wild-type (W^{1118}[5905]) and XLG-luc flies were exposed to 5 days of entrainment (LD) by either LD strobe or skeleton photoperiod protocols with 30, 15 or 5 minute pulses. Following entrainment, flies were maintained in constant darkness (DD) for 5 days. Cycle-P was used to quantify measures of period length and the percentage of rhythmic flies using 15 minute bins of individual fly locomotor activity. Individual flies were considered rhythmic by chi-square periodogram analysis if they met the following criteria: power ≥ 40, width ≥ 4 hours and period length of 24 ± 8 hours.

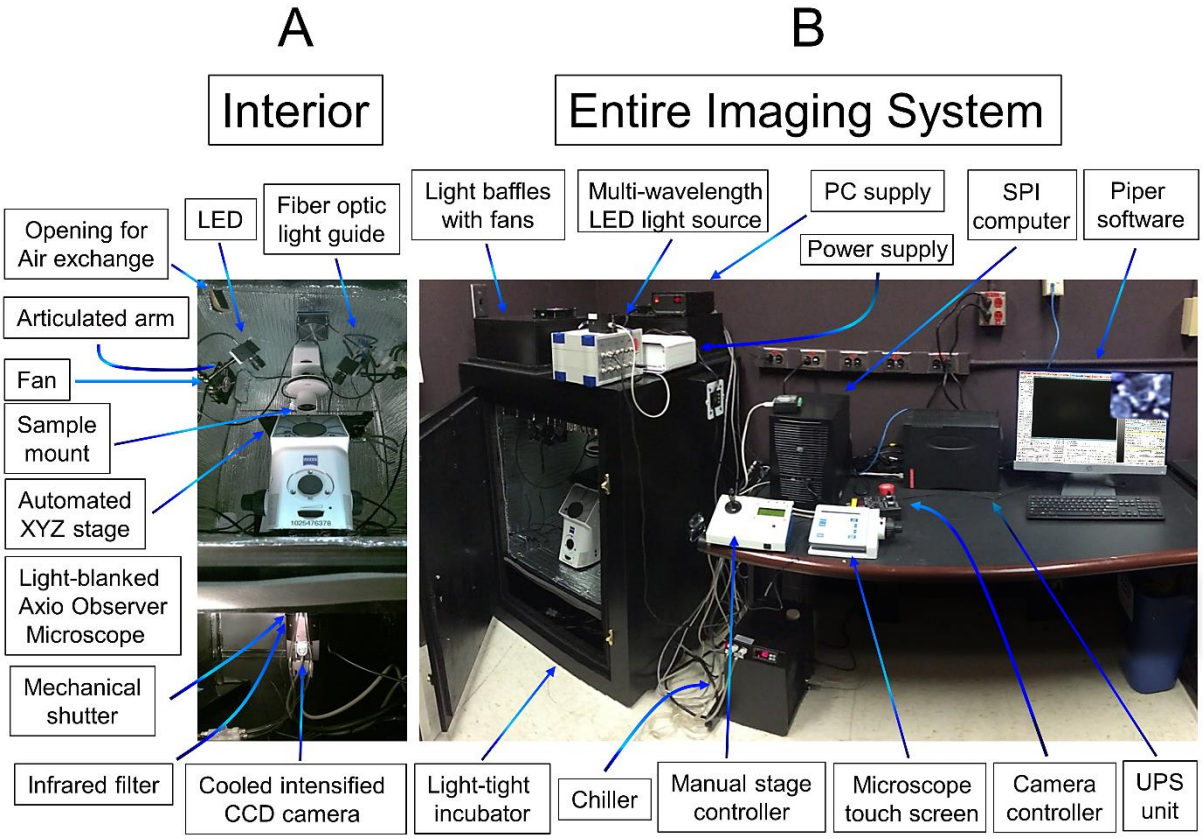

Figure 6.2. Setup of custom bioluminescence imaging system. The various components of our bioluminescence imaging system are shown for the **A:** interior of the light-tight incubator and the **B:** overall exterior setup. Within the interior, the cooled-intensified CCD camera and Axio Observer Microscope are visible. From the exterior, components such as the LED light sources, chiller, and computer are visible with all connections integrated into the incubator to ensure it remains light-tight. See Materials and Methods for details on how we have optimized the various components for increased signal-to-noise and functionality.

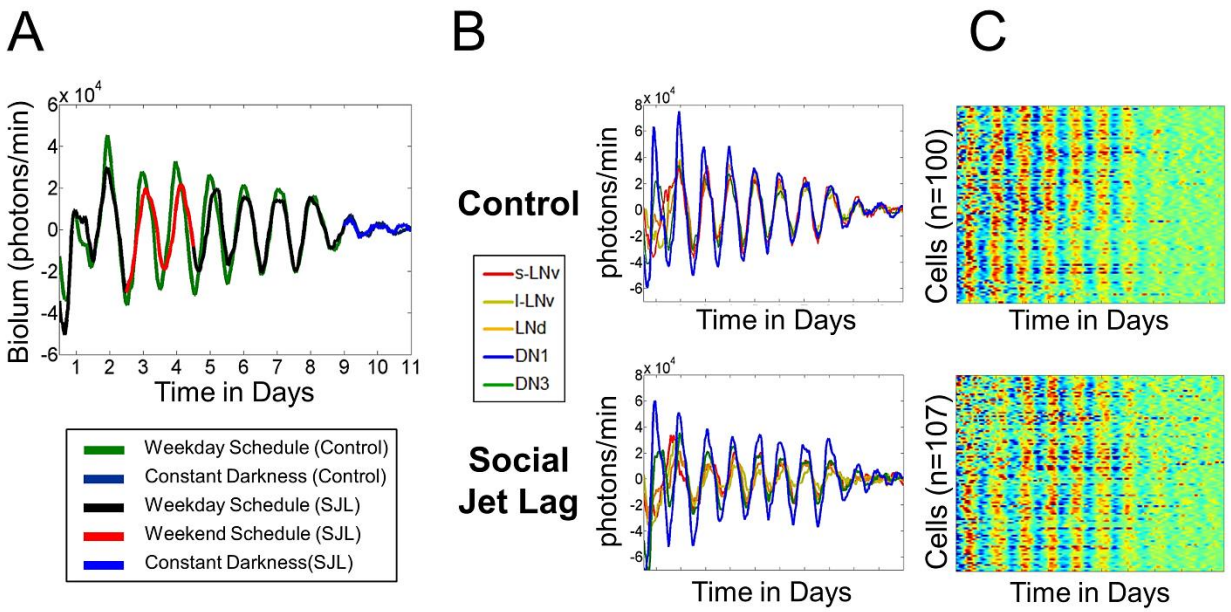

Figure 6.3. Social jet lag results in circuit-wide damped intrinsic rhythmicity and synchrony relative to day-night entrainment with no phase shifts. PERIOD (PER) activity as reported by 11 day bioluminescence recordings are shown at **A:** whole neural network, **B:** individual subgroup and **C:** single cell oscillator levels. **A:** Bioluminescence traces represent the activities of all circadian neurons (averaged from all subgroups) in either control (n=100 cells) or social jet lag (n=107 cells) conditions. Segments of the traces are color-coded to indicate whether they are in the weekday segment of the control (green), constant darkness (DD) segment of the control (dark blue), weekday segment of social jet lag (SJL, black), weekend segment of SJL (red), or DD segment of SJL (blue). See Materials and Methods for a detailed description of each of these experimental segments. **B:** Average bioluminescence traces are color-coded for each of the circadian neuron subgroups: s-LNv (red), l-LNv (yellow), LNd (orange), DN1 (blue) and DN3 (green). These are shown as overlapping traces for the control (**top row**) and SJL (**bottom row**) conditions. **C:** Raster pseudo-heat maps are shown representing the bioluminescence activities of single neuron oscillators in control (**top row**) and SJL (**bottom row**) conditions. Warmer colors indicate higher levels of bioluminescence activity whereas cooler colors indicate lower levels of bioluminescence activities. MATLAB scripts were used to generate bioluminescence traces and raster plots as previously described (Roberts et al., 2015).

Control (No Phase Shift)	n	R-value (Weekday)	R-value (Weekend)	R-Value (Weekday)	R-Value (DD)
All Circadian Neurons	100	0.31	0.59	0.58	0.097
s-LNv	18	0.41	0.65	0.71	0.16
l-LNv	19	0.36	0.66	0.66	0.16
LNd	18	0.36	0.52	0.66	0.095
DN1	27	0.52	0.67	0.56	0.14
DN3	18	0.49	0.54	0.46	0.11
Inter-Subgroup	5	0.69	0.96	0.98	0.74

Social Jet Lag (3 hr Phase Shift)	n	R-value (Weekday)	R-value (Weekend)	R-Value (Weekday)	R-Value (DD)
All Circadian Neurons	107	0.3	0.48	0.46	0.039
s-LNv	17	0.4	0.38	0.51	0.066
l-LNv	17	0.35	0.39	0.28	0.033
LNd	15	0.38	0.5	0.51	0.096
DN1	28	0.53	0.62	0.54	0.13
DN3	30	0.5	0.64	0.54	0.14
Inter-Subgroup	5	0.63	0.87	0.88	0.19

Table 6.2. **Quantification of order parameter R values during social jet lag and day-night entrainment conditions.** Order parameter R-values, as a measure of oscillator synchrony, are shown for “all circadian neurons” (summed from all subgroups), s-LNvs, l-LNvs, LNds, DN1s, and DN3s during light-exposed and constant darkness portions of control (no phase shift, **top row**) and social jet lag (SJL, **bottom row**) experiments. See Materials and Methods for a more detailed description of the experimental setup for these two conditions. To quantify changes in synchrony over time, custom MATLAB scripts calculated an order parameter ‘R’ over two day sliding windows as previously described (Gonze et al., 2005; Roberts et al., 2015). An R value of 1 indicates that the phase, period and waveform of all analyzed cells are in perfect synchrony, whereas an R value of 0 indicates uniform distribution.

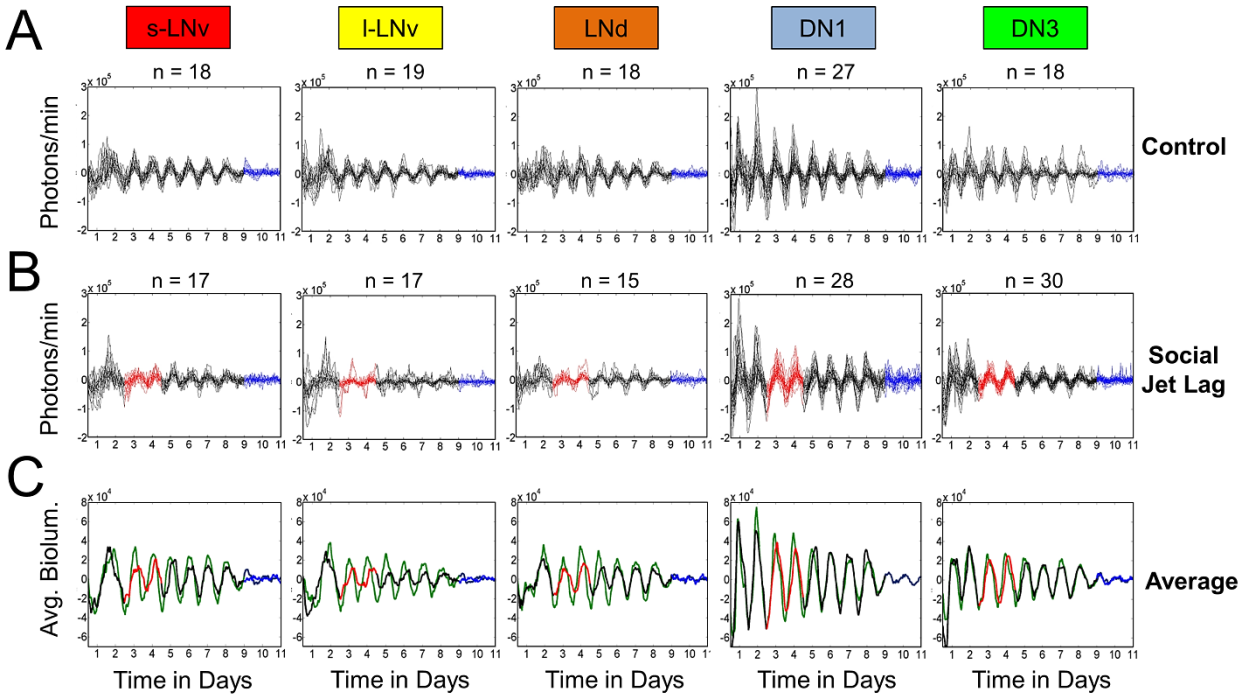

Figure 6.4. Circadian neuron subgroups exhibit distinct dynamics of activity in response to day-night entrainment and social jet lag. Bioluminescence traces are shown for the s-LNvs, l-LNvs, LNds, DN1s and DN3s in **A:** control (no phase shift) and **B:** social jet lag conditions. The number of cells in each condition and subgroup is shown on top of the traces. The traces are color-coded to indicate light schedules representing weekdays (black), weekends (red), and constant darkness (blue). **C:** Average bioluminescence traces are shown comparing control and social jet lag conditions for each subgroup. These traces were generated by MATLAB scripts and are color-coded with the same scheme as traces in **Figure 6.3A**.

6.8 References

A Quera Salva, M., Hartley, S., Barbot, F., C Alvarez, J., Lofaso, F., and Guilleminault, C. (2011). Circadian rhythms, melatonin and depression. Current pharmaceutical design *17*, 1459-1470.

Ahmad, M., and Cashmore, A.R. (1993). HY4 gene of A. thaliana encodes a protein with characteristics of a blue-light photoreceptor.

Allada, R., Emery, P., Takahashi, J.S., and Rosbash, M. (2001). Stopping time: the genetics of fly and mouse circadian clocks. Annual review of neuroscience *24*, 1091-1119.

Allada, R., White, N.E., So, W.V., Hall, J.C., and Rosbash, M. (1998). A mutant Drosophila homolog of mammalian Clock disrupts circadian rhythms and transcription of period and timeless. Cell *93*, 791-804.

Altun, A., and Ugur-Altun, B. (2007). Melatonin: therapeutic and clinical utilization. International journal of clinical practice *61*, 835-845.

An, S., Harang, R., Meeker, K., Granados-Fuentes, D., Tsai, C.A., Mazuski, C., Kim, J., Doyle, F.J., Petzold, L.R., and Herzog, E.D. (2013). A neuropeptide speeds circadian entrainment by reducing intercellular synchrony. Proceedings of the National Academy of Sciences *110*, E4355-E4361.

Arendt, J., and Marks, V. (1982). Physiological changes underlying jet lag. British medical journal (Clinical research ed) *284*, 144.

Aschoff, J. (1981). Freerunning and entrained circadian rhythms. In Biological rhythms (Springer), pp. 81-93.

Aschoff, J., Fatranska, M., Giedke, H., Doerr, P., Stamm, D., and Wisser, H. (1971). Human circadian rhythms in continuous darkness: entrainment by social cues. Science *171*, 213-215.

Ayaz, D., Leyssen, M., Koch, M., Yan, J., Srahna, M., Sheeba, V., Fogle, K.J., Holmes, T.C., and Hassan, B.A. (2008). Axonal injury and regeneration in the adult brain of Drosophila. The Journal of Neuroscience *28*, 6010-6021.

Barnard, A.R., and Nolan, P.M. (2008). When clocks go bad: neurobehavioural consequences of disrupted circadian timing. PLoS Genet *4*, e1000040.

Barrett, R.K., and Takahashi, J.S. (1995). Temperature compensation and temperature entrainment of the chick pineal cell circadian clock. The Journal of neuroscience : the official journal of the Society for Neuroscience *15*, 5681-5692.

Barski, O.A., Tipparaju, S.M., and Bhatnagar, A. (2008). The aldo-keto reductase superfamily and its role in drug metabolism and detoxification. Drug metabolism reviews *40*, 553-624.

Bell-Pedersen, D., Cassone, V.M., Earnest, D.J., Golden, S.S., Hardin, P.E., Thomas, T.L., and Zoran, M.J. (2005). Circadian rhythms from multiple oscillators: lessons from diverse organisms. Nature Reviews Genetics *6*, 544-556.

Belle, M.D., Diekman, C.O., Forger, D.B., and Piggins, H.D. (2009). Daily electrical silencing in the mammalian circadian clock. Science *326*, 281-284.

Benito, J., Houl, J.H., Roman, G.W., and Hardin, P.E. (2008). The blue-light photoreceptor CRYPTOCHROME is expressed in a subset of circadian oscillator neurons in the Drosophila CNS. Journal of biological rhythms *23*, 296-307.

Bergendahl, M., Evans, W.S., and Veldhuis, J.D. (1996). Current concepts on ultradian rhythms of luteinizing hormone secretion in the human. Human reproduction update *2*, 507-518.

Berndt, A., Kottke, T., Breitkreuz, H., Dvorsky, R., Hennig, S., Alexander, M., and Wolf, E. (2007). A novel photoreaction mechanism for the circadian blue light photoreceptor Drosophila cryptochrome. The Journal of biological chemistry *282*, 13011-13021.

Bjorvatn, B., and Pallesen, S. (2009). A practical approach to circadian rhythm sleep disorders. Sleep medicine reviews *13*, 47-60.

Blanchardon, E., Grima, B., Klarsfeld, A., Chélot, E., Hardin, P.E., Préat, T., and Rouyer, F. (2001). Defining the role of Drosophila lateral neurons in the control of circadian rhythms in motor activity and eclosion by targeted genetic ablation and PERIOD protein overexpression. European Journal of Neuroscience *13*, 871-888.

Blau, J., and Young, M.W. (1999). Cycling vrille expression is required for a functional Drosophila clock. Cell *99*, 661-671.

Bliss, R.D., Painter, P.R., and Marr, A.G. (1982). Role of feedback inhibition in stabilizing the classical operon. Journal of theoretical biology *97*, 177-193.

Blum, I.D., Zhu, L., Moquin, L., Kokoeva, M.V., Gratton, A., Giros, B., and Storch, K.-F. (2015). A highly tunable dopaminergic oscillator generates ultradian rhythms of behavioral arousal. Elife *3*, e05105.

Boivin, D.B., Duffy, J.F., Kronauer, R.E., and Czeisler, C.A. (1996). Dose-response relationships for resetting of human circadian clock by light.

Boulos, Z., Campbell, S.S., Lewy, A.J., Terman, M., Dijk, D.-J., and Eastman, C.I. (1995). Light treatment for sleep disorders: Consensus Report VII. Jet lag. Journal of biological rhythms *10*, 167-176.

Bouly, J.P., Schleicher, E., Dionisio-Sese, M., Vandenbussche, F., Van Der Straeten, D., Bakrim, N., Meier, S., Batschauer, A., Galland, P., Bittl, R.*, et al.* (2007). Cryptochrome blue light photoreceptors are activated through interconversion of flavin redox states. The Journal of biological chemistry *282*, 9383-9391.

Brainard, G.C., Hanifin, J.P., Greeson, J.M., Byrne, B., Glickman, G., Gerner, E., and Rollag, M.D. (2001). Action spectrum for melatonin regulation in humans: evidence for a novel circadian photoreceptor. The Journal of Neuroscience *21*, 6405-6412.

Brandes, C., Plautz, J.D., Stanewsky, R., Jamison, C.F., Straume, M., Wood, K.V., Kay, S.A., and Hall, J.C. (1996). Novel features of Drosophila period transcription revealed by real-time luciferase reporting. Neuron *16*, 687-692.

Broughton, S.J., Kitamoto, T., and Greenspan, R.J. (2004). Excitatory and inhibitory switches for courtship in the brain of Drosophila melanogaster. Current biology : CB *14*, 538-547.

Brown, T., Colwell, C.S., Waschek, J., and Piggins, H.D. (2007). Disrupted neuronal activity rhythms in the suprachiasmatic nuclei of vasoactive intestinal polypeptide-deficient mice. Journal of neurophysiology *97*, 2553-2558.

Buhr, E.D., and Van Gelder, R.N. (2014). Local photic entrainment of the retinal circadian oscillator in the absence of rods, cones, and melanopsin. Proceedings of the National Academy of Sciences *111*, 8625-8630.

Buhr, E.D., Yoo, S.H., and Takahashi, J.S. (2010). Temperature as a universal resetting cue for mammalian circadian oscillators. Science *330*, 379-385.

Busza, A., Emery-Le, M., Rosbash, M., and Emery, P. (2004). Roles of the two Drosophila CRYPTOCHROME structural domains in circadian photoreception. Science *304*, 1503-1506.

Cagnacci, A., Elliott, J., and Yen, S. (1992). Melatonin: a major regulator of the circadian rhythm of core temperature in humans. The Journal of Clinical Endocrinology & Metabolism *75*, 447-452.

Campomanes, C.R., Carroll, K.I., Manganas, L.N., Hershberger, M.E., Gong, B., Antonucci, D.E., Rhodes, K.J., and Trimmer, J.S. (2002). Kvβ subunit oxidoreductase activity and Kv1 potassium channel trafficking. Journal of Biological Chemistry *277*, 8298-8305.

Cao, G., and Nitabach, M.N. (2008). Circadian control of membrane excitability in Drosophila melanogaster lateral ventral clock neurons. The Journal of Neuroscience *28*, 6493-6501.

Cavanaugh, D.J., Geratowski, J.D., Wooltorton, J.R., Spaethling, J.M., Hector, C.E., Zheng, X., Johnson, E.C., Eberwine, J.H., and Sehgal, A. (2014). Identification of a circadian output circuit for rest: activity rhythms in Drosophila. Cell *157*, 689-701.

Cavey, M., Collins, B., Bertet, C., and Blau, J. (2016). Circadian rhythms in neuronal activity propagate through output circuits. Nature neuroscience *19*, 587-595.

Ceriani, M.F., Darlington, T.K., Staknis, D., Más, P., Petti, A.A., Weitz, C.J., and Kay, S.A. (1999). Light-dependent sequestration of TIMELESS by CRYPTOCHROME. Science *285*, 553-556.

Chang, D.C. (2006). Neural circuits underlying circadian behavior in Drosophila melanogaster. Behavioural processes *71*, 211-225.

Cho, K., Ennaceur, A., Cole, J.C., and Suh, C.K. (2000). Chronic jet lag produces cognitive deficits. The Journal of neuroscience : the official journal of the Society for Neuroscience *20*, Rc66.

Chouinard, S.W., Wilson, G.F., Schlimgen, A.K., and Ganetzky, B. (1995). A potassium channel beta subunit related to the aldo-keto reductase superfamily is encoded by the Drosophila hyperkinetic locus. Proceedings of the National Academy of Sciences *92*, 6763-6767.

Cohen, A.L., Leise, T.L., and Welsh, D.K. (2012). Bayesian statistical analysis of circadian oscillations in fibroblasts. Journal of theoretical biology *314*, 182-191.

Collins, B., Kane, E.A., Reeves, D.C., Akabas, M.H., and Blau, J. (2012). Balance of activity between LN_vs and glutamatergic dorsal clock neurons promotes robust circadian rhythms in *Drosophila*. Neuron *74*, 706-718.

Collins, B., Kaplan, H.S., Cavey, M., Lelito, K.R., Bahle, A.H., Zhu, Z., Macara, A.M., Roman, G., Shafer, O.T., and Blau, J. (2014). Differentially timed extracellular signals synchronize pacemaker neuron clocks. PLoS Biol *12*, e1001959.

Colwell, C.S., Michel, S., Itri, J., Rodriguez, W., Tam, J., Lelievre, V., Hu, Z., Liu, X., and Waschek, J.A. (2003). Disrupted circadian rhythms in VIP-and PHI-deficient mice. American Journal of Physiology-Regulatory, Integrative and Comparative Physiology *285*, R939-R949.

Coomans, C., Lucassen, E., Kooijman, S., Fifel, K., Deboer, T., Rensen, P., Michel, S., and Meijer, J. (2015). Plasticity of circadian clocks and consequences for metabolism. Diabetes, Obesity and Metabolism *17*, 65-75.

Cuesta, M., Aungier, J., and Morton, A.J. (2014). Behavioral therapy reverses circadian deficits in a transgenic mouse model of Huntington's disease. Neurobiology of disease *63*, 85-91.

Cymborowski, B., Lewis, R., Hong, S.-F., and Saunders, D. (1994). Circadian locomotor activity rhythms and their entrainment to light-dark cycles continue in flies (Calliphora vicina) surgically deprived of their optic lobes. Journal of Insect Physiology *40*, 501-510.

Cyran, S.A., Buchsbaum, A.M., Reddy, K.L., Lin, M.-C., Glossop, N.R., Hardin, P.E., Young, M.W., Storti, R.V., and Blau, J. (2003). vrille, Pdp1, and dClock form a second feedback loop in the Drosophila circadian clock. Cell *112*, 329-341.

Czeisler, C., Dumont, M., Duffy, J., Steinberg, J., Richardson, G., Brown, E., Sanchez, R., Rios, C., and Ronda, J. (1992). Association of sleep-wake habits in older people with changes in output of circadian pacemaker. The lancet *340*, 933-936.

Czeisler, C.A., Duffy, J.F., Shanahan, T.L., Brown, E.N., Mitchell, J.F., Rimmer, D.W., Ronda, J.M., Silva, E.J., Allan, J.S., and Emens, J.S. (1999). Stability, precision, and near-24-hour period of the human circadian pacemaker. Science *284*, 2177-2181.

Czeisler, C.A., Richardson, G.S., Zimmerman, J.C., Moore-Ede, M.C., and Weitzman, E.D. (1981). ENTRAINMENT OF HUMAN ORCADIAN RHYTHMS BY LIGHT-DARK CYCLES: A REASSESSMENT. Photochemistry and Photobiology *34*, 239-247.

Daan, S., and Slopsema, S. (1978). Short-term rhythms in foraging behaviour of the common vole, Microtus arvalis. Journal of comparative Physiology *127*, 215-227.

Dagan, Y., Yovel, I., Hallis, D., Eisenstein, M., and Raichik, I. (1998). Evaluating the role of melatonin in the long-term treatment of delayed sleep phase syndrome (DSPS). Chronobiology International *15*, 181-190.

Dahlitz, M., Alvarez, B., Parkes, J., English, J., Arendt, J., and Vignau, J. (1991). Delayed sleep phase syndrome response to melatonin. The Lancet *337*, 1121-1124.

Darlington, T.K., Wager-Smith, K., Ceriani, M.F., Staknis, D., Gekakis, N., Steeves, T.D., Weitz, C.J., Takahashi, J.S., and Kay, S.A. (1998). Closing the circadian loop: CLOCK-induced transcription of its own inhibitors per and tim. Science *280*, 1599-1603.

Das, A., Holmes, T.C., and Sheeba, V. (2015). dTRPA1 Modulates Afternoon Peak of Activity of Fruit Flies Drosophila melanogaster. PLoS One *10*, e0134213.

Das, A., Holmes, T.C., and Sheeba, V. (2016). dTRPA1 in Non-circadian Neurons Modulates Temperature-dependent Rhythmic Activity in Drosophila melanogaster. J Biol Rhythms *31*, 272-288.

Davidson, A.J., Castanon-Cervantes, O., Leise, T.L., Molyneux, P.C., and Harrington, M.E. (2009). Visualizing jet lag in the mouse suprachiasmatic nucleus and peripheral circadian timing system. The European journal of neuroscience *29*, 171-180.

Dawson, D., and Armstrong, S.M. (1996). Chronobiotics—drugs that shift rhythms. Pharmacology & therapeutics *69*, 15-36.

De Mairan, J. (1729). Observation botanique. Hist Acad Roy Sci *35*, 36.

Desan, P.H., Weinstein, A.J., Michalak, E.E., Tam, E.M., Meesters, Y., Ruiter, M.J., Horn, E., Telner, J., Iskandar, H., and Boivin, D.B. (2007). A controlled trial of the

Litebook light-emitting diode (LED) light therapy device for treatment of Seasonal Affective Disorder (SAD). BMC psychiatry *7*, 1.

DeWoskin, D., Myung, J., Belle, M.D., Piggins, H.D., Takumi, T., and Forger, D.B. (2015). Distinct roles for GABA across multiple timescales in mammalian circadian timekeeping. Proceedings of the National Academy of Sciences *112*, E3911-E3919.

Dijk, D.-J., and Archer, S.N. (2010). PERIOD3, circadian phenotypes, and sleep homeostasis. Sleep medicine reviews *14*, 151-160.

Dissel, S., Codd, V., Fedic, R., Garner, K.J., Costa, R., Kyriacou, C.P., and Rosato, E. (2004). A constitutively active cryptochrome in Drosophila melanogaster. Nature neuroscience *7*, 834-840.

Dissel, S., Hansen, Celia N., Özkaya, Ö., Hemsley, M., Kyriacou, Charalambos P., and Rosato, E. (2014). The Logic of Circadian Organization in Drosophila. Current Biology *24*, 2257-2266.

Dodson, E.R., and Zee, P.C. (2010). Therapeutics for circadian rhythm sleep disorders. Sleep medicine clinics *5*, 701-715.

Dowse, H.B., and Ringo, J.M. (1987). Further evidence that the circadian clock in Drosophila is a population of coupled ultradian oscillators. Journal of Biological Rhythms *2*, 65-76.

Emery, I.F., Noveral, J.M., Jamison, C.F., and Siwicki, K.K. (1997). Rhythms of Drosophila period gene expression in culture. Proceedings of the National Academy of Sciences *94*, 4092-4096.

Emery, P., So, W.V., Kaneko, M., Hall, J.C., and Rosbash, M. (1998). CRY, a Drosophila clock and light-regulated cryptochrome, is a major contributor to circadian rhythm resetting and photosensitivity. Cell *95*, 669-679.

Emery, P., Stanewsky, R., Hall, J.C., and Rosbash, M. (2000). Drosophila cryptochromes: A unique circadian-rhythm photoreceptor. Nature *404*, 456-457.

Evans, J.A., Leise, T.L., Castanon-Cervantes, O., and Davidson, A.J. (2011). Intrinsic regulation of spatiotemporal organization within the suprachiasmatic nucleus. PLoS One *6*, e15869.

Evans, J.A., Leise, T.L., Castanon-Cervantes, O., and Davidson, A.J. (2013). Dynamic interactions mediated by nonredundant signaling mechanisms couple circadian clock neurons. Neuron *80*, 973-983.

Evans, J.A., Pan, H., Liu, A.C., and Welsh, D.K. (2012). Cry1−/− circadian rhythmicity depends on SCN intercellular coupling. Journal of biological rhythms *27*, 443-452.

Ewer, J., Frisch, B., Hamblen-Coyle, M., Rosbash, M., and Hall, J. (1992). Expression of the period clock gene within different cell types in the brain of Drosophila adults and mosaic analysis of these cells' influence on circadian behavioral rhythms. The Journal of neuroscience *12*, 3321-3349.

Fadool, D.A., Holmes, T.C., Berman, K., Dagan, D., and Levitan, I.B. (1997). Tyrosine phosphorylation modulates current amplitude and kinetics of a neuronal voltage-gated potassium channel. Journal of neurophysiology *78*, 1563-1573.

Fernández, M.P., Berni, J., and Ceriani, M.F. (2008). Circadian remodeling of neuronal circuits involved in rhythmic behavior. PLoS Biol *6*, e69.

Fetveit, A., Skjerve, A., and Bjorvatn, B. (2003). Bright light treatment improves sleep in institutionalised elderly—an open trial. International journal of geriatric psychiatry *18*, 520-526.

Fido, A., and Ghali, A. (2008). Detrimental effects of variable work shifts on quality of sleep, general health and work performance. Medical principles and practice *17*, 453-457.

Filipski, E., Delaunay, F., King, V.M., Wu, M.W., Claustrat, B., Grechez-Cassiau, A., Guettier, C., Hastings, M.H., and Francis, L. (2004). Effects of chronic jet lag on tumor progression in mice. Cancer research *64*, 7879-7885.

Flourakis, M., Kula-Eversole, E., Hutchison, A.L., Han, T.H., Aranda, K., Moose, D.L., White, K.P., Dinner, A.R., Lear, B.C., Ren, D.*, et al.* (2015). A Conserved Bicycle Model for Circadian Clock Control of Membrane Excitability. Cell *162*, 836-848.

Fogle, K.J., Baik, L.S., Houl, J.H., Tran, T.T., Roberts, L., Dahm, N.A., Cao, Y., Zhou, M., and Holmes, T.C. (2015). CRYPTOCHROME-mediated phototransduction by modulation of the potassium ion channel β-subunit redox sensor. Proceedings of the National Academy of Sciences *112*, 2245-2250.

Fogle, K.J., Parson, K.G., Dahm, N.A., and Holmes, T.C. (2011). CRYPTOCHROME is a blue-light sensor that regulates neuronal firing rate. Science *331*, 1409-1413.

Foldvary-Schaefer, N. (2009). The Cleveland Clinic guide to sleep disorders (Kaplan Publishing).

Foley, N.C., Tong, T.Y., Foley, D., LeSauter, J., Welsh, D.K., and Silver, R. (2011). Characterization of orderly spatiotemporal patterns of clock gene activation in mammalian suprachiasmatic nucleus. European Journal of Neuroscience *33*, 1851-1865.

Freeman, G.M., Krock, R.M., Aton, S.J., Thaben, P., and Herzog, E.D. (2013). GABA networks destabilize genetic oscillations in the circadian pacemaker. Neuron *78*, 799-806.

Ganetzky, B., Robertson, G.A., Wilson, G.F., Trudeau, M.C., and Titus, S.A. (1999). The eag family of K+ channels in Drosophila and mammals. Annals of the New York Academy of Sciences *868*, 356-369.

Gao, S., Takemura, S.Y., Ting, C.Y., Huang, S., Lu, Z., Luan, H., Rister, J., Thum, A.S., Yang, M., Hong, S.T.*, et al.* (2008). The neural substrate of spectral preference in Drosophila. Neuron *60*, 328-342.

Geetha, L., Chandrashekaran, M.K., and Subbaraj, R. (1996). Responses of the circadian locomotor activity rhythm of Mus booduga to shifts in LD schedules. Chronobiol Int *13*, 103-112.

Gekakis, N., Saez, L., Delahaye-Brown, A.-M., Myers, M.P., Sehgal, A., Young, M.W., and Weitz, C.J. (1995). Isolation of timeless by PER protein interaction: defective interaction between timeless protein and long-period mutant PERL. Science *270*, 811-815.

Giebultowicz, J.M. (2001). Peripheral clocks and their role in circadian timing: insights from insects. Philos Trans R Soc Lond B Biol Sci *356*, 1791-1799.

Giebultowicz, J.M., and Hege, D.M. (1997). Circadian clock in Malpighian tubules. Nature *386*, 664-664.

Glaser, F.T., and Stanewsky, R. (2005). Temperature synchronization of the Drosophila circadian clock. Current biology : CB *15*, 1352-1363.

Godenschwege, T., Forde, R., Davis, C.P., Paul, A., Beckwith, K., and Duttaroy, A. (2009). Mitochondrial superoxide radicals differentially affect muscle activity and neural function. Genetics *183*, 175-184.

Gonnissen, H.K., Rutters, F., Mazuy, C., Martens, E.A., Adam, T.C., and Westerterp-Plantenga, M.S. (2012). Effect of a phase advance and phase delay of the 24-h cycle on energy metabolism, appetite, and related hormones. The American journal of clinical nutrition *96*, 689-697.

Gonze, D., Bernard, S., Waltermann, C., Kramer, A., and Herzel, H. (2005). Spontaneous synchronization of coupled circadian oscillators. Biophysical journal *89*, 120-129.

Green, C.B. (2004). Cryptochromes: tail-ored for distinct functions. Current Biology *14*, R847-R849.

Griffin, E.A., Staknis, D., and Weitz, C.J. (1999). Light-independent role of CRY1 and CRY2 in the mammalian circadian clock. Science *286*, 768-771.

Grima, B., Chélot, E., Xia, R., and Rouyer, F. (2004). Morning and evening peaks of activity rely on different clock neurons of the Drosophila brain. Nature *431*, 869-873.

Gulbis, J.M., Mann, S., and MacKinnon, R. (1999). Structure of a voltage-dependent K+ channel β subunit. Cell *97*, 943-952.

Gulbis, J.M., Zhou, M., Mann, S., and MacKinnon, R. (2000). Structure of the Cytoplasmic β Subunit--T1 Assembly of Voltage-Dependent K+ Channels. Science *289*, 123-127.

Hamada, F.N., Rosenzweig, M., Kang, K., Pulver, S.R., Ghezzi, A., Jegla, T.J., and Garrity, P.A. (2008). An internal thermal sensor controlling temperature preference in Drosophila. Nature *454*, 217-220.

Hamasaka, Y., Rieger, D., Parmentier, M.L., Grau, Y., Helfrich-Förster, C., and Nässel, D.R. (2007). Glutamate and its metabotropic receptor in Drosophila clock neuron circuits. Journal of Comparative Neurology *505*, 32-45.

Hao, H., Allen, D.L., and Hardin, P.E. (1997). A circadian enhancer mediates PER-dependent mRNA cycling in Drosophila melanogaster. Molecular and cellular biology *17*, 3687-3693.

Hardie, R. (1991). Voltage-sensitive potassium channels in Drosophila photoreceptors. The Journal of neuroscience *11*, 3079-3095.

Hardin, P.E. (2005). The circadian timekeeping system of Drosophila. Current biology : CB *15*, R714-722.

Harmar, A.J., Marston, H.M., Shen, S., Spratt, C., West, K.M., Sheward, W.J., Morrison, C.F., Dorin, J.R., Piggins, H.D., and Reubi, J.-C. (2002). The $VPAC_2$ Receptor Is Essential for Circadian Function in the Mouse Suprachiasmatic Nuclei. Cell *109*, 497-508.

Harvey, A.G. (2008). Sleep and circadian rhythms in bipolar disorder: seeking synchrony, harmony, and regulation. American Journal of Psychiatry.

Hasler, B.P., Dahl, R.E., Holm, S.M., Jakubcak, J.L., Ryan, N.D., Silk, J.S., Phillips, M.L., and Forbes, E.E. (2012). Weekend-weekday advances in sleep timing are associated with altered reward-related brain function in healthy adolescents. Biological psychology *91*, 334-341.

Hastings, M., Brancaccio, M., and Maywood, E. (2014). Circadian pacemaking in cells and circuits of the suprachiasmatic nucleus. Journal of neuroendocrinology *26*, 2-10.

Hastings, M.H. (1991). Neuroendocrine rhythms. Pharmacology & therapeutics *50*, 35-71.

Hastings, M.H., Reddy, A.B., and Maywood, E.S. (2003). A clockwork web: circadian timing in brain and periphery, in health and disease. Nature Reviews Neuroscience *4*, 649-661.

Hatori, M., Gill, S., Mure, L.S., Goulding, M., O'Leary, D.D., and Panda, S. (2014). Lhx1 maintains synchrony among circadian oscillator neurons of the SCN. Elife *3*, e03357.

Hattar, S., Lucas, R.J., Mrosovsky, N., Thompson, S., Douglas, R., Hankins, M.W., Lem, J., Biel, M., Hofmann, F., and Foster, R.G. (2003). Melanopsin and rod–cone photoreceptive systems account for all major accessory visual functions in mice. Nature *424*, 75-81.

Heisenberg, M., and Buchner, E. (1977). The rôle of retinula cell types in visual behavior ofDrosophila melanogaster. Journal of comparative physiology *117*, 127-162.

Helfrich-Forster, C. (1998). Robust circadian rhythmicity of Drosophila melanogaster requires the presence of lateral neurons: a brain-behavioral study of disconnected mutants. Journal of comparative physiology A, Sensory, neural, and behavioral physiology *182*, 435-453.

Helfrich-Förster, C. (1995). The period clock gene is expressed in central nervous system neurons which also produce a neuropeptide that reveals the projections of circadian pacemaker cells within the brain of Drosophila melanogaster. Proceedings of the National Academy of Sciences *92*, 612-616.

Helfrich-Förster, C., Winter, C., Hofbauer, A., Hall, J.C., and Stanewsky, R. (2001). The circadian clock of fruit flies is blind after elimination of all known photoreceptors. Neuron *30*, 249-261.

Helfrich-Förster, C. (2003). The neuroarchitecture of the circadian clock in the brain of Drosophila melanogaster. Microscopy research and technique *62*, 94-102.

Herzog, E.D., Aton, S.J., Numano, R., Sakaki, Y., and Tei, H. (2004). Temporal precision in the mammalian circadian system: a reliable clock from less reliable neurons. Journal of biological rhythms *19*, 35-46.

Hoang, N., Schleicher, E., Kacprzak, S., Bouly, J.P., Picot, M., Wu, W., Berndt, A., Wolf, E., Bittl, R., and Ahmad, M. (2008). Human and Drosophila cryptochromes are light activated by flavin photoreduction in living cells. PLoS Biol *6*, e160.

Hofbauer, A., and Buchner, E. (1989). Does Drosophila have seven eyes? Naturwissenschaften *76*, 335-336.

Hoffman, D.A., Magee, J.C., Colbert, C.M., and Johnston, D. (1997). K+ channel regulation of signal propagation in dendrites of hippocampal pyramidal neurons. Nature *387*, 869-875.

Holmes, T.C., Fadool, D.A., Ren, R., and Levitan, I.B. (1996). Association of Src tyrosine kinase with a human potassium channel mediated by SH3 domain. Science *274*, 2089-2091.

Hunter-Ensor, M., Ousley, A., and Sehgal, A. (1996). Regulation of the Drosophila protein timeless suggests a mechanism for resetting the circadian clock by light. Cell *84*, 677-685.

Hyun, S., Lee, Y., Hong, S.-T., Bang, S., Paik, D., Kang, J., Shin, J., Lee, J., Jeon, K., and Hwang, S. (2005). Drosophila GPCR Han is a receptor for the circadian clock neuropeptide PDF. Neuron *48*, 267-278.

Ibuka, N., Shin-ichi, T.I., and Kawamura, H. (1977). Analysis of sleep-wakefulness rhythms in male rats after suprachiasmatic nucleus lesions and ocular enucleation. Brain research *122*, 33-47.

Inagaki, N., Honma, S., Ono, D., Tanahashi, Y., and Honma, K.-i. (2007). Separate oscillating cell groups in mouse suprachiasmatic nucleus couple photoperiodically to the onset and end of daily activity. Proceedings of the National Academy of Sciences *104*, 7664-7669.

Ivanchenko, M., Stanewsky, R., and Giebultowicz, J.M. (2001). Circadian photoreception in Drosophila: functions of cryptochrome in peripheral and central clocks. Journal of Biological Rhythms *16*, 205-215.

Johansson, C., Willeit, M., Smedh, C., Ekholm, J., Paunio, T., Kieseppä, T., Lichtermann, D., Praschak-Rieder, N., Neumeister, A., and Nilsson, L.-G. (2003). Circadian clock-related polymorphisms in seasonal affective disorder and their relevance to diurnal preference. Neuropsychopharmacology.

Johard, H.A., Yoishii, T., Dircksen, H., Cusumano, P., Rouyer, F., Helfrich-Förster, C., and Nässel, D.R. (2009). Peptidergic clock neurons in Drosophila: ion transport peptide and short neuropeptide F in subsets of dorsal and ventral lateral neurons. Journal of Comparative Neurology *516*, 59-73.

Jones, C.R., Campbell, S.S., Zone, S.E., Cooper, F., DeSano, A., Murphy, P.J., Jones, B., Czajkowski, L., and Ptč, L.J. (1999). Familial advanced sleep-phase syndrome: A short-period circadian rhythm variant in humans. Nature medicine *5*, 1062-1065.

Jones, C.R., Huang, A.L., Ptáček, L.J., and Fu, Y.-H. (2013). Genetic basis of human circadian rhythm disorders. Experimental neurology *243*, 28-33.

Kalra, S.P., Bagnasco, M., Otukonyong, E.E., Dube, M.G., and Kalra, P.S. (2003). Rhythmic, reciprocal ghrelin and leptin signaling: new insight in the development of obesity. Regulatory peptides *111*, 1-11.

Kane, E.A., Gershow, M., Afonso, B., Larderet, I., Klein, M., Carter, A.R., de Bivort, B.L., Sprecher, S.G., and Samuel, A.D. (2013). Sensorimotor structure of Drosophila larva phototaxis. Proc Natl Acad Sci U S A *110*, E3868-3877.

Kaneko, M., and Hall, J.C. (2000). Neuroanatomy of cells expressing clock genes in Drosophila: transgenic manipulation of the period and timeless genes to mark the

perikarya of circadian pacemaker neurons and their projections. Journal of Comparative Neurology *422*, 66-94.

Kaneko, M., Helfrich-Förster, C., and Hall, J.C. (1997). Spatial and Temporal Expression of the period andtimeless Genes in the Developing Nervous System ofDrosophila: Newly Identified Pacemaker Candidates and Novel Features of Clock Gene Product Cycling. The Journal of neuroscience *17*, 6745-6760.

Kao, Y.T., Tan, C., Song, S.H., Ozturk, N., Li, J., Wang, L., Sancar, A., and Zhong, D. (2008). Ultrafast dynamics and anionic active states of the flavin cofactor in cryptochrome and photolyase. Journal of the American Chemical Society *130*, 7695-7701.

Karlsson, B., Knutsson, A., and Lindahl, B. (2001). Is there an association between shift work and having a metabolic syndrome? Results from a population based study of 27 485 people. Occupational and environmental medicine *58*, 747-752.

Kawato, M., and Suzuki, R. (1981). Analysis of entrainment of circadian oscillators by skeleton photoperiods using phase transition curves. Biological cybernetics *40*, 139-149.

Kayumov, L., Casper, R.F., Hawa, R.J., Perelman, B., Chung, S.A., Sokalsky, S., and Shapiro, C.M. (2005). Blocking low-wavelength light prevents nocturnal melatonin suppression with no adverse effect on performance during simulated shift work. The Journal of Clinical Endocrinology & Metabolism *90*, 2755-2761.

Keene, A.C., Mazzoni, E.O., Zhen, J., Younger, M.A., Yamaguchi, S., Blau, J., Desplan, C., and Sprecher, S.G. (2011). Distinct visual pathways mediate Drosophila larval light avoidance and circadian clock entrainment. The Journal of neuroscience : the official journal of the Society for Neuroscience *31*, 6527-6534.

Klarsfeld, A., Malpel, S., Michard-Vanhée, C., Picot, M., Chélot, E., and Rouyer, F. (2004). Novel features of cryptochrome-mediated photoreception in the brain circadian clock of Drosophila. The Journal of neuroscience *24*, 1468-1477.

Kleitman, N. (1982). Basic rest-activity cycle—22 years later. Sleep: Journal of Sleep Research & Sleep Medicine.

Knutson, K.L., Spiegel, K., Penev, P., and Van Cauter, E. (2007). The metabolic consequences of sleep deprivation. Sleep medicine reviews *11*, 163-178.

Koh, K., Zheng, X., and Sehgal, A. (2006). JETLAG resets the Drosophila circadian clock by promoting light-induced degradation of TIMELESS. Science *312*, 1809-1812.

Konopka, R.J., and Benzer, S. (1971). Clock mutants of Drosophila melanogaster. Proceedings of the National Academy of Sciences *68*, 2112-2116.

Konopka, R.J., Pittendrigh, C., and Orr, D. (1989). Reciprocal behaviour associated with altered homeostasis and photosensitivity of Drosophila clock mutants. Journal of neurogenetics *6*, 1-10.

Kreier, F., Kalsbeek, A., Sauerwein, H.P., Fliers, E., Romijn, J.A., and Buijs, R.M. (2007). "Diabetes of the elderly" and type 2 diabetes in younger patients: Possible role of the biological clock. Experimental gerontology *42*, 22-27.

Kumar, S., Chen, D., and Sehgal, A. (2012). Dopamine acts through Cryptochrome to promote acute arousal in Drosophila. Genes & development *26*, 1224-1234.

Lamba, P., Bilodeau-Wentworth, D., Emery, P., and Zhang, Y. (2014). Morning and evening oscillators cooperate to reset circadian behavior in response to light input. Cell reports *7*, 601-608.

Lau, E.Y.Y., Wong, M.L., Ng, E.C.W., Hui, C.-c.H., Cheung, S.F., and Mok, D.S.Y. (2013). "Social jetlag" in morning-type college students living on campus: Implications for physical and psychological well-being. Chronobiology international *30*, 910-918.

Lear, B.C., Merrill, C.E., Lin, J.-M., Schroeder, A., Zhang, L., and Allada, R. (2005). AG protein-coupled receptor, groom-of-PDF, is required for PDF neuron action in circadian behavior. Neuron *48*, 221-227.

Leise, T., and Siegelmann, H. (2006). Dynamics of a multistage circadian system. Journal of biological rhythms *21*, 314-323.

Leise, T.L., and Harrington, M.E. (2011). Wavelet-based time series analysis of circadian rhythms. Journal of biological rhythms *26*, 454-463.

Leise, T.L., Wang, C.W., Gitis, P.J., and Welsh, D.K. (2012). Persistent cell-autonomous circadian oscillations in fibroblasts revealed by six-week single-cell imaging of PER2:: LUC bioluminescence. PloS one *7*, e33334.

Lemmer, B. (2006). The importance of circadian rhythms on drug response in hypertension and coronary heart disease—from mice and man. Pharmacology & therapeutics *111*, 629-651.

Levandovski, R., Dantas, G., Fernandes, L.C., Caumo, W., Torres, I., Roenneberg, T., Hidalgo, M.P., and Allebrandt, K.V. (2011). Depression scores associate with chronotype and social jetlag in a rural population. Chronobiol Int *28*, 771-778.

Levine, J.D., Funes, P., Dowse, H.B., and Hall, J.C. (2002). Resetting the circadian clock by social experience in Drosophila melanogaster. Science *298*, 2010-2012.

Lewy, A.J., Ahmed, S., Jackson, J.M.L., and Sack, R.L. (1992). Melatonin shifts human orcadian rhythms according to a phase-response curve. Chronobiology international *9*, 380-392.

Lin, C., Robertson, D.E., Ahmad, M., Raibekas, A.A., Jorns, M.S., Dutton, P.L., and Cashmore, A.R. (1995). Association of flavin adenine dinucleotide with the Arabidopsis blue light receptor CRY1. Science *269*, 968-970.

Lin, C., and Todo, T. (2005). The cryptochromes. Genome biology *6*, 220.

Lin, F.J., Song, W., Meyer-Bernstein, E., Naidoo, N., and Sehgal, A. (2001). Photic signaling by cryptochrome in the Drosophila circadian system. Mol Cell Biol *21*, 7287-7294.

Lin, J.-M., Kilman, V.L., Keegan, K., Paddock, B., Emery-Le, M., Rosbash, M., and Allada, R. (2002). A role for casein kinase 2α in the Drosophila circadian clock. Nature *420*, 816-820.

Lin, Y., Stormo, G.D., and Taghert, P.H. (2004). The neuropeptide pigment-dispersing factor coordinates pacemaker interactions in the Drosophila circadian system. The Journal of neuroscience *24*, 7951-7957.

Liu, A.C., Welsh, D.K., Ko, C.H., Tran, H.G., Zhang, E.E., Priest, A.A., Buhr, E.D., Singer, O., Meeker, K., and Verma, I.M. (2007). Intercellular coupling confers robustness against mutations in the SCN circadian clock network. Cell *129*, 605-616.

Long, S.B., Campbell, E.B., and MacKinnon, R. (2005). Crystal structure of a mammalian voltage-dependent Shaker family K+ channel. Science *309*, 897-903.

Maemura, K., Takeda, N., and Nagai, R. (2007). Circadian rhythms in the CNS and peripheral clock disorders: role of the biological clock in cardiovascular diseases. Journal of pharmacological sciences *103*, 134-138.

Marrus, S.B., Zeng, H., and Rosbash, M. (1996). Effect of constant light and circadian entrainment of perS flies: evidence for light-mediated delay of the negative feedback loop in Drosophila. The EMBO Journal *15*, 6877.

Martinek, S., Inonog, S., Manoukian, A.S., and Young, M.W. (2001). A role for the segment polarity gene shaggy/GSK-3 in the Drosophila circadian clock. Cell *105*, 769-779.

Mazuski, C., and Herzog, E.D. (2015). Circadian Rhythms: To Sync or Not To Sync. Current Biology *25*, R337-R339.

McCormack, C.A., and McDonnell, M.T. (1994). Circadian regulation of teleost retinal cone movements in vitro. The Journal of general physiology *103*, 487-499.

Mertens, I., Vandingenen, A., Johnson, E.C., Shafer, O.T., Li, W., Trigg, J., De Loof, A., Schoofs, L., and Taghert, P.H. (2005). PDF receptor signaling in Drosophila contributes to both circadian and geotactic behaviors. Neuron *48*, 213-219.

Meyer, P., Saez, L., and Young, M.W. (2006). PER-TIM interactions in living Drosophila cells: an interval timer for the circadian clock. Science *311*, 226-229.

Michel, S., Geusz, M.E., Zaritsky, J.J., and Block, G.D. (1993). Circadian rhythm in membrane conductance expressed in isolated neurons. Science *259*, 239-241.

Mohawk, J.A., Green, C.B., and Takahashi, J.S. (2012). Central and peripheral circadian clocks in mammals. Annual review of neuroscience *35*, 445.

Monk, T.H. (2005). Aging human circadian rhythms: conventional wisdom may not always be right. Journal of Biological Rhythms *20*, 366-374.

Montell, C. (1999). Visual transduction in Drosophila. Annual review of cell and developmental biology *15*, 231-268.

Morgan, T.H. (1916). Sex-linked inheritance in Drosophila (Carnegie institution of Washington).

Morgenthaler, T.I., Lee-Chiong, T., Alessi, C., Friedman, L., Aurora, N., Boehlecke, B., Brown, T., Chesson, A.L., Kapur, V., and Maganti, R. (2007). Practice parameters for the clinical evaluation and treatment of circadian rhythm sleep disorders. Sleep *30*, 1445-1459.

Morioka, E., Matsumoto, A., and Ikeda, M. (2012). Neuronal influence on peripheral circadian oscillators in pupal Drosophila prothoracic glands. Nature communications *3*, 909.

Morse, D., Cermakian, N., Brancorsini, S., Parvinen, M., and Sassone-Corsi, P. (2003). No circadian rhythms in testis: Period1 expression is clock independent and developmentally regulated in the mouse. Molecular Endocrinology *17*, 141-151.

Murad, A., Emery-Le, M., and Emery, P. (2007). A subset of dorsal neurons modulates circadian behavior and light responses in Drosophila. Neuron *53*, 689-701.

Muraro, N.I., Pírez, N., and Ceriani, M.F. (2013). The circadian system: plasticity at many levels. Neuroscience *247*, 280-293.

Myers, M.P., Wager-Smith, K., Rothenfluh-Hilfiker, A., and Young, M.W. (1996). Light-induced degradation of TIMELESS and entrainment of the Drosophila circadian clock. Science *271*, 1736-1740.

Nagtegaal, J., Kerkhof, G., Smits, M., and Van Der Meer, Y. (1998). Delayed sleep phase syndrome: A placebo-controlled cross-over study on the effects of melatonin administered five hours before the individual dim light melatonin onset. Journal of sleep research *7*, 135-143.

Nakamura, W., Yamazaki, S., Takasu, N.N., Mishima, K., and Block, G.D. (2005). Differential response of Period 1 expression within the suprachiasmatic nucleus. The Journal of neuroscience *25*, 5481-5487.

Nawathean, P., and Rosbash, M. (2004). The doubletime and CKII kinases collaborate to potentiate Drosophila PER transcriptional repressor activity. Molecular cell *13*, 213-223.

Neikrug, A.B., Rissling, M., Trofimenko, V., Liu, L., Natarajan, L., Lawton, S., Parker, B.A., and Ancoli-Israel, S. (2012). Bright light therapy protects women from circadian rhythm desynchronization during chemotherapy for breast cancer. Behavioral sleep medicine *10*, 202-216.

Nitabach, M.N., Blau, J., and Holmes, T.C. (2002). Electrical silencing of Drosophila pacemaker neurons stops the free-running circadian clock. Cell *109*, 485-495.

Nitabach, M.N., Llamas, D.A., Araneda, R.C., Intile, J.L., Thompson, I.J., Zhou, Y.I., and Holmes, T.C. (2001). A mechanism for combinatorial regulation of electrical activity: Potassium channel subunits capable of functioning as Src homology 3-dependent adaptors. Proceedings of the National Academy of Sciences *98*, 705-710.

Nitabach, M.N., and Taghert, P.H. (2008). Organization of the Drosophila circadian control circuit. Current Biology *18*, R84-R93.

Nitabach, M.N., Wu, Y., Sheeba, V., Lemon, W.C., Strumbos, J., Zelensky, P.K., White, B.H., and Holmes, T.C. (2006). Electrical hyperexcitation of lateral ventral pacemaker neurons desynchronizes downstream circadian oscillators in the fly circadian circuit and induces multiple behavioral periods. The Journal of neuroscience *26*, 479-489.

Noguchi, T., Wang, L.L., and Welsh, D.K. (2013). Fibroblast PER2 circadian rhythmicity depends on cell density. Journal of biological rhythms *28*, 183-192.

Noma, A. (1983). ATP-regulated K+ channels in cardiac muscle.

Oishi, K., Fukui, H., Sakamoto, K., Miyazaki, K., Kobayashi, H., and Ishida, N. (2002). Differential expressions of mPer1 and mPer2 mRNAs under a skeleton photoperiod and a complete light-dark cycle. Brain research Molecular brain research *109*, 11-17.

Oishi, K., Shiota, M., Sakamoto, K., Kasamatsu, M., and Ishida, N. (2004). Feeding is not a more potent Zeitgeber than the light-dark cycle in Drosophila. Neuroreport *15*, 739-743.

Okawa, M., and Uchiyama, M. (2007). Circadian rhythm sleep disorders: characteristics and entrainment pathology in delayed sleep phase and non-24 sleep–wake syndrome. Sleep medicine reviews *11*, 485-496.

Okawa, M., Uchiyama, M., Ozaki, S., Shibui, K., and Ichikawa, H. (1998). Circadian rhythm sleep disorders in adolescents: clinical trials of combined treatments based on chronobiology. Psychiatry and clinical neurosciences *52*, 483-490.

Ono, D., Honma, K.-I., and Honma, S. (2015). Circadian and ultradian rhythms of clock gene expression in the suprachiasmatic nucleus of freely moving mice. Scientific reports *5*.

Ozturk, N., Selby, C.P., Annayev, Y., Zhong, D., and Sancar, A. (2011). Reaction mechanism of Drosophila cryptochrome. Proc Natl Acad Sci U S A *108*, 516-521.

Ozturk, N., Selby, C.P., Zhong, D., and Sancar, A. (2014). Mechanism of photosignaling by Drosophila cryptochrome: role of the redox status of the flavin chromophore. The Journal of biological chemistry *289*, 4634-4642.

Pan, Y., Weng, J., Cao, Y., Bhosle, R.C., and Zhou, M. (2008). Functional coupling between the Kv1. 1 channel and aldoketoreductase Kvβ1. Journal of Biological Chemistry *283*, 8634-8642.

Panda, S., Hogenesch, J.B., and Kay, S.A. (2002). Circadian rhythms from flies to human. Nature *417*, 329-335.

Parisky, K.M., Agosto, J., Pulver, S.R., Shang, Y., Kuklin, E., Hodge, J.J., Kang, K., Liu, X., Garrity, P.A., and Rosbash, M. (2008). PDF cells are a GABA-responsive wake-promoting component of the Drosophila sleep circuit. Neuron *60*, 672-682.

Parsons, M., Moffitt, T.E., Gregory, A., Goldman-Mellor, S., Nolan, P., Poulton, R., and Caspi, A. (2015). Social jetlag, obesity and metabolic disorder: investigation in a cohort study. International Journal of Obesity *39*, 842-848.

Pauley, S.M. (2004). Lighting for the human circadian clock: recent research indicates that lighting has become a public health issue. Medical hypotheses *63*, 588-596.

Peng, Y., Stoleru, D., Levine, J.D., Hall, J.C., and Rosbash, M. (2003). Drosophila free-running rhythms require intercellular communication. PLoS biology *1*, e13.

Pérez-García, M.T., López-López, J.R., and González, C. (1999). Kvβ1. 2 subunit coexpression in HEK293 cells confers O2 sensitivity to Kv4. 2 but not to Shaker channels. The Journal of general physiology *113*, 897-907.

Peschel, N., Chen, K.F., Szabo, G., and Stanewsky, R. (2009). Light-dependent interactions between the Drosophila circadian clock factors cryptochrome, jetlag, and timeless. Current biology : CB *19*, 241-247.

Petersen, C.I., McFarland, T.R., Stepanovic, S.Z., Yang, P., Reiner, D.J., Hayashi, K., George, A.L., Roden, D.M., Thomas, J.H., and Balser, J.R. (2004). In vivo identification of genes that modify ether-a-go-go-related gene activity in Caenorhabditis elegans may also affect human cardiac arrhythmia. Proc Natl Acad Sci U S A *101*, 11773-11778.

Pittendrigh, C.S. (1954). On temperature independence in the clock system controlling emergence time in Drosophila. Proceedings of the National Academy of Sciences *40*, 1018-1029.

Pittendrigh, C.S. (1960). Circadian rhythms and the circadian organization of living systems. Paper presented at: Cold Spring Harbor symposia on quantitative biology (Cold Spring Harbor Laboratory Press).

Pittendrigh, C.S., and Daan, S. (1976). A functional analysis of circadian pacemakers in nocturnal rodents. Journal of Comparative Physiology *106*, 223-252.

Pittendrigh, C.S., and Minis, D.H. (1964). The entrainment of circadian oscillations by light and their role as photoperiodic clocks. American Naturalist, 261-294.

Plautz, J.D., Kaneko, M., Hall, J.C., and Kay, S.A. (1997). Independent photoreceptive circadian clocks throughout Drosophila. Science *278*, 1632-1635.

Price, J.L., Blau, J., Rothenfluh, A., Abodeely, M., Kloss, B., and Young, M.W. (1998). double-time is a novel Drosophila clock gene that regulates PERIOD protein accumulation. Cell *94*, 83-95.

Quintero, J.E., Kuhlman, S.J., and McMahon, D.G. (2003). The biological clock nucleus: a multiphasic oscillator network regulated by light. The Journal of neuroscience *23*, 8070-8076.

Reddy, A.B., Karp, N.A., Maywood, E.S., Sage, E.A., Deery, M., O'Neill, J.S., Wong, G.K., Chesham, J., Odell, M., and Lilley, K.S. (2006). Circadian orchestration of the hepatic proteome. Current Biology *16*, 1107-1115.

Redfern, P. (1989). 'Jet-lag': Strategies for prevention and cure. Human Psychopharmacology: Clinical and Experimental *4*, 159-168.

Redfern, P., Minors, D., and Waterhouse, J. (1994). Circadian rhythms, jet lag, and chronobiotics: an overview. Chronobiology international *11*, 253-265.

Reeve, E.C. (2014). Encyclopedia of genetics (Routledge).

Renn, S.C., Park, J.H., Rosbash, M., Hall, J.C., and Taghert, P.H. (1999). A *pdf* neuropeptide gene mutation and ablation of PDF neurons each cause severe abnormalities of behavioral circadian rhythms in *Drosophila*. Cell *99*, 791-802.

Richter, C. (1965). Biological clocks in medicine and psychiatry Thomas. Springfield, Ill.

Rieger, D., Shafer, O.T., Tomioka, K., and Helfrich-Förster, C. (2006). Functional analysis of circadian pacemaker neurons in Drosophila melanogaster. The Journal of neuroscience *26*, 2531-2543.

Rieger, D., Stanewsky, R., and Helfrich-Förster, C. (2003). Cryptochrome, compound eyes, Hofbauer-Buchner eyelets, and ocelli play different roles in the entrainment and masking pathway of the locomotor activity rhythm in the fruit fly Drosophila melanogaster. Journal of Biological Rhythms *18*, 377-391.

Riganti, C., Gazzano, E., Polimeni, M., Costamagna, C., Bosia, A., and Ghigo, D. (2004). Diphenyleneiodonium inhibits the cell redox metabolism and induces oxidative stress. The Journal of biological chemistry *279*, 47726-47731.

Roberts, L., Leise, T.L., Noguchi, T., Galschiodt, A.M., Houl, J.H., Welsh, D.K., and Holmes, T.C. (2015). Light evokes rapid circadian network oscillator desynchrony followed by gradual phase retuning of synchrony. Current Biology *25*, 858-867.

Roenneberg, T., Allebrandt, K.V., Merrow, M., and Vetter, C. (2012). Social jetlag and obesity. Current Biology *22*, 939-943.

Rosato, E., Codd, V., Mazzotta, G., Piccin, A., Zordan, M., Costa, R., and Kyriacou, C.P. (2001). Light-dependent interaction between Drosophila CRY and the clock protein PER mediated by the carboxy terminus of CRY. Current biology : CB *11*, 909-917.

Rosenthal, N.E., Joseph-Vanderpool, J.R., Levendosky, A.A., Johnston, S.H., Allen, R., Kelly, K.A., Souetre, E., Schultz, P., and Starz, K. (1990). Phase-shifting effects of bright morning light as treatment for delayed sleep phase syndrome. Sleep *13*, 354-361.

Rutila, J.E., Suri, V., Le, M., So, W.V., Rosbash, M., and Hall, J.C. (1998). CYCLE is a second bHLH-PAS clock protein essential for circadian rhythmicity and transcription of Drosophila period and timeless. Cell *93*, 805-814.

Sack, R., Auckley, D., Auger, R., Carskadon, M., Wright, K., and Vitiello, M. (2007). Zhdanova IV. Circadian rhythm sleep disorders: Part I, basic prin-ciples, shift work and jet lag disorders. Sleep *30*, 1460-1483.

Sakai, T., Isono, K., Tomaru, M., Fukatami, A., and Oguma, Y. (2002). Light wavelength dependency of mating activity in the Drosophila melanogaster species subgroup. Genes & genetic systems *77*, 187-195.

Salcedo, E., Huber, A., Henrich, L., Chadwell, W., Chou, R.P., and Britt, S. (1999). Ectopic expression and physiological characterization of the R8 photoreceptor cell-specific Rh5 and Rh6 rhodopsins of Drosophila. J Neurosci *24*, 10716-10726.

Salcedo, E., Zheng, L., Phistry, M., Bagg, E.E., and Britt, S.G. (2003). Molecular basis for ultraviolet vision in invertebrates. The Journal of Neuroscience *23*, 10873-10878.

Santarelli, L.C., Wassef, R., Heinemann, S.H., and Hoshi, T. (2006). Three methionine residues located within the regulator of conductance for K+ (RCK) domains confer oxidative sensitivity to large-conductance Ca2+-activated K+ channels. The Journal of physiology *571*, 329-348.

Sasseville, A., Paquet, N., Sévigny, J., and Hébert, M. (2006). Blue blocker glasses impede the capacity of bright light to suppress melatonin production. Journal of pineal research *41*, 73-78.

Schaap, J., Pennartz, C.M., and Meijer, J.H. (2003). Electrophysiology of the Circadian Pacemaker in Mammals: REVIEW. Chronobiology international *20*, 171-188.

Scheer, F.A., Hilton, M.F., Mantzoros, C.S., and Shea, S.A. (2009). Adverse metabolic and cardiovascular consequences of circadian misalignment. Proceedings of the National Academy of Sciences *106*, 4453-4458.

Schibler, U., Ripperger, J., and Brown, S.A. (2003). Peripheral circadian oscillators in mammals: time and food. Journal of biological rhythms *18*, 250-260.

Scott, V.E., Rettig, J., Parcej, D.N., Keen, J.N., Findlay, J.B., Pongs, O., and Dolly, J.O. (1994). Primary structure of a beta subunit of alpha-dendrotoxin-sensitive K+ channels from bovine brain. Proc Natl Acad Sci U S A *91*, 1637-1641.

Sehadova, H., Glaser, F.T., Gentile, C., Simoni, A., Giesecke, A., Albert, J.T., and Stanewsky, R. (2009). Temperature Entrainment of *Drosophila's* Circadian Clock Involves the Gene *nocte* and Signaling from Peripheral Sensory Tissues to the Brain. Neuron *64*, 251-266.

Sehgal, A., Price, J.L., Man, B., and Young, M.W. (1994). Loss of circadian behavioral rhythms and per RNA oscillations in the Drosophila mutant timeless. Science *263*, 1603-1606.

Sei, H., Oishi, K., Morita, Y., and Ishida, N. (2001). Mouse model for morningness/eveningness. Neuroreport *12*, 1461-1464.

Sellix, M.T., Currie, J., Menaker, M., and Wijnen, H. (2010). Fluorescence/luminescence circadian imaging of complex tissues at single-cell resolution. Journal of biological rhythms *25*, 228-232.

Shafer, O.T., Helfrich-Förster, C., Renn, S.C.P., and Taghert, P.H. (2006). Reevaluation of Drosophila melanogaster's neuronal circadian pacemakers reveals new neuronal classes. Journal of Comparative Neurology *498*, 180-193.

Shafer, O.T., Rosbash, M., and Truman, J.W. (2002). Sequential nuclear accumulation of the clock proteins period and timeless in the pacemaker neurons of Drosophila melanogaster. The Journal of neuroscience *22*, 5946-5954.

Shalitin, D., Yang, H., Mockler, T.C., Maymon, M., Guo, H., Whitelam, G.C., and Lin, C. (2002). Regulation of Arabidopsis cryptochrome 2 by blue-light-dependent phosphorylation. Nature *417*, 763-767.

Shang, Y., Griffith, L.C., and Rosbash, M. (2008). Light-arousal and circadian photoreception circuits intersect at the large PDF cells of the Drosophila brain. Proceedings of the National Academy of Sciences *105*, 19587-19594.

Sharma, V.K., Singaravel, M., Chandrashekaran, M.K., and Subbaraj, R. (1997). Relationship between free-running period and minimum tolerable light pulse interval of skeleton photoperiods in field mice Mus booduga. Chronobiol Int *14*, 237-245.

Sheeba, V. (2008). The Drosophila melanogaster circadian pacemaker circuit. Journal of genetics *87*, 485-493.

Sheeba, V., Fogle, K.J., Kaneko, M., Rashid, S., Chou, Y.-T., Sharma, V.K., and Holmes, T.C. (2008a). Large ventral lateral neurons modulate arousal and sleep in *Drosophila*. Current Biology *18*, 1537-1545.

Sheeba, V., Gu, H., Sharma, V.K., O'Dowd, D.K., and Holmes, T.C. (2007). Circadian- and light-dependent regulation of resting membrane potential and spontaneous action potential firing of Drosophila circadian pacemaker neurons. Journal of neurophysiology *99*, 976-988.

Sheeba, V., Sharma, V.K., Gu, H., Chou, Y.-T., O'Dowd, D.K., and Holmes, T.C. (2008b). Pigment dispersing factor-dependent and-independent circadian locomotor behavioral rhythms. The Journal of Neuroscience *28*, 217-227.

Siwicki, K.K., Eastman, C., Petersen, G., Rosbash, M., and Hall, J.C. (1988). Antibodies to the period gene product of Drosophila reveal diverse tissue distribution and rhythmic changes in the visual system. Neuron *1*, 141-150.

Stanewsky, R., Jamison, C.F., Plautz, J.D., Kay, S.A., and Hall, J.C. (1997). Multiple circadian-regulated elements contribute to cycling period gene expression in Drosophila. The EMBO journal *16*, 5006-5018.

Stanewsky, R., Kaneko, M., Emery, P., Beretta, B., Wager-Smith, K., Kay, S.A., Rosbash, M., and Hall, J.C. (1998). The cryb mutation identifies cryptochrome as a circadian photoreceptor in Drosophila. Cell *95*, 681-692.

Stephan, F.K. (1983). Circadian rhythms in the rat: constant darkness, entrainment to T cycles and to skeleton photoperiods. Physiology & behavior *30*, 451-462.

Stevens, R.G., and Rea, M.S. (2001). Light in the built environment: potential role of circadian disruption in endocrine disruption and breast cancer. Cancer Causes & Control *12*, 279-287.

Stoleru, D., Nawathean, P., de la Paz Fernández, M., Menet, J.S., Ceriani, M.F., and Rosbash, M. (2007). The Drosophila circadian network is a seasonal timer. Cell *129*, 207-219.

Tang, C.-H.A., Hinteregger, E., Shang, Y., and Rosbash, M. (2010). Light-mediated TIM degradation within Drosophila pacemaker neurons (s-LNvs) is neither necessary nor sufficient for delay zone phase shifts. Neuron *66*, 378-385.

Tang, X.D., Garcia, M.L., Heinemann, S.H., and Hoshi, T. (2004). Reactive oxygen species impair Slo1 BK channel function by altering cysteine-mediated calcium sensing. Nature structural & molecular biology *11*, 171-178.

Tanoue, S., Krishnan, P., Krishnan, B., Dryer, S.E., and Hardin, P.E. (2004). Circadian clocks in antennal neurons are necessary and sufficient for olfaction rhythms in Drosophila. Current Biology *14*, 638-649.

Tauber, E., and Kyriacou, B.P. (2001). Insect photoperiodism and circadian clocks: models and mechanisms. Journal of Biological Rhythms *16*, 381-390.

Tsumoto, K., Kurosawa, G., Yoshinaga, T., and Aihara, K. (2011). Modeling light adaptation in circadian clock: Prediction of the response that stabilizes entrainment. PLoS One *6*, e20880.

Tyson, J.J. (2002). Biochemical oscillations. In Computational Cell Biology (Springer), pp. 230-260.

Vaidya, A.T., Top, D., Manahan, C.C., Tokuda, J.M., Zhang, S., Pollack, L., Young, M.W., and Crane, B.R. (2013). Flavin reduction activates Drosophila cryptochrome. Proc Natl Acad Sci U S A *110*, 20455-20460.

VanVickle-Chavez, S.J., and Van Gelder, R.N. (2007). Action spectrum of Drosophila cryptochrome. The Journal of biological chemistry *282*, 10561-10566.

Veleri, S., Brandes, C., Helfrich-Förster, C., Hall, J.C., and Stanewsky, R. (2003). A self-sustaining, light-entrainable circadian oscillator in the *Drosophila* brain. Current biology *13*, 1758-1767.

Videnovic, A., Noble, C., Reid, K.J., Peng, J., Turek, F.W., Marconi, A., Rademaker, A.W., Simuni, T., Zadikoff, C., and Zee, P.C. (2014). Circadian melatonin rhythm and excessive daytime sleepiness in Parkinson disease. JAMA neurology *71*, 463-469.

Vinayak, P., Coupar, J., Hughes, S.E., Fozdar, P., Kilby, J., Garren, E., Yoshii, T., and Hirsh, J. (2013). Exquisite light sensitivity of Drosophila melanogaster cryptochrome. PLoS Genet *9*, e1003615.

Wang, J., Zhang, J., Yuan, Z., Chen, A., and Zhou, T. (2008). Neurotransmitter-mediated collective rhythms in grouped Drosophila circadian clocks. Journal of biological rhythms *23*, 472-482.

Wang, T.A., Yu, Y.V., Govindaiah, G., Ye, X., Artinian, L., Coleman, T.P., Sweedler, J.V., Cox, C.L., and Gillette, M.U. (2012). Circadian rhythm of redox state regulates excitability in suprachiasmatic nucleus neurons. Science *337*, 839-842.

Waterhouse, J. (1999). Jet-lag and shift work:(1). Circadian rhythms. Journal of the royal society of medicine *92*, 398.

Webb, A.B., Taylor, S.R., Thoroughman, K.A., Doyle III, F.J., and Herzog, E.D. (2012). Weakly circadian cells improve resynchrony. PLoS Comput Biol *8*, e1002787.

Wegmann, H., and Klein, K. (1985). Jet-lag and aircrew scheduling. Hours of work, 263-276.

Welsh, D.K., Logothetis, D.E., Meister, M., and Reppert, S.M. (1995). Individual neurons dissociated from rat suprachiasmatic nucleus express independently phased circadian firing rhythms. Neuron *14*, 697-706.

Welsh, D.K., Takahashi, J.S., and Kay, S.A. (2010). Suprachiasmatic nucleus: cell autonomy and network properties. Annual review of physiology *72*, 551.

Welsh, D.K., Yoo, S.-H., Liu, A.C., Takahashi, J.S., and Kay, S.A. (2004). Bioluminescence imaging of individual fibroblasts reveals persistent, independently phased circadian rhythms of clock gene expression. Current Biology *14*, 2289-2295.

Weng, J., Cao, Y., Moss, N., and Zhou, M. (2006). Modulation of voltage-dependent Shaker family potassium channels by an aldo-keto reductase. Journal of Biological Chemistry *281*, 15194-15200.

Wheeler, D.A., Hamblen-Coyle, M.J., Dushay, M.S., and Hall, J.C. (1993). Behavior in light-dark cycles of Drosophila mutants that are arrhythmic, blind, or both. Journal of Biological Rhythms *8*, 67-94.

Whitton, J.L. (1978). Periodicities in self-reports of health, sleep and mood variables. Journal of psychosomatic research *22*, 111-115.

Wilson, G.F., Wang, Z., Chouinard, S.W., Griffith, L.C., and Ganetzky, B. (1998). Interaction of the K channel beta subunit, Hyperkinetic, with eag family members. The Journal of biological chemistry *273*, 6389-6394.

Winget, C.M., DeRoshia, C.W., Markley, C.L., and Holley, D.C. (1984). A review of human physiological and performance changes associated with desynchronosis of biological rhythms. Aviation, space, and environmental medicine *55*, 1085-1096.

Winter, S.L., Bosnoyan-Collins, L., Pinnaduwage, D., and Andrulis, I.L. (2007). Expression of the Circadian Clock Genes Pert, Per2 in Sporadic, Familial Breast Tumors. Neoplasia *9*, 797-800.

Wittmann, M., Dinich, J., Merrow, M., and Roenneberg, T. (2006). Social jetlag: misalignment of biological and social time. Chronobiology international *23*, 497-509.

Wittmann, M., Paulus, M., and Roenneberg, T. (2010). Decreased psychological well-being in late 'chronotypes' is mediated by smoking and alcohol consumption. Substance use & misuse *45*, 15-30.

Xiang, Y., Yuan, Q., Vogt, N., Looger, L.L., Jan, L.Y., and Jan, Y.N. (2010). Light-avoidance-mediating photoreceptors tile the Drosophila larval body wall. Nature *468*, 921-926.

Yamaguchi, S., Desplan, C., and Heisenberg, M. (2010). Contribution of photoreceptor subtypes to spectral wavelength preference in Drosophila. Proc Natl Acad Sci U S A *107*, 5634-5639.

Yamaguchi, S., Isejima, H., Matsuo, T., Okura, R., Yagita, K., Kobayashi, M., and Okamura, H. (2003). Synchronization of cellular clocks in the suprachiasmatic nucleus. Science *302*, 1408-1412.

Yamaguchi, Y., Suzuki, T., Mizoro, Y., Kori, H., Okada, K., Chen, Y., Fustin, J.-M., Yamazaki, F., Mizuguchi, N., and Zhang, J. (2013). Mice genetically deficient in vasopressin V1a and V1b receptors are resistant to jet lag. Science *342*, 85-90.

Yamazaki, S., Numano, R., Abe, M., Hida, A., Takahashi, R.-i., Ueda, M., Block, G.D., Sakaki, Y., Menaker, M., and Tei, H. (2000). Resetting central and peripheral circadian oscillators in transgenic rats. Science *288*, 682-685.

Yan, L., Karatsoreos, I., LeSauter, J., Welsh, D., Kay, S., Foley, D., and Silver, R. (2007). Exploring spatiotemporal organization of SCN circuits. Paper presented at: Cold Spring Harbor symposia on quantitative biology (Cold Spring Harbor Laboratory Press).

Yang, Z., Emerson, M., Su, H.S., and Sehgal, A. (1998). Response of the timeless protein to light correlates with behavioral entrainment and suggests a nonvisual pathway for circadian photoreception. Neuron *21*, 215-223.

Yang, Z., and Sehgal, A. (2001). Role of Molecular Oscillations in Generating Behavioral Rhythms in *Drosophila*. Neuron *29*, 453-467.

Yao, Z., and Shafer, O. (2014). The Drosophila circadian clock is a variably coupled network of multiple peptidergic units. Science *343*, 1516-1520.

Yasuyama, K., and Meinertzhagen, I. (1999). Extraretinal photoreceptors at the compound eye's posterior margin in Drosophila melanogaster. Journal of Comparative Neurology *412*, 193-202.

Yoshii, T., Ahmad, M., and Helfrich-Förster, C. (2009). Cryptochrome mediates light-dependent magnetosensitivity of Drosophila's circadian clock. PLoS biology *7*, e1000086.

Yoshii, T., Todo, T., Wülbeck, C., Stanewsky, R., and Helfrich-Förster, C. (2008). Cryptochrome is present in the compound eyes and a subset of Drosophila's clock neurons. Journal of Comparative Neurology *508*, 952-966.

Yu, W., and Hardin, P.E. (2006). Circadian oscillators of Drosophila and mammals. Journal of cell science *119*, 4793-4795.

Zerr, D., Hall, J., Rosbash, M., and Siwicki, K.K. (1990). Circadian fluctuations of period protein immunoreactivity in the CNS and the visual system of Drosophila. The Journal of Neuroscience *10*, 2749-2762.

Zhang, E.E., and Kay, S.A. (2010). Clocks not winding down: unravelling circadian networks. Nature reviews Molecular cell biology *11*, 764-776.

Zhang, L., Chung, B.Y., Lear, B.C., Kilman, V.L., Liu, Y., Mahesh, G., Meissner, R.-A., Hardin, P.E., and Allada, R. (2010a). $DN1_p$ Circadian Neurons Coordinate Acute Light and PDF Inputs to Produce Robust Daily Behavior in *Drosophila*. Current Biology *20*, 591-599.

Zhang, Y., Liu, Y., Bilodeau-Wentworth, D., Hardin, P.E., and Emery, P. (2010b). Light and Temperature Control the Contribution of Specific DN1 Neurons to *Drosophila* Circadian Behavior. Current Biology *20*, 600-605.

Zhao, J., Kilman, V.L., Keegan, K.P., Peng, Y., Emery, P., Rosbash, M., and Allada, R. (2003). Drosophila clock can generate ectopic circadian clocks. Cell *113*, 755-766.

Zhong, L., Bellemer, A., Yan, H., Ken, H., Jessica, R., Hwang, R.Y., Pitt, G.S., and Tracey, W.D. (2012). Thermosensory and nonthermosensory isoforms of Drosophila melanogaster TRPA1 reveal heat-sensor domains of a thermoTRP Channel. Cell Rep *1*, 43-55.

Zhu, E.Y., Guntur, A.R., He, R., Stern, U., and Yang, C.H. (2014). Egg-laying demand induces aversion of UV light in Drosophila females. Current biology : CB *24*, 2797-2804.

Zhu, L., and Zee, P.C. (2012). Circadian rhythm sleep disorders. Neurologic clinics *30*, 1167-1191.

Zylka, M.J., Shearman, L.P., Weaver, D.R., and Reppert, S.M. (1998). Three period homologs in mammals: differential light responses in the suprachiasmatic circadian clock and oscillating transcripts outside of brain. Neuron *20*, 1103-1110.